STRUCTURED NEURAL NETWORKS FOR MODELING AND IDENTIFICATION OF NONLINEAR MECHANICAL SYSTEMS

A THESIS SUBMITTED TO
THE GRADUATE SCHOOL OF NATURAL AND APPLIED SCIENCES
OF
MIDDLE EAST TECHNICAL UNIVERSITY

BY

ERGİN KILIÇ

IN PARTIAL FULFILLMENT OF THE REQUIREMENTS
FOR
THE DEGREE OF DOCTOR OF PHILOSOPHY
IN
MECHANICAL ENGINEERING

SEPTEMBER 2012

Approval of the thesis:

STRUCTURED NEURAL NETWORKS FOR MODELING AND IDENTIFICATION OF NONLINEAR MECHANICAL SYSTEMS

submitted by **ERGİN KILIÇ** in partial fulfillment of the requirements for the degree of **Doctor of Philosophy in Mechanical Engineering Department, Middle East Technical University** by,

Prof. Dr. Canan Özgen _____
Dean, Graduate School of **Natural and Applied Sciences**

Prof. Dr. Suha Oral _____
Head of Department, **Mechanical Engineering**

Asst. Prof. Dr. Melik Dölen _____
Supervisor, **Mechanical Engineering Dept., METU**

Asst. Prof. Dr. A. Buğra Koku _____
Co-supervisor, **Mechanical Engineering Dept., METU**

Examining Committee Members:

Prof. Dr. Tuna Balkan _____
Mechanical Engineering Dept., METU

Asst. Prof. Dr. Melik Dölen _____
Mechanical Engineering Dept., METU

Asst. Prof. Dr. Yiğit Yazıcıoğlu _____
Mechanical Engineering Dept., METU

Asst. Prof. Dr. Afşar Saranlı _____
Electrical and Electronics Engineering Dept., METU

Asst. Prof. Dr. Kutluk Bilge Arıkan _____
Mechatronics Engineering Dept., Atılım University

Date: 04.09.2012

I hereby declare that all information in this document has been obtained and presented in accordance with academic rules and ethical conduct. I also declare that, as required by these rules and conduct, I have fully cited and referenced all material and results that are not original to this work.

Name, Last name : Ergin KILIÇ

Signature :

ABSTRACT

STRUCTURED NEURAL NETWORKS FOR MODELING AND IDENTIFICATION OF NONLINEAR MECHANICAL SYSTEMS

Kılıç, Ergin
Ph.D., Department of Mechanical Engineering
Supervisor: Asst. Prof. Dr. Melik Dölen
Co-Supervisor: Asst. Prof. Dr. A. Buğra Koku

September 2012, 227 pages

Most engineering systems are highly nonlinear in nature and thus one could not develop efficient mathematical models for these systems. Artificial neural networks, which are used in estimation, filtering, identification and control in technical literature, are considered as universal modeling and functional approximation tools. Unfortunately, developing a well trained monolithic type neural network (with many free parameters/weights) is known to be a daunting task since the process of loading a specific pattern (functional relationship) onto a generic neural network is proven to be a NP-complete problem. It implies that if training is conducted on a deterministic computer, the time required for training process grows exponentially with increasing size of the free parameter space (and the training data in correlation). As an alternative modeling technique for nonlinear dynamic systems; this thesis proposed a general methodology for structured neural network topologies and their corresponding applications are realized. The main idea behind this (rather classic) divide-and-conquer approach

is to employ *a priori* information on the process to divide the problem into its fundamental components. Hence, a number of smaller neural networks could be designed to tackle with these elementary mapping problems. Then, all these networks are combined to yield a tailored structured neural network for the purpose of modeling the dynamic system under study accurately. Finally, implementations of the devised networks are taken into consideration and the efficiency of the proposed methodology is tested on four different types of mechanical systems.

Keywords: Structured Neural Networks, Position Error Estimation, Long-term Pressure Prediction, Timing-Belt Drive, Cable-Drum Mechanism.

ÖZ

DOĞRUSAL OLMAYAN MEKANİK SİSTEMLERİN MODELLEMESİNDE VE TANISINDA KULLANILAN YAPILANDIRILMIŞ YAPAY SİNİR AĞLARI

Kılıç, Ergin
Doktora, Makina Mühendisliği Bölümü
Tez Yöneticisi : Yrd. Doç. Dr. Melik Dölen
Ortak Tez Yöneticisi: Yrd. Doç. Dr. A. Buğra Koku

Eylül 2012, 227 sayfa

Mühendislik alanındaki sistemlerin çoğunun doğrusal-olmayan davranış göstermesi bu sistemler için güvenilir matematiksel modellerin oluşturulmasını zorlaştırmaktadır. Yapay sinir ağları kestirme, filtreleme, tanılama ve denetleme alanlarında sıklıkla kullanıldıklarından evrensel modelleme ve fonksiyon yaklaşıklama araçları olarak kabul görülmektedir. Bazı tip fonksiyonların genel tipteki sinir ağlarına uyarlanması NP karmaşıklık sınıfına girdiğinden, iyi eğitilmiş yekpare bir sinir ağı elde etmek oldukça zordur. Aslında, sinir ağının eğitilebilmesi için gereken süre, ağın sahip olduğu serbest değişken uzay boyutunun artmasıyla üstel bir biçimde artmaktadır.Doğrusal olmayan dinamik sistemlerin alternatif bir biçimde modellenebilmesi için bu tez kapsamında yapılandırılmış yapay sinir ağ topolojileri için bir yöntem dizisi önerilmekte ve bu yöntemlerin ağ yapıları ile birlikte uygulaması gerçekleştirilmektedir. Yöntemler dizisinin ana fikri sistemi temel yapılarına bölmektir. İrdelenen sistemin temel

yapılarına ayrılmasında kullanılacak olan ‘parçala ve çöz’ yöntemi ise, aslında sistem hakkında sahip olunan ön bilgiye önemli ölçüde bağlı olmaktadır. Böylelikle, ayrıştırılan bu yapılar nispeten küçük yapay sinir ağları ile kolaylıkla modellenebilmektedirler. Daha sonra, bu küçük yapay ağlar birbirleriyle tekrar birleştirilerek ve uygun hale getirilerek dinamik sistemi tam olarak modelleyebilecek bir yapılandırılmış yapay sinir ağı oluşturulur. Daha sonra, yöntemin etkinliği dört adet mekanik sistem üzerinde test edilmiştir.

Anahtar Kelimeler: Yapılandırılmış Yapay Sinir Ağları, Konum Hatası Tahmini, Uzun Vadeli Basınç Kestirimi, Dişli Kayış, Kablo Kasnak Mekanizması.

ACKNOWLEDGMENTS

I am deeply grateful to my thesis supervisor Asst. Prof. Dr. Melik Dölen and co-supervisor Asst. Prof. Dr. A. Buğra Koku for their advice, encouragement and invaluable help all throughout the study.

I also would like to thank to Prof. Dr. Tuna Balkan and to Asst. Prof. Dr. Afşar Saranlı for their precious advices, guidance and comments in my thesis progression.

I gratefully acknowledge Hakan Çalışkan, for his assistance in providing the experimental data about the hydraulic system.

Finally, I am grateful to my family for their endless love, support, trust and encouragement. I would like to thank my wife, Ferda Teltik Kılıç, for her invaluable support, kindness, and for being in my life with her endless love, forever.

This work has been supported by METU/BAP under contact (Project No: 1354).

TABLE OF CONTENTS

LIST OF TABLES

TABLES

LIST OF FIGURES

FIGURES

LIST OF SYMBOLS

P_A	hydraulic pressure in chamber A
P_B	hydraulic pressure in chamber B
P_S	supply pressure
P_T	tank pressure
Q_A	control flow in chamber A
Q_B	control flow in chamber B
M	mass of the piston
B	effective viscous damping
K	stiffness of the equivalent spring
F_{fric}	friction force
F_{ext}	external force
A_p	piston annulus area
x	hydraulic actuator position
v	velocity of the piston
V_A	volume of hydraulic oil in chamber A
V_{A0}	chamber A initial volume
V_B	volume of hydraulic oil in chamber B
V_{B0}	chamber B initial volume
I	coil current
V_c	control voltage
u_v	valve spool position
L_C	coil (solenoid) inductance
R_C	coil resistance

K_h	first stage servo-valve gain
ω_n	natural frequency
ζ	damping ratio
K_v	servo-valve flow gain
C_d	discharge coefficient of the orifice
w	gradient of the orifice area
ρ	density of the hydraulic oil
T	sampling period
σ_0	bristle-spring constant
σ_1	bristle-damping coefficient
σ_2	viscous friction coefficient
v_s	Stribeck velocity
z	average bristle deflection
F_c	Coloumb friction
F_s	static friction
β	bulk modulus of the hydraulic oil
φ	regression vector
θ	model parameter vector
Ψ	activation vector function
W	weight matrix
b	bias vector
m	order of the TDL actuator position signal
n	order of the TDL control voltage signal
p	order of the TDL pressure signals
k	discrete time index
s	Laplace variable
$\hat{y}$	model output
y	process output

u	process input
e	prediction error
i	imaginary unit
A	accuracy frequency response function
D	diagonal matrix
J_N	objective function
N	number of data sample
Δ	unit delay (memory)

LIST OF ABBREVIATIONS

AIC	Adaptive Inverse Control
ANN	Artificial Neural Network
AR	Auto-Regressive
ARMA	Auto-Regressive Moving Average
ARMAX	Auto-Regressive Moving Average with eXogeneous input
ART	Adaptive Resonance Theory
ARX	Auto-Regressive with eXogeneous input
BJ	Box-Jenkins
BSNN	B-Spline Neural Network
CGTLS	Constrained Generalized Total Least Squares
CUDA	Compute Unified Device Architecture
DFT	Discrete Fourier Transform
DNN	Dynamic Neural Networks
EHSS	Electro-Hydraulic Servo System
FIR	Finite Impulse Response
FNN	Feed-forward Neural Network
FODM	First Order Difference Method
FPAA	Field-Programmable Analog Array
FPGA	Field-Programmable Gate Array
FRF	Frequency Response Function

FRNN	Fully-Recurrent Neural Network
FWNN	Fuzzy Wavelet Neural Network
GDNN	General Dynamic Neural Network
GMN	Growing Multi-experts Network
GPU	Graphic Processing Units
HP	Home Position
IIR	Infinite Impulse Response
LM	Levenberg-Marquardt
LMN	Local Model Networks
LRFNN	Locally Recurrent Fuzzy Neural Network
LS	Least-Squares
LUT	Look-Up Table
ME	Mixture of Expert
MPC	Model Predictive Control
MRAC	Model Reference Adaptive Control
MSVME	Mixture of Support Vector Machine Expert
NARMAX	Nonlinear Auto-Regressive Moving Average with eXogeneous input
NARX	Nonlinear Auto-Regressive with eXogeneous input
NBJ	Nonlinear Box-Jenkins
NFIR	Nonlinear Finite Impulse Response
NN	Neural Network
NOE	Nonlinear Output Error
OBD	Optimal Brain Damage
OBS	Optimal Brain Surgeon

OE	Output Error
PE	Primary Encoder
PRMS	Pseudo-Random Multi-level Signal
PRNN	Pipelined Recurrent Neural Network
RBF	Radial Basis Function
RHONN	Recurrent High Order Neural Network
RLS	Recursive Least-Squares
RMS	Root-Mean-Square
RNN	Recurrent Neural Network
RTRL	Real-Time Recurrent Learning
SLN	Standard Library Network
SNN	Structured Neural Network
SRNN	Structured Recurrent Neural Network
SSNN	State Space Neural Network
SVM	Support Vector Machine
SVP	Smallest Variance Pruning
SVR	Support Vector Regression
TBD	Timing Belt Drive
TDL	Tapped-Delay-Line
ZRD	Zero Region Detector

CHAPTER 1

INTRODUCTION

In engineering domain, nearly all the systems are highly nonlinear so that one cannot easily derive their exact mathematical models which are based on the physical laws about the system behavior. This modeling technique is known as *white-box modeling* since all the model variables and parameters have a physical meaning about the system under study and give an insight into the system behavior. However, such a white-box modeling technique may not be appropriate for some systems due to the following reasons:

- The physical knowledge about a system could be insufficient to develop mathematical equations which will describe the system thoroughly.

- The measurement (or finding the exact value) of some physical parameters or coefficients used in the mathematical expressions could be limited or impossible.

- Mathematical expression of a system would most likely be an approximation of the investigated system since the real parameters of the process can never be known exactly.

- Although an exact mathematical modeling of a system is derived, the implementation of the resulting model would be difficult and time-consuming in a hardware platform.

As an alternative to mathematical modeling, some variables distinguishing the behavior of the nonlinear system could be measured and used to create approximate models (with desired accuracy). Here, the modeling is to devise a structure in which its parameters are determined in a way that when the same input(s) is applied to the nonlinear system and model, their corresponding outputs should match as much as possible. Simulating (or predicting) the outputs of a system accurately, the developed models could then be used for control purposes, fault-detection or estimating the systems' outputs directly (*soft sensor*). In the technical literature, it is seen that artificial neural networks (ANNs) are generally used for identification and control tasks of dynamic systems since they are highly efficient nonlinear modeling or decision making tools.

This chapter includes the following sections. An overview about ANNs is given in Section 1.1. Next, the motivation of the thesis is explained in Section 1.2. Following that, Section 1.3 gives the thesis statement. Finally, the outline of the thesis is given in Section 1.4.

1.1 Artificial Neural Networks

An *artificial neural network* (ANN) is a parallel processor in which a number of neurons are used to imitate the working principle of a biological brain. Indeed, a large number of neurons are connected to each other with different weight values and are activated by input signals to produce an intelligent behavior. They are mainly used for information processing while interacting with a system after a learning operation in which the weight values are adjusted to perform a computationally complex task. ANNs are especially useful in system identification and control (Narendra and Parthasarathy, 1990) where there is no way to write out the exact mathematical model of the nonlinear process under study. Robotics (King and Hwang, 1989) / optimization (Tagliarini et al., 1991) / decision making (Tan et al., 1996) / pattern recognition in radar systems (Orlando et al., 1990), face identification (Zhang and Fulcher, 1996), object recognition (Watanabe and Yoneyama, 1992) / sequence recognition such as speech recognition (Lippmann 1989) and handwritten text recognition (LeCun et al., 1989) / data processing

including filtering (Weber et al., 1991), clustering (Sato, 1995), blind signal separation (Girolami and Gyfe, 1997) and compression (Iwata et al., 1990) / medical diagnosis (Moallemi, 1991) / financial forecasting (Ankenbrand and Tomassini, 1996) and weather forecasting (Liu and Lee, 1999) are commonly used implementation areas of the ANNs.

The most critical phase of designing an ANN is absolutely the determination of the weight values. In fact, the weights, which are randomly initialized, should be placed in an appropriate location by a proper learning algorithm in the huge weight domain where the network will be globally stable. Optimization theory and statistical estimation techniques are generally used to train the ANNs in a straightforward fashion. Back-propagation by gradient descent (Werbos, 1974), genetic algorithms (Goldberg, 1989), simulated annealing (Kirkpatrick et al., 1983), Hebbian learning (Hebb, 1949), Boltzmann machine (Hinton et al., 1984), mean field annealing (Soukoulis et al., 1983), Gaussian machine, (Akiyema et al., 1991), expectation maximization (Dempster et al., 1977), k-means clustering algorithm (MacQueen, 1967) and winner-take-all learning rule (Hecht-Nielsen, 1987) are the names of frequently used methods for training a ANN.

In general, three major learning paradigms, which are the supervised, unsupervised and reinforcement learning, are used to become skilled at the assigned task to the ANN. In supervised learning, the weights of the network are changed to decrease the error between the output values of the system and those of the network for each input pattern. It is frequently used for system identification and control. Unsupervised learning is mostly used for clustering and pattern recognition where weight modifications are only realized with respect to the correlation among the input signals. Finally, in reinforcement learning, the weight modifications are done based on a numerical reward signal, which indicates how well the ANN performs. It is often used in systems that interact with an environment such as robots navigation, collision avoidance, learning autonomous agents and games. As the objective of this thesis is to devise ANN models for nonlinear systems, only supervised learning algorithms will be taken into consideration throughout the thesis study.

After a supervised learning operation, some criterions such as training error, learning speed, model generalization and interpretation are used to evaluate the utility of the ANN model. The training error only indicates the closeness of the network response to the target in the training scenario. It does not give any information about the stability of the network model. Therefore, the most important criterion is the generalization performance of the ANN. The modeling accuracy of the network must be tested with various input patterns which are not used in the training scenario. Moreover, a higher learning speed with minimum number of training samples is always sought due to the convenient real time implementation of the ANN models in a hardware platform. Lastly, the interpretation of a network architecture and its parameters are currently disregarded since most of the present networks' architectures are in *black-box* type. Eventually, the lack of interpretation prevents the incorporation of *a priori* engineering knowledge about the system into to the devised model.

1.2 Motivation of the Thesis

In mechanical engineering domain, nearly all the systems are highly non-linear (housing too much non-linearity such as *friction, dead-zone, saturation, backlash* and *hysteresis*) but some of them are beyond the boundary that one could define them in mathematical equations. Although, ANNs are used for the identification and control of nonlinear systems, they are not accepted as a widespread modeling methodology since a monolithic ANN could not be trainable for very complex systems and they are viewed as unstructured black-box models which makes them difficult to acquire an insight into the system under study.

On the other hand, there are numerous nonlinear mechanical systems about which *a priori* information is already exists. This knowledge of a system's dynamics could be used to increase the performance and also to determine the model structure of the devised ANNs. Therefore, the behavior of these systems could be emulated in a more accurate way by ANNs. The main motivation for embedding *a priori* information into the devised ANN will be to structure a network architecture which is convenient with the dynamics of the nonlinear system under study. For that

purpose four different types of mechanical systems are selected as the application domain of the ANNs in this thesis work.

First one is about a study where the position of a carriage in a timing-belt drive system is to be estimated via low-cost position sensor on the driver side. For this task, first the characteristics of the position error due to the transmission system will be explored. Next, this *a priori* information is to be utilized while devising a relevant neural network model since it will be seen that a monolithic ANN (a black-box model) could not estimate the hysteresis behavior of the position error dynamics at the desired levels. Therefore, the devised ANN model could be used as a viable position estimation scheme in cost-sensitive machines.

Next, valve controlled and a variable speed pump controlled hydraulic servo systems are chosen as a benchmark test platforms since it was found that there is not any study in the current literature about the long-term pressure prediction of hydraulic systems. After showing that classical black-box models were not sufficient for capturing the nonlinear behavior of the hydraulic systems, specific ANN models are to be proposed utilizing *a priori* information on the investigated systems to predict the pressure dynamics in the hydraulic cylinder chambers without using any pressure sensors. Consequently, an accurate pressure dynamic model may allow a pressure sensor to be replaced by an ANN model (*intelligent sensor*) to minimize the overall cost and the sensor-related malfunctions in the hydraulic systems.

Finally, a cable-drum (or capstan drive) mechanism, is chosen as the last benchmark test platform for another challenging prediction problem. It is aimed to predict the slippage between the cable and the drum; therefore, this type of mechanisms could be used as linear motion sensor. In that study, a carriage will house a cable-drum mechanism and the position of the carriage will be predicted via ANN, whose input will be only the position signal coming from a rotary encoder attached to the drum itself. Again, *a priori* knowledge will be used while designing network models so

that rigorous experimental tests are performed first to understand the nonlinear behavior of the slippage between the cable and drum.

1.3 Thesis Statement

Most engineering systems are highly nonlinear in nature and thus one could not develop efficient mathematical models for these systems. ANNs, which are used in prediction, filtering, identification and control in technical literature, are considered as universal modeling and functional approximation tools. Unfortunately, a conventional neural network development paradigm, which exclusively includes black-box approaches, is known as an exhaustive process and has some problems such as long training phases and (most notably) inaccuracy and instability problems for complex physical systems. Moreover, a well-trained ANN does not give any insight about the system to be modeled.

Currently, procedure for determining appropriate model structures for a specific system is still an unsolved problem in the neural network domain. Therefore, devising proper network structures for the system under investigation in a systematic fashion is extremely attractive in the related research field. As an alternative modeling technique for nonlinear dynamic systems; this thesis proposes a general methodology for the design of structured neural networks (SNNs) in a modular form with the sketchy guidance of *a priori* information on the related system. The applied approach adopted here is especially helpful while designing SNNs having an accurate prediction or estimation capability for the nonlinear dynamic systems whose exact physical models are not known exactly. However, the main problems remain that how to structure the system to be identified in modular neural network format and then how to combine the individual networks in order to form the unified one at the end. To clarify the aforementioned questions, some highly nonlinear mechanical systems are chosen as base platforms of application domain of the SNNs. Therefore, some practical implementations of SNNs will be realized on the chosen mechanical systems so that one can find the appropriate network architectures, which are to be used directly, for these types of systems later.

1.4 Outline of the Thesis

A general review of the state of the art about nonlinear system modeling and identification using ANNs is given in Chapter 2. Structured neural network methodology to model nonlinear dynamic systems is presented in Chapter 3. Chapter 4 introduces a feasible position estimation scheme for timing-belt drives that could eliminate the position errors due to the highly nonlinear behavior of the belt-pinion gear mechanism. In Chapter 5, black-box and structured neural network models are developed to predict the cylinder chamber pressures of a valve controlled hydraulic system in the long-term. Similarly, Chapter 6 focuses on the design of ANNs to predict the chamber pressures in hydraulic cylinder of a variable-speed pump controlled hydraulic system using traditional techniques and utilizing the sketchy guidance of *a priori* information about the process at hand. After that, another structured neural network is designed and proposed in Chapter 7 in order to predict the slippage in the cable-drum mechanisms, which could then be used as a linear motion sensor. Finally, Chapter 8 presents the contributions of this dissertation. This chapter also focuses on the future work of this research.

CHAPTER 2

REVIEW OF THE STATE OF THE ART

2.1 Introduction

This chapter presents a review of the state of the art about using ANNs for the system identification and modeling of nonlinear systems. Section 2.2 takes a close look at the literature about ANN architectures within the framework of nonlinear system modeling and identification of various processes. Next, Section 2.3 emphasizes the importance of developing accurate ANN models while designing nonlinear controllers for complex systems. Moreover, hardware implementations of the ANNs in parallel processors are investigated in Section 2.4. Following, Section 2.5 is about the literature review of the generalization of ANNs. The review of the modularity approach in the ANNs, which is highly needed for this thesis work, is presented in Section 2.6. Finally, the chapter closes with the identified research opportunity in Section 2.7 after a detailed literature survey work.

2.2 Nonlinear System Modeling and Identification

In literature, there exist many models (and accompanying identification techniques) such as autoregressive (AR), autoregressive with exogeneous input (ARX), autoregressive moving average (ARMA), autoregressive moving average with exogeneous input (ARMAX), output error (OE), Box-Jenkins (BJ), finite/infinite impulse response (FIR/IIR) filters and orthonormal basis functions with Laguerre/Kautz filters. (Ljung, 1999; Van den Hof et al., 2005; Lemma et al., 2010). Least-squares (LS), recursive least squares (RLS) with exponential forgetting and instrumental variables methods are generally used to find the

parameters of the aforementioned models. Unfortunately, these well known and frequently used models are insufficient for nonlinear systems. The most generic methodology for modeling and identification of nonlinear systems is based on black-box models whose main tools are ANNs, neuro-fuzzy networks (Te Braake et al., 1994), Volterra-series (Liu et al., 1998), Hammerstein and Weiner models (Aguirre et al., 2005), and wavelet networks (Zhang and Benveniste, 1992). In fact, ANNs could establish a model for the behavior of nonlinear system through the real system's input and output data for control- and/or fault-diagnostic purposes. However, the determination of the architecture (or structure) of the network, network size, memory model, training set while satisfying all the necessary conditions/constraints for accurate modeling remains an overwhelming task (Sorjamaa et al., 2007).

Despite the fact that the neural networks have performed well while predicting the response of nonlinear time series (one-step or multi-step ahead) (Mirzaee, 2009), the prediction of the nonlinear system's behavior in the long run (or in sufficiently "long" infinite time interval) is proven to be difficult (Maria et al., 2008). Nonlinear predictor models have received significant attention when the conventional ARX and ARMAX models were modified as nonlinear model architectures such as nonlinear autoregressive with exogenous input (NARX) and nonlinear autoregressive moving average with exogenous input (NARMAX) models (Parlos et al., 2000).

Especially, if the aim is to perform a long-term prediction task, it is obvious that the outputs of the predictor (for a finite number of time steps) must be utilized as an input to the model itself. In that case, the long-term prediction becomes an overwhelming task (Haykin and Li, 1995) due to the accumulation of errors and the lack of reliable estimates. Recurrent neural network (RNN) models have feedback connections and play important role in such complex tasks. RNN models are able to store information by the help of feedback loops which are not exist in feed-forward neural networks (FNN). Elman-type and Jordan-type networks were the first designed recurrent structures which are mainly comprised from feed-forward architectures but having some small number of local and/or global feedbacks inside

the network (Kolen and Kremer, 2001). Apart from that, NARX models, which could be easily adapted to model dynamic systems through a tapped-delay-line (TDL) of input(s) and measured output(s), constitute the well-known nonlinear output error (NOE) models encountered in the literature (Wong and Worden, 2007; Witters and Swevers, 2010) by feeding back the TDL of model output(s) into the input vector instead of measured output(s). This aforementioned recurrent network is usually trained by means of real-time recurrent learning (RTRL) algorithm (Williams and Zipser, 1989). However, network training operations, in which the input-output signals are related to each other with the temporal dependencies (of a dynamic system), are quite difficult especially in the long term intervals using the gradient based learning methods (Bengio et al., 1994; Lin et al., 1998).

Designing a very accurate model for a specific process is still a tough issue in the field of nonlinear dynamic system identification. Most of the designed models are used for only one-step ahead prediction tasks as they are highly needed in advanced controller topologies, which will be presented in Section 2.3. Some of them could be used in multi-step ahead prediction tasks but to capture the exact dynamics of a real complex process is doubtlessly a very challenging topic in the current literature.

Li (1995) used RNNs to emulate the dynamic behaviors of a two-link robot arm and a screw compressor. The RNNs have one hidden layer, in which the neurons feedback themselves, and a static output layer which collects the output of hidden layer in a linear way. It was shown that RNNs were well adapted to emulate the nonlinear behavior of such dynamic systems through their own dynamics.

Zamarreno and Vega (1998) proposed a RNN, whose structure was in the same way of a nonlinear state space equation, for the identification of nonlinear systems. This network model called state space neural network (SSNN) and used for the identification of a chemical reactor. Moreover, Schenker and Agarwal (1998) used a SSNN model in the output prediction of systems with backlash. It was shown that this state-feedback neural network structure could give out effective solution to the output prediction of simulation based systems with hysteresis or backlash. As an important feature, the structure of the proposed network model enables a linear model could be directly derived from its architecture so that linear control theorems

could be effectively applied to check the stability of the devised SSNNs. Next, Baruch et al. (2002) used the same network architecture for real time identification and adaptive tracking control of a DC motor after showing that the identification error is stable via Lyapunov function. Later, Baruch et al. (2005) proposed a fuzzy-neural model, containing two local RNNs, for the compensation of a gear backlash in a simulated mechanical system. Consequently, the states of the RNNs were used in a fuzzy rule based adaptive control system.

Hamrouni et al. (2011) trained a RNN to show that these models could be effectively used for modeling complex and nonlinear processes in the industry when the information about a process was not available to write out exact mathematical equations that accurately describe the unknown system. By using 28 variables related with a textile process (e.g. linear density of the yarn, strength of the fiber and heat setting, etc.), the color of denim fabrics are predicted in a successful manner.

Witters and Swevers (2010) designed a NOE type neural network for modeling of a semi-active hydraulic damper in a passenger car. It was found that the devised model could predict the damper forces in the long-term using the position, velocity and acceleration of the hydraulic cylinder plus the control signal applied to the valve. As it was clearly indicated in the study, the most difficult aspect of black-box modeling was choosing the variables and determining their TDL orders in the regression vector in order to describe the system behavior accurately.

Piroddi and Spinelli (2003) proposed an iterative regressor selection procedure and applied it for identification of a magneto-rheological damper by using a polynomial based NARX model. In each iteration, a new regression variable was added to the input vector and the model was tested after a training operation whether the accuracy of the model was improved or not. Lastly, an iterative algorithm was also applied to remove some regression elements for a model performance enhancement. Therefore, the optimum regression vector elements were determined after tedious iterations.

Han et al. (2011) proposed two dynamic neural networks (DNNs) with multi-time scales, in which the first one accepts the measured process output as an input to itself but the second one replaces the process output with the state variables of the model for the identification of nonlinear system. The developed DNNs were trained using a Lyapunov synthesis method and the success of the proposed identification method was only illustrated for some simulated systems based on the assumption that all the system states were completely measurable.

Dang and Tan (2007) used radial basis function (RBF) neural networks for modeling the hysteresis behavior of a piezo-ceramic actuators for only a one step ahead prediction task in order to compensate the error of the actuator in the controller. Indeed, these dynamic RBFs were utilized for transformations of phase lag and nonlinear magnitude to approximate the real output of the piezo-ceramic actuator. Later, Deng and Tan (2008) proposed a diagonal recurrent neural network, in which modified backlash operators were used as the activation functions of the hidden layer, to model the dynamic behavior of piezo-electric actuators for long-term prediction task.

Aadaleesan et al. (2008) proposed a Weiner type models to identify highly nonlinear systems. The inputs were first passed from a Laguerre basis filters in order to capture the linear dynamic part of the system. First, some *a priori* information about the process dynamics was used to find the poles of the Laguerre filter for capturing the linear dynamic part of the system. Next, the output of the Laguerre filters' states were used as input to the wavelet network for the mapping of static nonlinearities. The performance of the model was tested on a simulation based continuous bioreactor and a real-time process data taken from a pasteurization process. It was seen that the devised models could capture the output behavior of the processes efficiently.

Gonzalez-Olvera and Tang (2007) proposed a new structure of recurrent neuro-fuzzy network for black-box identification of nonlinear systems. One recurrent and another static fuzzy inference system were interconnected to form a state-space model structure. An initialization procedure was also proposed for the parameters of the model to get out of falling into a local minimum while using a gradient-based

training method. The proposed modeling scheme was successfully applied on identification of a simulated benchmark system, which is taken from Narendra and Parthasarathy (1990), and a nonlinear laboratory system (a three-tank array system). Later, Juang and Hsieh (2010) presented a locally recurrent fuzzy neural network with support vector regression (LRFNN-SVR) for modeling of nonlinear dynamic systems. The LRFNN-SVR was constructed by using a clustering algorithm and an iterative SVR learning approach which finds the feedback gains in the recurrent model. Model was used for the prediction of a chaotic discrete-time series and the identification of a simulated nonlinear dynamic system in a successful manner. Moreover, Yilmaz and Oysal (2010) proposed fuzzy wavelet neural network (FWNN) model for the prediction and the identification of nonlinear dynamic systems. In the proposed model, the traditional *THEN* parts of fuzzy rules were replaced by wavelet basis functions. It was seen that a model with reduced network size had been achieved by using the wavelets as the activation function in the hidden layer of the neural network. The successive performance of the proposed model was illustrated with using a Box-Jenkins time series data (gas furnace data), a Mackey Glass time series data and two simulated nonlinear plants; but, for only a one-step ahead prediction task. Furthermore, Treesatayapun (2010) introduces a multi-input fuzzy rules emulated network for system identification of an unknown system to be used in an adaptive control algorithm. The already gained knowledge about the system under study is utilized to set some initial parameters of the overall network model.

Ren and Lv (2011) proposed a new self-constructing neural network, called dynamic self-optimizing neural network, for a class of extended Hammerstein systems. The hidden layer was constructed online according to the plant dynamics with applying an algorithm which includes growing and pruning steps. Therefore, the algorithm is capable of adjusting both the network structure and weights without any a priori knowledge about the system under study. But, the efficiency of the model was only demonstrated for identification of three simulated Hammerstein type systems.

Broad range of publications on ANN literature use sigmoidal neural networks where the structure of the used neurons is fixed but only the connection weights are changed to capture the assigned task. Contrary to sigmoidal networks, weight coefficients are constant but the continuous activation functions are searched in Kolomogorov neural networks (Kurkova, 1991). But, the original Kolmogorov network was very complicated since finding the appropriate activation functions, to be used in the neurons, are not easy and the numerical implementation of the overall training algorithm is not practical (Sprecher, 1996). This problem was solved by introducing linear, polynomial or integer-valued function as the internal activation function of the Kolmogorov neural network. Next, this modified Kolmogorov neural network was used for the identification of Hammerstein and Weiner type nonlinear systems in Michalkiewicz (2012). Moreover, B-spline neural networks (BSNNs), in which global sigmoid activation functions are replaced with local B-spline activation functions, were also used for the identification of nonlinear systems. The information was stored locally in BSNNs as the RBFs maps the input-output data. Lightbody et al. (1997) used BSNN for modeling of a chemical plant (pH neutralization plant). Recently, Coelho and Pessoa (2009) used BSNN for one-step ahead forecasting of a gas combustion process and a ball-and-tube system. Moreover, a new complex-valued B-spline neural network was proposed by Hong and Chen (2011) for modeling of general complex-valued systems. The model was basis on the tensor product from the two univariate B-spline neural networks using the real and imaginary parts of the system input.

Some studies in the literature about the prediction of nonlinear time series and dynamic systems are presented in Table 2.1. It is observed that the system identification is mostly realized for one step or multi-steps ahead prediction tasks. The prediction performances of the black-box models were found to be inadequate in long time intervals as the system under study was highly nonlinear and complex. On the other hand, there could be some nonlinear models or observes which might be used as a soft sensor in the industry. Therefore, it is believed that this thesis, which concentrates on the accurate prediction of some highly nonlinear mechanical system's outputs for the possibility of eliminating costly sensors, is in line with the research efforts in the current state of the art.

Table 2.1 Prediction studies on time series and dynamic system modeling.

Research	Type of Model	Application Domain	Prediction
Maria et al., 2008.	NARX, Elman, Time Delay NN	Chaotic laser time series	60 steps
Zemouri at al., 2010.	Recurrent RBF, NARX	Mackey Glass time series	1 step
Zemouri et al., 2010.	Recurrent RBF+ NARX	Lorenz time series	10 steps
Ardalani et al., 2010.	ELMAN + NARX	Lorenz time series	1 step
Watton and Xue, 1997.	Biased-ARMAX (BARMAX)	Hydraulic system	Long-term
He and Sepehri, 1999.	NARMAX	Hydraulic system	15 steps
Parlos et al., 2000.	NARX	U Tube steam generator	Multi-steps
Sorjamaa et al., 2007.	Support vector machines	Poland Electricity Load	Long-term
Tufa et al., 2010.	Generalized orthonormal filter	A weakly damped linear system	1 to 5 steps
Chan and Lin, 2000.	Lateral Delay Neural Network (LDNN)	Time series prediction and dynamic modeling	1 step
Liberati et al., 2004.	Feed-forward neural network	Shock Absorber	1 step
Patel et al., 2010.	NARX	Hydraulic Suspension Dampers	1 step
Aquirre et al., 2005.	Hammerstein and Weiner Model	Electrical Heater	Long-term
Piroddi and Spinelli, 2003.	polynomial NARX	Dynamics of the arch dam	Long-term
Chen et al., 2008.	NARX	Direct injected Diesel engine	Long-term
Li, 1995.	RNN	Screw Compressor	Long-term
Barbounis and Theocharis, 2007.	RNN	Wind speed forecasting	Multi-steps
Coelho and Pessoa, 2009.	B-spline neural network	Ball-and-tube system / Gas combustion process	1 step
Wei et al., 2007	RBF network	Magnetosphere system	1 step
Mustafaraj et al., 2011	NARX	Thermal behavior of an open office	Multi-steps

2.3 Importance of ANN Models in Advanced Controller Design

Modeling the dynamic behavior of nonlinear systems is the most critical aspect in developing advanced algorithms for model predictive control (MPC) (Hunt et al., 1992), model reference adaptive control (MRAC) (Narendra and Parthasarathy, 1990) and adaptive inverse control (AIC) (Widrow and Walach, 1996). In MPC, the future responses of the actual system should be predicted in some way since these values are highly needed while calculating the optimum manipulation signal values as shown in Fig 2.1. Therefore, the control performance (e.g. command tracking, disturbance rejection and robustness, etc.) is often times directly related to that of the modeling and system identification (Atuonwu et al., 2010; Lawrynczuk, 2010).

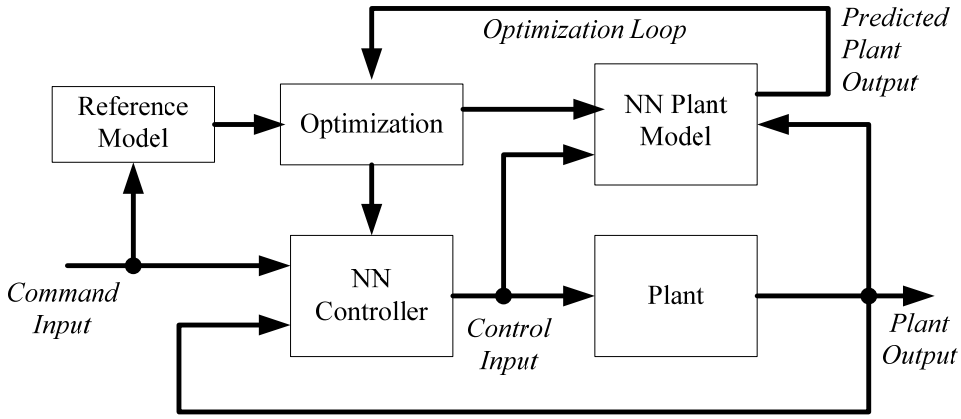

Fig 2.1 Model predictive control.

In MRAC, a NN plant is identified first with the recorded plant measurements, and then, a NN controller, whose parameters are randomly initialized, is located in front of this plant model as illustrated in Fig. 2.2. Later, the NN controller is trained based on the difference between the plant output and that of the reference model. But, this error value could not be back-propagated through the actual plant in the training session of the NN controller so that one will highly need a NN plant model for this task.

In AIC, the parameters of the controller, which is also a neural network (NN), are adaptively updated based on the difference between the output of a reference model and that of the plant. As could be seen from Fig. 2.3, the difference between the output of the NN plant model and the measured response of the actual plant is passed through the inverse plant model in order to generate the noise and/or disturbance at the plant output. Next, this signal is subtracted from the manipulation signal for cancelling the sensor noise and disturbance present in the plant.

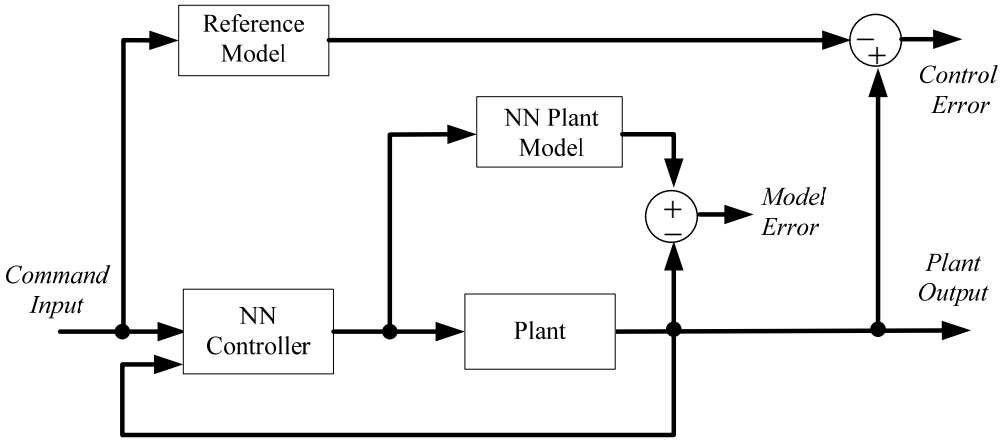

Fig 2.2 Model reference adaptive control.

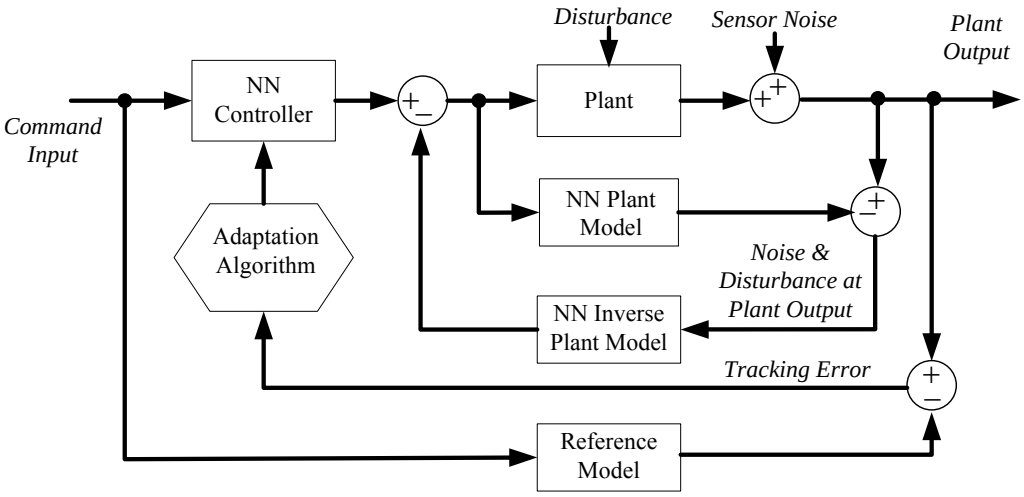

Fig 2.3 Adaptive inverse control.

Consequently, modeling is always the first step for the model-based control schemes. In these controller strategies, the model of the process is directly used in the implementation of the control structure; therefore, the quality of the control is highly related to the accuracy of the plant models.

2.4 Hardware Implementations of ANNs in parallel processors

It is well known that there are 100 billion neurons, which are highly connected to each other and work in a parallel way, in a human brain. Therefore, the greatest potential of ANNs remains in high-speed parallel processors. However, a tremendous part of the devised ANNs are utilized on software platforms in a serial manner. No doubt, if ANNs are implemented on hardware platforms with satisfying the full parallelism, their capabilities will be tested on various tasks and compared with biological brains. In order to implement fully parallel neural network architectures, all the parallelism of the ANNs such as training parallelism, layer parallelism and node parallelism must be taken into consideration to determine the most suitable hardware structure. Therefore, parallel processors such as field-programmable gate arrays, field-programmable analog arrays and graphic processing units are investigated in the current state of the art.

2.4.1 Field-programmable Gate Arrays

Parallelism of the neurons in a network model could be achieved well by field-programmable gate arrays (FPGAs), since there are a lot of cells, operating in parallel, in a generic FPGA in order to implement various digital circuits. Reconfigurable FPGAs provide an effective programmable resource to satisfy the parallelism of ANNs; but, a sigmoid type activation function could not be easily implemented by a digital circuit (Omondi and Rajapakse, 2006). A classical solution to this problem is the usage of lookup-tables (LUTs). Since a LUT is required for every neuron of a neural network, this method consumes much of the limited gate resources (Krips et al., 2002). Another solution proposed by Kwan (1992) is to use a second-order nonlinear function instead of the sigmoid function.

The other fundamental problem is the high cost of implementing a multiplication operation in a digital logic which consumes much of the resources in the FPGA. Unfortunately, ANNs needs a large number of multipliers at the same instant in order to satisfy the full parallelism. Bade and Hutchings (1994) proposed using a stochastic method to reduce the circuitry necessary for multiplication. In this technique, bits are serially sequenced and their values are probabilistically set (0 or 1) according to the numerical value of a variable. Therefore, the value of weights and neuron states in a network model are represented by bit streams. Next, basic logic gates are used to implement a multiplication operation on the randomly pulsed and sequenced inputs.

Hikawa (2003) devised and proposed a new digital circuit, called direct digital frequency synthesizer, for the multiplication operation in a neural network. In the proposed technique, the accuracy of the neuron output is improved via adding a voting circuit (a nonlinear adder) into the digital circuit and the performance of the activation function is increased by adding a pulse multiplier to the nonlinear adder. Moreover, Hikawa (1999) proposed an on-chip learning using a modified back-propagation algorithm that does not need any multiplication operation. But this modified learning is not easy to implement and requires some additional digital logic circuits (e.g. linear feedback shift register) to prevent the gradient of the activation function being zero in the training phase. On the contrary, Maeda and Tada (2003) adopt a learning rule named simultaneous perturbation that requires only twice forward operations which is more convenient for hardware implementations of ANNs. In this simple method, the gradient of the cost function is approximated by using only the two successive error values.

On the other hand, spiking neural networks are becoming an important research area and emerging as a new generation of neural networks due to the similarity of the biological neurons (Zhuang et al., 2007; Schrauwen et al., 2008; Nuno-Maganda et al., 2009). In this architecture, the information among neurons is transferred via pulses or spikes. Indeed, the information is carried out by the number and the timing of the pulses. Therefore, FPGAs are suitable for that architecture because the

generation of pipelined pulses is well suited to the digital circuits and the pulse transitions could be easily captured by the intrinsic high speed of FPGAs. The learning algorithm for spiking models is generally based on evolutionary strategies. On the other hand, Bohte et al. (2002) developed an error back-propagation algorithm to be used in spiking neural networks.

In the current literature, it is possible to verify that several implementation problems have already been resolved in the FPGA context. Nevertheless, the solutions that were found do not allow the direct usage of the ANN models (which had been designed in software platforms) on the FPGAs. Filling this gap, between the software and the hardware platforms, will be an important issue in the hardware implementation field of the ANNs.

2.4.2 Field-programmable Analog Arrays

Field-programmable analog arrays (FPAAs) are emerged as parallel processors for analog version of its digital partner FPGAs. The biggest advantage of using FPAAs is that they don't need any data converter while interacting with the outside. Therefore, delay, noise and quantization error problems are all eliminated in a real time application. Dong et al. (2006) managed to design a neural network model on a FPAA but having neurons with affine activation functions. Moreover, Maher et al. (2006) developed a genetic algorithm for the evolution of a network model on a FPAA. Later, Maeda et al. (2009) realized the analog implementations of NNs on FPAAs where neurons are modeled with integrate and fire type spiking.

2.4.3 Graphic Processing Units

Graphic processing units (GPUs) are getting more popular since they have a huge amount of processors satisfying a massive parallelism with using floating point arithmetic. In fact, GPUs have many core processors (i.e. hundreds of parallel processing elements) which could perform more than 10^{12} floating point operations per second (Che et al., 2008). Therefore, GPUs are well suited to satisfy the full parallelism of the ANNs. On the other hand, they are also used for problem solving

in different fields such as finite element analysis and fluid mechanics. GPUs could be programmed with a C extension software language called compute unified device architecture (CUDA) (Januszewski and Kostur, 2010).

CUDA has been already utilized in neural networks applications. For instance, multiplication operations (in floating point) of a neural network are implemented by matrices in Jang et al. (2008). Therefore, a huge amount of time is saved by this matrix multiplication. Recently, Cernansky (2009) use CUDA for linear algebra operations of an extended Kalman filter in order to train a RNN. Experiments showed that this achieves a great amount of time saving while training (deep) larger ANNs. Moreover, Nageswaran et al. (2009) devised spiking neural networks using a CUDA platform in which a great conformity was satisfied with biological neurons. Consequently, GPUs make the hardware implementations of ANNs very suitable since they have extreme number of threads running concurrently and specialized functional units that could perform trigonometric and arithmetic functions at the same instant. But, the main problem of GPUs is that although one could perform complex operations very fast utilizing the full parallelism of the hardware, the data transfer between the GPU and outer world (giving the inputs and then retrieving the outputs) could only be realized in a serial manner which brings a bottleneck for the processing speed of the overall computations.

2.5 Generalization of Artificial Neural Networks

ANNs would be more efficient if any generalization (or optimization) methods are applied after a training operation. Therefore, a detailed literature survey is also conducted about generalizations of ANNs in this section.

Using too many parameters (weight values), ANN does not capture the assigned task (poor generalization) and only memorizes the training scenario in the learning operation (over fitting). Therefore, a network model should not only learn the training scenario but generalize the given task well. As indicated by Baum and Haussler (1989), ANNs satisfy better generalization performance with minimal free parameters. Moreover, one can easily interpret a small network and can extract

simple arithmetic rules from the structure of the network (Ni and Song, 2006). Furthermore, less hardware resources are used for the implementation of a small network. On the other hand, using a small network structure at the beginning make the network easily trapped into a local minimum rather than a global optimum point.

Three main approaches have been proposed to increase the generalization performance of a network model (Xu and Ho, 2006). The first one is the *pruning* algorithm which trims the unnecessary part of a huge amount of the network until a reasonable solution is found (Reed 1993). The second approach is the constructive algorithm in which a network having small parameters is taken first, and then, new parameters (it could be a neuron or a weight) are added until an acceptable generalization performance is satisfied (Fahlman and Lebiere, 1990; Kwok and Yeung, 1997; Tenorio and Lee, 1990). In the third approach which is called regularization, the objective function to be minimized is modified by adding a penalty term on it (Girosi et al., 1995; Ishikawa, 1996; Schittenkopf et al., 1997). The implementation of the third approach is simple. But, the inserted penalty term may cause a problem; for instance, creating additional local minima on the weight domain (Engelbrecht, 2001). Of the three well-known generalization methods given above, the most used one is the pruning technique since starting the training session with large number of parameters enables the network to learn the training scenario almost all. Next, excessive parameters are removed from the network in order to enhance the generalization performance of the network.

As explained before, the main attitude of pruning is to decrease the redundant parameters from the network. First, an importance factor, correlated with the efficacy of a neuron or a weight, is generally calculated for each of the network parameters in a generic pruning operation. Next, sorting the importance factor of the parameters, the specified parameter which has the least importance factor is deleted from the network architecture. No doubt, a simple method is sorting the magnitude of weights as an importance factor (Finnoff et al., 1993). In this method, the smallest weight in the network is removed and then the network is retrained to

compensate the effect of the deleted weight until, recursively. Another very simple method proposed by Mozer and Smolensky (1989) is to define an importance factor for each neuron from the variation of the network output error when an arbitrary neuron is deleted. Similarly, Karnin (1990) calculated an importance factor for the weights of a network by performing a sensitivity analysis on the error function. Moreover, Sietsma and Dow (1991) proposed a smallest variance pruning (SVP) method in which the hidden neuron having the smallest variance in the output of its activation function is removed.

More advanced pruning techniques are the optimal brain damage (OBD) (Cun et al., 1990) and optimal brain surgeon (OBS) (Hassibi and Stork, 1992; Hassibi et al., 1993) methods. In these methods, importance factor for the weights, called saliency term, is calculated with using the inverse of the second derivative of the error function with respect to the each weight (inverse Hessian information). In OBD, Hessian matrix is assumed to be diagonal in order to decrease the computation burden of taking the inverse of a matrix in the calculations. Furthermore, no corrections are made on the remaining weights after removal of a weight having the smallest saliency term. On the other hand, OBS method utilizes the full Hessian information in the calculations but the remaining weights are automatically updated to minimize the error function without a retraining operation. Although the OBS method could effectively eliminate the unnecessary weights one by one, the overall pruning process is very time-consuming and difficult especially for large networks as the dimension of the Hessian matrix will be equal to the number of weights used in the network. Therefore, the OBS method is not very efficient for large scale neural networks. As the efficiency can be improved by deleting a neuron rather than removing a weight, a unit-OBS method was developed by Stahlberger and Riedmiller (1996) in which redundant neurons were pruned directly. Therefore, the overall computation time is considerably reduced so that it is suitable for large scale problems. But, the performance of the neural network could decay very much due the removal of an entire neuron which may accommodate an important weight in it.

Next, the advantages of both the unit-OBS and OBS methods are combined in the multi weight-OBS (mw-OBS) pruning method (Han et al., 2006). The mw-OBS method could delete multiple weights from different neurons according to their contribution for the network performance. Moreover, a fast unit pruning algorithm is proposed solving the time and complexity problems of the OBS method (Qiao et al., 2008). In the proposed algorithm, Hessian matrix is correlated with each hidden unit instead of each hidden weights in order to reduce the dimension of the Hessian matrix so that the pruning time is effectively shortened. Moreover, Xu and Ho (2006) proposed a pruning algorithm in which the outputs of the neurons are investigated whether there are some highly dependent neurons to each other. Next, the dependent neurons (if exist) (and also their corresponding weights) are deleted but excluding one of them. Later, the remaining but independent neurons are retrained to keep up the network performance almost same.

In a recent publication (Pukrittayakameei et al., 2009), both the error and gradient of the error are utilized in the cost (or objective) function. When this cost function is optimized in a training session, the network outputs are forced to pass through the target data points with their exact slope values. Therefore, over fitting problems are avoided with this modified objective function.

Moreover, many researchers have used genetic algorithms for a stochastic search of the weight values (Stepniewski and Keane, 1997). Following that, Siebel et al. (2009) developed a genetic algorithm in which excessive network's parameters are deleted so that complex analytical calculations are all avoided in this pruning technique. It is important to note that evolutionary methods can be easily implemented but they are difficult to analyze theoretically.

2.6 Modularity in Artificial Neural Networks

It is well known that some training problems such as inaccuracy, divergence, instability and long training phases are frequently happened when a complex dynamic system is to be modeled via traditional NN development paradigms, which exclusively use black-box approaches. In traditional approach, the training data set

is the only information that an ANN must form its own representation while identifying a system in a learning operation. But, recent studies have shown that the modularity is a key for the solution of the above-mentioned training problems. In a modular neural network design, some small networks are trained individually to capture the characteristics of the sub-elements in the whole system. No doubt, simple networks could be easily designed and trained on the small domain of the sub-element without any stability and convergence problem. Therefore, the probability of getting into a local minima point, training time and computational cost are all decreased. Model complexity reduction, robustness, high learning capacity, computational efficiency and knowledge integration are the most attractive factors for the design of modular neural networks (Azaam, 2000). Divide and conquer approach is used in the concept of modularity; but, how a modular network structure could be obtained is not given in a systematic way, yet.

Knowledge about the physical system, input/output characteristics of the system and the relationship between the sub-elements of the entire system could be used to modularize the overall system. A good decomposition for a modular design could be realized by input-output domain knowledge about the system as indicated by Tseng et al (2009). Decomposition task could be done before the learning operation by the help of already gained information about the system or it could be realized in the progress of learning (Lu and Ito, 1999). The last important part of the modularization is the aggregation of the smaller networks to form the main model. Using a weighted average of outputs produced by small networks is one of the most used aggregation method (Tseng et al., 1995). Furthermore, Chi et al. (1997) proposed an adaptive aggregation method in which the connection gains of the modular networks are continuously updated since the sub-elements of the process could be interconnected to each other in a nonlinear way. In the literature, there are a lot of modular neural network architectures which are diversifying with their decomposition and aggregation methodologies.

In *ensemble network* (Tumer and Ghosh, 1996), separate networks are trained to learn the same task. In fact, distinct networks are individually trained with using randomly initialized weight values, changing the number of neurons (or layers) and

varying the training data (e.g. re-sampling, cross-validation and injecting randomness, etc.) so that the networks will converge to different local minima while making them uncorrelated to each other. Next, the outputs of individual networks are combined by some averaging techniques as could be seen from Fig. 2.4. But, for an effective aggregation, nonlinear combination methods such as rank based information (Al-Ghoneim and Kumar, 1995), Dempster-Shafer belief algorithm (Rogova, 1994), voting schemes (Battiti and Colla, 1994) and probability based combination methods (Jacobs, 1995) are used. Consequently, the main intention of the ensemble network is to obtain a modular model which could make a more accurate estimate for a given task rather than using only a one network model for the same task.

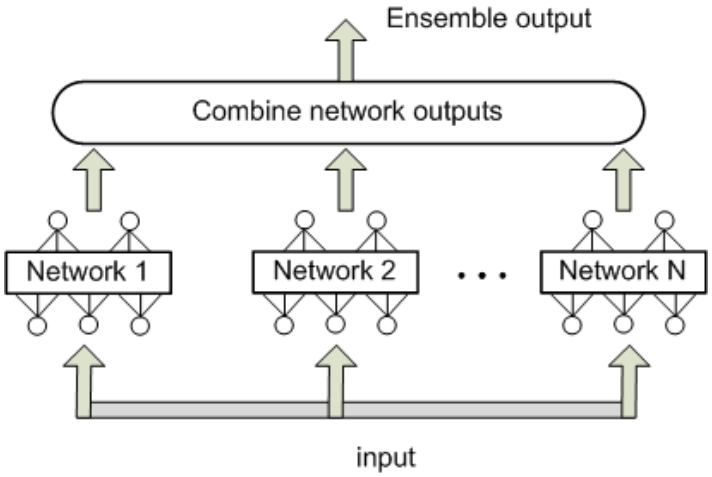

Fig 2.4 Ensemble of neural networks.

In *decoupled* modularity approach, input is first categorized into groups based on similarity by using an adaptive resonance theory (ART). Note that ART network has a special architecture which enables the network to remember the previously captured information while learning new things (*stability-plasticity* dilemma) (Bartfai, 1994). Later, each group is further trained with supervised modules in a parallel form without any interaction between them. The absolute maximum of the

module outputs is chosen as the final output of the overall network model as could be seen from Fig. 2.5.

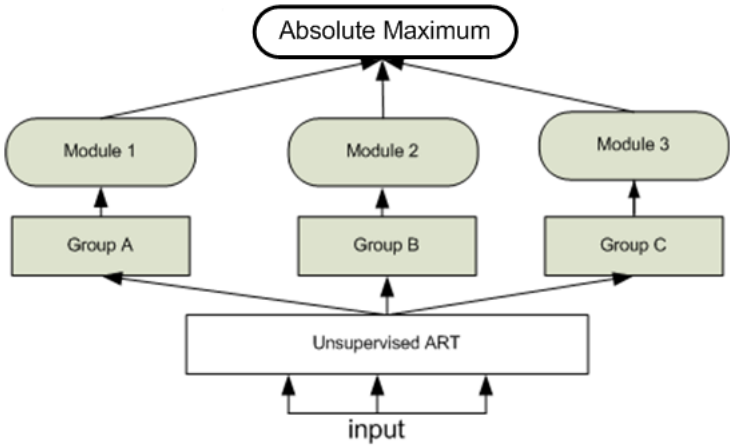

Fig 2.5 Decoupled modularity approach.

The architecture of the *other output* modularity approach resembles very much to the structure of the decoupled approach. But, the individual modules have an extra binary output in this topology as could be seen from Fig. 2.6. These binary outputs are utilized in the decision strategy among the parallel modules instead of using the absolute maximum decision strategy (Auda and Kamel, 1998).

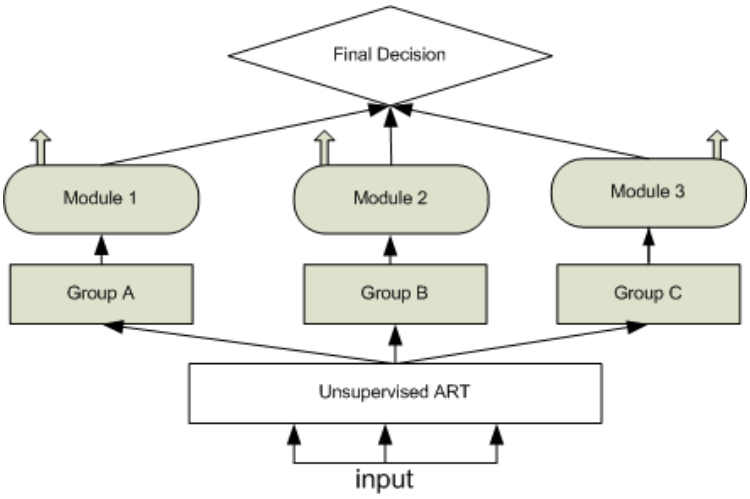

Fig 2.6 Other output modularity approach.

In *hierarchical networks,* a supervised back-propagation module is used at the bottom level in order to perform a coarse partitioning of the input space, and then, a fine-tune learning is realized at the higher level by separate and parallel modules as shown in Fig. 2.7 (Corwin et al., 1994).

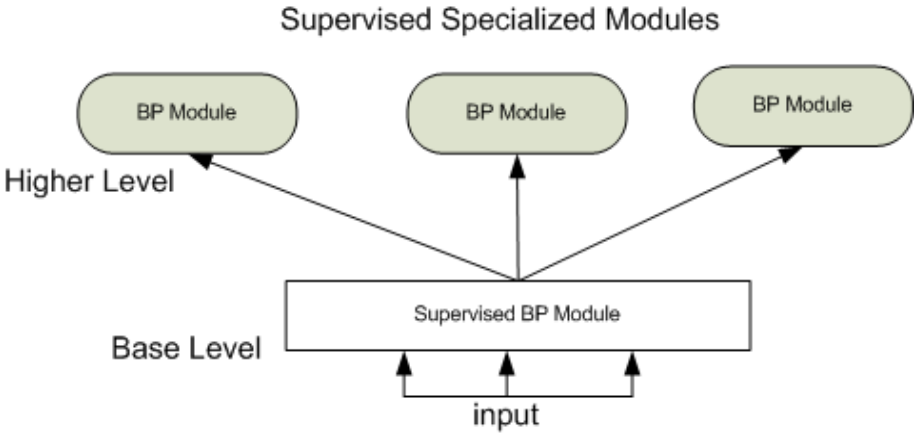

Fig 2.7 Hierarchical networks.

Mixture of experts composed of some local experts and gating networks in a modular and hierarchical way. Each expert is attached a probability for different regions of the input space and gating networks are used to determine the value of the connection gains of the individual modules at the junction points in order to produce the correct output at the end (Jordan and Jacobs, 1994). Therefore, this architecture seems to apply a divide and conquer approach for the input domain as shown in Fig. 2.8. Expectation maximization algorithm is used for the training of hierarchical mixture of experts.

In *merge and glue networks* (Waibel 1989), the task is first decomposed and assigned to individual network models according to the knowledge available about the system. Next, the decomposed tasks are learned separately by these small networks via supervised learning algorithms. Finally, a global network is formed by merging the individual networks without changing their architecture and weight values. Furthermore, some additional network models, called *glue,* could be added

to correct the erroneous behavior of the global network as the overall architecture of this modular network model is presented in Fig. 2.9.

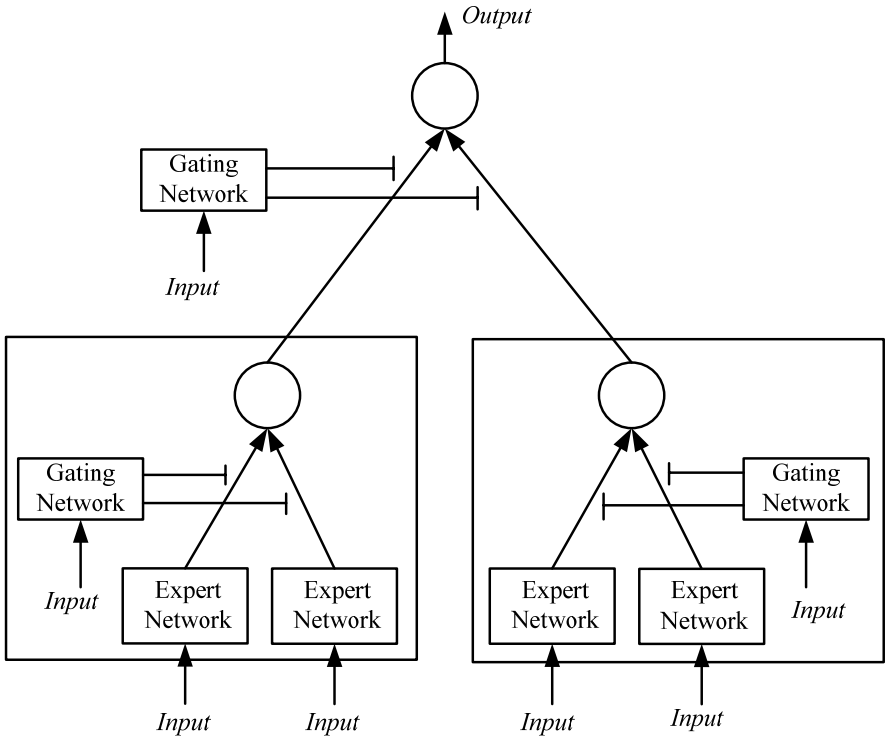

Fig 2.8 Mixture of experts.

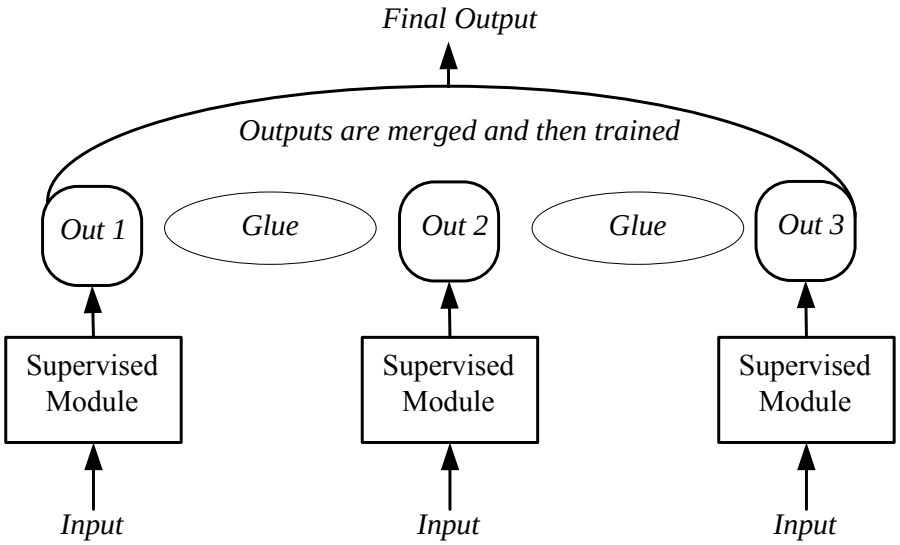

Fig 2.9 Merge and glue network.

Hence a nonlinear dynamic system can be considered as a multi-variable surface, a number of modules could be used to capture the behavior of the system in different operating space. Johansen and Foss (1995; 1997) proposed using a combination of local model networks, which were identified over the different operating regimes of the workspace, for the modeling and control of nonlinear systems. But, it was seen that this type of network could model the system accurately only for the points where the local models had been specialized before.

Surveying the recent studies in the literature, modular networks are constantly emerging; for example, an algorithm for incrementally growing ANNs is developed to control the body-plan of a robot as shown by Macleod et al. (2009). In that study, the network is expanded by adding new sub-networks or modules and trained by evolutionary algorithm. Every time a new network is added to the existed main network, only the latest added network (or module) is trained. Therefore, complex and large networks could occur with a high performance since the search space will be so small in each of the iterations. Lima et al. (2007) proposed a novel model, named as mixture of support vector machine experts (MSVME), by combining the complementary properties of both support vector machines (SVMs) and mixture of expert (ME) models for the identification of nonlinear dynamic systems. It is seen that hybridization of SVM and ME could accurately predict the output of some simulation based nonlinear dynamic systems, given in Narendra and Parthasarathy (1990). Moreover, Tokunaga et al. (2009) used modular networks for the prediction of weather dynamics. For this task, small network models (modules) are arrayed for the construction of a self-organizing feature map (SOM). In this study, it was shown that the possibility of trapping into a local minimum point had been highly diminished as more modules were utilized in the SOM. Furthermore, Wang et al. (2010) develop a new sequential Bayesian learning (SBL) which will be used for the aggregation of modular neural networks. Some benchmark functions such as Mexican hat, Friedman and Gabor were used to show the efficiency of the proposed unification technique.

Looking to the literature, one can see that modular neural networks are effectively used in target recognition (Wang et al., 1998), pattern classification (Lu and Ito, 1999), texture processing (Van Hulle and Tollenacre, 1993), image compression (Watanabe and Mori, 2001), language processing (Sibte and Abidi, 1996), inverse kinematics model learning (Oyama et al., 2001), controller design for a flexible manipulator (Sharma et al., 2003), complex economic time series forecasting (Melin et al., 2007), real-time video coding (Ramirex-Agundis et al., 2008), medical diagnosis (Pan and Sensen, 2005) and fault diagnosis (Kim and Park, 1993). But, it is found that their application on nonlinear system modeling and system identification is very limited especially for the long-term prediction task.

Haykin and Li (1995) proposed a pipelined recurrent neural network (PRNN) as a nonlinear adaptive predictor for nonlinear time series. Later, this modular model, which consists of a number of computationally efficient RNNs, has been widely used for speech processing (Baltersee and Chambers, 1998; Goh and Mandic, 2005; Stavrakoudis and Theocharis, 2007) instead of nonlinear system identification. Next, Zhao and Zhang (2009) proposed another version of this modular network, called pipelined functional link artificial recurrent neural network (PFRNN), to model nonlinear dynamic systems by combining a PRNN module with an ANN in which the dimensionality of the input signal is increased by using a set of linearly independent functions such as trigonometric and Chebyshev orthogonal polynomials. The effectiveness of the model was tested with simulation based benchmark systems, given in Narendra and Parthasarathy (1990), but only for a one step ahead prediction task.

Kiong et al. (2003) proposed a constructivism procedure for identification of nonlinear dynamic systems via growing multi-experts network (GMN). A redundant removal algorithm and a growing neural gas algorithm were used in the proposed methodology to find the optimal network structure. In GMN, local expert models were used to be skilled on the decomposed region of the problem, and then, the combination of the expert models determined the output of the network. The proposed algorithm was only applied for a set of simulation based discrete-time

nonlinear dynamical systems, adopted from Narendra and Parthasarathy (1990) again.

Wong and Worden (2007) constructed an ensemble model by merging an ANN with the exact mathematical model of a friction process (Maxwell slip model) that frequently seen in mechanical contacts. It was seen that the ensemble model could predict the dynamical behavior accurately.

Ge et al. (2008) suggested a new model called particle swarm optimization based Elman neural network to be used in identification and control of nonlinear systems. Structure developing and degenerating operations are realized via evolutionary computation technique. Units of the swarm change their position over time in the huge work space and search a possible location which could be the solution of the problem. It was seen that the proposed dynamic identifier could accurately approximate the nonlinear behavior of an ultrasonic motor.

Tellez et al. (2010) presented an identification and control methodology for nonlinear systems using a modularity approach. In the proposed methodology, the overall system is seen as a group of sub-systems which are connected in any way. Next, a recurrent high order neural network (RHONN) is trained for each of the subsystems. Once a RHONN identifier is developed for one step ahead prediction task, a sliding mode controller is designed to guarantee the robustness of the each subsystem. Extended Kalman filter is used to train the RHONNs; but, assuming that all the states of the system are measurable. The performance of the methodology was tested on a two DOF planar robot where a unique identifier and controller had been designed for each link of a robot for an accurate trajectory tracking.

Hametner and Jacubek (2011) proposed using a priori information about a process to reduce the black-box model complexity. The splitting of the training data into smaller pieces allows the local interpretation of the model in small operating regimes. Local model networks (LMN) were used to capture the behavior of the local pieces of the input-output mapping process. Parameter estimations of the

LMNs were realized by using a developed constrained generalized total least squares (CGTLS) algorithm with equality constraints. Expectation maximization algorithm was used for the partitioning process of the training data. Prior knowledge about a process such as the differential behavior of the system and the tapped delay order of the input signals were used to reduce the degrees of freedom of the parameters and the complexity of the split optimization problem. The efficiency of the LMN with equality-CGTLS model was demonstrated on identification of a supercharged natural gas engine and estimation of a tire-road friction.

Banakar and Azeem (2012) used a combination of a tangent sigmoid and a wavelet function as an activation function of neurons in a recurrent neural network for predicting the nonlinear behavior of dynamic systems. Indeed, the product of the different type activation functions and a delay element, which is used to feedback the output of the activation functions to each other, determine the structure of the hidden layer neurons in the proposed network model. Therefore, the presented study proposes a network using a mixture of local experts not in the network architecture but in the neuron structure. The output of the wavelet neuron acts as gate to the output of sigmoidal neuron. Therefore, the localize property of a wavelet neuron (capturing the sharp temporal changes in system dynamics) is merged with the functional capability of a sigmoidal neuron (capturing low frequency response of the system dynamics). But the devised network model is only tested for one step ahead prediction task on a simulation based systems which are a linear regression with nonlinear input model and a Box-and-Jenkins gas furnace data.

It is seen that there are lots of different RNN architectures in the literature and which one is the most appropriate for a system to be modeled is another challenging task. Although RNNs are capable of identifying a nonlinear system accurately, determining the number of layers and the number of neurons in the hidden layers, and also, the layout of the connections between the layers is unavailable in the current literature.

Seidl (1996) proposed an original idea called structured neural networks (SNNs) as an application-driven methodology and it has been successfully applied to process identification/modeling (Artmeyer et al., 1995), motion control (Seidl et al., 1993; Seidl et al., 1992) and power electronics (Seidl and Lorenz, 1993). In this methodology, the system under study is first divided into its sub-systems with the help of *a priori* knowledge on the process. Next, some small networks are individually trained to learn the characteristics of the sub-systems. Later, all the network modules are combined to construct a SNN model for capturing the exact dynamic behavior of the nonlinear system at hand.

Dolen (2000) designed a SNN to estimate the milling forces for an ideal machining in CNC machine tools and Garcia et al. (2007) developed a SNN for sensorless control of AC machines. Furthermore, the signal flow chart of a multi stand rolling system is matched with the architecture of a SNN by Hintz et al. (2000). Lastly, Endisch et al. (2009) designed another SNN to identify a nonlinear two-mass system with friction and backlash. Again, the designed network is of the same structure as the nonlinear system since it is assumed that matching the structural knowledge (found by engineering approach) of the nonlinear system with the network architecture, the SNN will emulate the exact behavior of the plant.

It is seen that the SNNs only mimic the known processes (not giving any additional information about the processes) and their network architectures are not generic (only Σ- neurons with sigmoidal activation functions and some delay elements should be used in a generic ANN). Nonstandard activation functions (exponential, logarithmic, hyperbolic, trigonometric, Boolean functions etc.) and neurons with multiply ability (ΣΠ-neurons) are used and amorphous networks are developed in the existed SNN methodology. On the other hand, a network model developed via SNN methodology should be generic in order to be designed for similar physical plants later. Therefore, Dolen and Lorenz (2002) introduced some general methodologies for neural network programming so that a conversion from an amorphous network model to a generic network model is now available.

2.7 Research Opportunity

In the preceding sections, the state-of-the-art relevant to this research has been presented in detail. It is observed that black-box models are frequently used for modeling and identification of various dynamic systems. However, long-term prediction could not be realized efficiently with such models in the current literature. On the other hand, despite the apparent success of the SNN methodology, this is purely an application driven technique. Furthermore, it lacks the ability to accommodate (unknown) unaccounted system dynamics that may be present in the actual system under study. Unfortunately, the implementation of the SNN models in the current literature constantly need the exact mathematical descriptions of the processes under study so that the resulting neural network models do not provide any further information about the physical models at hand.

To summarize, the aim of this thesis is to develop a design methodology for SNNs in which nonlinear dynamic systems will be modeled exactly via utilizing the sketchy guidance of *a priori* information on the investigated systems. Therefore, this research will seek to design accurate predictors or estimators for some nonlinear mechanical systems via using ANNs and utilizing the already existed (or gained) knowledge about the dynamic systems under investigation.

CHAPTER 3

STRUCTURED NEURAL NETWORK METHODOLOGY

3.1 Introduction

In Chapter 2, it is seen that identification, modeling and control of nonlinear systems are generally realized with ANNs. However, it is known that training a black-box network models which have enormous number of weights (free parameters) is not an easy task. This issue is categorized as non-polynomial-time (NP-complete) problem (Blum and Rivest, 1992) since the time required for this training task exponentially increases with the size of the network parameters and the length of the training data in correlation. On the other hand, Baum (1991) indicated that using error back-propagation algorithms while training networks for large-size problems were not effective. Therefore, some training problems such as instability and divergence frequently emerge while developing a conventional NN (black-box model) for the identification/modeling of complex systems in mechanical engineering domain. Since many mechanical systems comprised of hard nonlinearities such as dead-zone, backlash, friction and hysteresis, which increases the size and complexity of the problem to be solved.

On the other hand, SNN design methodology is utilized to handle these training problems. In this methodology, *a priori* knowledge about the system under study is especially used for not only the selection of a proper structure but also the decomposition of the system into its subsystems. Furthermore, only generic neural network topologies such as FNN and RNN architectures (excluding Hopfield,

Kohonen and associated memory networks) are utilized and supervised learning algorithms are taken into consideration while designing NN modules for the investigated systems in this modeling technique. Therefore, the finalized NN models will be a collection of only generic network architectures.

After this brief introduction, modeling nonlinear dynamic systems using black-box structures is given in a detailed manner in Section 3.2. A general methodology of designing SNNs is proposed in Section 3.3. Following that, some standard library networks are developed in Section 3.4 as they frequently needed at the unification stage of the proposed SNN methodology. Furthermore, well-known standard network architectures from the current literature are given in Section 3.5 for a proper model selection procedure. Next, an entropy based pruning algorithm is developed in Section 3.6 for the parameter reduction of the trained ANNs. Finally, Section 3.7 summarizes the key points of this chapter.

3.2 Black-box Modeling

Black-box approach, which employs weak assumptions about the process under investigation, follows a systematic procedure as illustrated in Fig. 3.1. In this scheme, one should perform the experiments involving the choice of excitation signal, selection of sampling period, measurement (recording) of the input-output data sets and pre-processing of the data. The design of an excitation signal is very important for gathering the identification data. Excitation signal has to be chosen with extreme care in order to capture relevant (and statistically significant) data points that cover all the operating regimes of interest. On the other hand, to excite the dynamic system around its equilibrium points, the excitation signal must have low frequency components. Moreover, the full-range of the input signal must also be applied to the system in order to maximize the signal-to-noise ratio (Nelles, 2001).

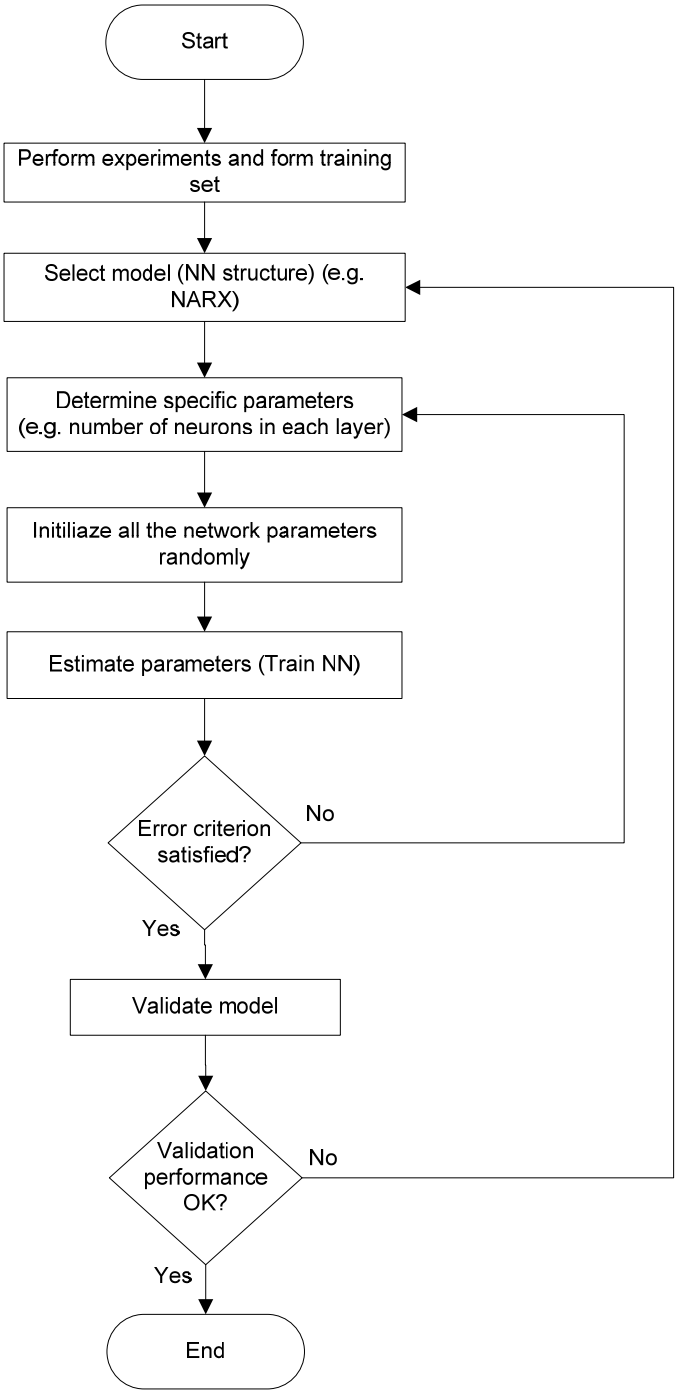

Fig 3.1 Flow chart of black-box modeling process.

To that end, a pseudo-random multi-level signal (PRMS), chirp-signal, band-limited white noise, and all their combinations could be utilized to create an input signal for exciting the system at the frequencies of interest (Xue-miao et al., 2010). The

selection of a suitable sampling period is another important factor that affects the identification performance. A short sampling period should be generally preferred to cover more range. On the other hand, if the sampling frequency is chosen very high, the successive measurements in the recorded data would be nearly same ($u(k) \approx u(k-1) \approx u(k-2)$). In that case, the order of the tapped-delay-line (TDL) should be increased to create an uncorrelated (or more informative) input vector space for the network model since the TDL of input(s) are especially utilized in the regression vector in order to create an external dynamic input space, which should capture the variations in the related input variables. However, another problem, called curse of dimensionality, will occur, if one increases the dimensions of the regression space while trying to make the inputs uncorrelated. In machine learning, the computation needed for training an ANN grows exponentially as the dimensionality of the input space is enlarged. On the other hand, a principal component analysis could be used in order to create uncorrelated input elements via transforming some input elements into axes of another dimensionality space instead of increasing the order of the TDL of input(s). For instance, $u(k), \nabla u(k), \nabla^2 u(k)$ (where ∇ is the difference operator) could be used instead of using $u(k), u(k-1), u(k-2)$ in the elements of the regression vector. However, it is important to note that the noise effects will exaggerate as the order of the differentiation operation is increased. Furthermore, one needs to pay a careful attention to the length of a training data since the training session (including computational and storage/memory costs) for RNNs grows exponentially as the training data length step up dramatically with a higher sampling frequency. As indicated by Shannon sampling theorem, it is advisable to choose the sampling frequency greater than (at least) twice the maximum frequency of the interested variables. After recording the signals at a proper sampling rate, the captured data should be preprocessed. That is, some pre-processing operations could be applied to remove the noise, outliers, delays, offsets and drifts (due to sensors or cross-talks between the channels of the data acquisition card) from the raw-data. Furthermore, normalization of the training data is highly recommended. In fact, the tangent sigmoid activation functions used in ANNs are centered around 0 and their outputs varied between -1 and 1. Scaling the input variables across the working range of the activation functions has an effect on the training performance since the activation

functions will be more sensitive to the all elements of the input data at the beginning of the training session. Therefore, matching the range of input data with the range of the activation function makes the training of ANNs numerically faster convergence as this situation is well demonstrated by Sola and Sevilla (1997).

After performing the experiments and preparing the training- and validation data sets, one needs to select an appropriate black-box model structure such as NARX, NARMAX, NOE, nonlinear finite impulse response (NFIR) and nonlinear Box-Jenkins (NBJ) for the investigated dynamic system. This choice should be based on the dynamics and complexity of the network model which is most likely to match with the system under study. For instance, if one wants to model a system which has a hysteretic behavior; at least a RNN type model should be taken into consideration rather than feed-forward models as all the hysteresis systems have some local and global memory properties. Furthermore, if one is specifically interested in a longer prediction horizon (or infinite prediction), it is better to consider NOE type models. Choosing a suitable model structure is the most difficult step of the black-box modeling procedure since there is not an exact procedure defined in the current literature for this task. Therefore, this choice could be done based on some engineering ingenuity, intuition, and experience. Otherwise, several model structures should be tested in an iterative way, which will increase the duration of identification process significantly. No doubt, an inconsistent model will not be trained effectively to give out a satisfactory predictor or estimator regardless of the quality of the training data set and the chosen of the training algorithm.

Nonlinear black-box models, in general, could be expressed in the form of $\hat{y}(k) = f(\varphi(k),\theta)$ as illustrated in Fig. 3.2 for NARX and NOE, respectively. In general, the regression vector, $\varphi(k)$=[$u(k), u(k-1), u(k-2),....y(k-1), y(k-2),..., \hat{y}(k-1), \hat{y}(k-2), ..., e(k-1), e(k-2),...]^T$, can contain previous (and possibly current) process inputs (u), previous process (or model) outputs (y or $\hat{y}$) and previous prediction errors ($e = y-\hat{y}$). Note that the regression vectors of the various black-box models are given in Table 3.1. On the other hand, θ represents the model parameters to be determined.

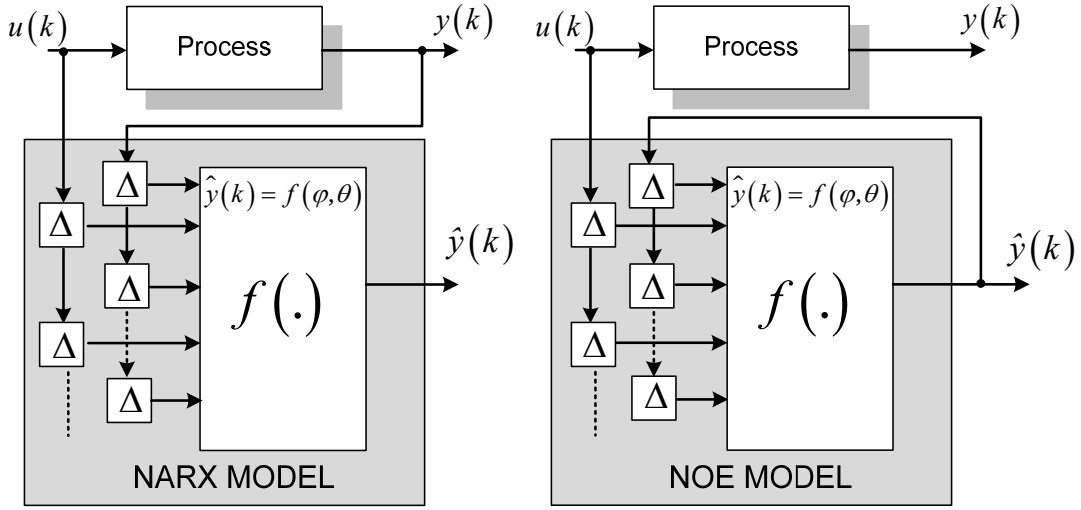

Fig. 3.2 NARX and NOE model structures.

Table 3.1 Regression vectors of the well-known black-box models.

Structure	Regression vector
NARX	$\varphi(k)=\left[u(k)\ldots u(k-n)\quad y(k-1)\ldots y(k-m)\right]^T$
NARMAX	$\varphi(k)=\left[u(k)\ldots u(k-n)\quad y(k-1)\ldots y(k-m)\quad e(k-1)\ldots e(k-m)\right]^T$
NOE	$\varphi(k)=\left[u(k)\ldots u(k-n)\quad \hat{y}(k-1)\ldots \hat{y}(k-m)\right]^T$
NFIR	$\varphi(k)=\left[u(k)\ldots u(k-n)\right]^T$
NBJ	$\varphi(k)=\left[u(k)\ldots u(k-n)\quad \hat{y}(k-1)\ldots \hat{y}(k-m)\quad e(k-1)\ldots e(k-m)\right]^T$

As could be seen from Fig. 3.1, the number of neurons at each hidden layer should be determined after choosing a proper model structure. The choice of how many neurons to be used at each layer is not an easy decision to make. It is well known that using too little or too many neurons will result in under-fitting or over-fitting problems, respectively. There are some rule-of-thumbs which could be used as a rough starting point to determine the adequate number of neurons at hidden layers. For instance, this number could be 1/10 of the length of the training data set or it could be (Heaton, 2008):

- between the size of the inputs and the size of the outputs.
- two-thirds of the size of the inputs plus the size of the outputs.
- less than twice the size of the inputs.

After choosing a proper network structure populated with adequate number of neurons, the problem boils down to find the parameter set, θ, for which below objective (cost) function, J_N, is minimized for a particular training scenario:

$$J_N = \frac{1}{2N}\sum_{k=1}^{N}\left[y(k)-\hat{y}(k)\right]^2 + \frac{1}{2N}\theta^T D\theta \tag{3.1}$$

where D is a diagonal matrix in which the main diagonal are equal to the weight decay and N is the number of collected samples. Levenberg-Marquardt (LM) method could be used for the numerical solution of this problem ($\theta = \arg\min_{\theta}\{J_N\}$).

It is well known that conventional (black-box) NN development paradigms especially for long-term prediction task of nonlinear dynamic systems using an error back-propagation algorithm have significant drawbacks such as divergence and instability. In the LM technique, if the previous model outputs are to be used in the regression vector, there will be feedback loop while taking the gradient of the cumulative error with respect to the parameter vector in the cost function. In fact, this feedback might lead to instability and divergence problems in the training phase of a RNN. For instance, Xu (1997) designed NARX and NOE type of black-box models to predict the control flow of a variable displacement hydraulic pump under various loading conditions. It was found that NARX has superior convergence rate and always reached a stable solution in the training scenarios. On the other hand, as emphasized by Narendra and Parthasarathy (1989), NOE also encounters similar problems. Nørgaard (2000) demonstrated that such problems can be avoided in a training session when the initial conditions of the network weights are nearly selected from their optimum values. Consequently, the classical design procedure (where dynamic systems are the main focus) can be summarized in the following steps: **i)** NARX model is developed (i.e. its free parameters are adapted)

conveniently (without any instability or convergence problem) since the model outputs are not used in the regression vector of NARX models. However, this model will not work for extended time periods due to the lack of the information about the process outputs; **ii)** with the estimated parameter vector θ (of the NARX model) used as the initial condition for the parameters of the NOE type model, an RNN is trained without experiencing divergence / instability problems.

Finally, one must perform the model validation tests of the network with using a scenario which should be different from the training case. Some statistical tests on residuals (i.e. differences between the model- and actual process outputs) could be performed to check the validity of the devised network model. Ideally, residuals (i.e. innovation sequence) should be statistically independent from the inputs and resemble a band-limited (zero-mean) Gaussian noise (or white noise). Additionally, a cross-correlation function test could be performed as (Billings and Zhu, 1994)

$$R_{ue}(l)=\frac{\sum_{k=1}^{N}\left[\left(u(k)-\bar{u}\right)\left(e(k-l)-\bar{e}\right)\right]}{\sqrt{\sum_{k=1}^{N}\left(u(k)-\bar{u}\right)^2\sum_{k=1}^{N}\left(e(k)-\bar{e}\right)^2}} \tag{3.2}$$

where $R_{ue}(l)$ is the cross-correlation function for all lags (l), $\bar{u}$ is the mean of the input signal and $\bar{e}$ is the mean of prediction error. After calculating the value of the cross-correlation coefficients for some lag values, it should be checked that these coefficients are within the confidence band. For instance, the confidence band is $\pm 1.96/\sqrt{N}$ for a 95% confidence interval. If this not the case, it means that some parts of the actual process have not been learned properly by the devised neural network.

Note that some techniques such as wavelet and Fourier transforms could also be utilized in order to perform a model validation in different domains (other than time domain). Such transform techniques open different point of views to analyze the system in a better way. Consequently, one should consider proper transformation

techniques as an essential component of the model validation phase. For instance, accuracy frequency response functions (FRFs) could be easily used for performing the model validation test in the frequency domain as,

$$A(\omega)=\frac{\hat{Y}(\omega)}{Y(\omega)} \tag{3.3a}$$

In this expression, $\hat{Y}(\omega)$ is the discrete Fourier transform (DFT) of the neural network model output while $Y(\omega)$ is the DFT of the actual process output and could be expressed as

$$\hat{Y}(\omega)=\sum_{k=0}^{N-1}\hat{y}(k)e^{-i\omega kT} \tag{3.3b}$$

$$Y(\omega)=\sum_{k=0}^{N-1}y(k)e^{-i\omega kT} \tag{3.3c}$$

where $\omega = (2\pi n) / (NT)$, $n = 1,2,\ldots,N/2$ and i is the imaginary unit (Ljung, 1999).

As could be seen from Fig. 3.1, the paths going from decision blocks and back to the previous stages indicate that the identification process is executed in an iterative manner. If the training session cannot be finished successfully, the parameter estimation step should be repeated with different (random) choices of initial conditions for the weight values. This will decrease the possibility of being caught in local minima of the objective function. But, the corresponding error may not reach a predetermined threshold value after all trials. In that case, one must consider playing with the number of neurons in the layers of the previously chosen NN architecture. The common (trial-and-error) procedure to determine a sufficient number of neurons is to start with a small number of neurons and then increase their number gradually while evaluating the error criterion. No doubt, this procedure increase the duration of the identification process, enormously. Furthermore, the

path leading back to model structure selection is generally followed in case the error criterion could not be satisfied in any way or the well-trained model could not pass the validation tests.

Consequently, black-box model design for nonlinear dynamic systems is an exhaustive process since different network architectures and different initial conditions (i.e. initial weights) are iteratively tried to find out a well performed network model. Moreover, the network may entirely be unsuccessful to capture the desired functional relationship after a painful training process if the network architecture (or structure) is incompatible with the dynamics of the system under study. On the other hand, a well-trained black-box model does not give any information about the inner nature of the physical system under study. This makes the network model lack of any interpretability since the user could only interact with the input- and output signals of the network. Another major factor that limits the use of black-box type neural network model is that instability and divergence. The dynamic system under investigation could be very complex and it may require long training sessions and may not always converge to optimum network weight values for satisfying the guaranteed stability especially in real time or on-line training situations. In that case, it will be difficult to guarantee the asymptotic stability of the model and some techniques such as perturbation analysis, interval analysis, describing function analysis, harmonic analysis etc. should be used to check the robustness of the model.

As a result, designing black-box type NNs from generic structures is a very difficult feat for highly nonlinear dynamic systems. On the other hand, the main nonlinear features common to the most engineering systems could be investigated to gain an intuition about the overall estimator/predictor topology. To solve the problem of stability and convergence of a monolithic network, a number of modular neural network models can be developed utilizing *a priori* knowledge on the system through *divide and conquer* strategy. This methodology, named as SNN methodology in the current literature of ANNs, is nowhere complete and has been currently evolving in time.

3.3 Structured Neural Network Methodology

As outlined in Chapter 2, the structure neural network (SNN) appearing in the current literature were generally devised to “imitate” the known processes and hence did not give any additional knowledge about the systems at hand. Therefore, if some features of the nonlinear system, which could not be taken into consideration during the design of the SNN, exist, they will not be captured by the devised SNN in the further training sessions. On the other hand, the proposed SNN methodology in this thesis is especially based on a sketchy guidance of *a priori* knowledge on the studied systems. Unlike previous studies, the approach adopted here is helpful while designing SNN models for the nonlinear dynamic systems whose exact physical models are unknown. It is important to note that this methodology does not offer a new training algorithm but suggests a step-wise procedure in which the finalized outcome of this methodology is an optimized gray-box model (a model between a black-box and a white-box model). The presented methodology determines the overall ANN architecture for a specific application in a systematic fashion. Another advantage of the methodology is that the devised model could be easily used to identify/model similar processes by simply augmenting the system with new networks representing the unaccounted dynamics. After a brief training session, compact SNNs can be designed in a modular fashion. The proposed SNN methodology is illustrated in Fig. 3.3.

First, it is checked that a system model is available or not. If an exact mathematical model of the system under study exists, the complex dynamic system (or physical process) is decomposed into a series and/or parallel sub-systems in order to reveal the interactions among them. That is, a complex nonlinear system can be conveniently divided into its subsystems/components where casual-relationship among the inputs and outputs may be clearly identified. From the identified interactions, important information about the order of the inputs and the nonlinearity inherent to the subsystem could be generally seen. Thus, this procedure often times yields an efficient sub-system models for a specific application domain. In this step, *a priori* knowledge about the system could be effectively used since many engineering systems from electrical and mechanical domain are extensively

investigated in terms of physical modeling, model order, input/output properties and range of model parameters etc. Therefore, pertinent knowledge is generally ready for use to decompose the system into its sub-systems using the engineering intuition. A good example for this step is well applied in Chapter 5 (and Chapter 6, also) where the nonlinear pressure dynamics of a hydraulic system is divided into sub-systems based on the available mathematical models of the system. In case the lack of any physical model at hand, one could inspect the behavior of the complex system from its input-output data, and then, divide the overall training data into sets in order to perform some tasks. Here, one can speculate about desired tasks which should be realized by network models and their corresponding inputs in a systematic fashion. Again, a relevant example to this case could be seen from Chapter 4 in which only the output of a timing-belt drive system is investigated based on a recorded data from the experimental setup. Then, the output behavior of the above-mentioned system is divided into regions which are correlated with the operating regimes of the drive system rather than deriving a detailed mathematical model, and then, dividing its physical model into sub-systems. Consequently, the main idea behind this (rather classic) “divide” approach is to employ a priori knowledge on the process to separate the problem into its primary functions.

Next, each subsystem is taken into consideration and then queried whether or not it could be represented by a standard library network (SLN). It is obvious that there are some unique nonlinear features common to the various complex systems. Individual neural network models could be devised for these unique nonlinear elements. Next, these task-specialized network models could be categorized as a SLN. They could be utilized later to model similar systems. SLNs will be explained in a detailed manner in Section 3.4. Therefore, if there exists a network model which was already designed for the desired function in the network library; it will be taken and directly used for the modeling of the sub-system under consideration. Otherwise, a black-box model should be developed for this sub-system. Decomposing the system into a group of sub-systems over their operating regions, relationships between the sub-systems gives out the input-output variables of the sub-models. Furthermore, the physical nature of the sub-system can be utilized

while determining the order of the TDL of input signals and the layout of the feedback connections between the layers of the NN_i's (Agarwal, 1997). Therefore, one will need some standard network architectures in order to start the training session of a black-box network with an appropriate model structure. For that purpose, some generic NN templates are also given in Section 3.5 since selecting a proper model structure is the most important stage of a black-box modeling approach. Furthermore, all the input-output signals to the sub-systems should be normalized while training NN_i's so that the trained network modules could then be used for the full scale nonlinear mapping of other similar systems by only playing with their normalization coefficients (or connection gains). At the end of this stage, each sub-system is separately modeled by unique (and small) neural network modules (NN_i; $i=1...n$) which could be easily debugged, also (Tseng and Almogahed, 2009).

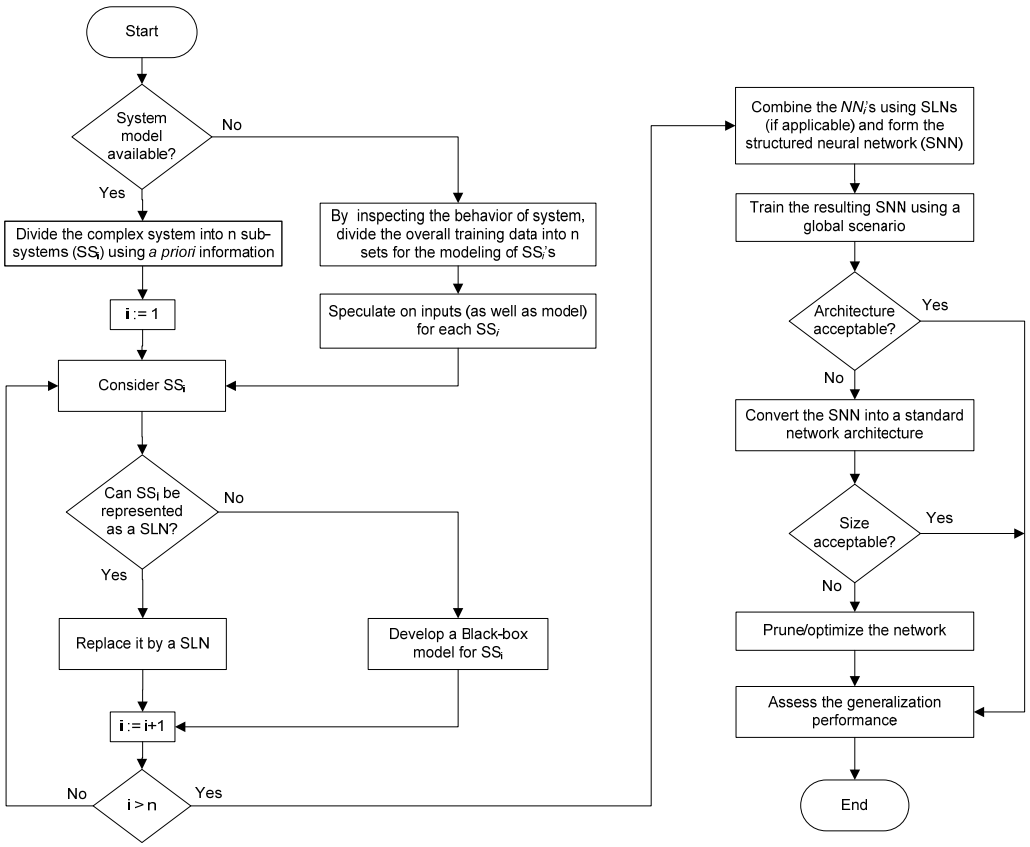

Fig 3.3 Proposed SNN methodology.

Next, the NN_i's, which are trained in a piecewise fashion, are aggregated with SLNs (if they are utilized) to construct a unified ANN. Both the stability/convergence along with the accuracy of the overall network is to be maintained since all the NN_i's trained individually via compact training sets. Therefore, the resulting network at this step is expected to converge rapidly to the global optima since the aggregated network will not start the final training session at an arbitrary location in the huge weight (parameter) space but at a location in close proximity to the global optimum. Hence, the learning computation cost will be decreased and local minima problem which large monolithic neural networks frequently trapped will also be avoided.

Furthermore, SNN is trained in a unified manner using a global scenario. This step is important since the entire network modules are only trained for their specific operating regimes in order to implement the sub-system behavior. Up to this stage, it is important to note that NN_i's have never been trained in a unified form to capture the dynamic behavior of the nonlinear system using a case scenario which is based on the functionality of the overall system. Therefore, this training operation will fine-tune all the SNN parameters and will further increase the performance of the SNN model. Moreover, if the devised SNN model is to be used for other similar systems, this step will be crucial in which the parameters of the SNN should be adapted to capture the dynamic behavior of the new system. At the end of this step, one could end up the identification process after performing model validation tests if the architecture of the model is acceptable.

Otherwise, it would be advantageous to convert the SNN model into a generic (standard) type network model since the SNN model may have several successive feed-forward network modules with linear output units and connection gains between some hidden layers. As the weights of the linear layers could be easily merged with the next layer weights (Dolen and Lorenz, 2002) and the connection gains could be easily embedded into the corresponding hidden layers, an architecture simplification procedure could be applied at this stage of the

methodology in order to enhance the implementation of the network in a more generic way.

Finally, the excessive (or irrelevant) parameters of the network could be removed to increase the generalization performance and to reduce the computational burden (processing speed) of the model. No doubt, a pruning process (model refinement) will ease the implementation of the network model on hardware platforms (e.g. FPGAs). It is important to note that a new entropy based pruning algorithm is proposed and explained in a detailed manner in Section 3.6.

3.4 Standard Library Networks

Some network models could be readily devised for the approximation of well-known functional relationships such as arithmetic, logical, trigonometric and logarithmic operations that frequently appear when a complex system is decomposed into its components. These networks are categorized as SLNs since their functionality is always same and independent from the input or output signals which are connected to them.

Dolen (2000) devised some SLNs for performing arithmetic ($x_1.x_2$), trigonometric ($cos(x)$), inverse trigonometric ($cos^{-1}(x)$), Gaussian ($exp(-x^2/2)$) and piecewise continuous operations (e.g. $|x|$, $min\{1,max\{x,0\}\}$, $min\{1,max\{x,-1\}\}$) and gave all the values of the network parameters to be used directly for similar tasks. For self containment, some SLNs are also developed in this thesis work in order to augment the SNN library. It is important to note that the network models presented are intuitively designed in a piecewise fashion without any prior training.

3.4.1 Switching Networks

A switching (or *gating*) network that essentially performs multiplexing operations among the network inputs is especially be needed to form a “mixture of experts” model. Two types of switching network, which are elaborated in the following sections, are designed in this thesis work.

3.4.1.1 Switching Network Type 1

In the first type of the switching network, the output is equal to the first input (u_1) when s = 1 while the second argument (u_2) passes if s = -1. As illustrated in Fig. 3.4, this network is a two layered feed-forward network that could be expressed as:

$$y = V_2\, \Psi\left(W_1\, u + b_1\right) + V_1 u \tag{3.4a}$$

$$W_1 = \begin{bmatrix} \kappa^{-1} & 0 & \kappa \\ 0 & \kappa^{-1} & \kappa \end{bmatrix}, \qquad b_1 = \begin{bmatrix} -\kappa \\ \kappa \end{bmatrix} \tag{3.4b}$$

$$V_1 = \begin{bmatrix} 0 & 0 & -\kappa \end{bmatrix}, \qquad V_2 = \begin{bmatrix} \kappa & \kappa \end{bmatrix} \tag{3.4c}$$

where $u = [u_1\ u_2\ s]^T$ is the input vector; y is the output of the network; $\Psi(.)$ is an activation (tangent sigmoid) vector function. To transmit the signal through the activation function without any distortion, the value of κ should be high enough to scale down input of the neuron (by κ^{-1}) into the linear part of the tangent sigmoid. Then, the output of the activation function is rescaled with κ to form the original input signal.

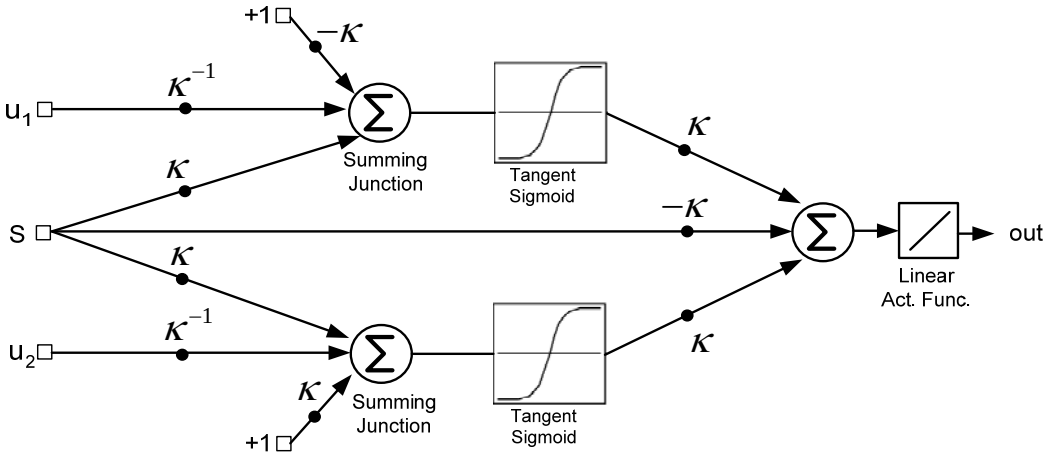

Fig. 3.4 Switching Network Type 1.

3.4.1.2 Switching Network Type 2

The switch input must be exactly 1 or -1 to canalize one of the inputs to the output in the above mentioned switching network (*Type 1*). However, one can need a switching network which should implement the below task

$$y = \begin{cases} u_1, & s \geq 0 \\ u_2, & s < 0 \end{cases} \tag{3.5}$$

For that purpose, a RNN (with three neurons) architecture is devised that could be expressed as

$$q^+ = \Psi(V_1 q^- + W_1 u + B_1) \tag{3.6a}$$

$$y = W_2 q^+ \tag{3.6b}$$

where q^- and $q^+ \in \Re^{3\times 1}$ indicate the state vector of neurons before and after the update respectively. Correspondingly, the weight matrices and bias of (3.6) can be given as

$$V_1 = \begin{bmatrix} 0 & 0 & 10 \\ 0 & 0 & 10 \\ 0 & 0 & 0 \end{bmatrix}, \qquad W_1 = \begin{bmatrix} 0.01 & 0 & 0 \\ 0 & 0.01 & 0 \\ 0 & 0 & 10^5 \end{bmatrix} \tag{3.7a}$$

$$B_1 = \begin{bmatrix} -10 & 10 & 0 \end{bmatrix}^T, \qquad W_2 = \begin{bmatrix} 100 & 100 & -100 \end{bmatrix} \tag{3.7b}$$

3.4.2 Exclusive-OR Network

An exclusive-OR (XOR) is frequently needed when one needs to determine a direction change from the position signal ($x(k)$) of a mechanical system. Defining the network input as $u = [u_1\ u_2]^T$, where $u_1 = x(k) - x(k-1)$ and $u_2 = x(k-1) - x(k-2)$, the below function should be implemented by a XOR network.

$$y = \begin{cases} -1, & sgn(u_1) = sgn(u_2) \\ 1, & else \end{cases} \tag{3.8}$$

The analytical expression of the XOR network could be written as

$$y = W_3 \Psi(W_2 \Psi(W_1 u) + B_2) + B_3 \tag{3.9a}$$

where the weight matrices and biases become

$$W_1 = \begin{bmatrix} K & 0 \\ 0 & K \end{bmatrix}, \quad W_2 = \begin{bmatrix} K & -K \\ K & -K \end{bmatrix}, \quad B_2 = \tfrac{1}{2}\begin{bmatrix} -K \\ K \end{bmatrix} \tag{3.9b}$$

$$W_3 = \begin{bmatrix} 1 & -1 \end{bmatrix}, \quad B_3 = 1 \tag{3.9c}$$

In (3.9b), K refers to a large gain (typically 10^5) in order to drive the tangent sigmoid functions into the saturation.

3.5 Standard Network Architectures

Although some widely known black-box model architectures are given in Section 3.2, they may not be an appropriate model structures when devising a network model for a discrete-time sub-system at the second step of the proposed SNN methodology. Covering all the black-box models, other network architecture templates are given in Fig. 3.5. As could be seen, all the standard network architectures are comprised from the basic operations of delay elements (TDL), feed-forward multi-layered networks having tangent sigmoid neurons (illustrated as *f(.)* and *g(.)*), and summation blocks. Using the multi-layered networks in cascade and feedback configurations with the TDL inputs to such models, arbitrary discrete-time nonlinear sub-systems could be modeled efficiently. Table 3.2 indicates which template should be used for which type of discrete-time sub-system.

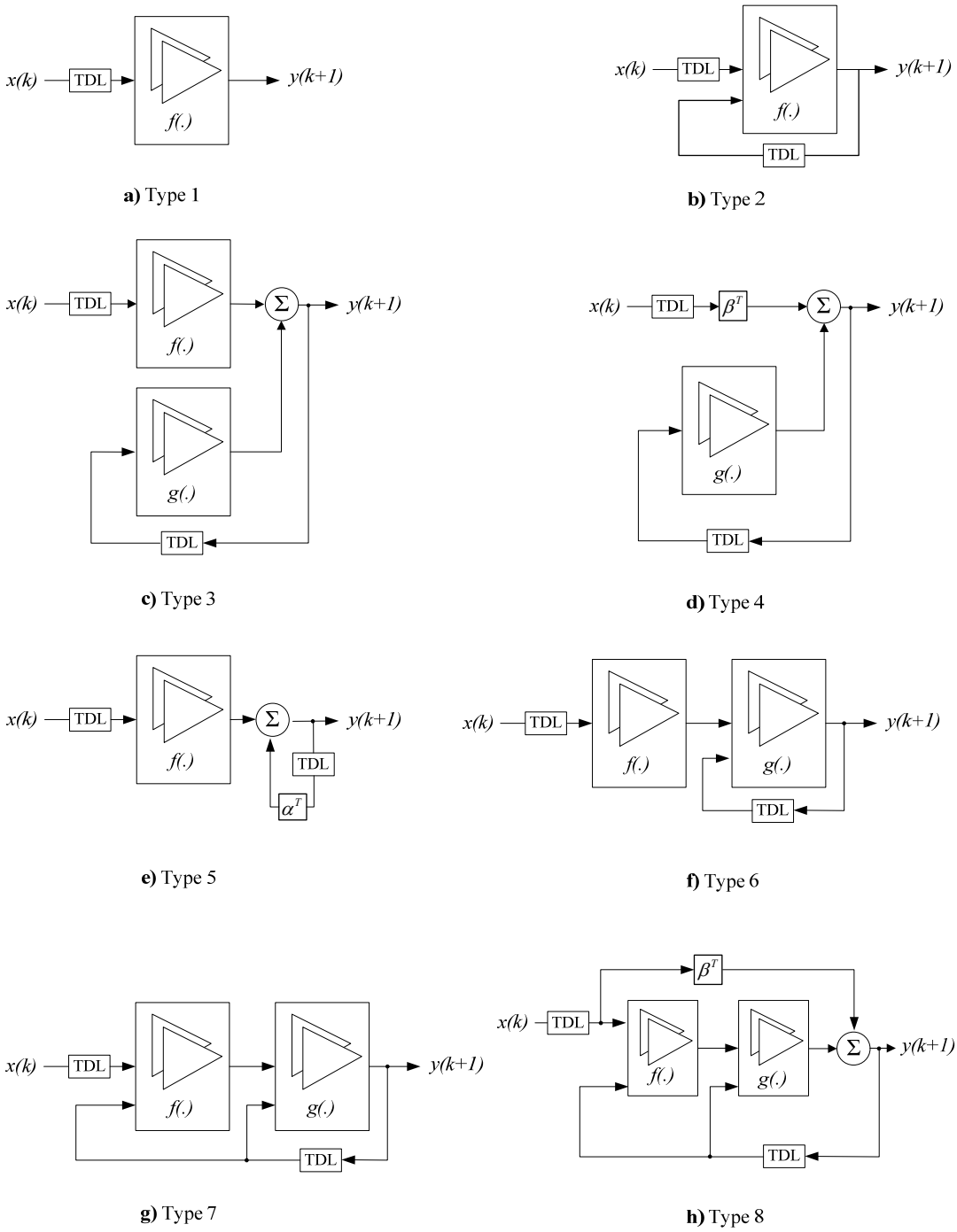

Fig. 3.5 Standard network templates.

Table 3.2 Discrete-time systems and their corresponding network templates.

Type	Discrete-time System Model
1	$y(k+1) = f[x(k), x(k-1), x(k-2),\ldots]$
2	$y(k+1) = f[y(k), y(k-1),..,x(k), x(k-1), x(k-2),\ldots]$
3	$y(k+1) = g[y(k), y(k-1), y(k-2),\ldots] + f[x(k), x(k-1), x(k-2),\ldots]$
4	$y(k+1) = g[y(k), y(k-1), y(k-2),\ldots] + \sum_{i=0} \beta_i x(k-i)$
5	$y(k+1) = \sum_{i=0} \alpha_i y(k-i) + f[x(k), x(k-1), x(k-2),\ldots]$
6	$y(k+1) = g\{y(k), y(k-1), y(k-2),\ldots, f[x(k), x(k-1), x(k-2),\ldots]\}$
7	$y(k+1) = g\{ y(k), y(k-1), y(k-2),\ldots, f[x(k), x(k-1), x(k-2),\ldots y(k), y(k-1), y(k-2),\ldots]\}$
8	$y(k+1) = g\{ y(k), y(k-1), y(k-2),\ldots, f[x(k), x(k-1), x(k-2),\ldots y(k), y(k-1), y(k-2),\ldots]\} + \sum_{i=0} \beta_i x(k-i)$

3.6 Entropy Based Pruning Algorithm

Although there are a lot of different pruning methods as could be seen from the literature survey in Chapter 2, an entropy based pruning algorithm, which is mainly adapted from the smallest variance pruning (SVP) method, is utilized whenever a pruning operation will be needed for a devised neural network. In SVP, the units, which have approximately constant (or smallest variance) outputs across the training set, are deleted. The primary problem with this simple and effective pruning algorithm is that the inessential units must be identified manually and there is not a built-in mechanism which automates the procedure for large and complex networks (Guan and Chen, 2005). In this thesis work, this problem is solved through calculating the uncertainty of each hidden neuron output via entropy (*H*) approach.

Entropy is defined as the uncertainty of a single random variable in statistical mechanics. On the other hand, information theory uses the entropy as a measure of

information. In fact, entropy is a function of a probability (i.e. *H(p)*); therefore, it does not rely on the apparent value of the random variables. It is obvious that if an event with a low probability is happened, one will get the most information (i.e. information is inversely related to the probability of occurrence). Therefore, entropy is frequently used to measure the uncertainty, or to get the information content of an interested variable.

Now, an entropy function *H(p)* will be constructed based on the three properties about entropy and probability laws as

1. $H(p) \geq 0$ (entropy always increases)
2. $H(p_1.p_2) = H(p_1) + H(p_2)$ (independent events are additive)
3. $H(p)$ is a continuous function of p ($0 \leq p \leq 1$).

From second property, some manipulations could be written as below

$$H\left(p^n\right) = n\,H\left(p\right) \tag{3.10a}$$

$$p^n = y, \quad p = y^{1/n} \tag{3.10b}$$

$$H\left(y\right) = n\,H\left(y^{1/n}\right) \tag{3.10c}$$

$$H\left(y^{m/n}\right) = \frac{m}{n} H\left(y\right) \tag{3.10d}$$

From the above manipulations, it is seen that an entropy function obeys the logarithmic function rules and could be written for some base of the log system for any constant k as below

$$H\left(p\right) = k \log\left(p\right) \tag{3.11}$$

From first property, k must be non-positive and could be chosen as -1. Moreover, considering p_i as the probability of getting the information $H(p_i)$, one will get all the information $H(p)$ on the average with using the third property as

$$H(p) = \sum_{i=1}\left[p_i \log\left(\frac{1}{p_i}\right)\right] \tag{3.12}$$

It does not matter which base of the log system is used. If the base is chosen as 2, the resulting units of information will a bit (binary digit). Furthermore, if the used base is *e*, then the unit of information is called a *nat* (Hamming, 1986). For the idea of entropy, let's consider an example in which the output variable is either 1 or 0. It is obvious that if the probability of the output being 1 is *p*, then the probability of being 0 will be 1-*p*. Based on these assumptions, the entropy function of this event (in bit units) could be written as

$$H(p) = p\ log_2\left(\frac{1}{p}\right) + (1-p)\ log_2\left(\frac{1}{1-p}\right) \tag{3.13}$$

The graph of this entropy function is given in Fig. 3.6. It is seen that *H(p)* gets its maximum value (1 bit) when *p = 1/2* (uncertainty is maximum). On the other hand, it is 0 when *p* equals 0 or 1, meaning that the output variable is not random but constant (no uncertainty).

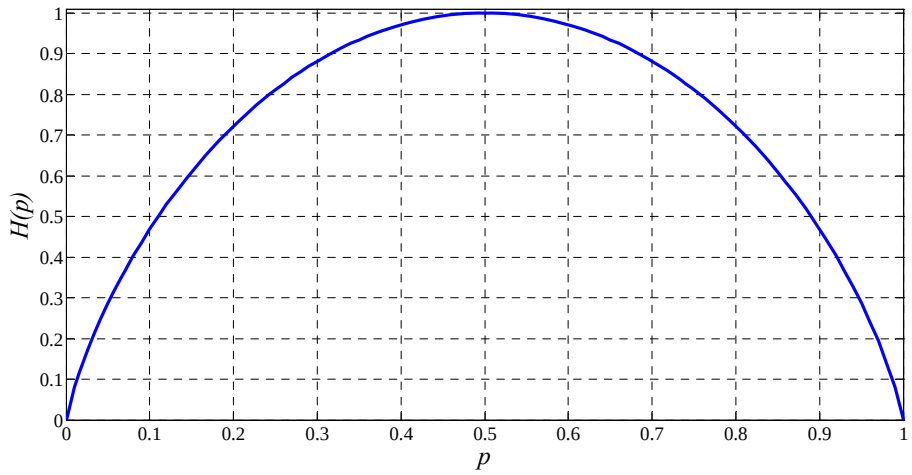

Fig 3.6 Entropy functions for two probabilities.

Considering that the output of a hidden layer neuron is an information source, one can use the entropy to evaluate the uncertainty of a neuron. The flowchart of the entropy based pruning algorithm is shown in Fig.3.7. In the proposed pruning method, entropy is defined as the weighted average of the natural logarithms of the reciprocals of the probability density function (*pdf*) of the neuron output in its whole working range (-1 ≤ working range ≤ +1 for tangent sigmoid neurons) and calculated as below

$$H = \sum_{i=1}\left[pdf_i \ \log_e\left(1 \Big/ pdf_i \right)\right] \ = -\sum_{i=1}\left[pdf_i \ \log_e\left(pdf_i \right)\right] \tag{3.14}$$

Consequently, neurons with a small entropy value (or uncertainty) could be removed from the network in an automated fashion. But, the mean output of the removed neurons should be added as the bias weights of the neurons in connection with the removed one in order to keep the network's performance (almost) unchanged. Following that, the pruned network should be retrained for fine tuning of the remaining parameters. After the retraining operation, if the network could not reach the predetermined error threshold value, one should revert to the previous network architecture (undo last pruning operation) and terminate the pruning process. In the next sub-sections, two benchmark systems are utilized to show the efficiency of the proposed algorithm for a pruning process. The first system is taken from Lazar and Pastravanu (2002) and the second system is adapted from Narendra and Parthasarathy (1990).

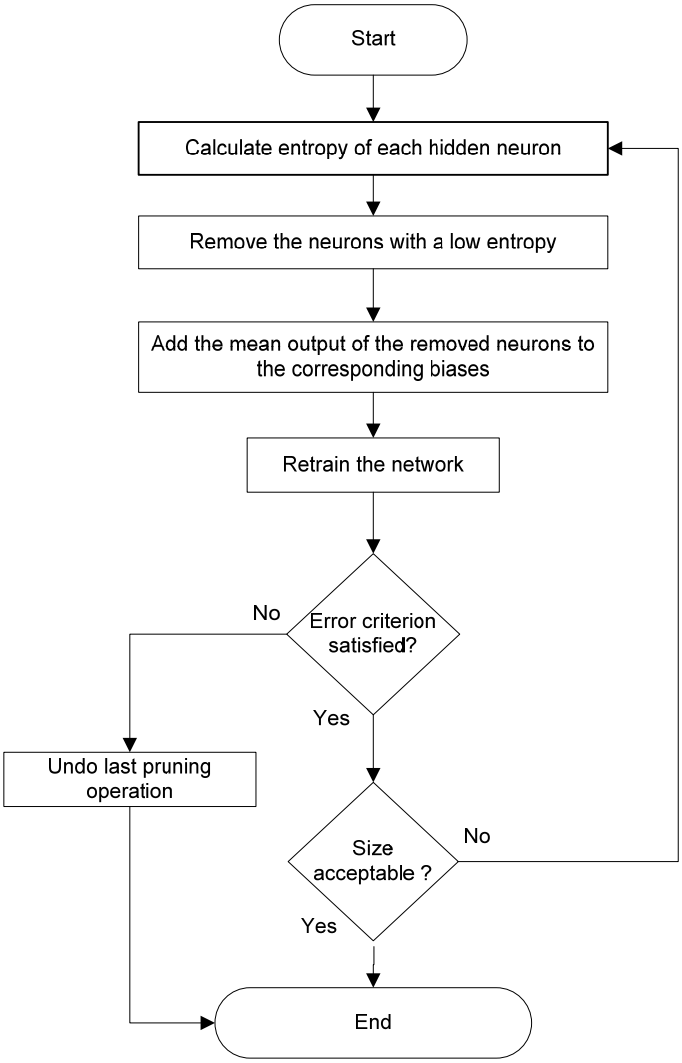

Fig 3.7 Flowchart of the entropy based pruning algorithm.

3.6.1 Benchmark System 1

The first benchmark system is defined as below

$$y(k)=\frac{2.5\,y(k-1)y(k-2)}{1+y^2(k-1)+y^2(k-2)} + 0.3\cos\left[0.5\left(y(k-1)+y(k-2)\right)+1.2u(k-1)\right] \tag{3.15}$$

where y is the output and u is the input of the discrete-time nonlinear system. The dynamic system in (3.15) resembles the *Type2* architecture in Fig. 3.5. Note that

training such a recurrent model with randomly initialized parameters is known to be very difficult. For that reason, first a NARX type model (with ten neurons in its first hidden layer) is trained. Following that, its parameters are used as the initial conditions of the Type2 structure (NOE type black-box model). Fig. 3.8 shows the applied input signal to the plant and the target response that are used in the training session.

Consequently, a NOE model is trained by taking the initial conditions (weights) of the parameters from the NARX model. Table 3.3 shows the training performance of the network. As can be seen in Fig. 3.9, some instability and divergence problems are encountered while validating the *NOE#1*. As previously suggested, the number of the hidden layer neurons are not increased gradually but increased extremely (from 10 to 30) not to make a lot of trials. In this way, a NARX model having 30 neurons in the first layer is trained first and; then, again a NOE model is devised by taking the initial conditions of the parameters from the NARX. At the end, a well trained recurrent network model (*NOE#2*) but having an excessive number of neurons in its hidden layer is achieved as could be seen from Table 3.3. Although this model passes the model validation test successfully, one may demand to finish the identification process with a network model having a less number of neurons.

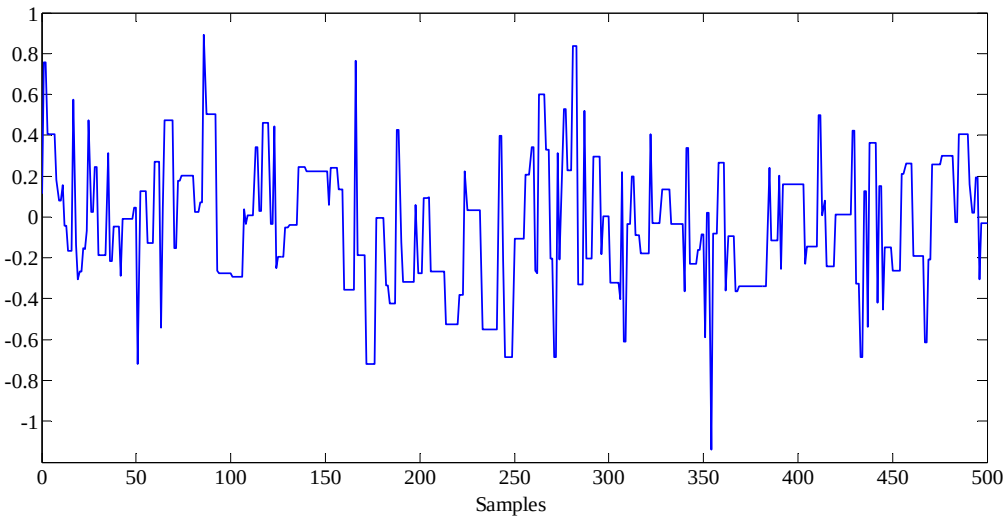

a) Input signal applied to the plant.

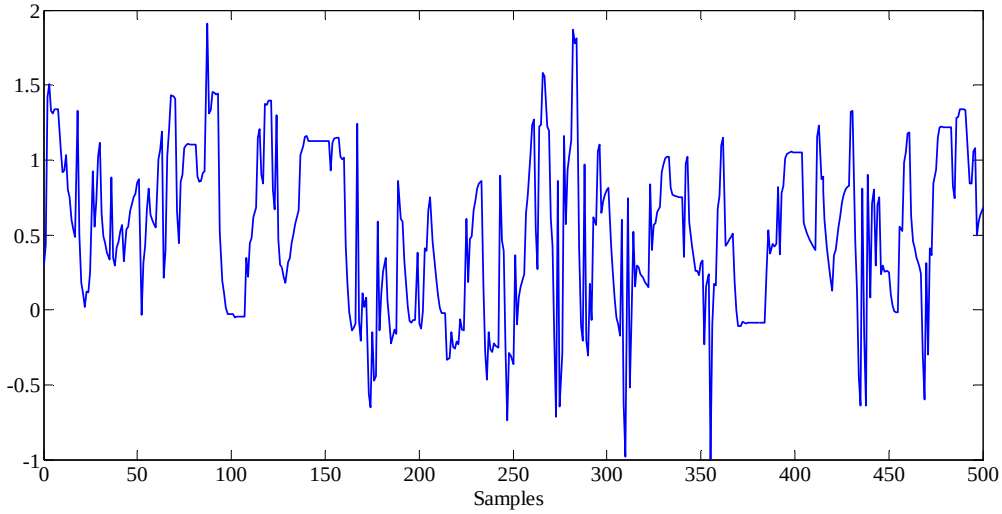

b) Target response.

Fig 3.8 Training scenario used for benchmark system 1.

Table 3.3 Black-box networks for benchmark system 1*.

Model	***NARX#1***	***NARX#2***	***NOE#1***	***NOE#2***
Input(s)	*u(k-1), y(k-1), y(k-2)*		*u(k-1)*	
Output	*y(k)*			
Training data	*501 Samples*			
1st layer neurons	*10*	*30*	*10*	*30*
Training time (seconds)	*57*	*98*	*57*	*63*
Epochs	*5000*		*50*	
Mean-square training error	1.11×10^{-6}	6.43×10^{-10}	1.38×10^{-6}	7.4×10^{-10}
Activation Function	*Tangent (Bipolar) Sigmoid*			

[*] Linear activation functions are utilized at their output layers.

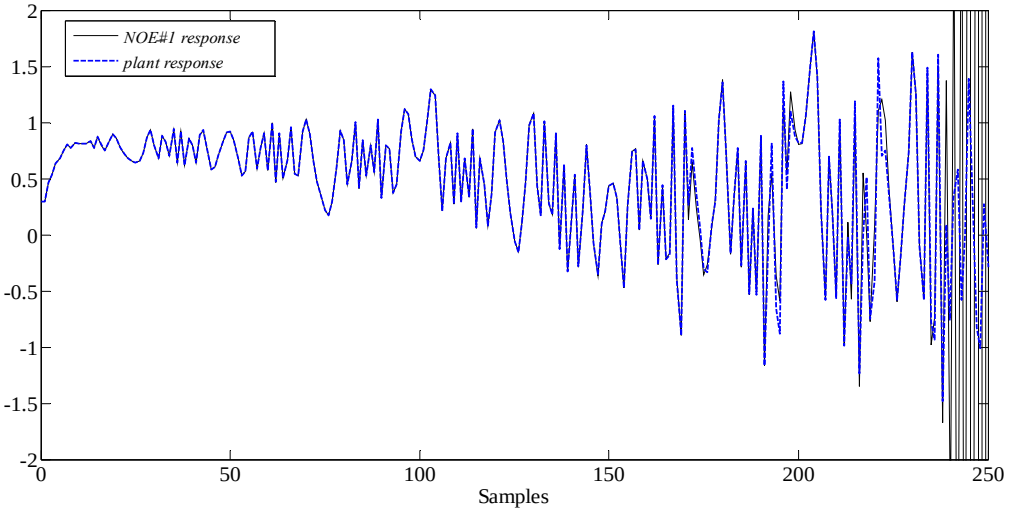

Fig 3.9 Validation performance of *NOE#1*.

For a pruning operation, probability density functions of the hidden layer neurons in *NOE#2* are calculated first, and then, (3.14) is used to calculate the entropy value of the each neuron separately. As could be seen from Fig. 3.10, neurons indexed with 16, 28 and 30 have an entropy value closer to zero, meaning that their activation function outputs are not changing too much during the training process. After pruning these three neurons from *NOE#2*, another network named as *NOE#3* is created, and then, trained for fine tuning of the network parameters. Again, the entropy of the neurons in *NOE#3* is recalculated and given in Fig 3.11. Now, the neurons indexed with 11, 21 and 25 are removed and a network called *NOE#4* is formed after this operation.

One more iteration is carried out via looking to the entropy diagram of *NOE#4*, given in Fig. 3.12, in which the neurons indexed with 13 and 21 are pruned and a network called *NOE#5* is created at last. From that point on, it is seen that no further neuron could be pruned and the rest network parameters could be trained in an effective way. Eventually, after 3 iterations, the number of the neurons is decreased from 30 to 22 by using this simple and effective pruning technique. Fig. 3.13 shows the validation performances of the *NOE#2* and *NOE#5*. It is seen that the *NOE#2* was easily pruned without deteriorating its modeling performance.

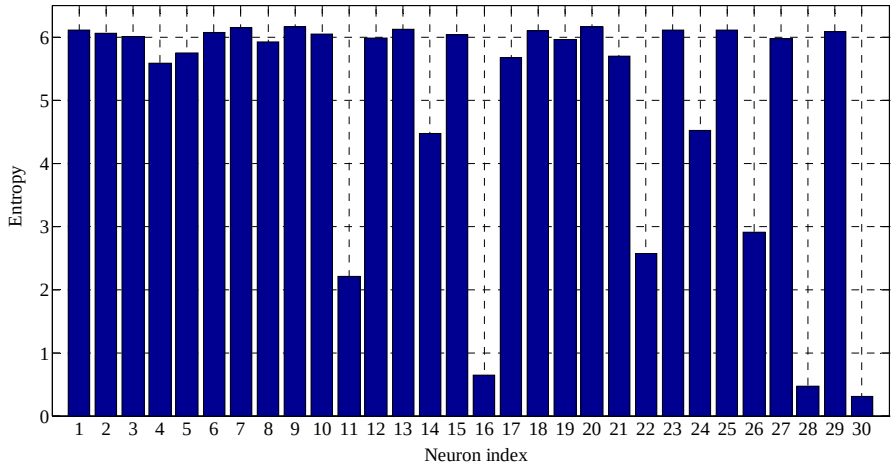

Fig 3.10 Entropy of the hidden layer neurons in *NOE#2*.

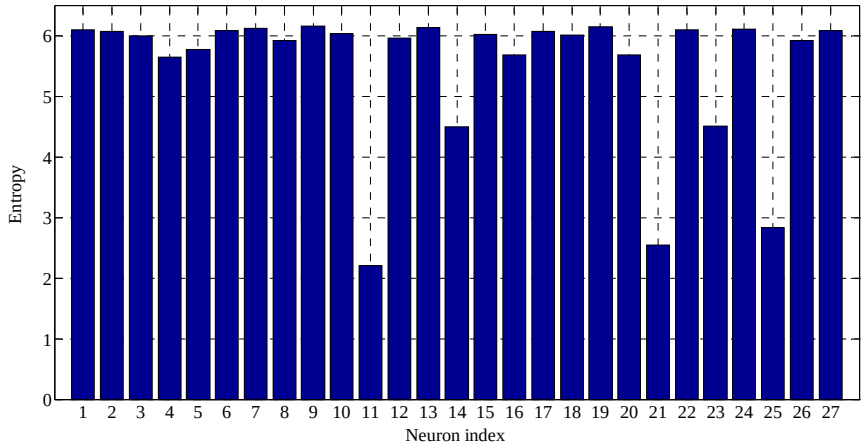

Fig 3.11 Entropy of the hidden layer neurons in *NOE#3*.

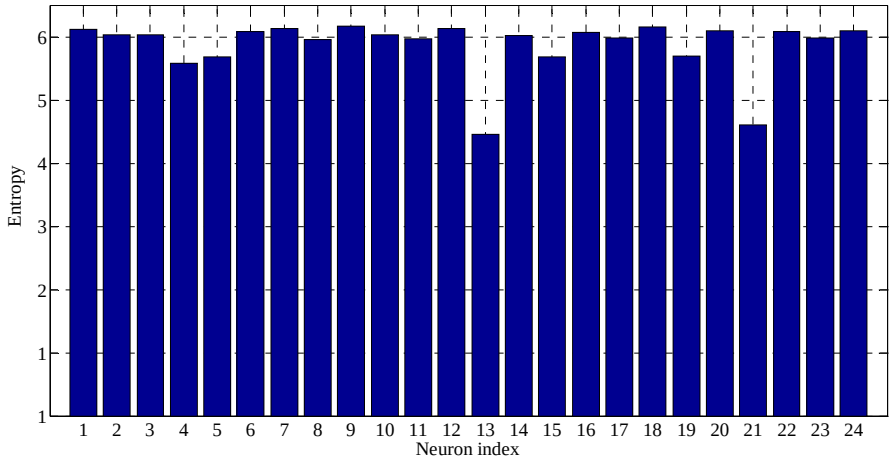

Fig 3.12 Entropy of the hidden layer neurons in *NOE#4*.

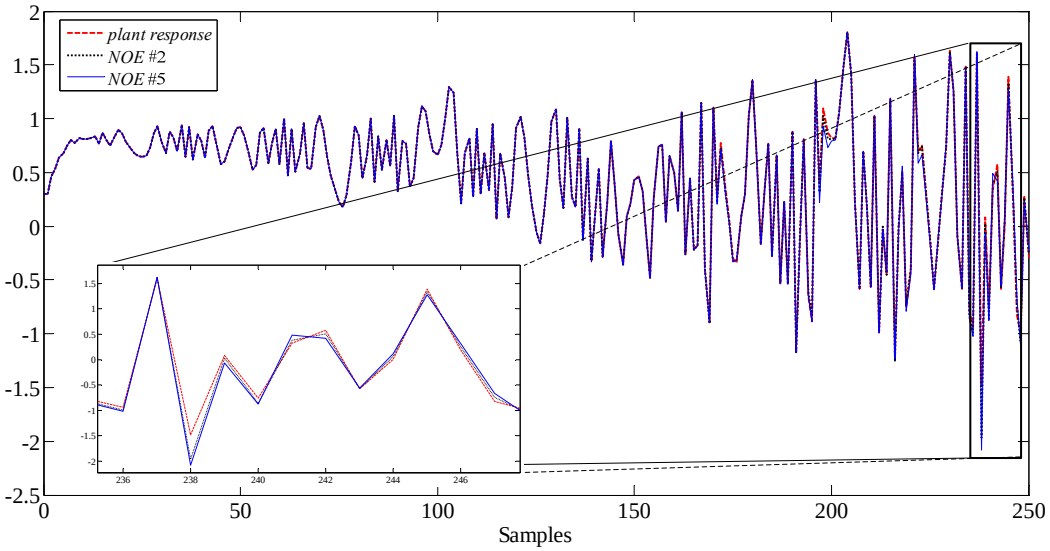

Fig 3.13 Validation performance of *NOE#2* and *NOE#5*.

3.6.2 Benchmark System 2

In the second benchmark example, the system is assumed to be of the form

$$y(k+1)=\frac{y(k)y(k-1)y(k-2)u(k-1)\left[y(k-2)-1\right]+u(k)}{1+y^2(k-2)+y^2(k-1)} \tag{3.16}$$

where y is the output and u is the input of the discrete-time nonlinear system. In the identification process, as used by Narendra and Parthasarathy (1990), a three-layered NOE-type network model structure is chosen. The number of tangent sigmoid neurons is 20 and 10 in the first and second layers, respectively while one linear neuron is used in the output layer. As mentioned earlier, this network model is trained first in a feed-forward manner (i.e. a NARX model is created), meaning that the measured output values are used in the regression vector. Then, using the values of estimated parameter of the NARX model as the initial conditions of the NOE parameters, a recurrent learning is performed. A uniformly distributed random input signal is used in the training session as depicted in Fig. 3.14.a and the corresponding output of the plant is illustrated in Fig. 3.14.b.

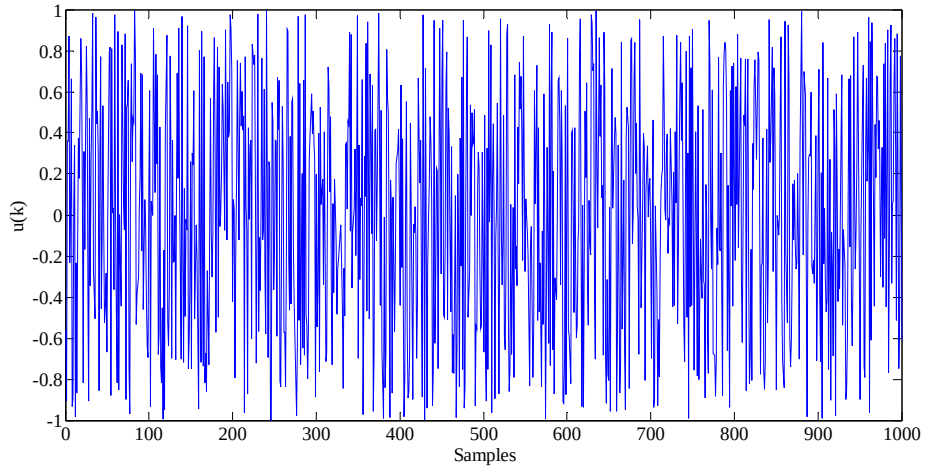

a) Input signal applied to the plant.

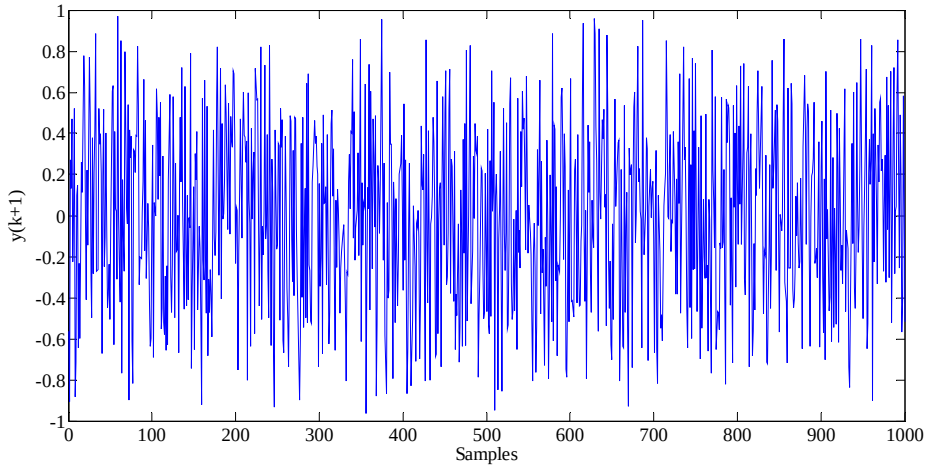

b) Target response.

Fig 3.14 Training signals used for benchmark system 2.

Next, the entropy value of the each neuron in the hidden layers of the network is calculated. Fig. 3.15 presents the entropy diagrams for the first- and second hidden layers of the recurrent neural network (NOE-type). The entire procedure given in the flowchart of the entropy based pruning algorithm (see Fig. 3.7) is followed step-by-step in 3 iterations. The neuron indexed with 2 in first hidden layer and the neuron indexed with 10 in the second hidden layer is purged in the first iteration. In the second iteration, only the neuron indexed with 1 is removed from the first layer.

It is seen that no further neuron could be pruned from the second layer after pruning one neuron from it at the first iteration. Lastly, the indexed neurons with 11, 12 and 17 in Fig. 3.15.a are purged in the third iteration. Table 3.4 shows the training performances of the devised network models.

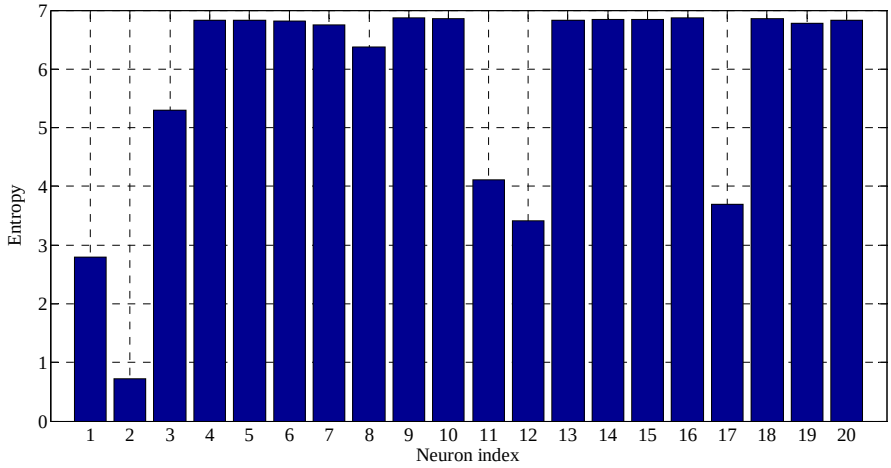

a) Entropy diagram of the first hidden layer.

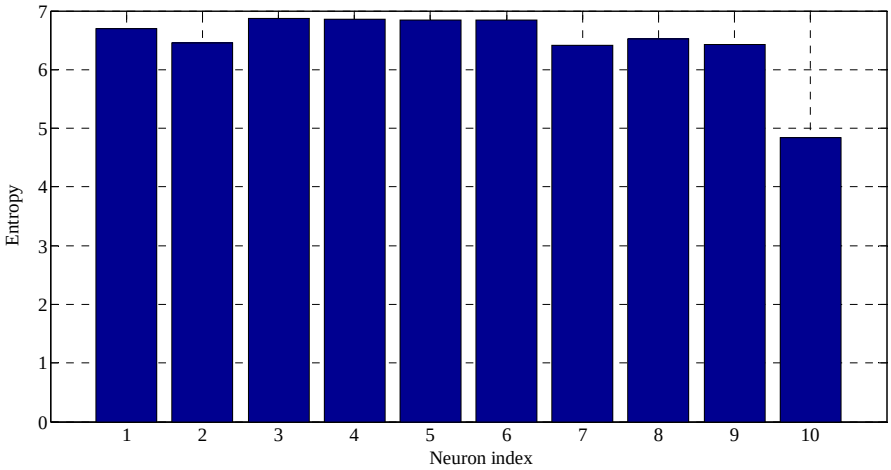

b) Entropy diagram of the second hidden layer.

Fig 3.15 Entropy diagrams of the hidden layer neurons in NOE.

After finishing the pruning operation, the original NOE and pruned NOE are compared via applying an input signal defined as

$$u(k)=\begin{cases}\sin(2\pi k/250), & k\le 500\\ 0.8\sin(2\pi k/250)+0.2\sin(2\pi k/25), & k>500\end{cases} \tag{3.17}$$

Table 3.4 Black-box networks for benchmark system 2*.

Model	***NARX***	***NOE***	***pruned NOE***
Input(s)	*y(k), y(k-1), y(k-2), u(k), u(k-1),*	*u(k), u(k-1)*	
Output	*y(k+1)*		
Training data	*1001 Samples*		
1st layer neurons	*20*	*20*	*15*
2nd layer neurons	*10*	*10*	*9*
Training time (seconds)	*64*	*190*	*184*
Epochs	*1000*	*50*	
Mean-square error	1.04×10^{-7}	8.57×10^{-8}	8.65×10^{-8}
Activation Function	*Tangent (Bipolar) Sigmoid*		

[*] Linear activation functions are utilized at their output layers.

Fig. 3.16 shows the outputs of both models for this input signal and the plant response. Moreover, Fig. 3.17 illustrates the prediction errors of the compared models throughout the validation scenario. Root-mean-square-errors are calculated as 0.0042 for NOE and 0.0052 for pruned NOE. It is observed that the prediction performance of the pruned NOE model is almost same as that of the original NOE. On the other hand, deleting these 6 neurons from the network considerably decreases the computation burden of the model (as well as memory requirements) as the total number of network parameters is decreased from 341 to 244 (28.4% reduction). It is seen that the proposed pruning method is simple and very effective as the redundant neurons are pruned directly rather than pruning the individual weights.

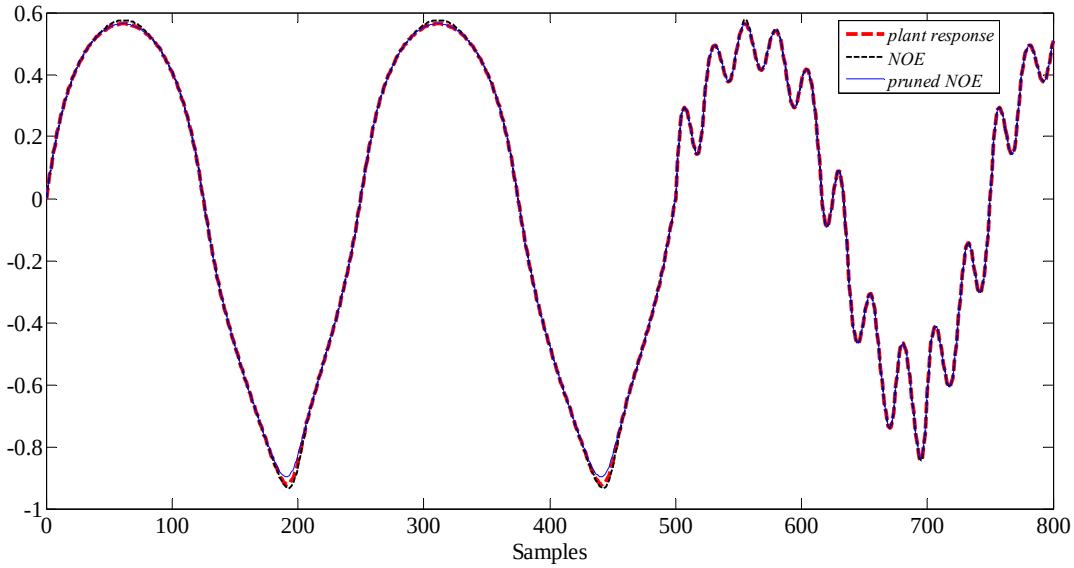

Fig 3.16 Validation performances of NOE and pruned NOE.

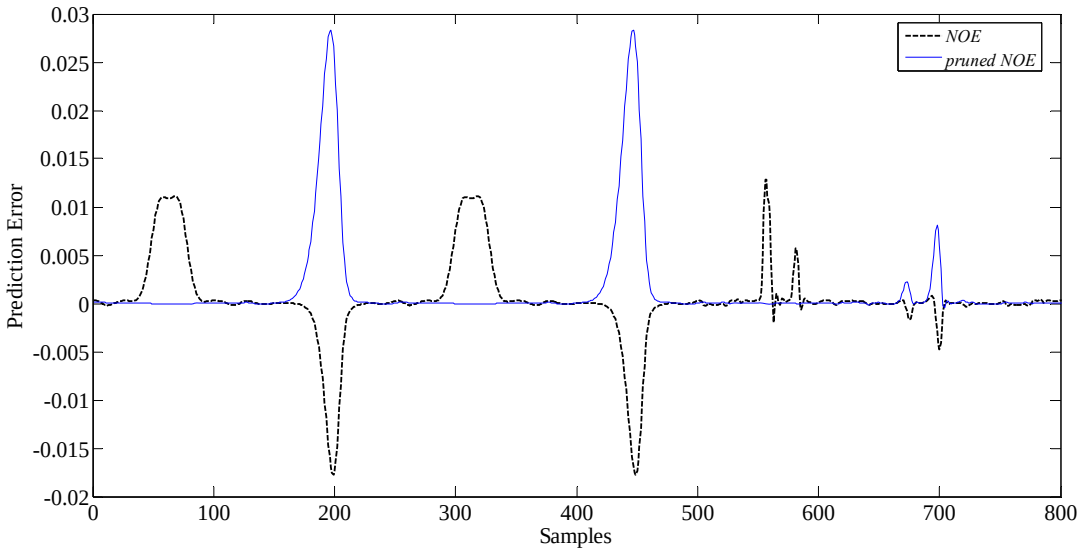

Fig 3.17 Prediction errors of *NOE* and pruned *NOE*.

3.7 Closure

This chapter has presented a modeling and identification procedure for nonlinear dynamic systems using ANNs. First, black-box modeling procedure has been explained. Every step of this identification process (the data preparation, model

structure selection, parameter estimation and model validation) was elaborated in a detailed manner. The procedure was known to be very time-consuming since one need to consider a number of issues (i.e. different model structures, different number of neurons in the chosen model architecture and different initial conditions while starting the training of the parameters). Hence, a general methodology to model nonlinear dynamic systems using SNNs was proposed. Several stages of the proposed methodology (division, unification, and pruning) were all explained in a step wise procedure. Furthermore, some standard library networks were developed and an iterative entropy based pruning algorithm was also proposed, which is one of the contributions of the thesis work.

CHAPTER 4

POSITION ESTIMATION FOR TIMING BELT DRIVES OF PRECISION MACHINERY

4.1 Introduction

Precision positioning systems are used in a wide variety of applications in manufacturing-, automation-, semiconductor-, and biomedical industries (Kulkarni and El-Sharkawi, 2001). Almost all of these systems use a rotary actuator (such as a brushless DC motor) where its angular motion is converted into translation by mechanical power transmission elements like belts, chains, rack-and-pinion, traction (friction) drives, and ball/lead-screws. The drive system is usually selected by considering various issues including positioning accuracy/repeatability sought, travel span, maximum speed, load capacity, and cost. At present, high precision systems (requiring repeatability less than 100 microns) frequently employ rigid (or stiff) elements like ball-screws owing to the fact that comparable performance cannot be achieved with elastic transmission elements like timing belts, cable, chain etc. For the systems with elastic elements, positioning accuracy is obtained through direct load position measurement devices (like linear encoders) at the increased hardware cost (Zhao and Cai, 1996). Furthermore, elastic elements in such arrangements is known to introduce nonlinearities (backlash, spatial variations in stiffness, friction, etc.) to the system which may in turn lead to limit cycles in the controlled system (Li and Rehani, 1996). This drawback oftentimes calls for more elaborate control- and estimation schemes that can compensate for such effects to improve system's stability and performance by incorporating advanced system models (Hace et al., 2005; Zaki et al. 2008). Consequently, the main motivation of

this work is to propose a feasible estimation scheme for timing-belt drives (TBDs) that utilize the information emanating from a low-cost sensor on the driver side (pulley). Hence, the position of the carriage driven through a timing belt could be estimated for cost-sensitive computer numerical control (CNC) applications.

To predict the transmission error of TBDs, detailed dynamic (and kinematic) models must be taken into consideration. Surprisingly, TBDs are somewhat neglected in the technical literature and thus (unlike gears) their dynamic attributes have not been fully investigated. In fact, the transmission error of a TBD depends on many different factors such as belt-pinion material pair, form errors in elements, eccentricity of the pinion, radial/axial vibrations of the belt, belt-tension, interface temperature, etc. Hence, the functional dependency between the actual position of the carriage and that of the pinion is quite complicated. On the other hand, NNs, which are capable of learning complex mappings, are the most suitable tools to approximate these error patterns. Unfortunately, large number of cited nonlinearities makes it quite difficult for a single (recurrent) NN topology to learn the complete task satisfactorily due to weak initial assumptions associated with the NN models. That is, the learning goal cannot be attained through a properly-sized NN topology within a reasonable time frame. As an alternative, a structured neural network topology is also proposed in this chapter for the solution of this challenging estimation problem.

In the presented work, the TBD under study is divided into its components employing the physical models. Unlike classical SNN approach, the inputs of the presented neural networks are speculated via sketchy guidance of the relevant processes under investigation. Hence, the resulting neural networks are trained to explore their sub-domains via extensive training data sets. As a consequence, the overall network is expected to go beyond the physical model at hand so as to capture unaccounted system attributes.

The organization of this Chapter 4 is as follows: After the introduction part, Section 4.2 elaborates the generic TBD considered in this work. Then, Section 4.3

introduces the experimental setup along with a number of accompanying evaluations to investigate the transmission characteristics of a TBD. Based on the information collected, various neural network topologies are proposed in Section 4.4 and Section 4.5. Next, Section 4.6 illustrates the estimation performance of the proposed model. Finally, the key points of the work are discussed in detail in Section 4.7.

4.2 Timing Belt Drive

Fig. 4.1 illustrates the generic TBD considered in this work. There exist two distinct modes of operations in such mechanisms:

i. Teeth of driving pinion and the (driven) timing belt are fully engaged and thus the resulting dynamic system acts like (lower order) lumped system;

ii. Teeth are disengaged due to backlash but (unlike gears) the torque is still transmitted through the friction coupling between these elements.

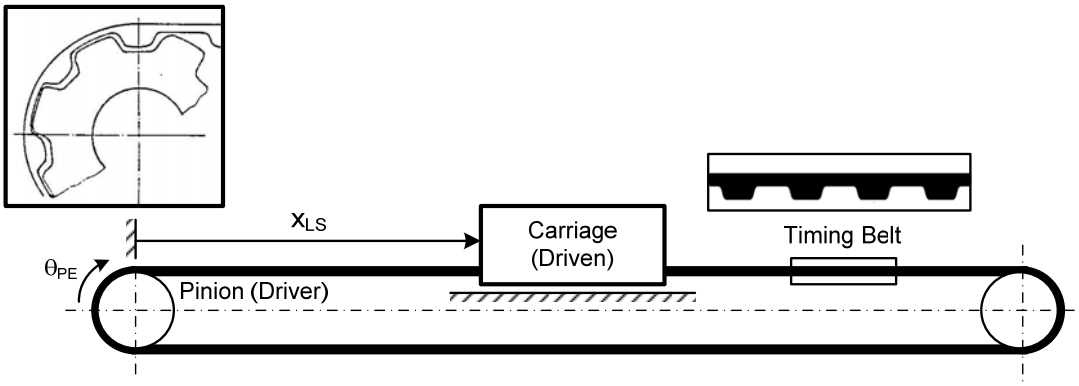

Fig. 4.1 A generic timing (synchronous) belt drive system.

Kilic (2007) offers a dynamic model that takes into account the properties of these regimes. The presented model reveals hysteresis-type nonlinearity. In fact, there exist a significant number of research efforts on systems with hysteresis. The most popular hysteresis model (which is a carry-over from the studies on electro-magnetism and ferromagnetic materials) is the Preisach model (Mayergoyz, 1991).

This domain-independent modeling technique has well-defined features (such as its ability to model complex hysteresis types, identification algorithm, and implementation) which make it a suitable candidate for control applications. Unfortunately, the Preisach model is not particularly adequate to model the hysteretic effects of TBDs since such dynamic systems evidently incorporate both local- and global memory which is a condition violating the congruent minor-loop property of basic Preisach model.

Note that devising general-purpose estimator/observer (with nonlinear properties), which directly embodies such complex dynamic models, is quite challenging due to obvious implementation difficulties such as numerical instability, divergence, high real-time computational cost, etc. Hence, this study proposes a feasible “gray-box” approach for the estimation problem at hand.

4.3 Experimental Studies

To develop a general-purpose estimator, the transmission error of a TBD (not subjected to any external load or any other change in its operation parameters) should be repeatable (i.e. deterministic). Thus, a test setup is designed to test the validity of this basic assumption first. Remaining of this section introduces the test setup and the experimental procedure implemented on this setup.

4.3.1 Test Setup

Figs.4. 2 and 4.3 show the experimental setup and its corresponding schematic. Here, the preload of TBD can be adjusted by changing the location of the free wheel. Note that the belt preload is not measured but indirectly estimated by considering the nominal stiffness of the timing belt. A high resolution linear scale (LS) is integrated into this setup for modeling and verification purposes. This experimental setup is used to simulate several scenarios where the velocity and acceleration profiles of the carriage are accurately controlled to investigate the slip dynamics of the mechanism.

To detect the error of primary encoder (PE) measuring the displacement of transmission system, the position measurements of the PE are to be compared to those of the high-resolution LS that is directly coupled to the carriage. Due to the limitations of physical layout of the stage, the measurement axes of the LS and that of the PE do not coincide as illustrated in Fig. 4.3. In order to come up with an accurate kinematic model, the Abbe offset errors have to be considered:

$$e \hat{=} x_{LS} - x_{PE} = \delta_x(x_{PE}) + A_z\varepsilon_y(x_{PE}) - A_y\varepsilon_z(x_{PE}) \tag{4.1}$$

where x_{LS} and x_{PE} refer to the position measurements of the LS and PE, respectively. A_y, A_z are the Abbe offsets (positive); ε_y, ε_z are the small angular rotations (a few arc-seconds) about principal axes; δ_x denote the displacement error introduced by the transmission system. Thus, *e* in (4.1) includes the geometric/kinematic errors associated with the support elements (anti-friction bearings, rails) as well.

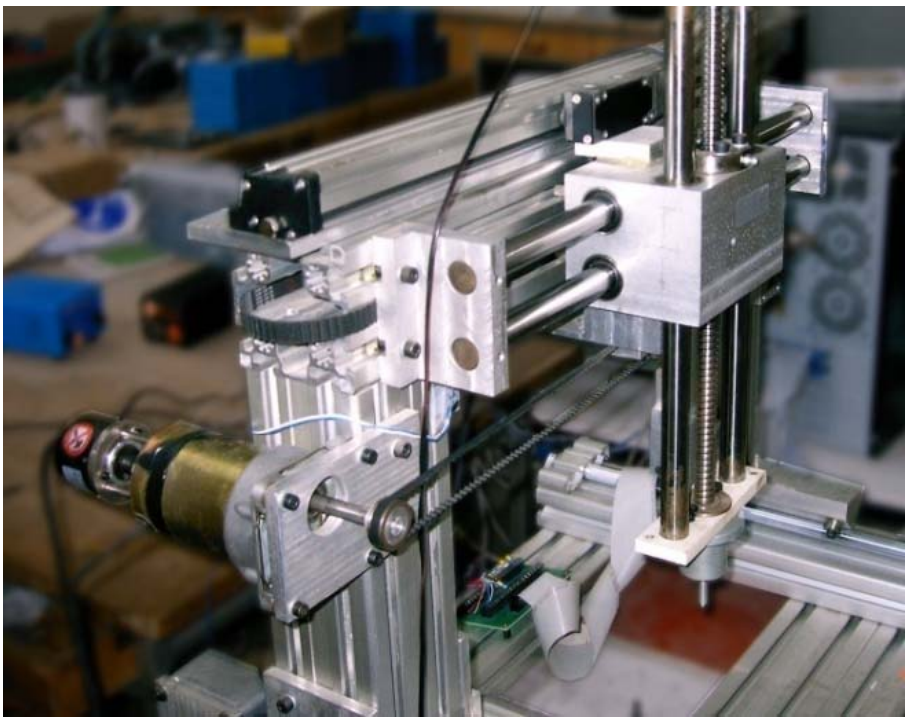

Fig. 4.2 General view of the setup.

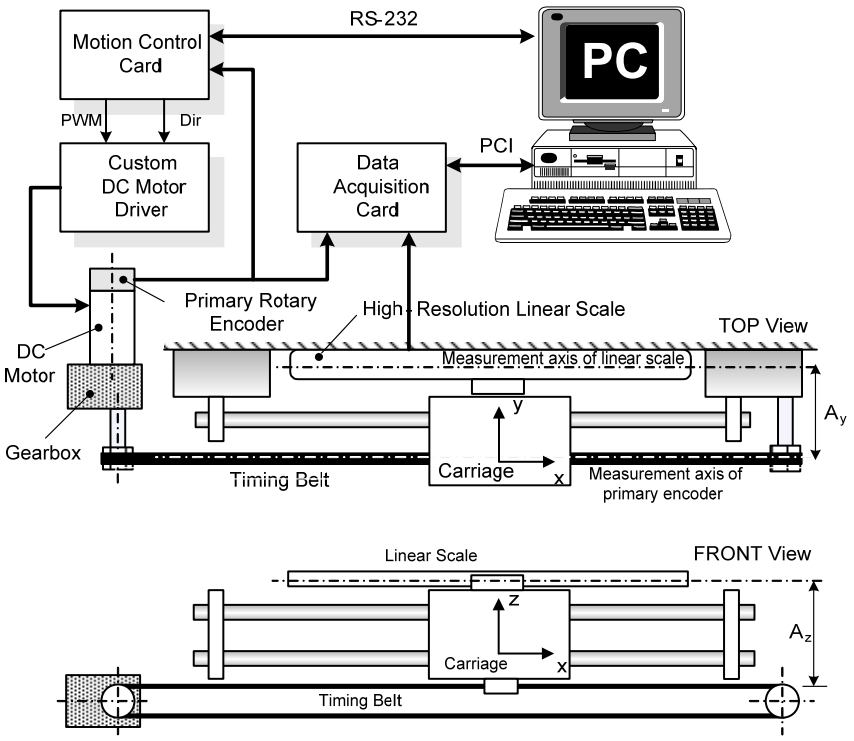

Fig. 4.3 Schematic of experimental setup.

4.3.2 Experiments

In this work, several tests are conducted to show the repeatability of the motion which is a prerequisite to devise reliable reference models. In all tests, the motor's velocity is accurately controlled along a trapezoidal path as shown in Figure 4.4. This velocity pattern corresponds to a carriage round-trip along a 300mm path. Thereafter, the carriage is driven with constant velocity (assumed to be in steady-state, i.e., the acceleration / deceleration of the system is negligible) along its full span, the positioning error patterns (e) for twelve different (overlaid) trajectories are plotted in Fig. 4.5.a. Fig. 4.5.b shows the zoom window in Fig. 4.5.a. Note that the waveform (with low-frequency content) in Fig. 4.5.a (shown as dashed red line) is the (low-pass filtered) positioning error and is employed as a reference for the major hysteresis band. As can be seen from Fig. 4.5.b, the positioning errors are quite repeatable (systematic) which in turn encourages the development of advanced estimator models. Despite its high repeatability, the tooth-passing frequency component is deliberately neglected in this work owing to the fact that

this component is mainly a function of form errors associated with the timing belt and pinion. Hence, it highly depends on starting position (i.e. initial conditions) of the mechanism.

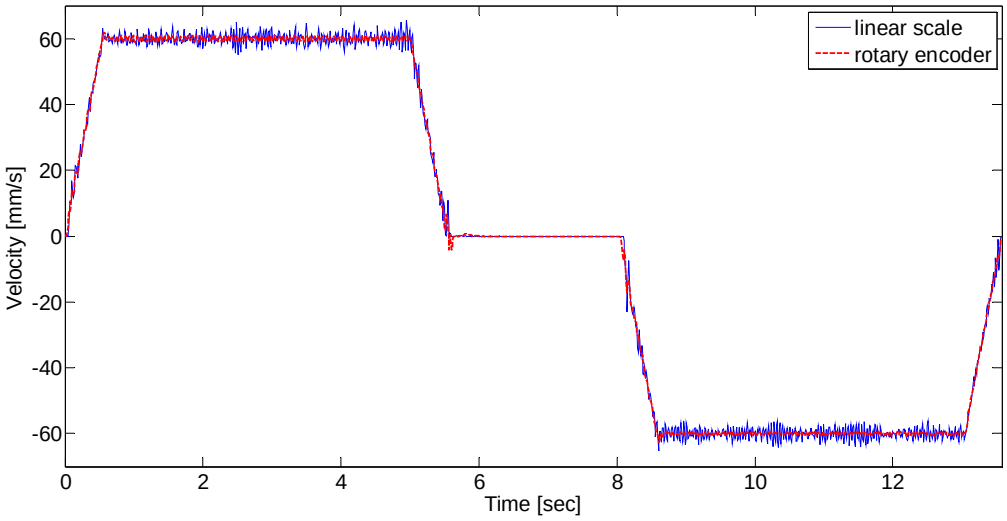

Fig. 4.4 Velocity profile of the carriage measured from the LS and the PE.

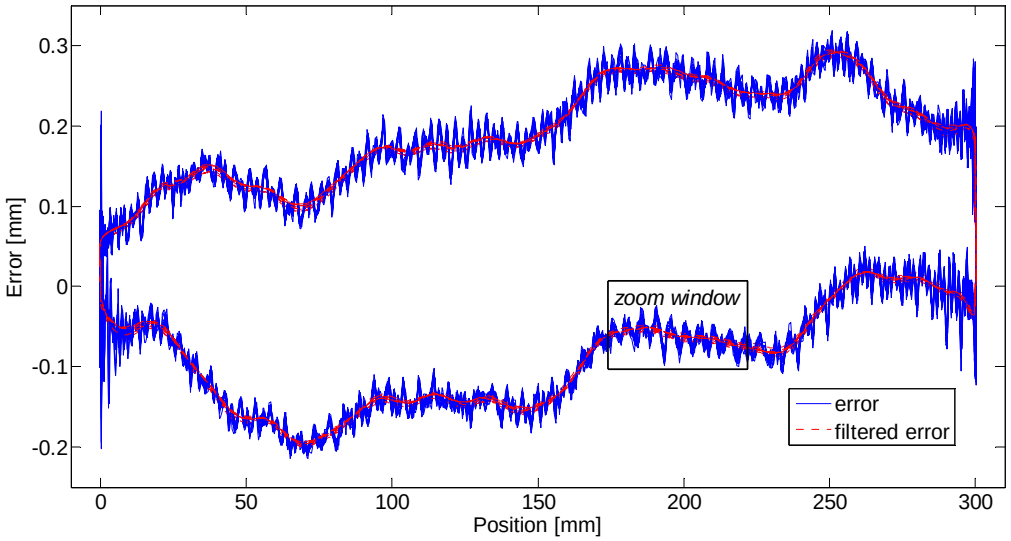

a) Error trajectories.

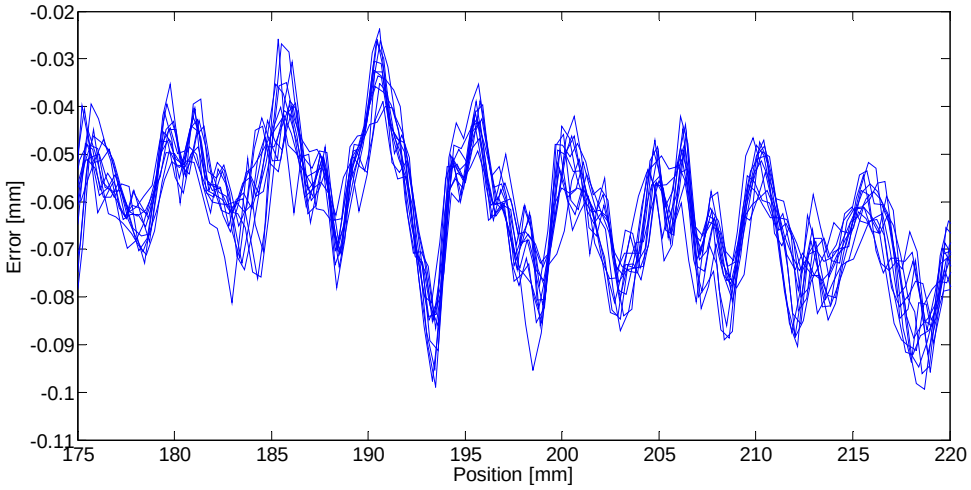

b) Exploded view.

Fig. 4.5 Position error trajectories of 12 different cases.

Close examination of the error patterns in Fig. 4.5 reveals critical points about the attributes of the system under investigation:

- Hysteresis band, which is roughly 0.3 *mm* for the test cases, is apparently a consequence of the backlash between the timing belt and the driving pinion (pulley). It is obvious that an increase or decrease in the belt tension will create contraction or expansion in the length of the timing belt which in turn modifies dead-zone characteristic of meshing teeth pairs (Kulkarni, El-Sharkawi, 2001). Note that in all the experiments the operating conditions (carriage mass, ambient temperature) along with belt preload are kept constant.
- As mentioned earlier, unless A_y and A_z are zero [see (4.1)], the Abbe offset errors manifest themselves as the waveforms on the upper and lower boundaries. Hence, mechanical manipulations on the bearing elements usually impress a different texture on these bounds. That is, the use of different linear bearing elements (with different geometric form errors, running parallelism and straightness errors) and/or corresponding assembly errors creating geometric

congruence between interfacing elements might alter the spatial attributes of the major hysteresis band.

- A fundamental harmonic component (with a magnitude of 15 microns) superimposed onto the band is at the tooth-passing (meshing) frequency (i.e. carriage velocity ÷ pitch) of the timing belt and thus the observed variations could be mainly attributed to the effect of belt-climbing as well as the form errors of the belt (Kagotani et al., 2001).

Harmonics injected by the two-stage gearbox of the motor appear to be quite negligible while the transition in the backlash zone (of which has bandwidth of 0.12 mm) is extremely fast (< 1 *ms*) when a change in the direction of motion is observed.

The next set of experiments focuses on the effect of velocity and inertial forces on the transmission error. As can be seen from Fig. 4.6, the dramatic changes at the steady-state velocity have some influences on the nature of the nonlinear relationship. Moreover, the effect of inertial forces is investigated by modifying the acceleration and deceleration profile of the controlled motor such that the sliding motion inside the hysteresis band is induced under the action of these inertial forces. The inertial forces do not have a considerable effect on the closing distances as illustrated in Fig. 4.6. To identify the reversal path inside the hysteresis band, the TBD mechanism is programmed to reverse its course at every 25 *mm* and go back to its starting point. This procedure is repeated in both directions (forward and backward). Similarly, the collected (and low-pass filtered) data shown in Fig. 4.7 reveal the closing distances when the direction of motion is reversed at the above mentioned intervals. It is obvious that when the direction of travel is reversed, the power transmitting teeth disengage and micro-slip under external excitation comes into play. As a consequence, the belt slowly slides until the different set of teeth pairs engage into transmission. Unfortunately, developing dynamic models that explain the observed phenomena satisfactorily is known to be quite challenging and is an active research field in tribology (Astrom and Canudas-De-Wit, 2008).

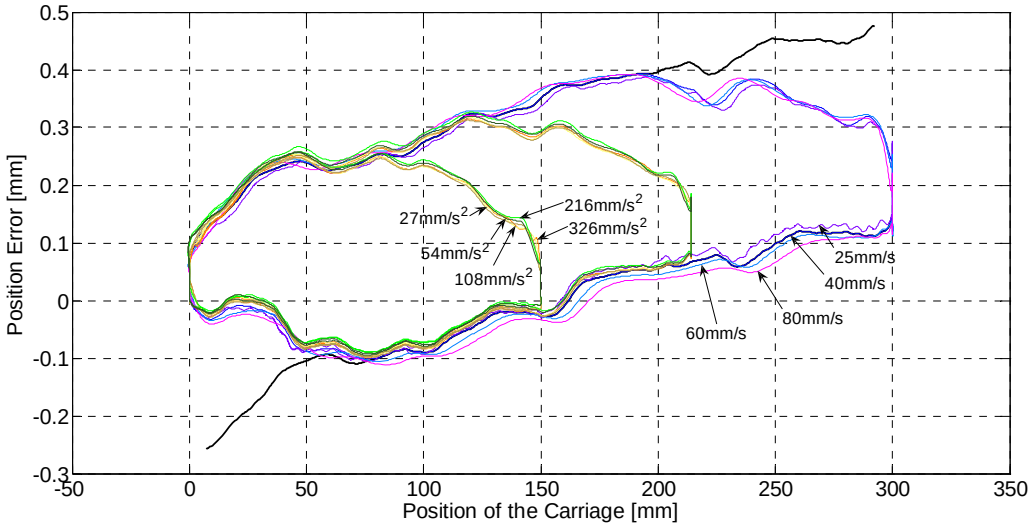

Fig. 4.6 Effect of velocity and inertial forces on the transmission error.

These preliminary experimental studies show that the response of an unloaded system is quite repeatable. Thus, the changes due to velocity and acceleration can be stored and may be recalled (and interpolated) later for corrective actions ("compensation"). This suggests the development of an estimator so that the position of the carriage, $\hat{x}(k)$, can be calculated using the indirect measurements of the PE as

$$\hat{x}(k) = x_{PE}(k) + e(k) \tag{4.2}$$

where k is the time index.

4.4 Conventional Neural Network Designs

Functional relationship between the transmission error of the mechanism and the PE readings is dominated by hysteretic effects as can be seen in Fig. 4.7. To develop a conventional NN to capture the desired functional dependency, one needs to identify the relevant inputs and outputs of the network. Kilic et al. (2007) propose a number of interpolation algorithms to approximate the above-mentioned function. All of the presented algorithms can be generically expressed as

$$e(k) = f(x_{PE}(k), x_{PE}(k-1), x_{PE}(k-2), x_{PE}(k-d), e(k-d)) \tag{4.3}$$

where $x_{PE}(k)$, $x_{PE}(k-1)$, $x_{PE}(k-2)$ refer to the history of the PE readings while d (a time-variant positive integer) denotes the time index when the direction change takes place. Here, $f:\Re^5 \rightarrow \Re$ represents a Borel measurable function. A RNN can theoretically capture the desired mapping when all necessary states are presented to the network at a particular instant (Seidl and Lorenz, 1991).

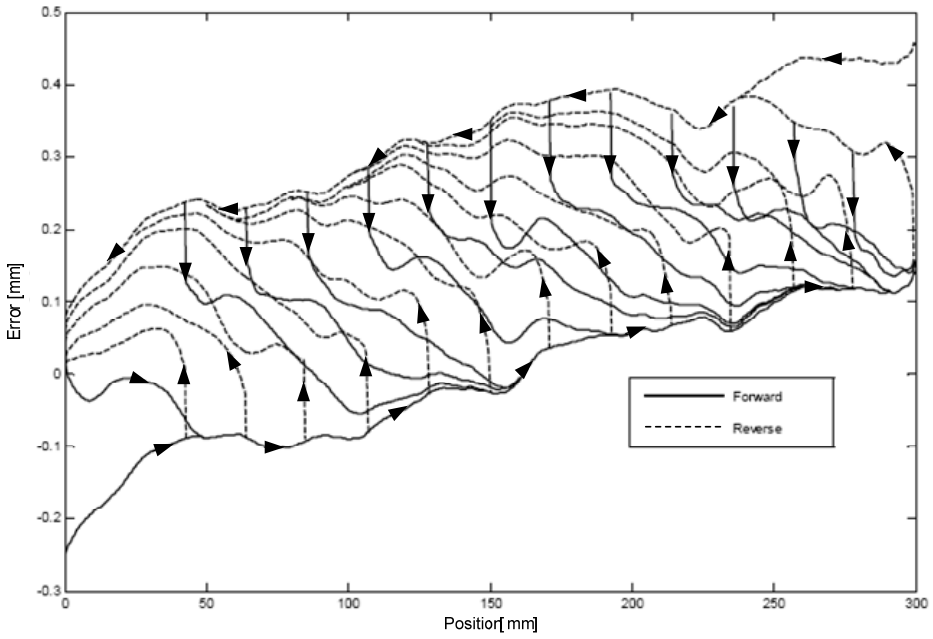

Fig. 4.7 Position errors on motion reversals at various locations.

In fact, there exists an extensive literature on modeling/identification of hysteretic systems using ANNs. Previous studies deal with the hysteresis-type problems using the outputs of the elementary hysteresis operators of the Preisach model as inputs to the designed FNNs (Zhang and Tan, 2010). For example, Zhao and Tan (2008) propose a hysteretic operator that was based on the classical Preisach model to construct an expanded input space of the hysteresis. Moreover, there are some recent studies which design hysteresis-type ANN models by changing the activation

function of the neurons whose characteristic is hysteretic (Lien et al., 2010; Deng and Tan, 2008).

Within the framework of transmission error estimation, several (supervised) RNN topologies such as Elman-type RNNs, NOE and fully-recurrent neural network (FRNN) are considered to approximate the nonlinear relationship. It is well known that the Elman-type networks are based on FNNs except that they have feedback connections from hidden layer units to the context units. In NOE, the output of the second layer is directly connected to the first hidden layer as input. Moreover, all the layers have feedback connections to the other layers (including self-feedback) in FRNN. The major assumption here is that the output feedback and the internal feedback connections of these ANNs are sufficient to form a relevant memory model (i.e. long-term) implicitly to capture the relationship in (4.3).

The training results of the various RNN models using the input signals in (4.3) are shown in Table 4.1. As could be seen, the Elman-type RNN (with 50 neurons in its hidden layer), whose training performance is presented in Fig.4.8, has the smallest training error. Unfortunately, this network's generalization performances on some arbitrary motion scenarios (which will be elaborated in Section 4.7) are unsatisfactory as could be seen from Fig. 4.9. When the number of hidden-layer neurons of the network is increased, the training error reaches to an acceptable level (about 15 μm) after a long training session on a high-end PC (with Intel Core i5 processor and a SDRAM of 4GB). However, the Elman-type networks fail in the validation scenarios due to various reasons including well-known bias/variance dilemma (German et al., 1992). Furthermore, when gradient-descent based training methods are utilized, the developed NNs are not guaranteed to converge to a global minimum (in a vast parameter space) within a reasonable training period. Within this context of this study, the Elman-network was clearly not able to form a long-term memory that allows the recall of the nominal position as well as the error estimate [namely, x_{PE}(k-d) and e(k-d)] when the direction had changed. Therefore, independent of the network architecture, the obtained results are unacceptable for estimation and modeling purposes (i.e. modeling error >> 15 μm).

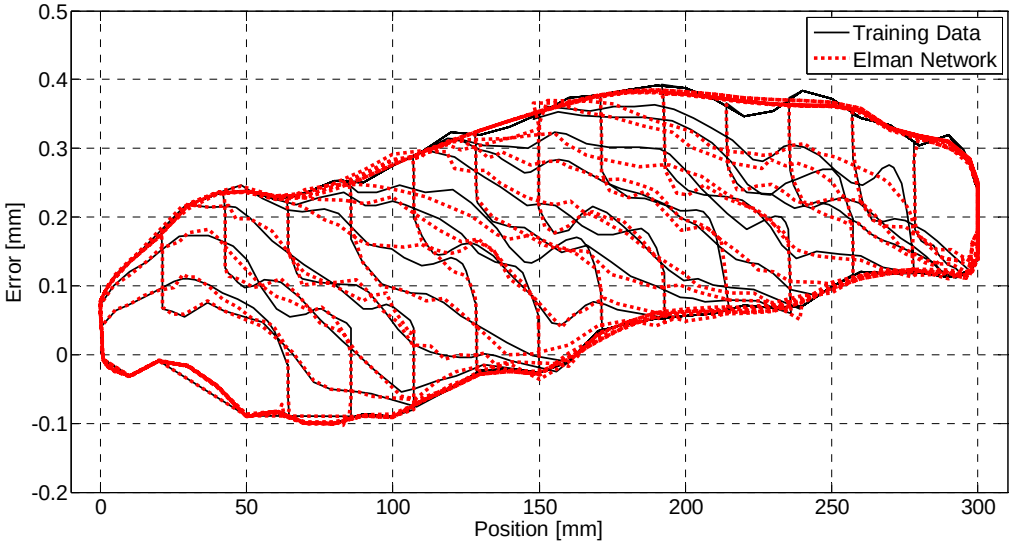

Fig. 4.8 Training performance of the Elman-type RNN.

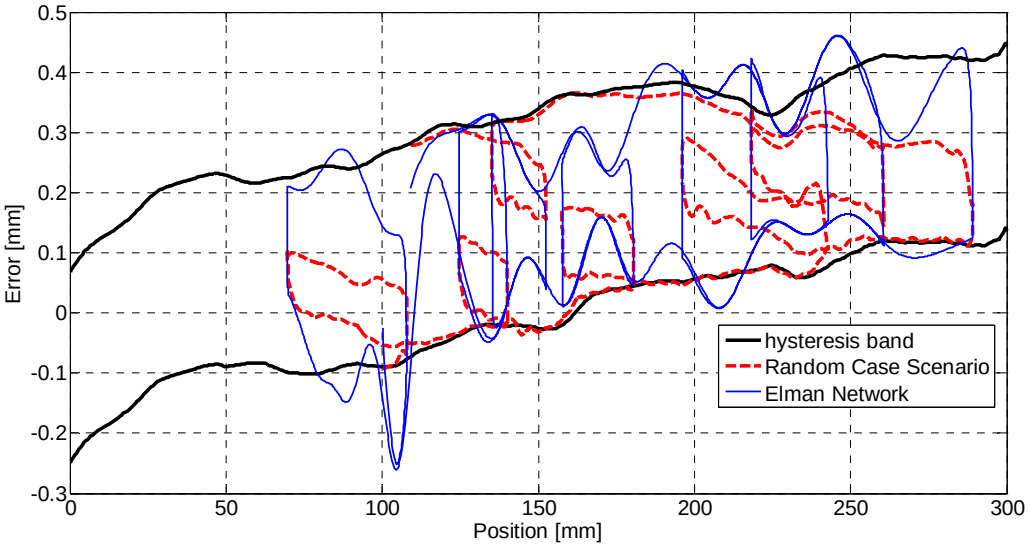

Fig. 4.9 Generalization performance of the Elman-type RNN on Scenario 2.

Table 4.1 Training results of the Elman-type RNN, NOE, and FRNN [*]

Inputs	x(k), x(k-1), x(k-2)								
Output	Position Error								
Training Data	1067 Samples								
Act. Func.	Tangent Sigmoid								
Training Method	Levenberg-Marquardt								
Architecture	**Elman-type RNN**			**NNOE**			**FRNN**		
1st Layer Neurons	10	25	50	10	25	50	10	25	50
Training error in (μm)	23	19	15	34	33	28	27	22	17
Epochs	125								
Training time in (*min*)	7.5	15.5	55	4	5	6	13	26	85

[*] Linear activation functions are utilized at their output layers.

4.5 Structured Neural Network Architecture

Estimation problem at hand can be decomposed into a number of well-defined sub-problems that are known to be associated with different operating regimes of the mechanism. Once a NN is devised to capture the characteristics of each regime, the corresponding networks can be transformed into a single network to represent the overall dynamics of the system accurately.

Looking at Fig. 4.7, one can directly identify four different operating regimes for the given mechanism:

1. Mechanism moves in the forward direction (left to right) while the power/torque transmitting teeth are fully engaged. The carriage follows the lower bound of the hysteresis band.

2. Mechanism moves in the reverse (backward) direction (right to left) while the power transmitting teeth are fully engaged. The carriage follows the upper bound of the hysteresis band.

3. Mechanism changes its course towards the forward direction and thus the power transmitting teeth become disengaged. In this transient regime, the driving torque is transmitted through the friction coupling between the pinion and the belt. Depending on the reversal position, a path inside the hysteresis band (indicated by solid lines) is followed.

4. Mechanism changes its course towards the reverse direction and thus the power transmitting teeth become disengaged. The driving torque is again transmitted through the friction coupling between the pinion and the belt. Depending on the reversal position, a path inside the hysteresis band (indicated by dashed lines) is followed.

Hence, four different ANNs can be designed to capture/model the mechanism's behavior in each region: ANN_e^+, ANN_e^-, ANN_d^+, ANN_d^- where the superscripts **+** and **–** denote the forward- and reverse directions while the subscripts "e" and "d" indicate the engagement / disengagement status of the power transmitting teeth in the mechanism. Fig. 4.10 illustrates the SNN incorporating these units. It is critical to note that the physical parameters of the timing belt (e.g. pitch of the timing belt, width, length, mass, number of pinion teeth etc.) are not directly utilized in the overall network. Since each ANN is trained separately, the weights of the overall SNN is to implicitly encode the relevant physical parameters.

In this configuration, ANN_e^+ and ANN_e^- represent the lower- and upper boundaries of the hysteresis band in Fig. 4.7. Since there is a one-to-one correspondence between x(k) (carriage position) and e(k) (estimated error), these networks employ x(k) as input. Similarly, ANN_d^+ and ANN_d^- are trained to approximate a family of trajectories (curves) lying inside the hysteresis band between the upper and lower boundaries. In other words, these networks are expected to model the "creep" behavior of the timing-belt beginning from the disengagement of teeth until the engagement on the other side of the dead-band. Notice that these two networks have two inputs: **i)** reversal (starting) point on the boundaries of hysteresis band; **ii)** relative (incremental) position with respect to the starting point on the boundary. If

direction reversal takes place inside the hysteresis band (i.e. when the torque/force is transmitted through friction coupling), the correct course of return needs to be determined. Hence, two different networks (ANN_{sp}^{+} and ANN_{sp}^{-}) are specifically designed to determine "starting point" (of reversal) on the target boundary using the information available at the turnaround point inside the band.

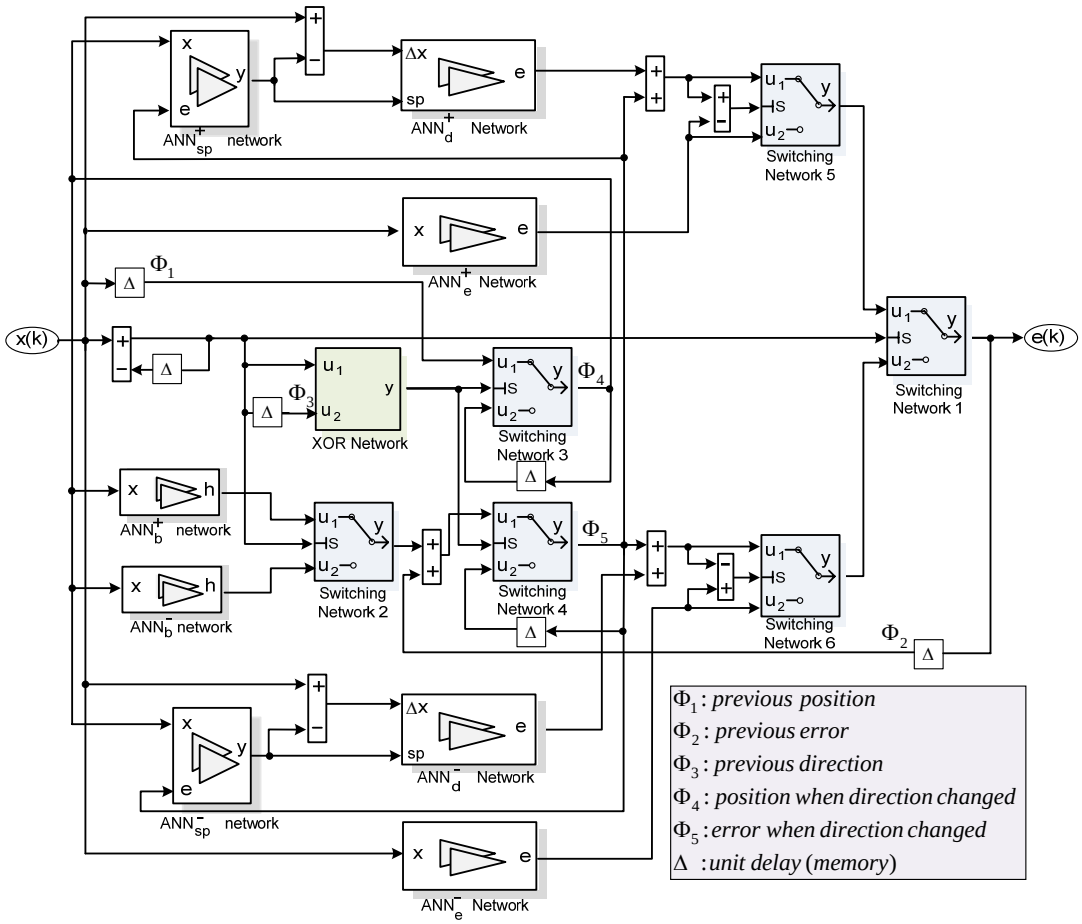

Fig. 4.10 SNN topology for estimating the position error of the carriage.

Notice that when the direction is reversed (in Fig. 4.7), a considerable jump is observed at the starting point of a traversed path owing to the fact that the built-in gearbox of the motor used in this study does have a significant gear backlash. Hence, two ANNs (namely, ANN_b^{+}, ANN_b^{-}) are included to the SNN to calculate

the play introduced by this gearbox. Note that ANN_d^+ and ANN_d^- could be trained to learn this hard-nonlinearity as well. However, when included, the corresponding approximation error does increase drastically despite the addition of neurons. Hence, predicting this (easy-to-model) nonlinearity through the use of separate networks provides a more effective solution.

As a result, eight separate ANNs are connected together to form a "mixture of experts" via switching (or gating) networks that essentially perform multiplexing operations among the network outputs. Design of such NNs is discussed in Section 3.5.1. Here, switching networks Type 2 are used for the implementation of the below task

$$y = \begin{cases} u_1, & s \geq 0 \\ u_2, & s < 0 \end{cases} \tag{4.4}$$

The resulting SNN can be viewed as a finite state machine with five states (Φ_1 … Φ_5). In this topology, the *Switching Network 1* selects the outputs of the relevant networks depending on the current direction of the carriage (i.e. *sgn*{x(k) – x(k-1)}). Moreover, the direction change is detected via the FNN (with 2 hidden layers) performing logical exclusive-OR (XOR) operation.

Note that if a change in direction is detected, the *Switching Network 3* immediately latches the last position onto the Φ_4 state. Similarly, the *Switching Network 4* updates the Φ_5 state that essentially holds the last error value including the backlash calculated by ANN_b^+or ANN_b^-.

When the direction is changed inside the hysteresis band (i.e. teeth are disengaged), the error could be calculated by first adding the backlash value. Then, the resulting value is used to find the starting point on the hysteresis boundaries using ANN_{sp}^+or ANN_{sp}^-. It is critical to note that in the presented SNN architecture, the states must continuously monitored to switch to the output of "correct" network (i.e. choose the proper alternative). For instance, the transition from dead-band to its boundary is

determined by comparing the outputs of ANN_d and ANN_e: if the output of ANN_d^+ is less than that of ANN_e^+, the output of ANN_e^+ becomes effective. When the output of ANN_d^- is greater than that of ANN_e^-, the output of ANN_e^-should be selected.

For the ANNs in the proposed architecture, a number of standard neural networks available in the literature can be utilized. Among these alternatives, FNN, RBF and RNN are considered. Table 4.2 summarizes these networks and their corresponding properties. The next section evaluates the performance of the proposed SNN employing these networks as its components.

Table 4.2 Architectures of the FNN, RBF and RNN networks*

		ANN_e^+	ANN_e^-	ANN_d^+	ANN_d^-
	Input(s):	Position		Incremental Position and Starting Position	
	Output(s):	Position Error		Incremental Position Error	
	Training Data:	601 Samples		2×1961 Samples	
	Training (rms) error:	< 10 μm			
	Epochs:	50		225	
FNN	**1st Layer Neurons:**	8		60	
	Activation Function:	Tangent Sigmoid			
	Training Method:	Error Back-propagation / Gradient Descent			
RBF	**1st Layer Neurons:**	24	26	233	237
	Activation Function:	Gaussian			
	Training Method:	K-means clustering & Recursive Least Squares			
RNN	**1st Layer Neurons:**	12		90	
	Activation Function:	Tangent (Bipolar) Sigmoid			
	Training Method:	Levenberg-Marquardt			

[*] Linear activation functions are utilized at their output layers.

4.6 Results and Discussions

The estimation capabilities of the proposed SNN are investigated by considering four arbitrary motion scenarios for the carriage. In each case, the user controls the velocity and the direction of the carriage manually (at will). The attributes of these cases are summarized as follows:

- **Scenario 1**. During its forward motion course, the carriage loops (i.e. oscillates) around 75, 150, 245 and 295 mms respectively. Similarly, while in the reverse course the carriage performs these loops at 80, 150 and 230 mms respectively. Fig. 4.11 shows the trajectory (position and velocity) of the carriage for this case. The carriage maintains an average velocity of 32 mm/s on the overall course (when meshing teeth fully engage). While looping, the pinion- and timing belt teeth disengage at the beginning and then re-engage when reaching the starting point at the end of the reversal course.

- **Scenario 2.** This case is similar to the first scenario except that this case contains longer loops which commence at different points on the course as could be seen from Fig. 4.12. Note that this case, in which the corresponding average velocity is 28 mm/s, is selected such that the loop starting points are distributed out quite evenly throughout the whole travel span.

- **Scenario 3.** This case, which is illustrated in Fig. 4.13, constitutes five loops on the forward course and five loops on the backward one. Some of the loops are cascaded such that the direction is reversed before the meshing teeth fully engage. For this case, the carriage maintains an average velocity of 24 mm/s when meshing teeth are fully engaged.

- **Scenario 4.** This case, which is shown in Fig. 4.14, resembles its predecessor except the loop starting points. The average velocity maintained on the loops (i.e. in the region where meshing teeth disengage) is slightly higher than its counterpart.

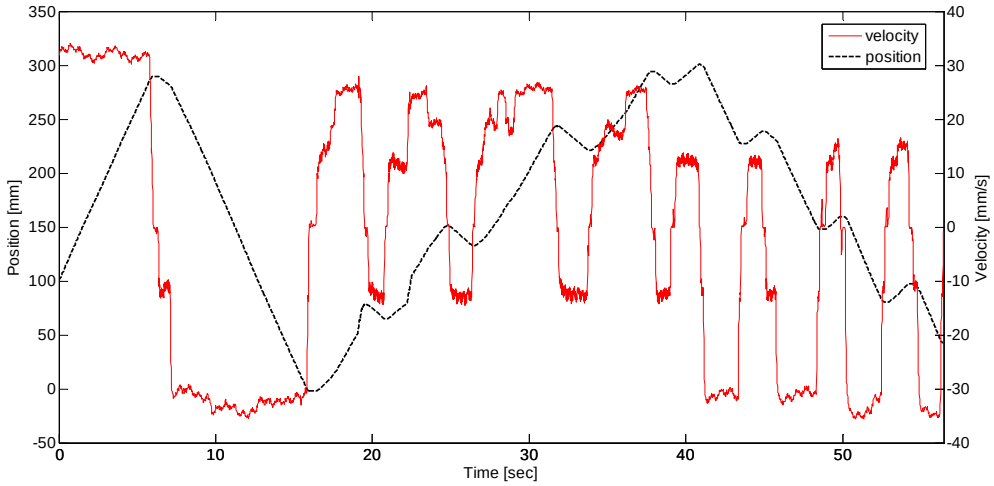

Fig. 4.11 Position- and velocity-states of the carriage in Scenario 1.

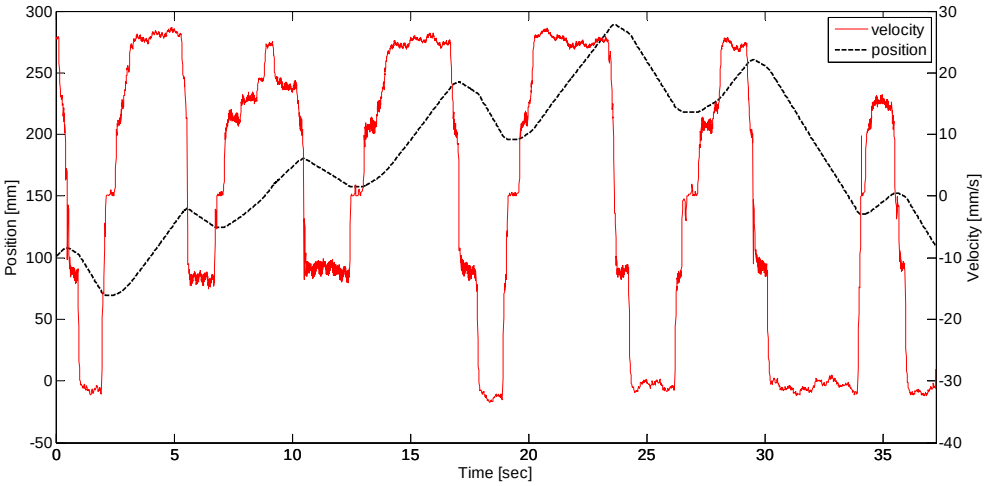

Fig. 4.12 Position- and velocity-states of the carriage in Scenario 2.

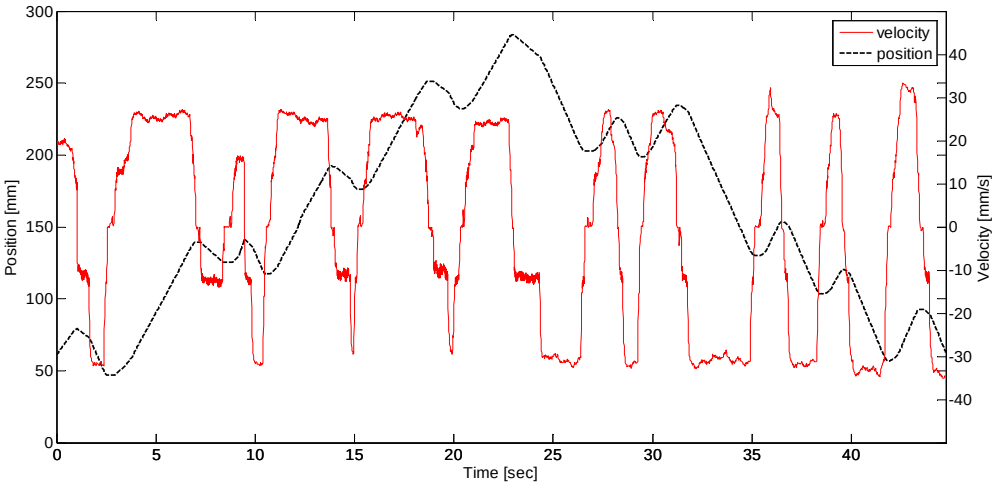

Fig. 4.13 Position- and velocity-states of the carriage in Scenario 3.

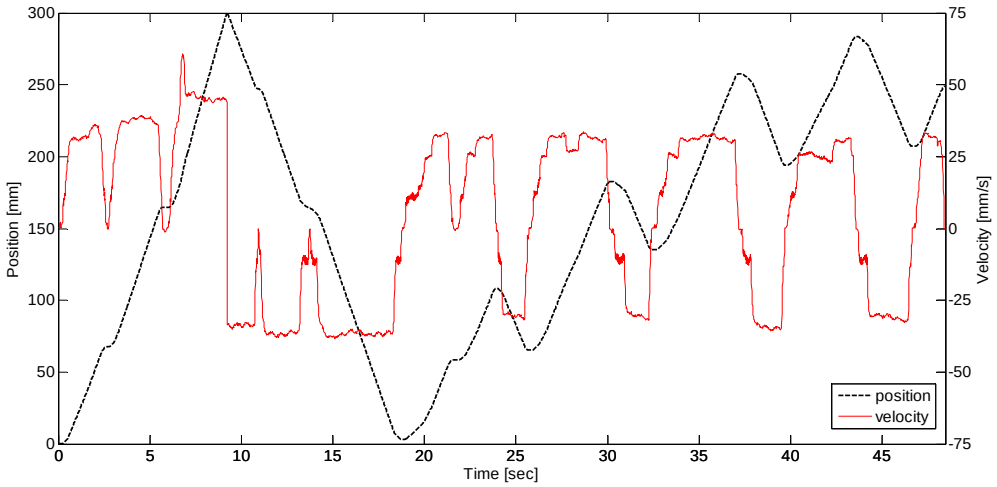

Fig. 4.14 Position- and velocity-states of the carriage in Scenario 4.

Figs. 4.15 to 4.26 demonstrate the estimation performances of the SNN topology on each case. As for quantitative analysis, the key results [in terms of "estimation error" characteristics along the traversed trajectory for a SNN incorporating three different NN types (FNN, RBF, RNN)] are summarized in Table 4.3. Moreover, Table 4.4 gives the estimation errors on major – and minor hysteresis loops separately. Note that the major loop is associated with the motion where belt teeth essentially mesh with pinion teeth. That is, it corresponds to the motion on the upper- and lower bounds of the hysteresis band. On the other hand, the minor loop refers to the motion inside the band where the meshing teeth of the mechanism are fully disengaged and the motion is transmitted by friction coupling. Figs. 4.15, 4.16, and 4.17 show the results of the considered networks for Scenario 1.

Table 4.3 Estimation errors (in μm) for each NN employed in the SNN.

	Scenario:	**1**	**2**	**3**	**4**
FNN	**Max**	145.2	116.1	92.5	132.6
	Min	-133.6	-92.2	-149.3	-127.2
	RMS	24.1	25.4	30.1	26.8
RBF	**Max**	101.1	113.4	102.3	129.5
	Min	-169.2	-85	-192.8	-136.7
	RMS	25.9	25.5	33.8	27.3
RNN	**Max**	76.7	109	92.5	127.8
	Min	-142.7	-100.7	-176.9	-91.1
	RMS	24.9	26.1	34.2	25.9

Table 4.4 Estimation errors (in μm) on major- and minor hysteresis loops.

Scenario	1		2		3		4	
	Major	**Minor**	**Major**	**Minor**	**Major**	**Minor**	**Major**	**Minor**
FNN	12.7	30.6	16.6	27.9	21.8	33	18.4	28.8
RBF	12.8	32.9	16.4	28.2	21.6	37.6	19.7	30.2
RNN	14.8	31	19.9	28	22.7	37.9	20.3	29.7

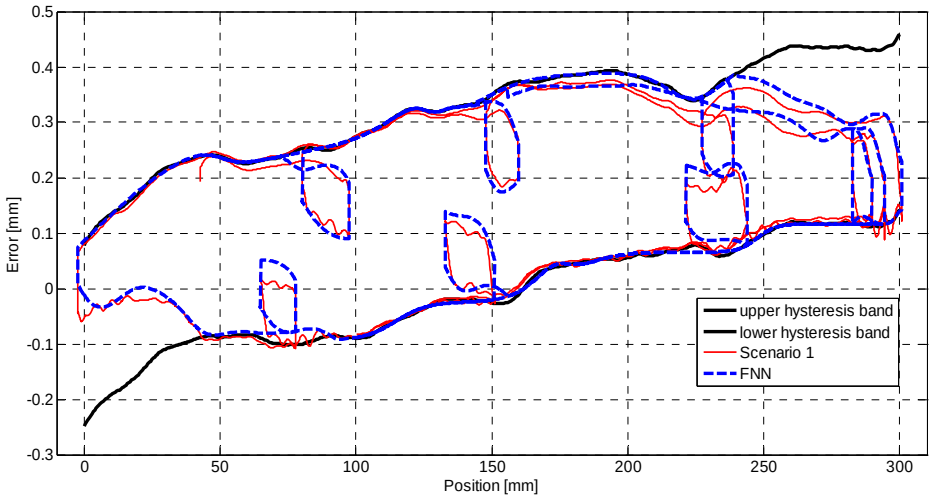

Fig. 4.15 Response of the SNN comprising FNNs for Scenario 1.

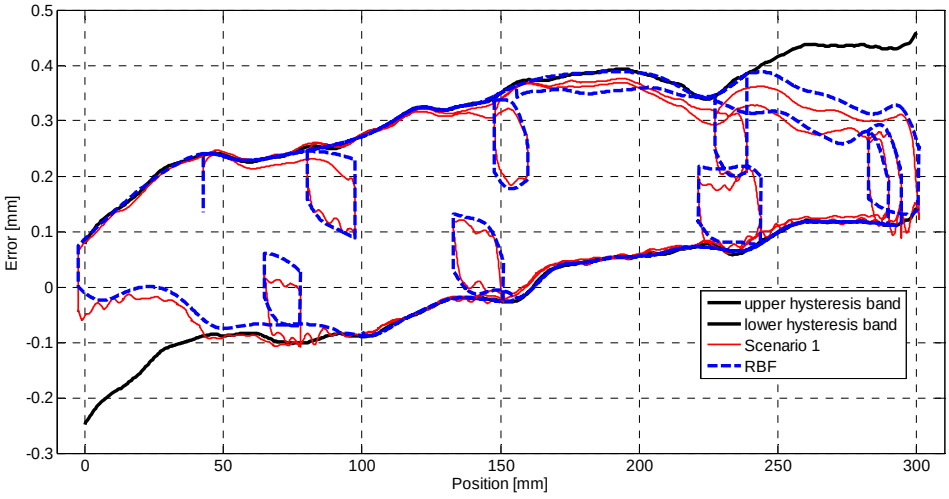

Fig. 4.16 Response of the SNN comprising RBFs for Scenario 1.

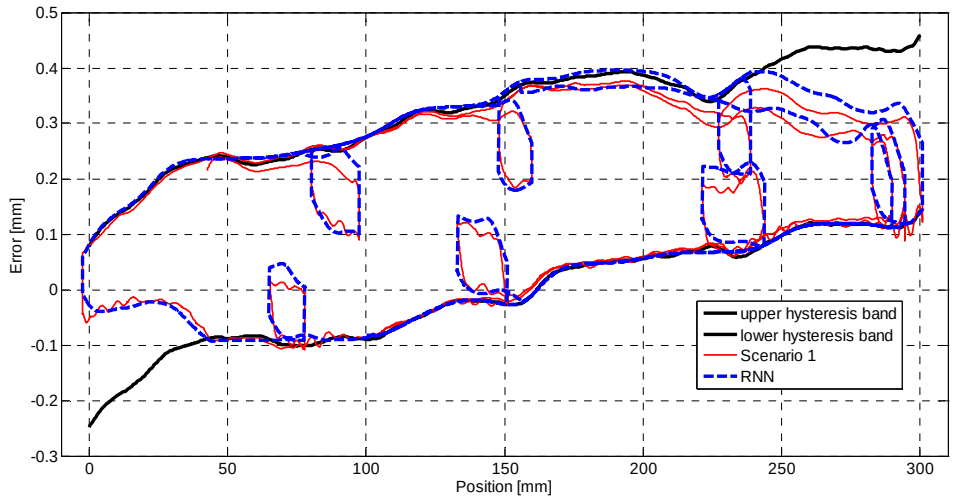

Fig. 4.17 Response of the SNN comprising RNNs for Scenario 1.

As could be seen, the positioning errors generally vary between 10 and 15 μm on the main (upper and lower) hysteresis bands whereas the positioning errors are about 30 μm on the minor loops. Similarly, the performance of the tested networks for Scenario 2 could be seen from Figs. 4.18, 4.19, and 4.20 for SNN with FNNs, RBFs, and RNNs respectively.

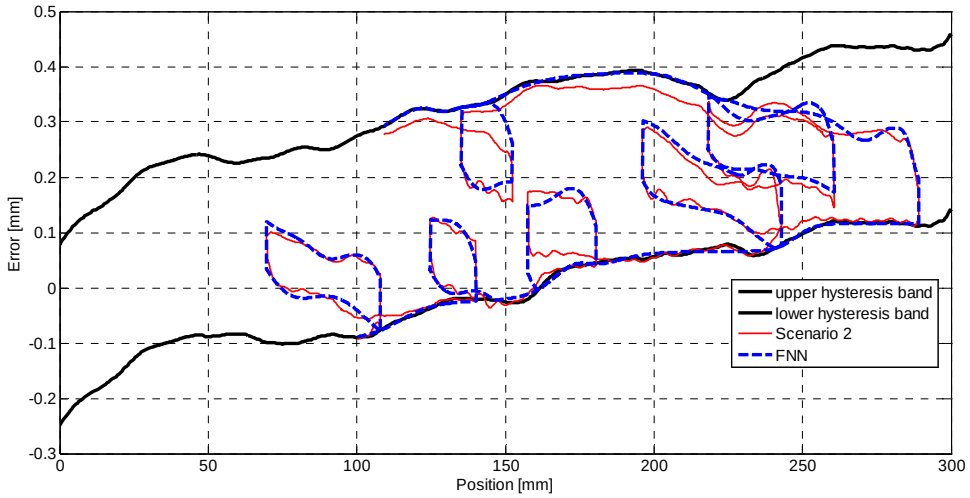

Fig. 4.18 Response of the SNN comprising FNNs for Scenario 2.

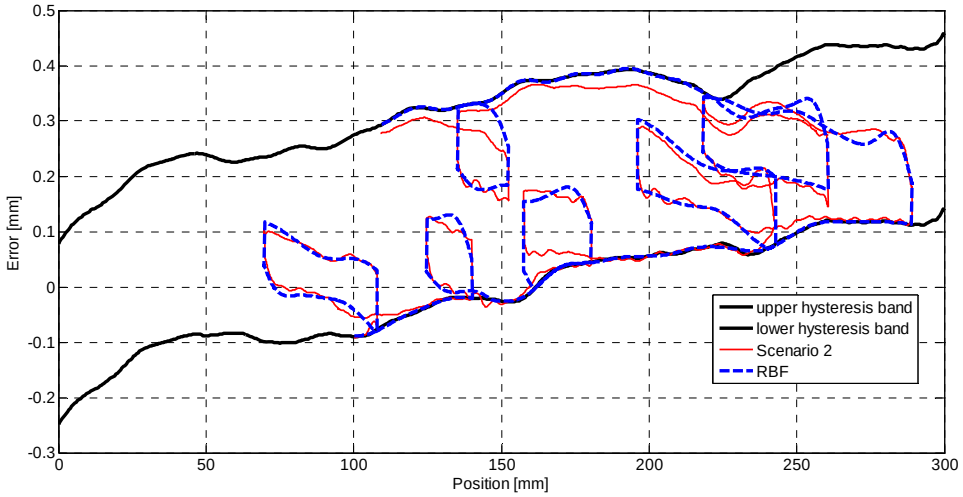

Fig. 4.19 Response of the SNN comprising RBFs for Scenario 2.

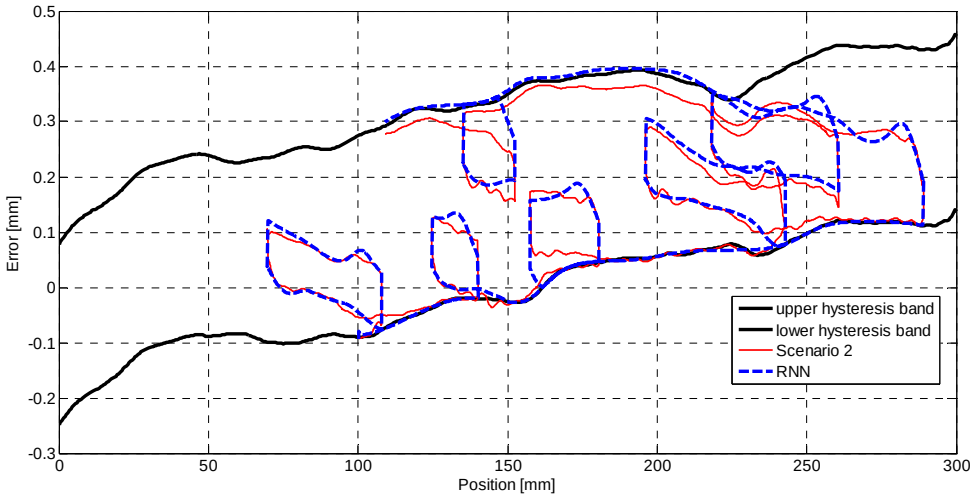

Fig. 4.20 Response of the SNN comprising RNNs for Scenario 2.

As illustrated, the position estimation errors are again about 30 μm and 16-20 μm on the minor loops and major loops respectively. Note that the estimation errors on the major loop are slightly elevated in this case owing to the fact that the average velocity on major loops (28 mm/s) deviates from the velocity in the training case (40 mm/s). Similarly, Figs. 4.21, 4.22, and 4.23 demonstrate the NNs performances on the Scenario 3.

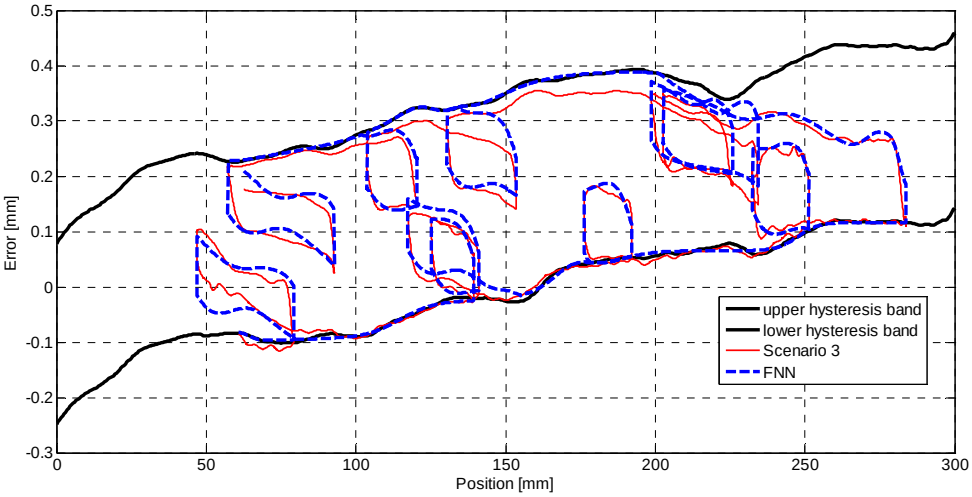

Fig. 4.21 Response of the SNN comprising FNNs for Scenario 3.

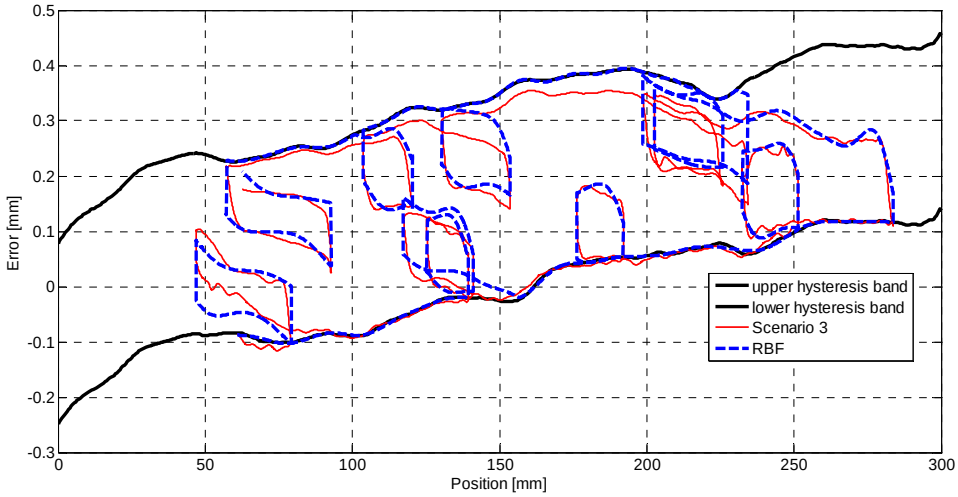

Fig. 4.22 Response of the SNN comprising RBFs for Scenario 3.

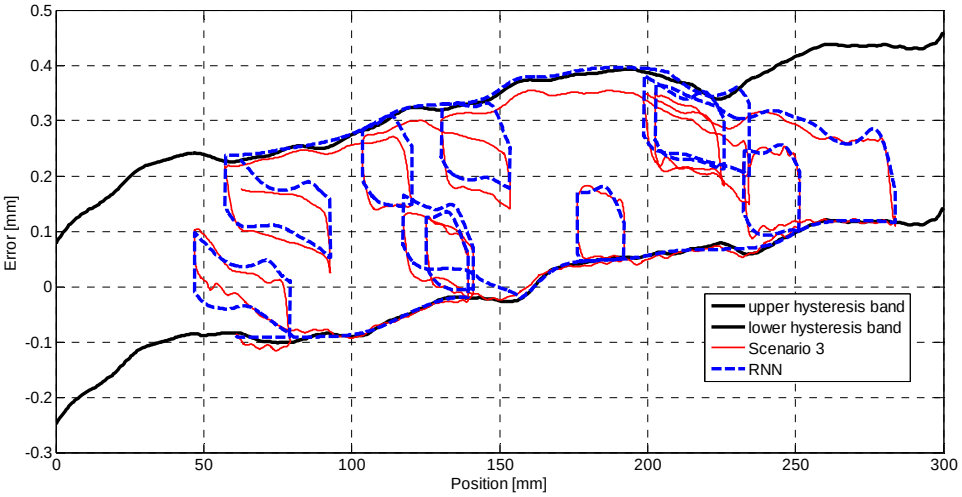

Fig. 4.23 Response of the SNN comprising RNNs for Scenario 3.

As expected, the position estimation errors on major- and minor hysteresis loops are getting bigger in Scenario 3 since the calculated average velocity on major loop (24 mm/s) significantly differs from that of the training scenario. Furthermore, this case constitutes cascaded minor loops which deteriorate the performance of the NNs due to the error contributions of ANN_{sp} networks which predict the starting point of the new trajectory. Finally, the Figs. 4.24, 4.25, and 4.26 present the overall performances of the NNs for Scenario 4. The major loop performances of the NNs for this scenario are worst than those for Scenario 1 and Scenario 2 since the conditions in this case (e.g. the average velocity of 25.5 mm/s) are significantly different from the ones in the training session.

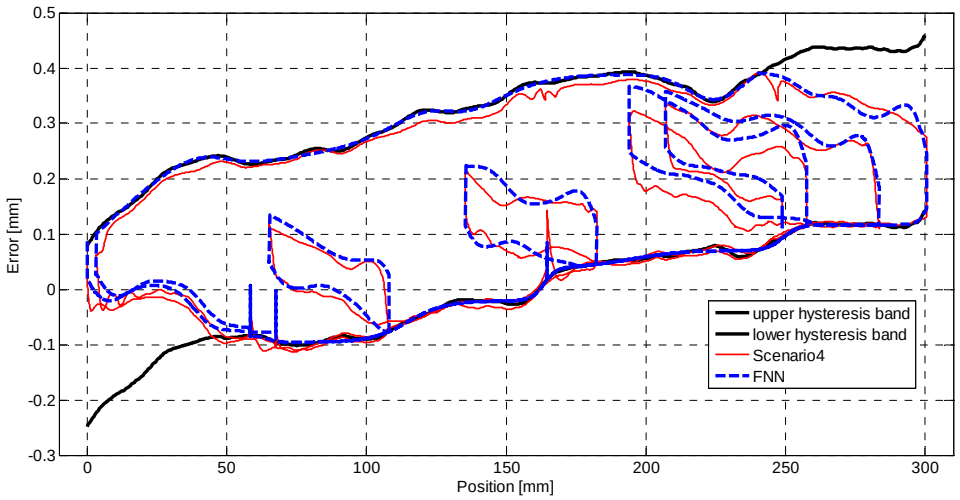

Fig. 4.24 Response of the SNN comprising FNNs for Scenario 4.

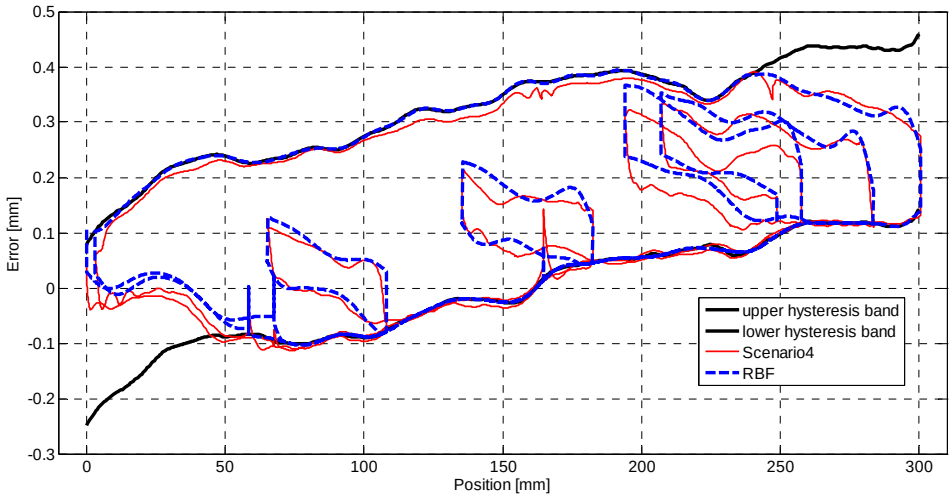

Fig. 4.25 Response of the SNN comprising RBFs for Scenario 4.

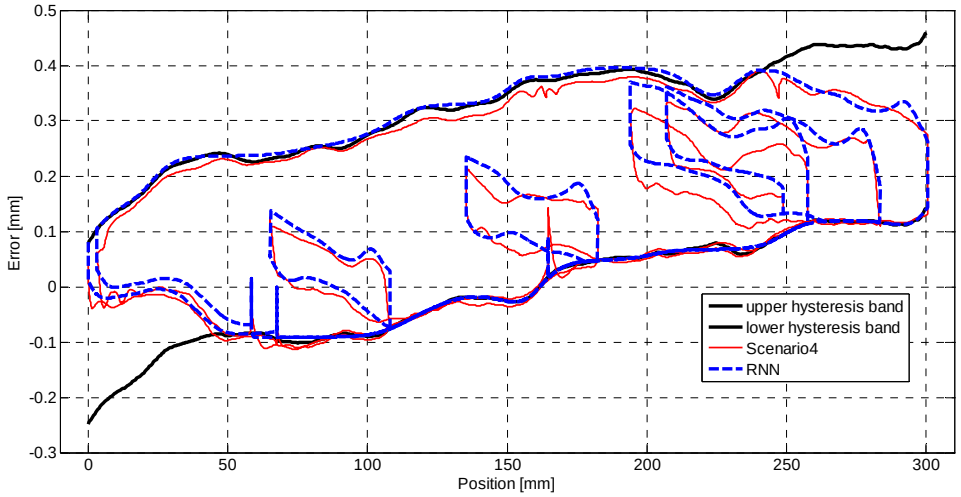

Fig. 4.26 Response of the SNN comprising RNNs for Scenario 4.

The type of NNs used in the SNN does not have a major influence on the results owing to the fact that the training errors associated with them are comparable in magnitude. Consequently, for a TBD that constitutes a large hysteresis band of 300 microns (plus a gearbox backlash of 120 microns), the presented network can estimate the carriage's position with an overall root-mean-square error of 25-35 microns utilizing the position measurements at the actuator (driver) side.

Note that the estimation performance of the SNN utilizing the FNN is slightly better the others. That is, all RMS error values for FNN on major- and minor loops are less than 30 μm. This network is presumed sufficient for error compensation in precision applications (Kulkarni and El-Sharkawi, 2001).

It is evident from Table 4.4 that the main error comes from the transient regimes (minor loops) where the motion could only be transmitted by friction forces. Unfortunately, modeling the friction characteristics in such regimes is quite challenging as it involves a large number of variables including the radial- and axial vibrations of the belt (Abrate, 1992). For that reason, the developed NN models, which lack the relevant inputs, could not fully capture the complex micro-slip phenomenon which is quite dominant in this operating regime. Furthermore, other

physical variables (such as belt tension, interface temperature, form errors of the pinion and belt teeth, etc.) could be incorporated to the developed NN models to increase the performance. However, such attempts would clearly defy the practicality (and the goal) of the presented method.

4.7 Closure

In this chapter, a TBD, which is not subjected to any external load, was considered. It has been shown that the transmission error patterns of such (elastic) mechanisms are repeatable to a certain extent. Hence, this feature motivates the design of an estimator that makes good use of indirect measurement techniques.

As suggested by the previous studies, various interpolation paradigms could be used to compute these (quasi-static) error patterns (possibly in real-time). However, huge numbers of data points are required to represent the corresponding patterns accurately. Furthermore, complex decisions are still necessary to switch among various interpolation schemes. A natural choice is to capture the “essence” of error patterns via NNs.

As briefly shown in this work, a generic RNN topology could not be developed to establish the desired relationship effectively within a reasonable time frame. On the other hand, the study has illustrated the performance of the presented SNN via a number of practical test cases. Using the sketchy guidance of the model at hand, a number of smaller NNs (with different architectures like FNN, RBF, RNN) were designed to tackle with these elementary “mapping” problems. Finally, seven NNs performing glue logic were designed to combine these individual networks. Hence, a SNN topology was tailored to estimate the transmission error efficiently.

Despite the fact that the mechanical system under study was far from ideal, the presented network yielded a satisfactory estimation performance provided that no external forces were acting on the carriage of the mechanism. Even though this (“no load”) condition seems to be seriously restricting the application of the presented paradigm; it is crucial to recall that most mechanisms encountered in practice (e.g.

printer/plotters, scanners, plasma/laser beam cutters, rapid prototyping machines, etc.) do not operate under the presence of external loads. Thus, the presented approach (which conveniently embodies an actuator with a crude position sensor) can be easily incorporated to the advanced motion controllers for such applications.

CHAPTER 5

PRESSURE PREDICTION OF A SERVO-VALVE CONTROLLED HYDRAULIC SYSTEM

5.1 Introduction

Hydraulic systems are widely used in many applications such as manufacturing equipment, construction machinery, rolling and paper mills, aircrafts, etc. If compared to their electrical counterparts, they could provide large forces at higher speeds with a high power-to-weight ratio. In hydraulic control systems, the relevant physical quantities such as position, velocity, acceleration, pressure, flow-rate and actuator force are measured via precision sensors to carry out a specific control task. Among these quantities, the pressures in cylinder chambers of the electro-hydraulic servo systems (EHSSs) play a key role in both the implementation of closed-loop force and/or position control and estimation of disturbances on the hydraulic actuator. Generally, accurate trajectory tracking control of hydraulic actuators is realized by the application of advanced control techniques such as adaptive robust control (Yao et al., 2000; Kaddissi et al., 2011; Mohanty and Yao, 2011), cascade control (Guo et al., 2008) and sliding-mode control (Guan and Pan, 2008; Pi and Wang, 2011). Despite the fact that position sensors, accelerometers, and force sensors are frequently utilized for tracking control of hydraulic systems, the above-mentioned control applications exclusively require the measurement of hydraulic (actuator chamber) pressures. Note that the introduction of pressure sensors increases the cost and complexity of the overall control system while reducing its reliability due to extra sensors and interface circuitry incorporated to the system. Likewise, in many industrial applications, the number of dedicated pressure sensors

(or any other sensors like PZT or strain-gage based load cells for that matter) is sought to be minimized for the purpose of reducing both the overall cost and the sensor-related malfunctions. Hence, an accurate pressure dynamic model, which could also be used for maintenance and fault-detection purposes, may allow a pressure sensor to be replaced by a relevant model (a soft-sensor or observer).

Note that accurate models for the dominant dynamics of the system must be also incorporated to the controller design so as to obtain a high bandwidth response (Jelali, 2003). A dramatic increase in control system performance can be accomplished via the use of predictive control schemes that employ stable models to forecast the behavior of the plant in foreseeable future (Lawrynczuk, 2010). On the other hand, the dynamic behavior of an EHSS is known to be highly nonlinear due to the compressibility of the hydraulic fluid, the complex characteristics of the flow-control device (i.e. servo-valve), the friction- and the leakage in the hydraulic actuators which in turn create problems in the model development efforts / control for such systems. Yet, nonlinear control system development for EHSSs remains a challenging task and is an active area in fluid power research (Karpenko and Sepehri, 2010).

There is not a single study that could predict accurately the long-term pressure dynamics of a valve-controlled EHSS in the current literature. For instance, Zhang (1997) and Watton et al. (1997) reveal the problem of creating reliable ANN models for hydraulic systems. Furthermore, He and Sepehri (1999) deal with the prediction problem and they were able to predict (15 step ahead) chamber pressures of an electro hydraulic test setup using a NARMAX-type network with prediction accuracy about ±5-10 bar (using a pressure sensor with a measurement accuracy of 1% within the range of 0-138 bar). Hence, the objective of this study is to predict the long-term pressure dynamics of an EHSS without the use of any extra sensors. The signals, which are exclusively used for the long-term pressure prediction task, are the control voltage to the servo valve driver and the measured position of the hydraulic actuator. No doubt, the pressure sensors would be used in the training operation and then they would have to be removed in the validation phases. This

study considers only the problem of design of an ANN model to predict the chamber pressure variables in a hydraulic cylinder actuator. The long-term prediction performances of the proposed network are demonstrated through a number of simulation studies. Therefore, the objective of this study is not only to elaborate the performance within the framework of realistic case scenarios but also to study the adaptation of a network model to a new hydraulic system with different physical parameters.

The rest of the Chapter 5 is organized as follows: Section 5.2 describes the simulation based hydraulic system employed in this study. Section 5.3 focuses on the design of RNN architectures to predict the hydraulic pressures using traditional techniques and utilizing the sketchy guidance of *a priori* knowledge at hand. Section 5.4 shows the practical usage of the devised neural network models for a hydraulic experimental test set up. Finally, concluding remarks are presented in Section 5.5.

5.2 Hydraulic System Model

The hydraulic actuation system considered in this study is composed of a fixed-displacement pump, a pressure relief valve, an accumulator, a critical-centered (or zero lapped) servo-valve and a double-action cylinder that is coupled to a load operating in a high-friction environment as shown in Fig. 5.1. For the sake of keeping the study in focus (and succinct), the mathematical models of the pump, the pressure relief valve, the accumulator and the pipe lines (along with the interactions among themselves) are not given below. However, the models of these systems are given in appendix A in a detailed manner.

Consequently, the models of the key hydraulic circuit elements (i.e. servo-valve and a double-action cylinder) that would allow the development of reduced-order pressure estimators are to be discussed here. Referring to Fig. 5.1, the nonlinear (differential) equations describing the relationships among the servo-valve control flows (Q_A and Q_B) and the actuator position (x) can be written as

$$M\ddot{x} + B\dot{x} + Kx + F_{fric} + F_{ext} = \left(P_A - P_B\right) A_p \tag{5.1}$$

$$\dot{P}_A = \frac{\beta}{V_A(x)}\left(Q_A - A_p\dot{x}\right) \tag{5.2a}$$

$$\dot{P}_B = \frac{\beta}{V_B(x)}\left(-Q_B + A_p\dot{x}\right) \tag{5.2b}$$

where M is the mass of the piston/load; B is the effective viscous damping; K is the stiffness of the equivalent spring, A_p is the piston annulus area and β refers to the bulk modulus of the hydraulic fluid. P_A and P_B denote the hydraulic pressures in each actuator chamber. Note that the volumes of hydraulic oil on each side of the piston are expressed by $V_A(x) = V_{A0} + A_p x$ and $V_B(x) = V_{B0} - A_p x$ where V_{A0} and V_{B0} are the initial chamber volumes when the piston is located at the center of the cylinder. Please note that the internal leakage between the chambers of a hydraulic actuator is generally characterized as a laminar flow (where the associated Reynolds number is smaller than 2000) and could be given as

$$Q_{leakage} = C_L\left(P_A - P_B\right) = C_L\,\Delta P \tag{5.3}$$

where C_L (leakage coefficient) generally ranges in between $10^{-12} m^3/(Pa \cdot s)$ (Kaddissi et al, 2007) and $10^{-15} m^3/(Pa \cdot s)$ (Guan and Pan, 2008) for hydraulic actuators. Despite the fact that C_L depends on many different physical parameters, this important coefficient can be approximately expressed as

$$C_L \propto \frac{D c^3}{\mu L} \tag{5.4}$$

where D is the piston diameter; c is the clearance between the piston and the cylinder; μ is the dynamic viscosity coefficient; L is the length of the piston (Merritt, 1967). As can be seen from (5.4), the clearance has the biggest impact on

the leakage flow. In practice, the internal leakage could be omitted if the seal between the chambers is considered intact. That is, the clearance between the piston and cylinder is extremely low. Otherwise, the resulting flow will affect the pressure dynamics and one must incorporate (5.3) to (5.2). In that case, a cross-coupled pressure model must be utilized. Note that, in this experimental (and simulation) study, the leakage in the hydraulic actuator is neglected since a brand-new actuator (with virtually no wear whatsoever) is employed.

The valve flow rates (which depend on the valve displacement from neutral) are also nonlinear in nature and could be given as

$$Q_A = \begin{cases} K_v\, u_v \sqrt{P_S - P_A}, & u_v > 0 \\ K_v\, u_v \sqrt{P_A - P_T}, & u_v < 0 \end{cases} \tag{5.5a}$$

$$Q_B = \begin{cases} K_v\, u_v \sqrt{P_B - P_T}, & u_v > 0 \\ K_v\, u_v \sqrt{P_S - P_B}, & u_v < 0 \end{cases} \tag{5.5b}$$

$$K_v = C_d w \sqrt{2/\rho} \tag{5.6}$$

where P_S refers to the hydraulic supply pressure and P_T denotes the tank (reservoir) pressure; K_v is the servo-valve flow gain; w is the orifice area gradient of the servo-valve. The servo-valve orifice coefficient of discharge is given by C_d while ρ denotes the density of the hydraulic oil. Here, u_v refers to the displacement of the valve spool.

Moreover, the friction force in (5.1) can be characterized by a dynamic friction process model like the LuGre model (Mihajlov et al., 2002) as

$$F_{fric} = \sigma_0 z + \sigma_1 \dot{z} + \sigma_2 v \tag{5.7}$$

$$\frac{dz}{dt} = v - \frac{|v|}{g(v)} z, \quad g(v) = \frac{1}{\sigma_0}\left(F_c + (F_s - F_c) e^{-(v/v_s)^2}\right) \tag{5.8}$$

where v is the velocity of the piston; z is an internal state representing the average bristle deflection; v_s is the Stribeck velocity; F_s is the static friction, F_c is Coloumb friction; σ_0 is the bristle-spring constant; σ_1 is the bristle-damping coefficient and σ_2 is viscous friction coefficient.

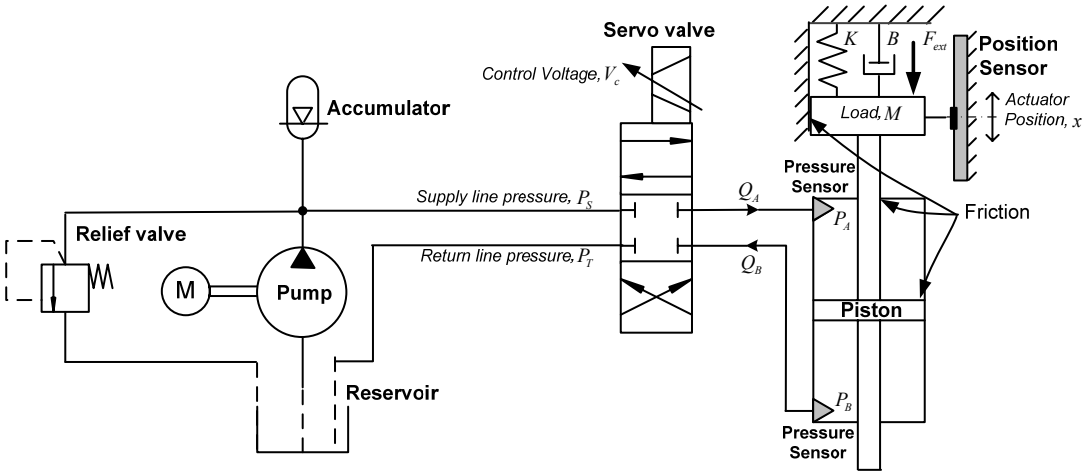

Fig. 5.1 Valve controlled hydraulic system.

A servo-valve is a complicated electro-mechanical device that includes a torque motor, a flapper-nozzle, and a valve spool. The manufacturers of such devices often times provide (linearized) models that characterize accurately the dynamics of their devices within the frequency response band of interest. For the servo-valve considered in this study, the current drive along with the valve-spool dynamics can be described in Laplace (s) domain as

$$\frac{I(s)}{V_c(s)} = \frac{1}{L_C s + R_C} \tag{5.9}$$

$$\frac{u_v(s)}{I(s)} = \frac{K_h \omega_n^2}{s^2 + 2\zeta\omega_n s + \omega_n^2} \tag{5.10}$$

In these equations, L_C is the valve-coil (solenoid) inductance; R_C is the coil resistance; V_c is the control voltage; I is the current in the coil; K_h is the first stage servo valve gain. Moreover, ζ and ω_n is the damping ratio and natural frequency of the servo-valve. Manufacturers' catalogues provides the relevant parameters of these linear models.

In the simulation study, a fixed-step integration (0.1 *ms*) was performed via MATLAB® Simulink using Dormand-Prince solver. The parameters of the afore-mentioned models are presented in Table 5.1. Note that the advanced simulation model is primarily used to provide the data needed for not only designing the structured NNs but also assessing their (preliminary) prediction performance.

Table 5.1 Some of the key model parameters used in the simulation study.

Par.	**Value**	**Par.**	**Value**	**Par.**	**Value**
M	9 kg	V_{A0}	0.00005 m^3	K_h	0.0401 m/A
B	2000 $N{\cdot}s/m$	V_{B0}	0.00005 m^3	ω_n	1256 rad/s
K	10 $N{\cdot}m$	β	1.4×10^9 Pa	ζ	0.7
A_P	645×10^{-6} m^2	σ_0	12×10^5 N/m	L_C	0.59 H
P_s	2×10^7 Pa	σ_1	300 Ns/m	R_C	100 Ω
K_v	3.2×10^{-5} $m^{5/2}/kg^{1/2}$	σ_2	60 Ns/m	Q_{max}	6×10^{-5} m^3/s
C_d	0.625	F_c	100 N	u_{v_max}	0.6×10^{-3} m
w	1.08 mm	F_s	130 N	x_{max}	0.05 m
ρ	890 kg/m^3	v_s	0.1 m/s	I_{max}	15 mA

5.3 Prediction Models and Parameter Estimation

The problem of creating accurate ANN models for the long-term pressure prediction in the cylinder chambers of a valve-controlled hydraulic system is to be solved by using black-box- and gray-box (SNN) modeling approaches in Sections

5.3.1 and 5.3.2, respectively. Next, prediction performances of the designed network models are evaluated in Section 5.3.3.

5.3.1. Black-box Approach

Now, black-box regression models are to be designed to predict the chamber pressures (P_A and P_B) in extended time periods without any feedback (at any rate) from the (simulated) pressure sensors. Hence, only the position sensor output *x(k)* along with the control voltage for the servo-valve $V_c(k)$ are to be utilized in the designed predictor.

Before developing any black-box model, its regression vector, which could be generically expressed in the form of (5.11), must be determined:

$$\begin{aligned}\varphi(k) = [&x(k),\ldots, x(k-m),\ V_c(k),\ldots, V_c(k-n),\\ &P_A(k-1),\ldots,P_A(k-p),\quad P_B(k-1),\ldots,P_B(k-p)]^T\end{aligned} \tag{5.11}$$

The selection for the model orders (*m, n, p*) [i.e. the size of TDL for various signals of interest] used in the regression vector closely governs the prediction performance. In literature, there exist well-known techniques like the Lipschitz quotients method (He and Asada, 1993) to determine the model orders. However, the pragmatic approach is to select these orders via trial-and-error or to use the prior knowledge about the process when applicable.

When the (simplified) equations governing the pressure dynamics [i.e. (5.2) and (5.5)] are examined closely, one can infer that the pressure states of the hydraulic system are decoupled and that two multiple-input single-output (MISO) predictors can be developed if the spool position (u_v) is accurately estimated using (5.9) and (5.10). That is, a discrete-time model (i.e. a constant coefficient difference equation) to estimate the spool position can be conveniently devised as

$$u_v(k) = \sum_{n=1}^{3} a_n u_v(k-n) + b_n V_c(k-n) \tag{5.12}$$

where a_n and b_n are the constants of the difference equation.

Note that the selection of sampling period *(T)* plays a key role in discrete-time modeling of dynamic systems. Reuter (1995) studies the system identification of hydraulic servo-systems and shows that a sampling period in between 0.86 *ms* and 1.3 *ms* is sufficient for modeling purposes of such systems. Therefore, in this study, 1 *ms*, which is a common choice in the current state of the art (Yousefi et al., 2008), is selected as the sampling period. Note that when (5.2) and (5.5) are discretized via backward difference method (i.e. Euler method), the prediction models simply boil down to

$$P_x(k) = f_x(\varphi_x(k), \theta_x) \tag{5.13a}$$

$$\varphi_x(k) = [u_v(k),\, x(k),\, v(k),\, P_x(k-1)]^T \tag{5.13b}$$

where θ_x is the weight vector; the subscript x denotes a placeholder for letters A and B.

Before the training session, one should select a proper excitation signal in order to create input-output data set. Looking to the literature, it is seen that PRMS is the most suitable choice of input signal form for identification of hydraulic systems (Jelali and Kroll, 2003; He and Sepehri, 1999; Xue-miao et al., 2010; Barbosa et al., 2011). Therefore, the servo-valve manipulation signal, shown in Fig. 5.2.a, is applied for gathering the training data. Fig. 5.2.b represents the position and velocity profile of the hydraulic actuator. Furthermore, Figs. 5.2.c and 5.2.d show the pressure dynamics for this training scenario in chamber A and B, respectively. It is seen that the pressure dynamics is getting more vibratory when the piston approaches to its stroke limits (0.05 *m*) at about 7.8 seconds.

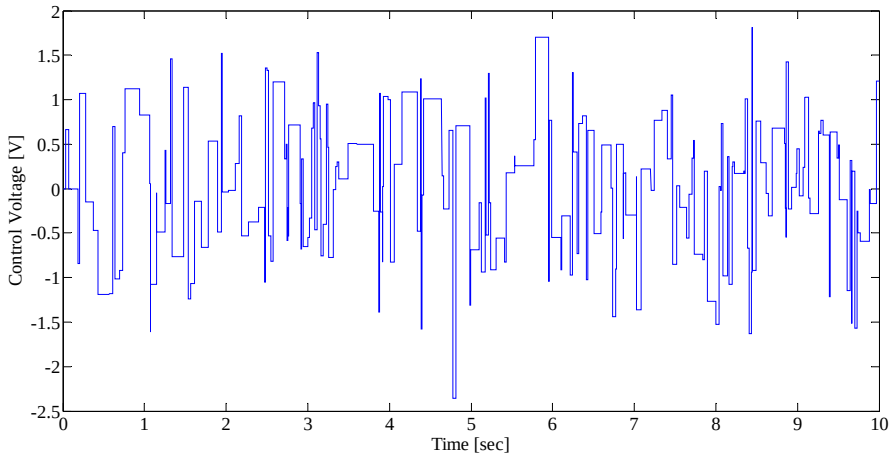

a) Servo-valve manipulation signal.

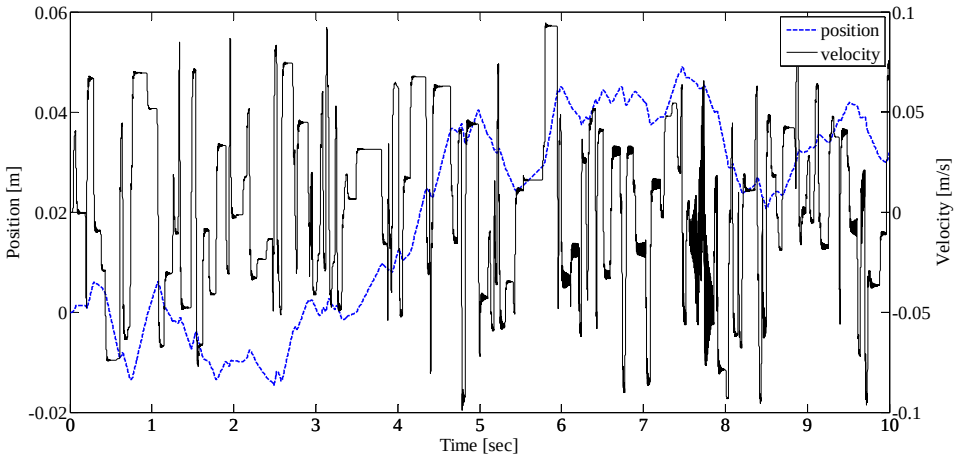

b) Cylinder position and velocity.

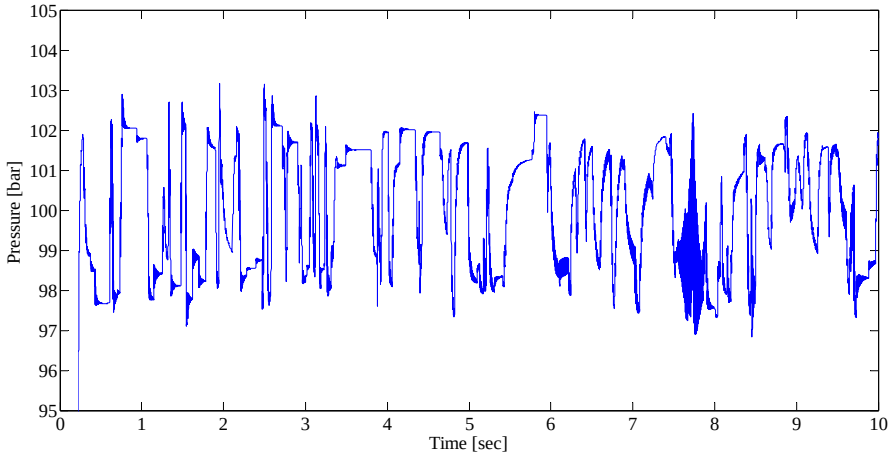

c) Pressure dynamics in chamber *A*.

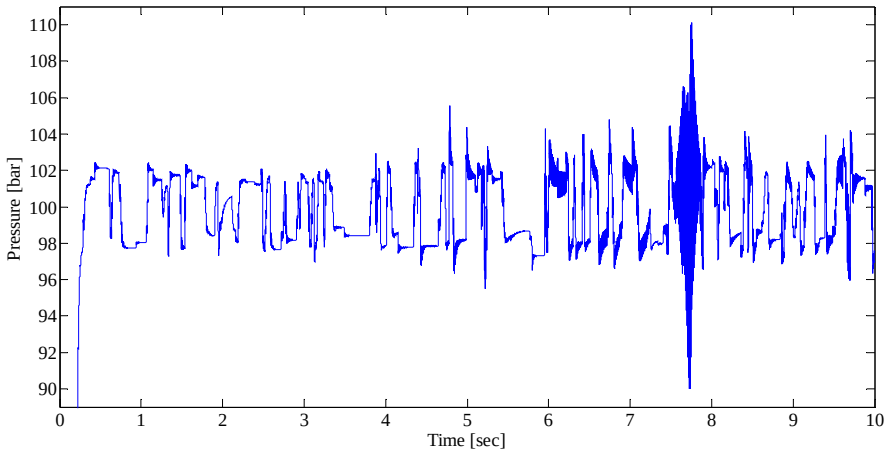

d) Pressure dynamics in chamber *B*.

Fig. 5.2 Training data used for the modeling of servo-valve controlled hydraulic system.

First of all, a NARX model is devised to model the pressure dynamics as can be seen from Fig. 5.3. The network is trained via MATLAB® (2008a) NN toolbox that runs on a PC with Intel Core i5 processor and a SDRAM of 4GB. Due to poor training performance, the regression vector in (5.13.b) is modified as

$$\varphi_x(k) = [u_v(k), u_v(k-1), x(k), x(k-1), v(k), v(k-1), P_x(k-1), P_x(k-2)]^T \qquad (5.14)$$

Table 5.2 summarizes the properties of this network. Even though this model exhibits excellent training performance, the resulting network alone is of little practical use owing to the fact that the model requires the history of the pressure state. It is important to note that a fully recurrent neural network, which produces self-sustaining predictions, cannot be trained to the desired accuracy when the weights of the network are initialized randomly. As for the next step, the output of this network is directly fed back as could be seen from Fig. 5.3. The resulting network, which is commonly referred to as NOE model, is further trained via RTRL algorithm. The summary of the training session is also given in Table 5.2. Hence,

the final RNN is able to predict the pressure states without the need for pressure sensors.

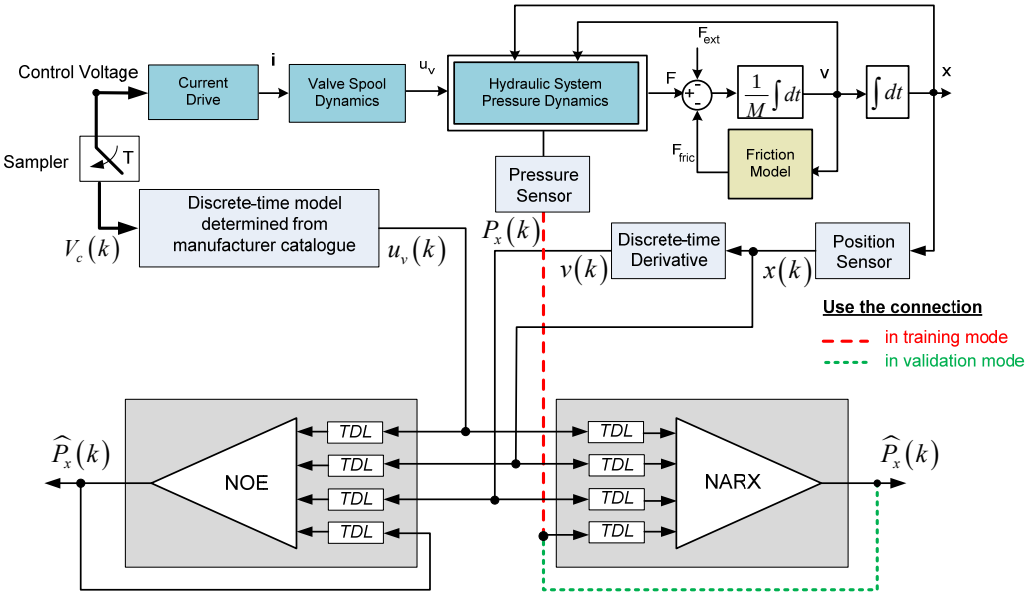

Fig. 5.3 Connections of the NARX and NOE models to the system.

Table 5. 2 Architecture and performance of the black-box networks*.

Architecture		***NARX***	***NOE***
Inputs		$u_v(k), u_v(k-1), x(k), x(k-1)$ $v(k), v(k-1), P_x(k-1), P_x(k-2)$	$u_v(k), u_v(k-1), x(k), x(k-1)$ $v(k), v(k-1), \hat{P}_x(k-1), \hat{P}_x(k-2)$
Training Data		10001 Sample	
Training error in RMS	for P_A	0.011 *bar*	0.506 *bar*
	for P_B	0.017 *bar*	0.777 *bar*
Epochs		1000	50
Training time (min)		1.5	40
1st Layer Neurons		10	10
Activation Function		Tangent (Bipolar) Sigmoid	
Training Method		Levenberg-Marquardt	LM / RTRL

[*] Linear activation functions are utilized at their output layers.

5.3.2 Gray-box (SNN) Approach

A close examination of the (simplified) model presented in Section 5.2 reveals that it can be conveniently divided into two parts: *flow-rate model* and *pressure model*. Hence, the pressure states may be predicted accurately when the flow-rates for each chamber (rather than $u_v(k)$ input) is provided. Fig. 5.4 illustrates the schematic of the proposed structured recurrent neural network where $G_1 = K_v u_{v\_\max}\sqrt{P_S}/Q_{\max}$ and $G_2 = (\beta Q_{\max} T)/(V_{x0} P_S)$ refers to two gains with lumped parameters. The following sections elaborate the NN designs in the topology.

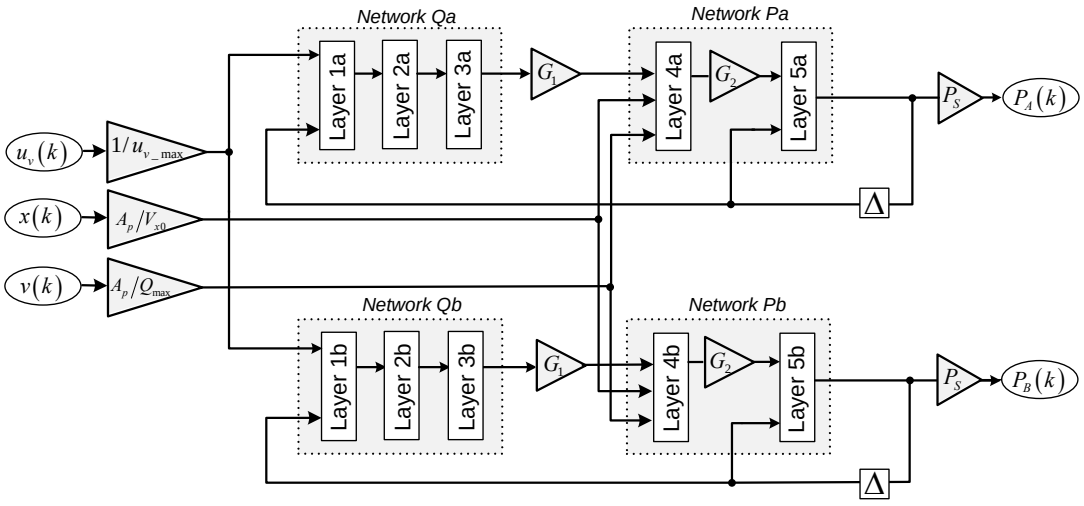

Fig. 5.4 Schematic of the structured recurrent neural network.

5.3.2.1 Flow-rate Model

Flow-rate can be estimated by a NN model using *a priori* information about the process. If the pressure states in (5.5) are normalized by the maximum pump supply pressure (P_S) while the spool displacement is scaled by the maximum allowable valve-spool displacement (u_{v_max}), the nonlinear flow characteristic [as expressed by (5.5) in its simplified form] can be learned by a FNN. That is, training data set (i.e. normalized flow rate) could be generated for all the ranges of normalized pressure

and spool position. Presuming that the normalized pressure is available, a FNN can be trained to learn this nonlinear mapping.

Table 5.3 summarizes some of the FNN architectures considered in this study. As can be seen, the fourth architecture, which yields the minimum root-mean-square (RMS) training error, is utilized to estimate the corresponding flow rates (see the networks labeled *Network Qa* and *Network Qb* in Fig. 5.4).

It is critical to notice that to estimate the flow rate at time instant kT, the network requires not only the valve-spool displacement (u_v) but also the pressure estimate at $t = kT$. Since such an estimate is usually not available for that instant, the previous value of that state must be employed for all intensive purposes. Hence, this practical implementation necessity implies that the pressure does not change significantly within one sampling interval and that $P_x(k) \cong P_x(k\text{-}1)$.

Table 5.3 Characteristics of various networks designed for Q_A*.

Architecture	**# 1**	**# 2**	**# 3**	**# 4**
1st layer neurons	10	30	5	10
2nd layer neurons	-	-	5	10
Output layer neurons	1	1	1	1
Number of epoch	1000	1000	1000	2500
Training time in (*min*)	< 1	< 3	< 1	< 7
RMS training error in (m^3/s)	4.37×10^{-7}	5.22×10^{-8}	2.31×10^{-7}	8.52×10^{-9}
Training data	9801 Sample			
Training method	Levenberg-Marquardt			
Activation function	Tangent (Bipolar) Sigmoid			

[*] Linear activation functions are utilized at their output layers.

5.3.2.2 Pressure Model

Once the flow rates are estimated to the desired accuracy, the chamber pressure (rates) can be approximately computed via (5.2) in a straightforward fashion. Considering the discrete-time equivalent of (5.2) [as computed via a Euler integration method], a RNN should implement the below pressure dynamics as

$$P_A(k)=P_A(k\text{-}1)+T\beta\left[\frac{Q_A(k)-A_p\,v(k)}{V_{A0}+A_p\,x(k)}\right] \tag{5.15a}$$

$$P_B(k)=P_B(k\text{-}1)+T\beta\left[\frac{-Q_B(k)+A_p\,v(k)}{V_{B0}-A_p\,x(k)}\right] \tag{5.15b}$$

One needs to design a specific FNN to implement the division operation in (5.15) since it is tested and seen that a generic RNN could not learn the pressure dynamics directly using a regression vector whose elements constitute from $Q_x(k)$, ,$x(k)$, $v(k)$ and $P_x(k\text{-}1)$.For that purpose a FNN, called *divider network*, is trained with normalized inputs in such a way that Ω is between [-1 +1] and Γ is between [-0.9 +0.9]. This network model will be used as the main part of the *pressure model* as shown in Fig. 5.5.

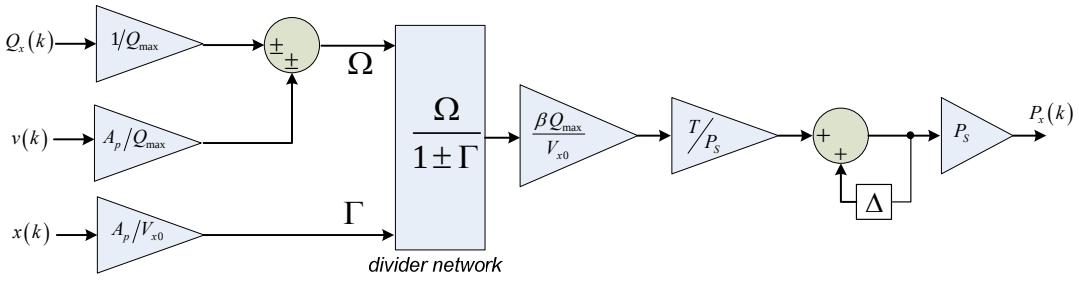

Fig. 5.5 Schematic of the pressure model.

The overall *pressure model* could be represented with a 2 layered RNN model as given below

$$\bar{P}_x(k)=G_2\left\{W_2\,\psi\left[W_1\,\bar{\varphi}(k)+b\right]\right\}+\bar{P}_x(k-1) \tag{5.16a}$$

$$\bar{\varphi}(k)=\left[\bar{Q}_x(k),\bar{v}(k),\bar{x}(k)\right]^T \tag{5.16b}$$

where $\Psi(\cdot)$ is the activation vector function (bipolar sigmoid); the weight matrices are $W_1 \in \Re^{20x3}$, $W_2 \in \Re^{1x20}$, and bias vector is $b \in \Re^{20x1}$. As described before, G_2 is a constant in (5.16a) and comes into existence due to the normalization procedure. Two *pressure models*, named as *Network Pa* and *Network Pb*, are created based on this architecture and 20 tangent sigmoid neurons are used in the 1st layer of these network models. After training a number of modular NN models using the "divide-and-conquer" approach, these subsystems are combined to construct a unified SRNN. Therefore, a specific network architecture for that system is established. The SRNN network could be further trained in the unified form for fine tuning of its weight parameters. It is seen that the training error of the SRNN for P_A decreases from 0.396 *bar* level to 0.190 *bar* level within 5 epochs while training session lasts about 85 minutes. Table 5.4 summarizes the training properties of the SRNN network. The performance of the resulting network is evaluated in the next section.

Table 5.4 Properties of the structured recurrent neural network.

Input(s)	$u_v(k)$, $x(k)$ $v(k)$	
Output(s)	$P_A(k)$, $P_B(k)$	
Layer 1a	10 Tangent Sigmoid	
Layer 2a	10 Tangent Sigmoid	
Layer 3a	1 Linear	
Layer 1b	10 Tangent Sigmoid	
Layer 2b	10 Tangent Sigmoid	
Layer 3b	1 Linear	
Layer 4a	20 Tangent Sigmoid	
Layer 5a	1 Linear	
Layer 4b	20 Tangent Sigmoid	
Layer 5b	*1 Linear*	
Error of the SRNN after unification	*for* P_A	0.396 *bar*
	for P_B	0.773 *bar*
number of training data	10001 Sample	
training method	*LM / RTRL*	
number of epoch	*5*	
training time	*85 minute*	
Error of the SRNN after training	*for* P_A	0.190 *bar*
	for P_B	0.598 *bar*

5.3.3 Prediction Results

To assess the prediction performances of the developed RNNs, a validation study (called v1) is conducted via generating a servo-valve manipulation signal that constitutes another PRMS as depicted in Fig. 5.6. With this input applied to the detailed model in Fig. 5.1, the hydraulic system is simulated and a 5000 step-ahead prediction test is realized with the SRNN and NOE models.

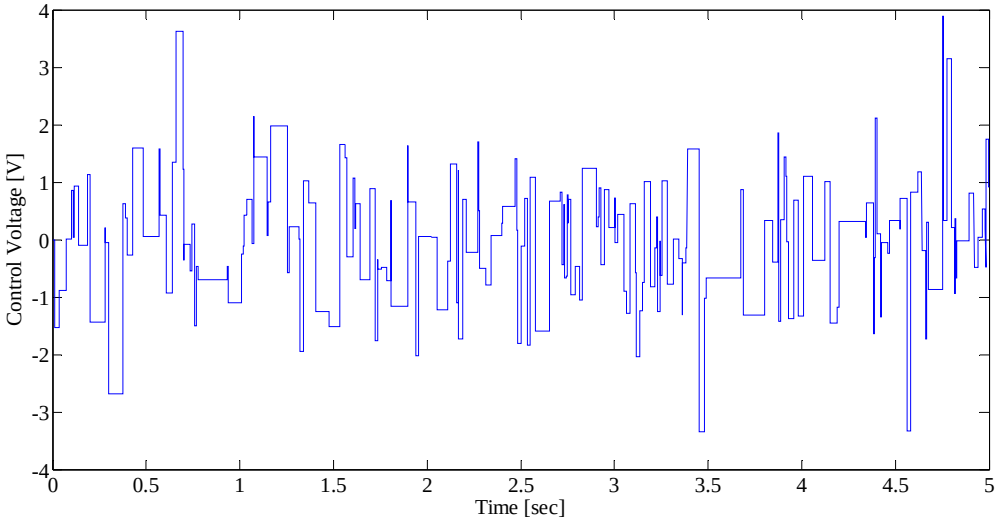

Fig 5.6 Servo-valve manipulation signal used in model validation.

Note that in the simulation study, the sensor- and data conversion dynamics are also taken into consideration. The networks are only provided with the relevant digital information: $x(k)$ and $V_c(k)$. In this scenario, the position of the piston $x(k)$ is assumed to be measured by a linear scale with a resolution of 5 microns. Similarly, the velocity $v(k)$ (as required by the networks) is to be estimated via a first-order backward difference: $v(k) = [x(k) - x(k-1)]/T$. Furthermore, the servo-valve manipulation voltage $V_c(k)$, which is to be generated by a digital control system, is sampled and converted to the digital representation via a 12-bit analog-to-digital converter (ADC). Therefore, the inputs to the networks do constitute quantization noise to some extent.

Model validation results are presented in Fig. 5.7 for the NOE and SRNN models. Fig. 5.7.a represents the temporal pressure changes of chamber *A* as calculated from the simulated system's response (i.e. exact pressure change) for SRNN and NOE model. Fig. 5.7.b illustrates the accuracy frequency response function (FRF) that is spectrally averaged to reduce the noise content.

Similarly, Figs. 5.7.c and 5.7.d show the (temporal) pressure changes of chamber *B* as well as the corresponding accuracy FRFs. From accuracy FRFs, it has been observed that the SRNN model outputs are very close to actual states (since the ratio is about 1). Furthermore, the RMS errors of the SRNN model are 0.552 and 0.43 *bars* for prediction of P_A and P_B respectively while the corresponding RMS errors of the NOE model are 5.592 (for P_A) and 2.946 *bars* (for P_B) respectively.

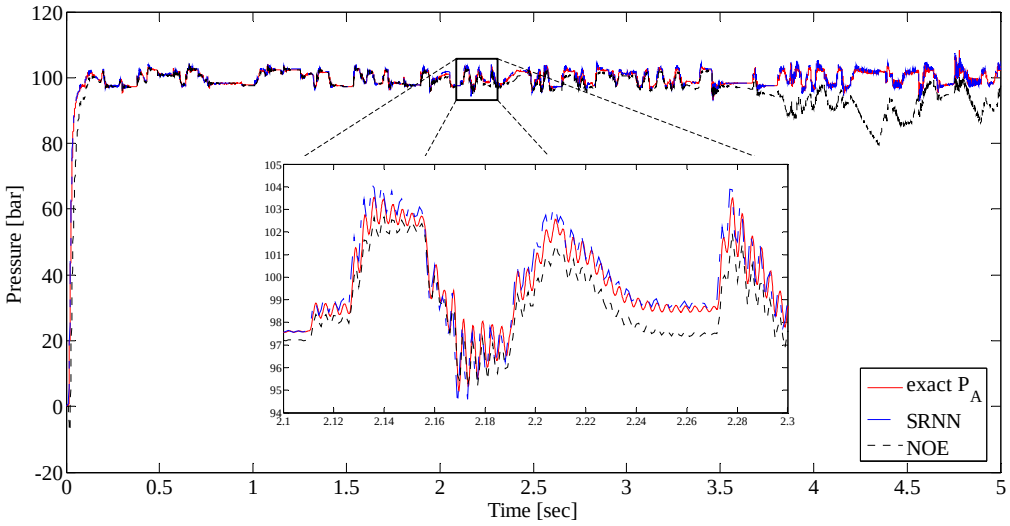

a) Pressure change in chamber *A*.

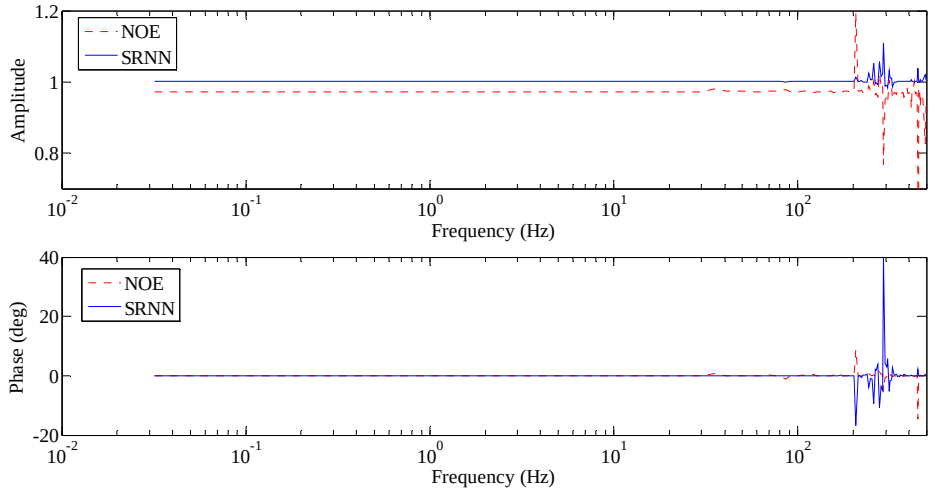

b) Accuracy frequency response functions when predicting P_A.

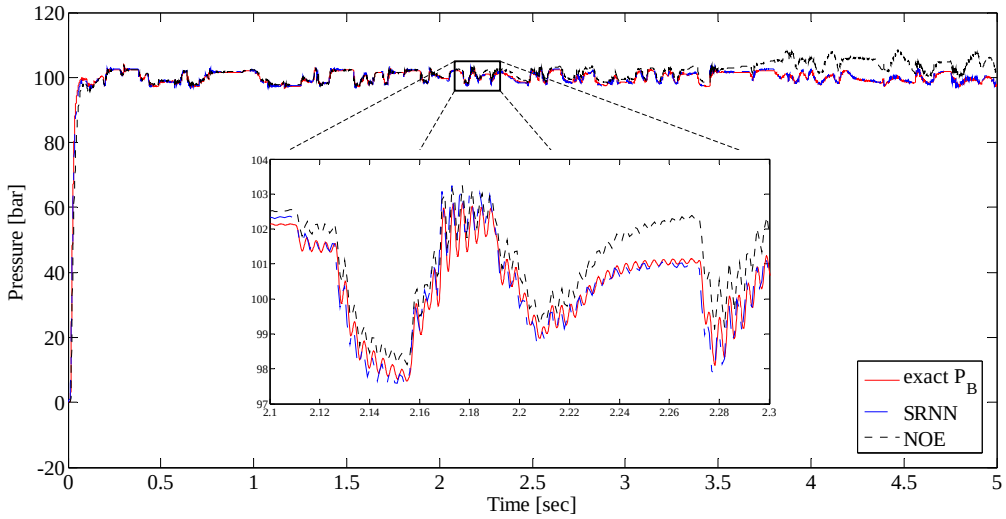

c) Pressure change in chamber *B*.

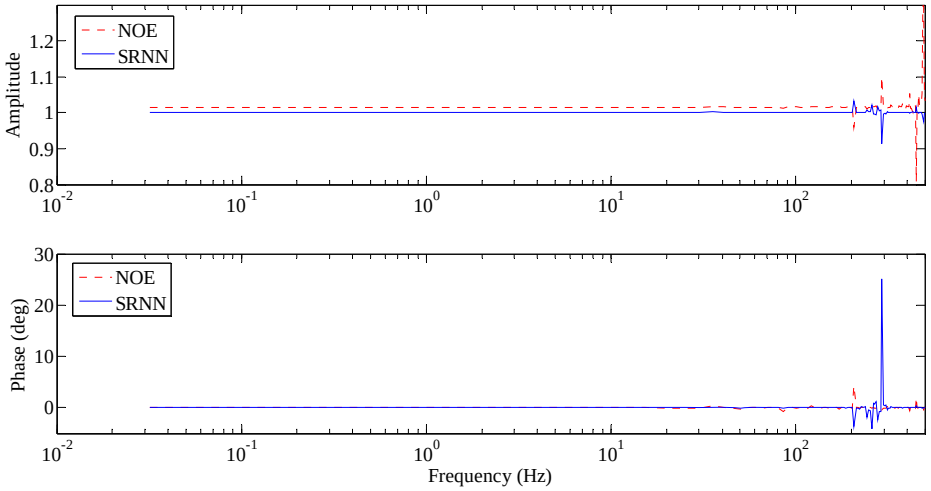

d) Accuracy frequency response functions when predicting P_B.

Fig. 5.7 Validation test (v1) results.

It is critical to note that all conditions in the validation test v1 (including the friction) are exactly the same as those of the training case. Consequently, another verification test (called v2) is carried out for a different set of mechanical system parameters. That is, the LuGre model parameters in the simulation are changed to increase the friction force four times if compared to the previous case. Furthermore, a load (external) force (in the form of a chirp signal with amplitude of 3000 *N* and a frequency range from 0.1 *Hz* to 5 *Hz* in 5 seconds) is applied to load in order to fluctuate the chamber pressures in a broader range (70-130 *bar*) around $P_S/2$ level (100 *bar*). The results of this validation scenario are presented in Fig. 5.8. Again, the pressure changes in both chambers are shown in Figs. 5.8.a and 5.8.b. Not surprisingly, the SRNN, which apparently captures the essential features of the hydraulic system, yields excellent long-term prediction performance (where the RMS error is 0.758 *bar* and 0.540 *bar* for the prediction of P_A and P_B, respectively) while the NOE model fails to predict the pressure states accurately. It could be inferred that the estimation accuracy at the frequency band of interest (including extrapolation capability) of the SRNN models are quite exceptional as indicated by the accuracy FRFs of the SRNNs in Fig. 5.8.c.

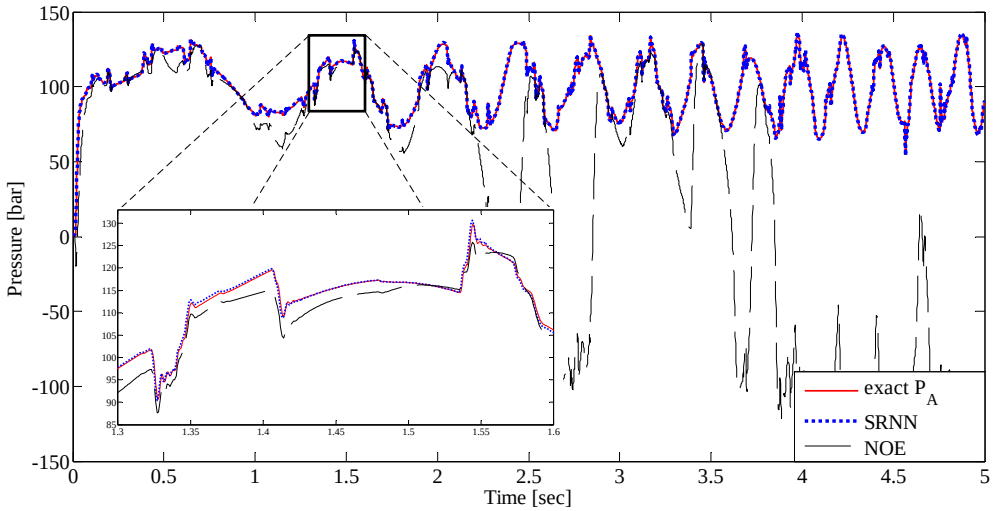

a) Pressure change in chamber *A*.

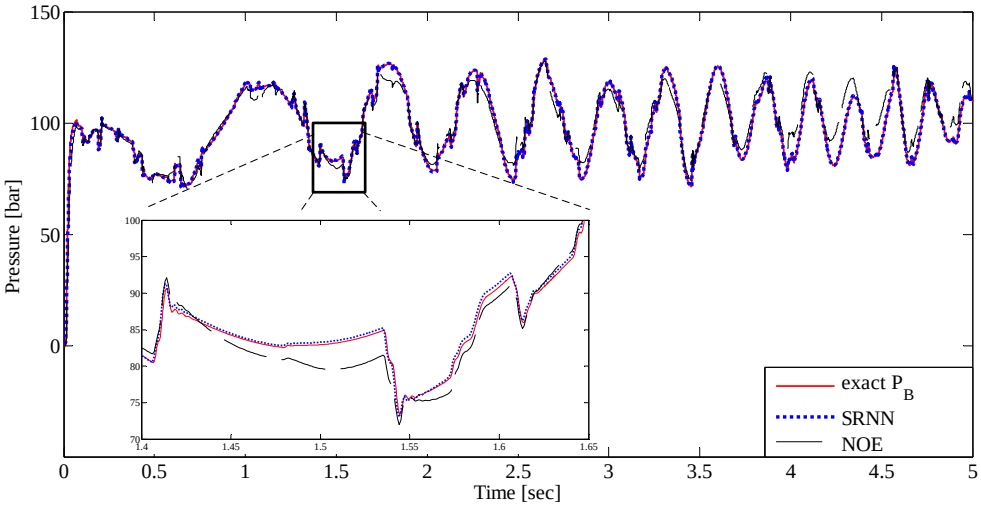

b) Pressure change in chamber *B*.

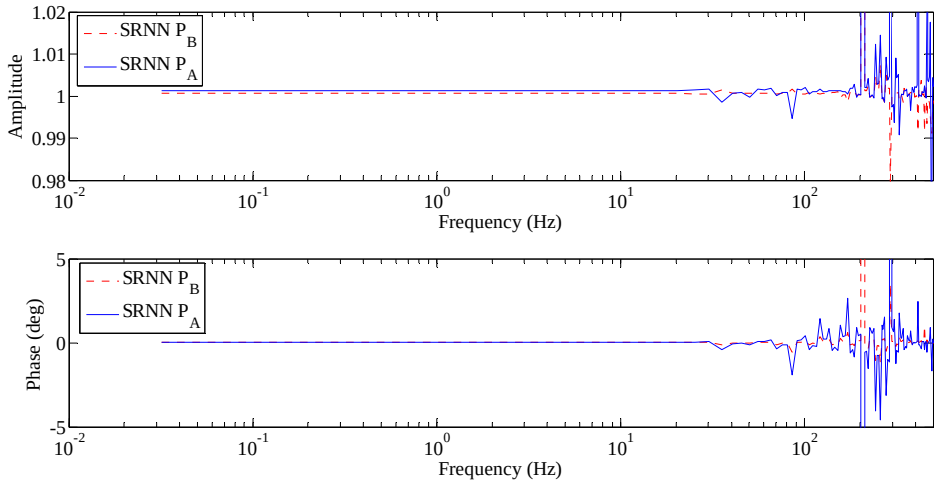

c) Accuracy frequency response functions of the SRNN.

Fig.5.8 Validation test (v2) results.

Moreover, the robustness of the SRNN is tested via applying an external force. Fig. 5.9.a shows the applied external force in time domain while the magnitude of the (time-varying) prediction errors in chambers *A* and *B* are presented in Figs. 5.9.b and 5.9.c, respectively. A (sampled) cross-correlation coefficient between external force and prediction error is also calculated as

$$R = \frac{\sum_{k=1}^{N}\left[\left(F_{ext}(k)-\bar{F}_{ext}\right)\left(e(k)-\bar{e}\right)\right]}{\sqrt{\sum_{k=1}^{N}\left(F_{ext}(k)-\bar{F}_{ext}\right)^2\sum_{k=1}^{N}\left(e(k)-\bar{e}\right)^2}} \tag{5.18}$$

where $\bar{F}_{ext}$ is the mean of applied external force and $\bar{e}$ is the mean of prediction error. It is found that the cross-correlation coefficient is 0.076 (7.6%) for prediction error in chamber *A* and -0.116 (11.6%) for prediction error in chamber *B*, respectively. Furthermore, Fig. 10 shows the prediction error (in *bars*) of the SRNN while applying sinusoidal type external forces with different amplitudes and frequencies. It has been observed that as the magnitude and frequency of the external force are increased, the prediction performance of the SRNN slightly deteriorates. However, there exist a significant potential to improve the training performance of the resulting network via an enhanced training data set (at the expense of increased training time).

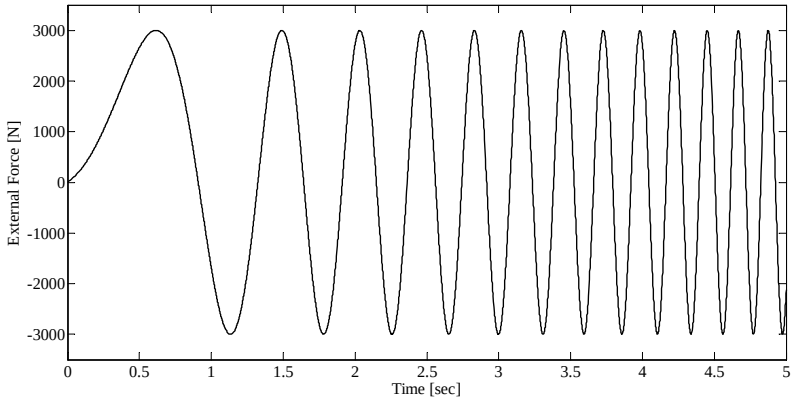

a) Applied external force.

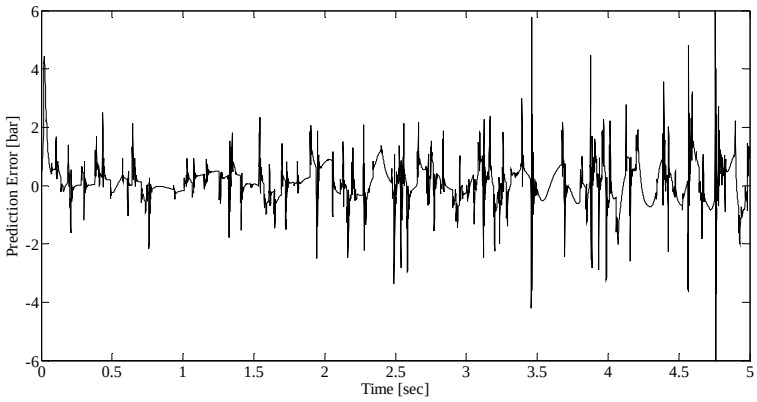

b) Prediction error in chamber *A*.

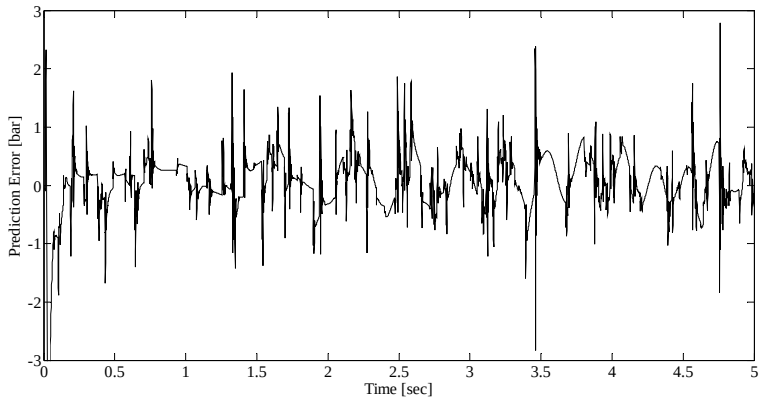

c) Prediction error in chamber *B*.

Fig. 5.9 Test for sampled cross-correlation between external force and prediction error.

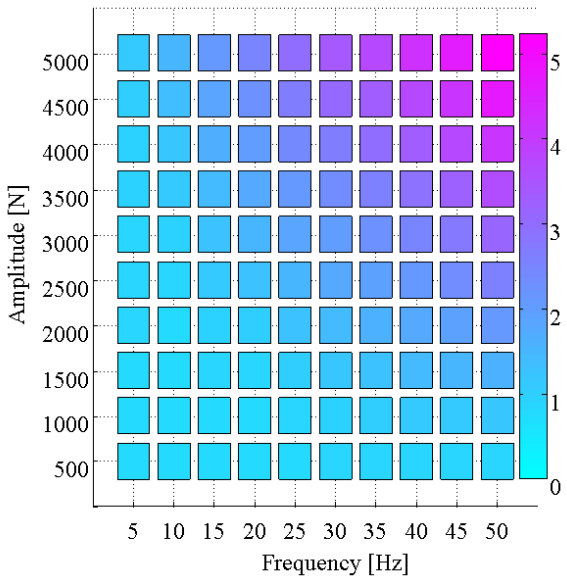

Fig. 5.10 Prediction error (in *bars*) of the SRNN to the applied external force.

The above-mentioned claim merely states the fact that if the neural network based predictor/estimator/observer was "tuned" (or trained) ideally, its estimation error would approach to zero (within its bandwidth) even if its inputs (u_v, x, v) were highly correlated with the disturbance (or applied external force). Unfortunately, the theoretical treatment of the above-mentioned aspect using well-known techniques such as perturbation analysis, interval analysis, describing function analysis, harmonic analysis etc. is known to be quite challenging for highly nonlinear systems (i.e. systems with a number of discontinuities). For instance, devising even an operating-point model for the (simplified) hydraulic system considered in this study is not straightforward. To be specific, one cannot develop a linear time-invariant (LTI) (operating point) model when the servo-valve is operated at its neutral point ($u_v = 0$) while the piston is to be centered around a specific location ($x = x_0$). Consequently, one needs to employ further assumptions in order to perform a manageable analysis. To that end, let us assume the followings:

1) Piston is operated at the middle section of the hydraulic cylinder. The volume changes (in both chambers) as a function of piston position are presumed negligible.
2) Friction force and linear elastic force component (i.e. spring force) are embedded to the external force.
3) Piston is assumed to be extending with $u_v>0$.

After defining the perturbation variables as $u_v = u_{v0} + \delta u_v$ ($u_v>0$), $v = v_0 + \delta v$, $P_A = P_{A0} + \delta P_A$, $F_{ext} = F_{ext0} + \delta F_{ext}$ …; one can "linearize" (5.2) and (5.5) via Taylor series expansion to get

$$\delta P_A(j\omega) = \frac{K_{uA\_ext}}{\frac{V_A}{\beta} j\omega + K_{PA\_ext}} \delta u_v - \frac{A_p}{\frac{V_A}{\beta} j\omega + K_{PA\_ext}} \delta v \qquad (5.19a)$$

$$\triangleq \frac{k_{1A}}{j\omega + k_{3A}} \delta u_v - \frac{k_{2A}}{j\omega + k_{3A}} \delta v$$

$$K_{uA\_ext} \triangleq \left. \frac{\partial Q_A}{\partial u_v} \right|_{\substack{u_v = u_{v0} \\ P_A = P_S/2}} = K_v \sqrt{P_S/2} \qquad (5.19b)$$

$$K_{PA\_ext} \triangleq \left.\frac{\partial Q_A}{\partial P_A}\right|_{\substack{u_v = u_{v0} \\ P_A = P_S/2}} = \frac{K_v u_{v0}}{\sqrt{2 P_S}} \tag{5.19c}$$

where the excitation frequency is $\omega = 2\pi f$ *(rad/s)* ($0 < f < f_{bandwidth}$). The terms K_{uA_ext} and K_{PA_ext} are referred to as the valve spool position gain and the valve pressure gain of the orifice respectively. In practice, the valve spool position (i.e. control input voltage) along with actuator velocity is correlated to the external force provided that a motion-control loop is realized. That is, $\delta u_v \sim \delta F_{ext}$ and $\delta v \sim \delta F_{ext}$. Assuming that the neural network based predictor closely mimics the actual pressure dynamics, the pressure prediction error in chamber *A* could be defined as

$$\delta e_A \triangleq \delta P_A - \delta \hat{P}_A = \left(\frac{k_{1A}}{j\omega + k_{3A}} - \frac{\hat{k}_{1A}}{j\omega + \hat{k}_{3A}} \right) \delta u_v - \left(\frac{k_{2A}}{j\omega + k_{3A}} - \frac{\hat{k}_{2A}}{j\omega + \hat{k}_{3A}} \right) \delta v \tag{5.20}$$

Here, the quantities with ^ denote the ones associated with the SNN model. It is clear from the equation above that $\delta e_A \to 0$ as model coefficients converge to the actual system parameters $\left(\hat{k}_{1A} \to k_{1A}, \hat{k}_{2A} \to k_{2A}, \hat{k}_{3A} \to k_{3A} \right)$. In that case, the prediction error would be independent from the external force (i.e. its amplitude and excitation frequency). As mentioned previously, the SRNN in this study were not trained perfectly since the training session had to be terminated when the corresponding error reached a predetermined threshold value. For the sake of creating a practical training scenario, the data set included only a limited number of operation regimes where the application of the external force and wideband excitation of the system via this force was also excluded. As explained before, the duration of the training session grows exponentially as the network size (i.e. free parameters) along with the size of the training data set step up dramatically. Under the given circumstances, one might expect some correlation (or functional dependence) between the external force and the prediction errors of the developed network.

5.4. Long-term Pressure Prediction of an Experimental Hydraulic Test Setup

The black-box- and gray-box (SNN) modeling approaches devised in Section 5.3 are to be evaluated experimentally and thus this section focuses on the practical usage of the devised SRNN using an experimental hydraulic test set up.

5.4.1. Experimental Test Setup

The experimental test set up used in this study is illustrated in Fig. 5.11. This set up was assembled for the evaluation of state feedback control techniques on two different operating modes (valve controlled and variable-speed pump controlled mode) of a hydraulic system (Caliskan, 2009). These two circuit schemes can be selected at will. The components of this setup are listed in Table 5.5.

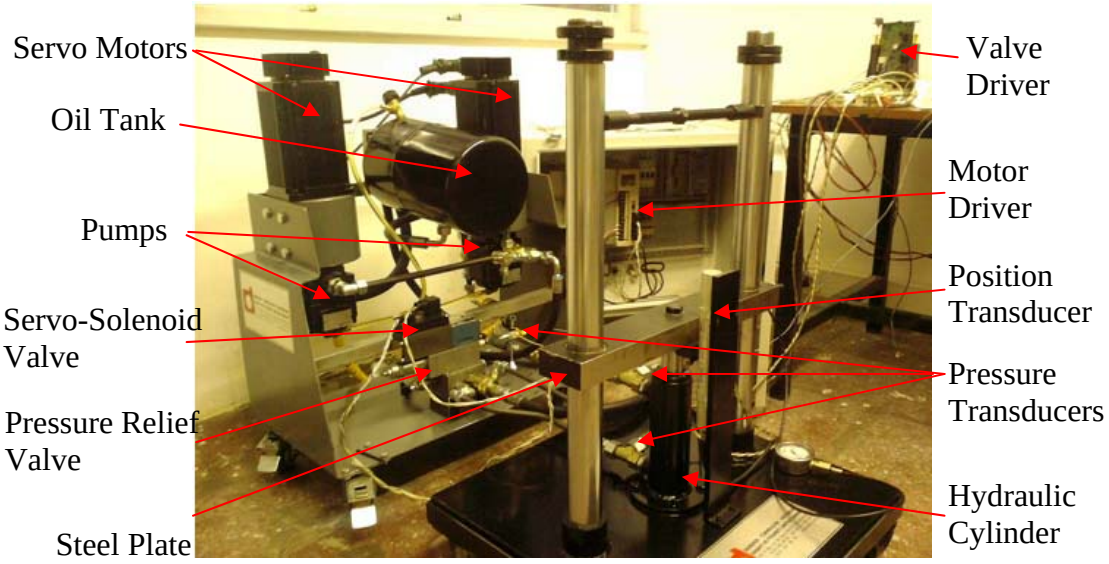

Fig. 5.11 Experimental test setup (Caliskan, 2009).

Since the presented study concentrates on the pressure estimation of the valve controlled hydraulic circuit, the experimental set up shown in Fig. 5.12 is operated in that mode. Note that in this test set up, a double acting asymmetric cylinder is used as the hydraulic actuator where it is rigidly connected to a steel plate being

supported by two sliders at each end to restrict its rotation. The masses of the steel plate and cylinder rod and the friction acting on the seals of the actuator and the bearings of the supports constitute the load. The pumps are driven in one direction with constant speed and their outlet pressure (i.e. the supply pressure of the valve) is limited by the pressure relief valve. Similarly, a servo solenoid valve regulates the flow rate through the double acting asymmetric cylinder. The valve driver has a spool position controller accepting spool position feedback from the LVDT on the valve and receives its reference spool position command (±10 *V*). The position of the actuator, the chamber pressures of the hydraulic cylinder and the valve supply pressure are measured in the set up. In fact, the spool position of the solenoid valve can be read from the valve driver via a data acquisition (DAQ) card.

Table 5.5 Components of the hydraulic test setup.

Components	***Remarks***
Hydraulic pumps	Effective displacement: *15.6 cm^3/rev* Max. operating pressure: 250 *bar*
Hydraulic actuator	Cap side area: 1963.5 *mm^2* Rod side area: 1001.4 *mm^2* Stroke: 100 *mm* Cap side chamber volume: 154387 *mm^3* Rod side chamber volume: 82455 *mm^3*
Load	Steel plate: 11.6 *kg* Actuator rod: 0.7 *kg*
Transmission line elements	Steel tubes with diameter 12 *mm*
Hydraulic oil	Bulk modulus: 1300 *MPa* Kinematic viscosity at 20º*C* is 100 *mm^2/s*
Servo proportional valve & driver	BOSCH 4WRPH Nominal flow rate: 24 *l/min* Valve gain: 2.138×10^{-8} *$m^{7/2}/(kg^{1/2}.V)$*
Servo motors and motor drivers	Nominal power 1 *kW*
DAQ card	National Instruments 16 Analog Input 2 Analog Output
Sensors	Pressure sensors 0-400 *bar*, 4-20 *mA* output LVDT with ±10 *V* output

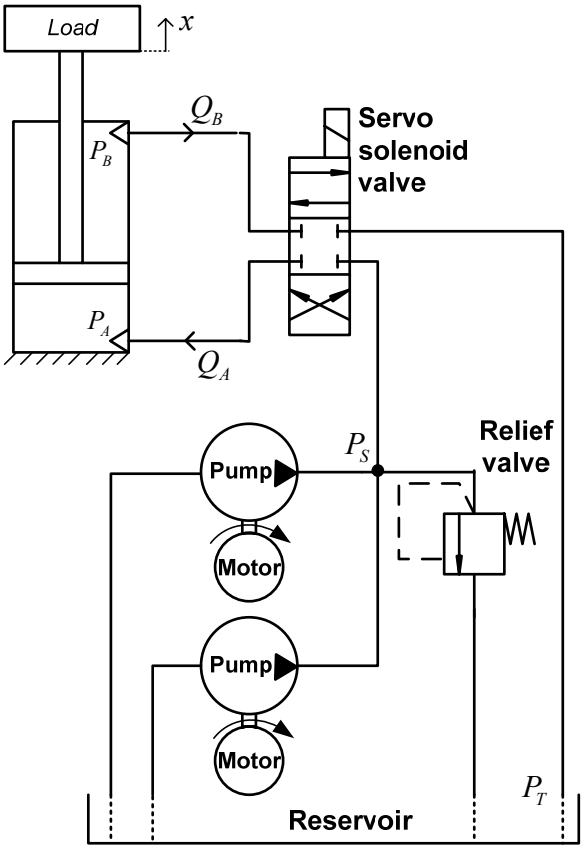

Fig. 5.12 Schematic diagram of the experimental test setup.

5.4.2. Adaptation of Black-box Model

To identify the nonlinear black-box models for the given experimental setup, the measured servo-valve spool position (control signal) shown in Fig. 5.13.a, is applied to the valve driver for gathering the regression (i.e. training) data. Fig. 5.13.b shows the measured position of the actuator position. As could be seen, the noise on the position transducer aggravates the noise on the calculated velocity significantly. Therefore, the position signal must be filtered before the velocity calculation operation. For this purpose, a discrete-time low-pass filter with a cut-off frequency of 20 *Hz* is used to smooth the position signal. Fig. 5.13.c presents the calculated actuator velocity (which is an element in the regression vector) from the filtered actuator position signal using first order difference method (FODM). Furthermore, the pressure changes in each chamber are presented in Fig. 5.13.d. As

can be seen, some noise is also observed in the measured pressure as well as valve spool position signals due to the (pump) motor drivers. Thus, these signals are filtered with a discrete-time low-pass filter with a cut off frequency of 100 *Hz*. Architecture and training performances of the black-box models are presented in Table 5.6 for this training case.

Table 5.6 Architecture and performance of the black box networks*.

Architecture		***NARX***	***NOE***
Input(s)		$u_v(k), u_v(k-1), x(k), x(k-1)$ $v(k), v(k-1), P_x(k-1), P_x(k-2)$	$u_v(k), u_v(k-1), x(k), x(k-1)$ $v(k), v(k-1), \hat{P}_x(k-1), \hat{P}_x(k-2)$
Output(s)		$P_x(k)$	$P_x(k)$
Training data		50001 Sample	
Training error (bar)	*for* P_A	0.021	2.243
	for P_B	0.024	2.891
Epochs		500	10
Training time (min)		6	225
1st layer neurons		10	10
Activation function		Tangent (Bipolar) Sigmoid	
Training method		Levenberg-Marquardt	LM / RTRL

[*] Linear activation functions are utilized at their output layers.

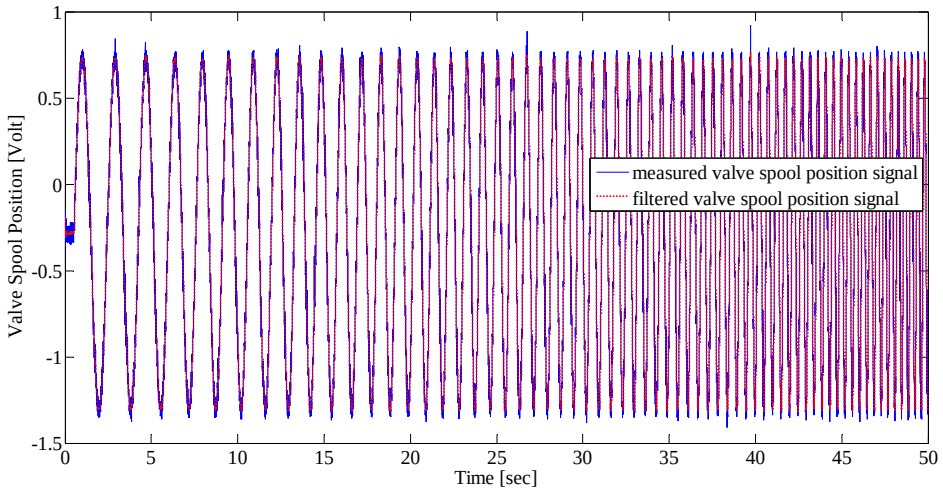

a) Valve spool position.

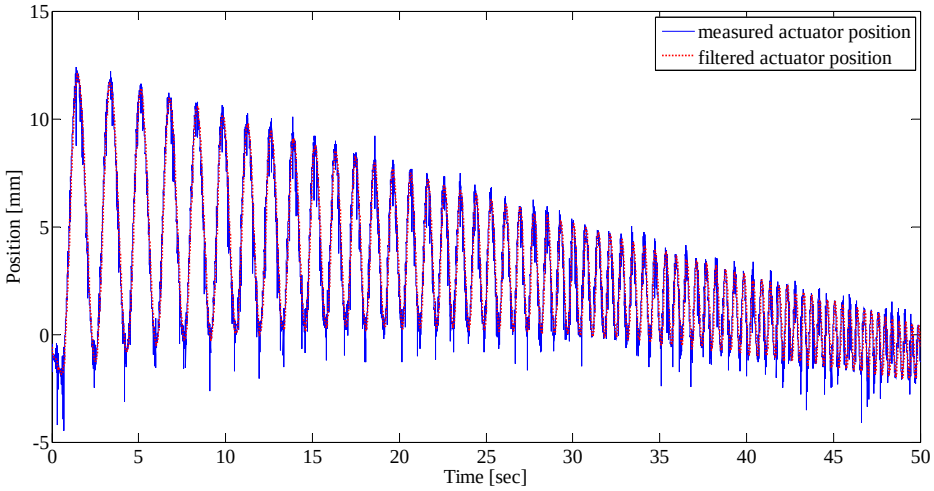

b) Actuator position.

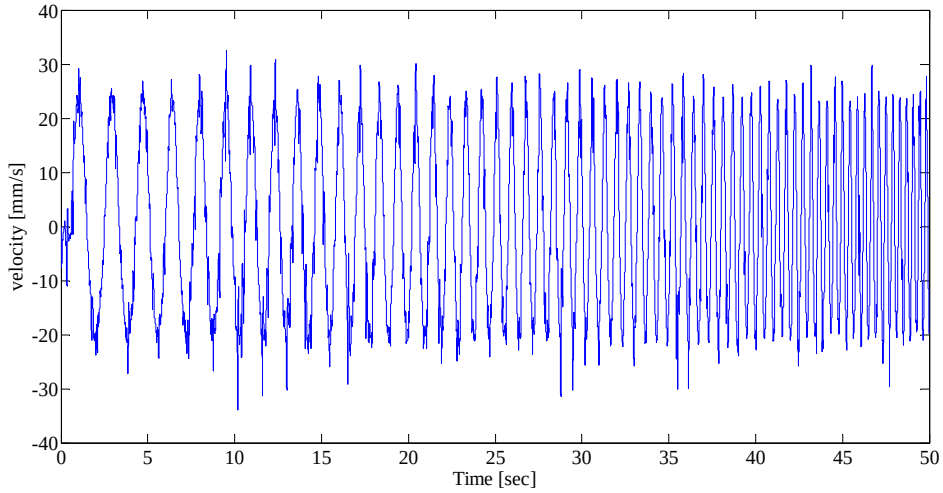

c) Calculated actuator velocity from filtered position signal.

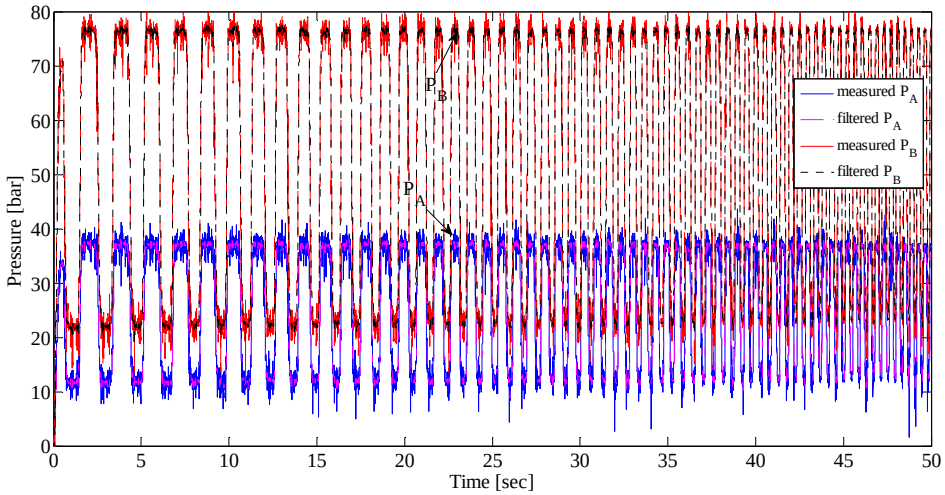

d) Cylinder chamber pressures.

Fig. 5.13 Measured and filtered signals that will be used for training.

5.4.3 Adaptation of Gray-box (SNN) Model

Due to similarity in the hydraulic system architecture (including zero-lapped servo valve), the SRNN devised in Section 5.3.2 can be directly adapted for the long term pressure prediction of the hydraulic cylinder chambers. However, if the servo-valve in the experimental setup were of a different type (i.e. an overlapped or under lapped type), the FNNs estimating the flow rates (i.e. *Network Qa* and *Network Qb*) would have to be modified (or redesigned to be exact) to accommodate the unique nonlinearities associated with these valves. Furthermore, G_1 and G_2 weights (see Fig. 5.4) can be calculated provided that the valve gain constant, maximum spool displacement, pump supply pressure, maximum flow rate of the valve, bulk modulus of the hydraulic oil, sampling time of the predictor model and initial chamber volumes are known. All these values, which could be found in Table 5.5, are used to form the specific SRNN model for this experimental setup.

Again, the filtered signals presented in Fig. 5.13 are used in the training session of SRNN. The training results are given in Table 5.7. In fact, the SRNN commences training in close proximity to an acceptable solution in (huge) multi-dimensional weight space. Hence, the overall network will quickly converge to the best global solution within a few epochs. The weights of the SRNN layers from *1a* to *5a* (shown in Fig. 5.4) are investigated for the purpose of determining the changes in free weights after the training. Figs. 5.14, 5.15 and 5.16 show the percentage change of the bias, input and layer weights of the SRNN with respect to the ones before the training operation. Note that, in these figures, every square indicates the percentage change of the (bias/input/layer) weight value associated with a unique neuron in the specified layer shown along the ordinate. It is observed that overall network could learn the dynamics of the experimental hydraulic system quite easily by making only a minor weight changes. It is interesting to note that when this SRNN architecture is initialized with arbitrary weights, the network totally fail to learn the dynamic behavior of the system. Therefore, the determination of the right architecture along with the optimal size of the network is not a sufficient condition to capture the desired functional relationship.

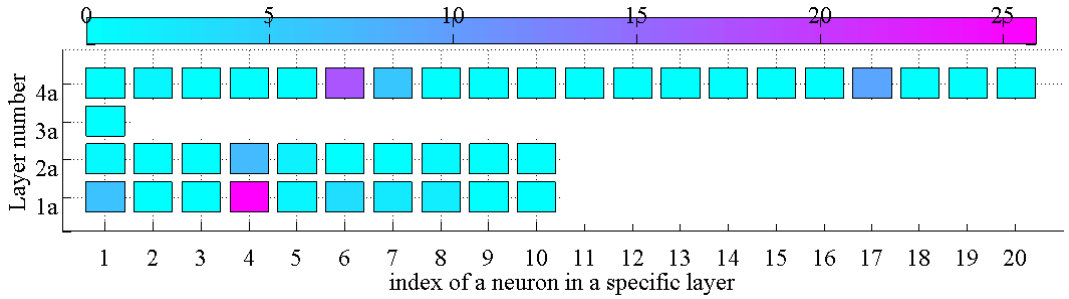

Fig. 5.14 Percentage change of the bias weights with respect to the initial model weights.

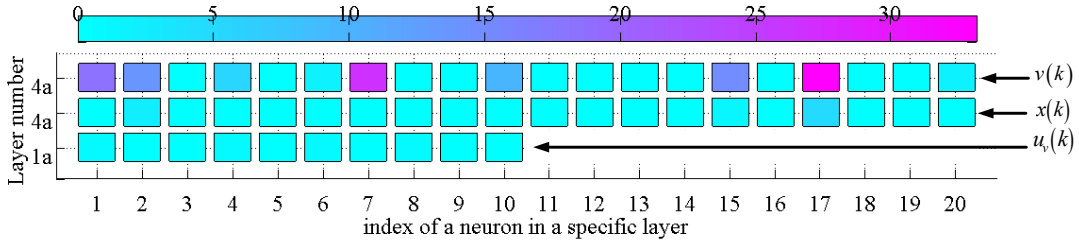

Fig. 5.15 Percentage change of the input weights with respect to the initial model weights.

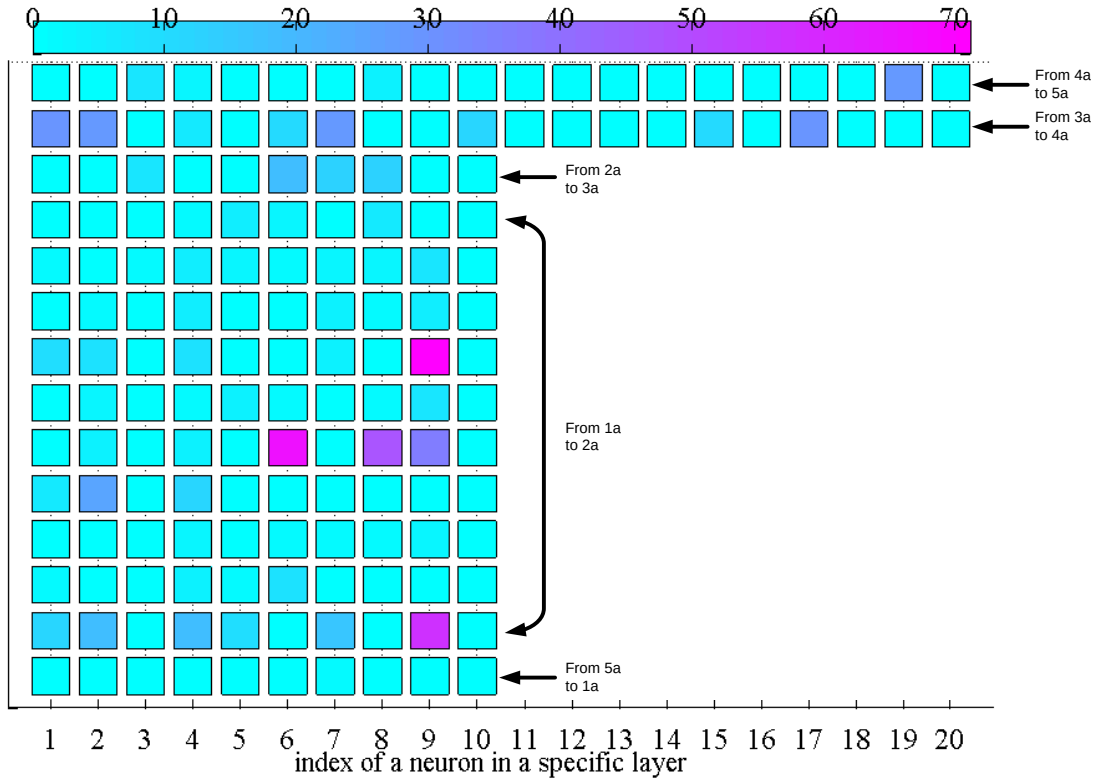

Fig. 5.16 Percentage change of the layer weights with respect to the initial model weights.

Table 5.7 Training results of the structured recurrent neural network.

Input(s)		$u_v(k),\quad x(k)\quad v(k)$
Output(s)		$P_A(k),\quad P_B(k)$
Layer 1a		10 Tangent Sigmoid
Layer 2a		10 Tangent Sigmoid
Layer 3a		1 Linear
Layer 1b		10 Tangent Sigmoid
Layer 2b		10 Tangent Sigmoid
Layer 3b		1 Linear
Layer 4a		20 Tangent Sigmoid
Layer 5a		1 Linear
Layer 4b		20 Tangent Sigmoid
Layer 5b		1 Linear
Training error	*for* P_A	18.980 *bar*
	for P_B	22.064 *bar*
Training data		50001 Sample
Training method		LM / RTRL
Epochs		10
Training time (*min*)		835
Error after training	*for* P_A	1.232 *bar*
	for P_B	1.720 *bar*

5.4.4 Prediction Results

To assess the prediction performances of the RNNs developed in Sections 5.4.2 and 5.4.3, a validation study (called **v3**) is conducted via generating a servo-valve manipulation signal (u) for a duration of 2.5 seconds which correspond to a 2500 step-ahead prediction test as depicted in Fig. 5.17.a. With this input, the velocity profile of the hydraulic actuator is presented in Fig. 5.17.b. Using these two signals, model validation results are presented in Fig. 5.17.c for the NOE and SRNN models. Not surprisingly, the SRNN captures the essential features of the hydraulic system while the NOE model fails to predict the pressure states accurately. On the other hand, an exact mathematical model of this experimental setup was tried to be constructed by Caliskan (2009) and the performance of that white-box modeling for the pressure estimations in actuator chambers are presented in Fig. 5.18. It is obvious that such modeling efforts yield poor performance on the long-term pressure predictions of hydraulic system considered.

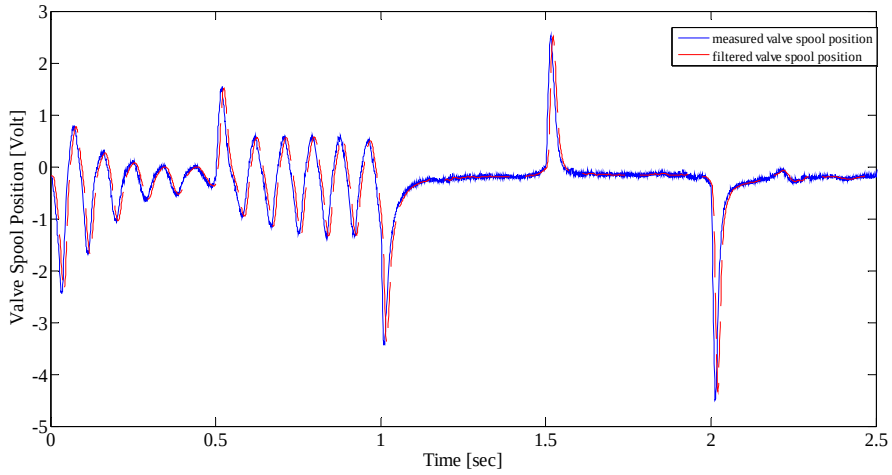

a) Valve spool position.

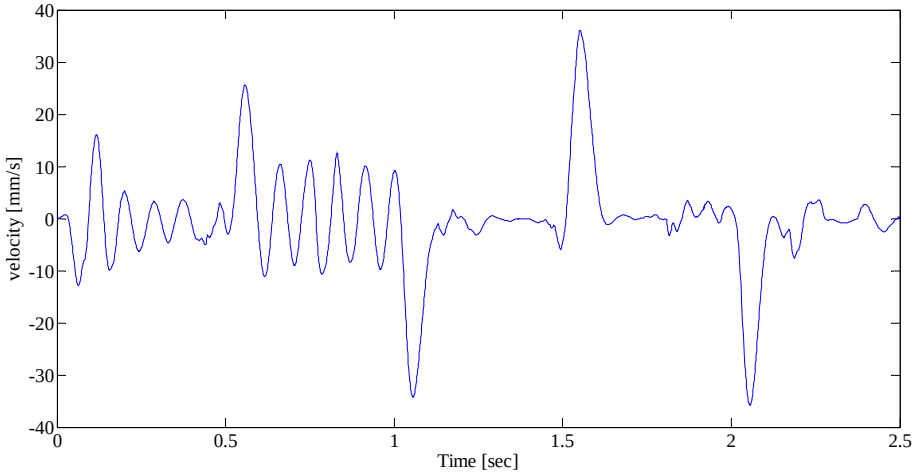

b) Calculated actuator velocity from filtered position signal.

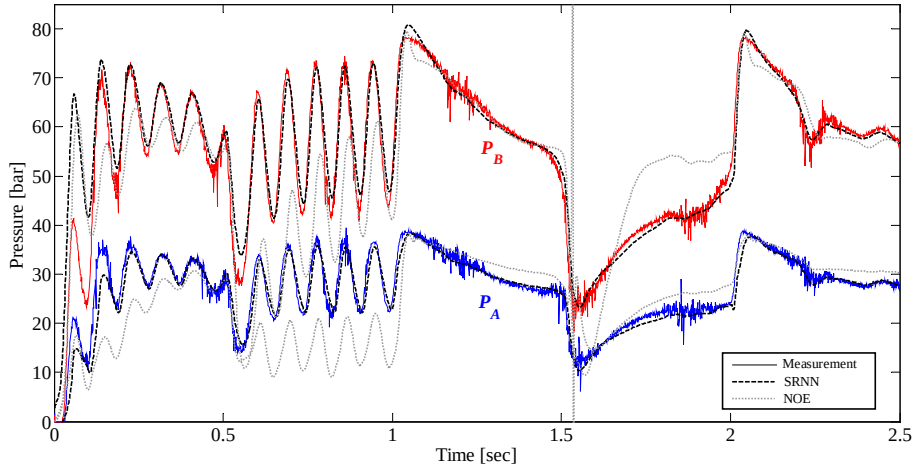

c) Cylinder chamber pressures.

Fig. 5.17 Validation study (v3**)** results.

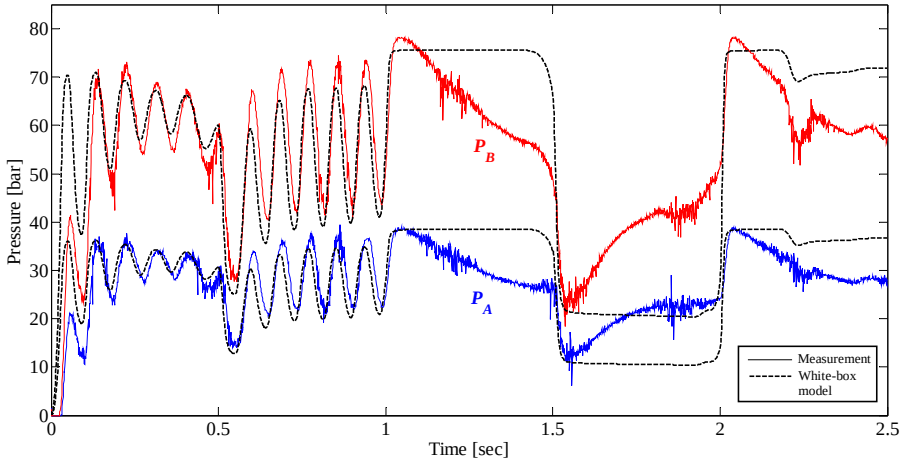

Fig. 5.18 Pressure prediction via white-box modeling approach.

Three more validation tests are realized to check the stability and convergence of the SRNN model when realizing some closed-loop position control tests on the hydraulic system. In validation test **v4**, a 10000 step-ahead prediction test is realized with the servo-valve signal applied to the servo-valve driver as shown in Fig. 5.19.a. The other necessary signal (the actuator velocity) for the predictor model is shown in Fig. 5.19.b. Furthermore, Fig. 5.19.c represents the temporal pressure changes measured by pressure sensors and the predicted ones using the SRNN model. It is found that the RMS error value of the SRNN model is 1.76 *bars* for the prediction of P_A and 3.61 *bars* for the prediction of P_B. Moreover, it can be easily seen that the accuracy FRF of the SRNN model outputs, which are shown in Fig. 5.19.d, are close to actual state for a very broad bandwidth since the ratio is about 1.

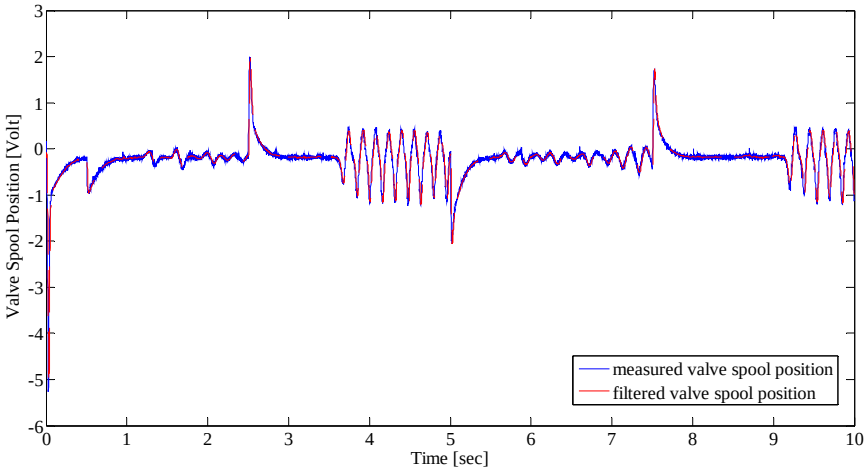

a) Valve spool position.

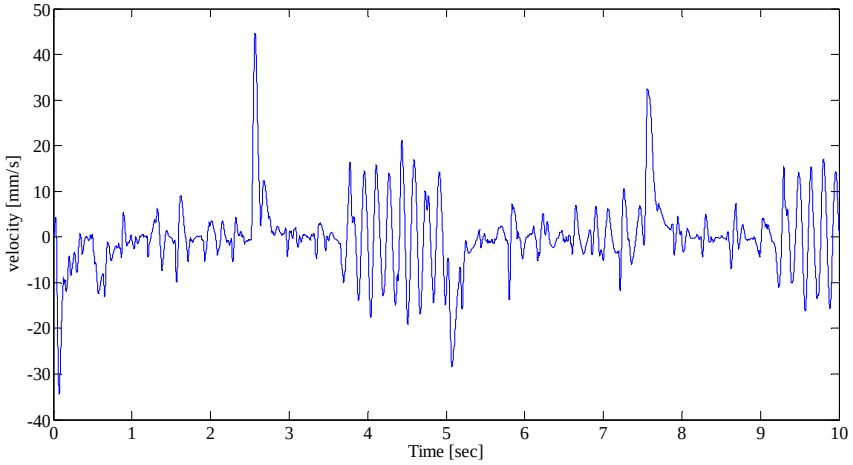

b) Calculated actuator velocity from filtered position signal.

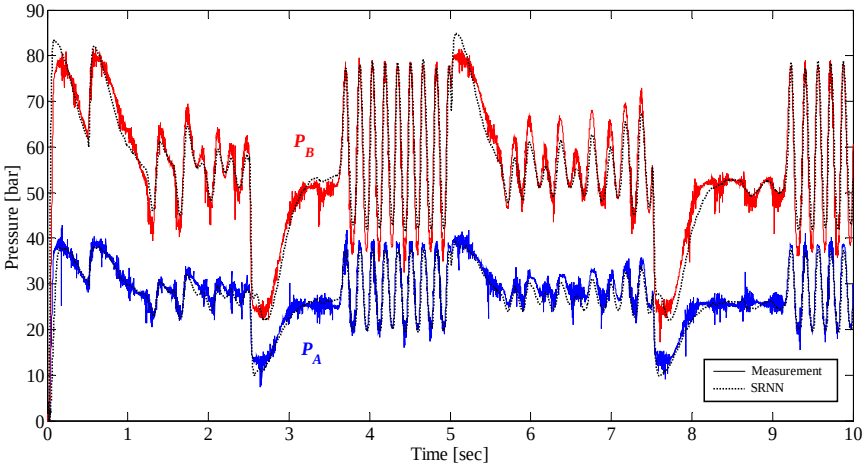

c) Cylinder chamber pressures.

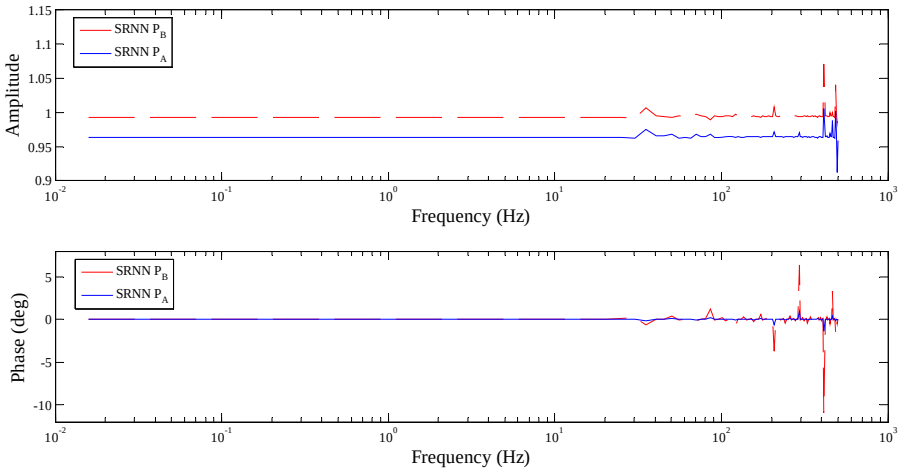

d) Accuracy frequency response functions.

Fig. 5.19 Validation study (v4) results.

In the next validation test (called **v5**), the signals that will be used for the validation of SRNN were shown in Fig. 5.20.a and Fig. 5.20.b, again for a 10000 step ahead prediction task. The measured and predicted pressures are presented in Fig. 5.20.c and it is found that the RMS error values of the SRNN are 1.66 *bars* and 5.48 *bars* when predicting P_A and P_B, respectively. Again, the model accuracy is very high (prediction error is about 2%) up to frequency of 400 *Hz* (except at the frequencies of 35 *Hz* and 210 *Hz*) as indicated by the accuracy FRF of the SRNN model presented in Fig. 5.20.d. It could be said that there is no stability and convergence problem in the long-term pressure prediction (10000 steps) of the servo-valve controlled hydraulic system and the validation performance of the SRNN is quite acceptable.

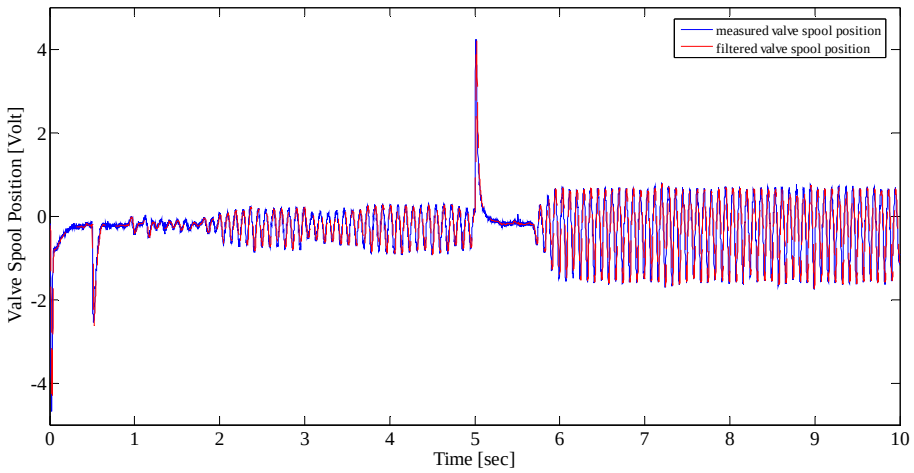

a) Valve spool position.

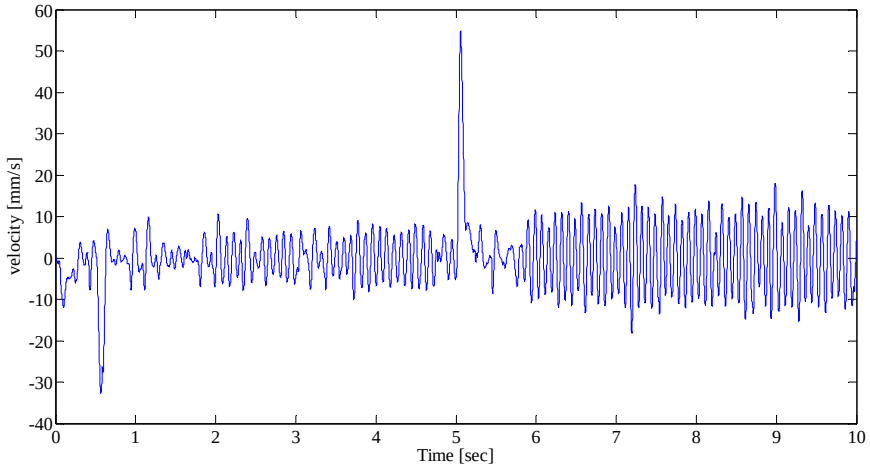

b) Calculated actuator velocity from filtered position signal.

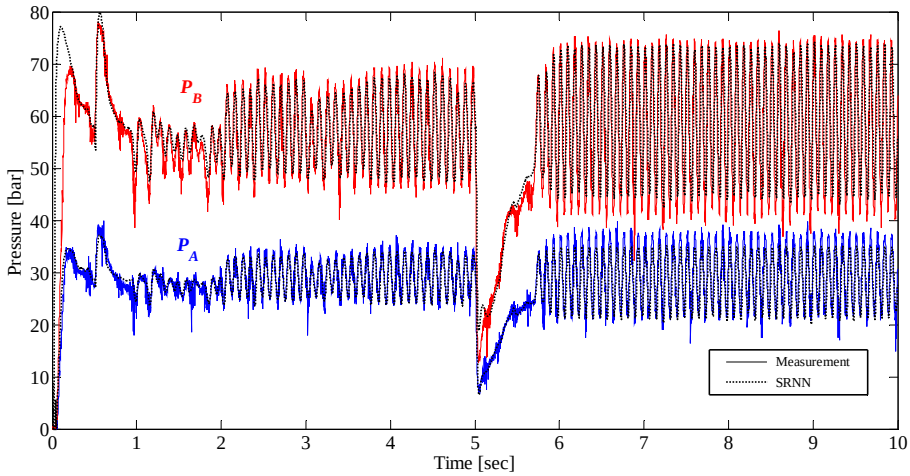

c) Cylinder chamber pressures.

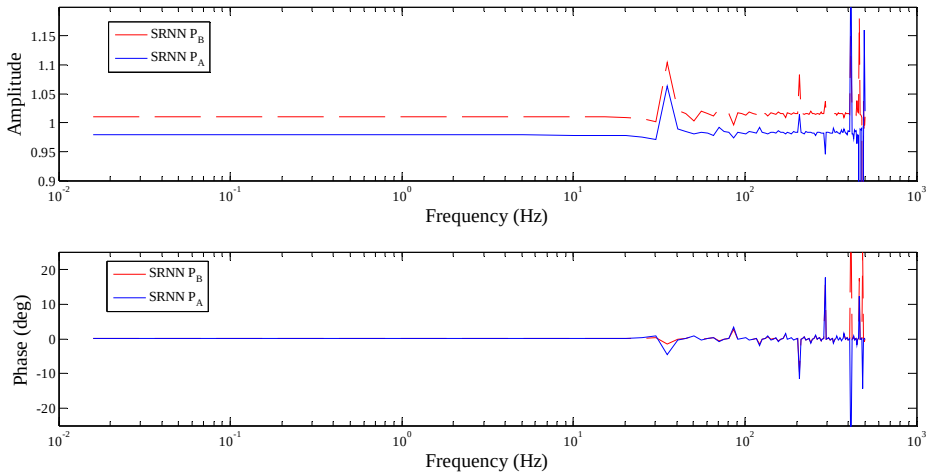

d) Accuracy frequency response functions.

Fig. 5.20 Validation study (v5) results.

In the last validation test scenario (called **v6**), the reference- (command) and the measured position of the actuator are illustrated in Fig. 5.21.a while the other input signals (e.g. the valve position and the velocity of the actuator) for the SRNN are shown in Figs. 5.21.b and 5.21.c. Similarly, Fig. 5.21.d represents the measured pressure changes and the predicted ones using the SRNN model during a very long-prediction period (50000 steps). It is found that the SRNN outputs are in good agreement with the actual pressure states as the corresponding RMS error values simply become 2.646 *bars* and 3.496 *bars* in the cylinder chamber *A* and *B*, respectively. Finally, Fig. 5.21.e illustrates the accuracy FRF of the SRNN for the frequency band of interest. Consequently, the prediction performance of SRNN for this experimental case is quite acceptable for all practical purposes. Hence, the SRNN demonstrates its potential in predicting the chamber pressures for a servo-valve controlled hydraulic system in extended time periods.

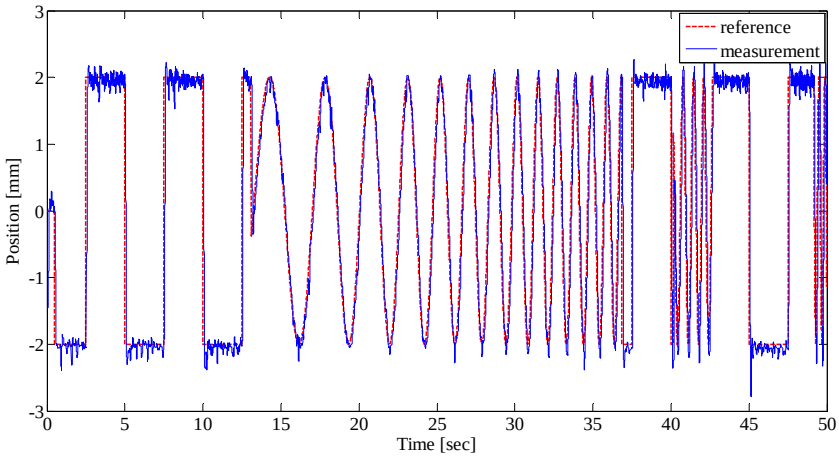

a) Reference and measured actuator position signal.

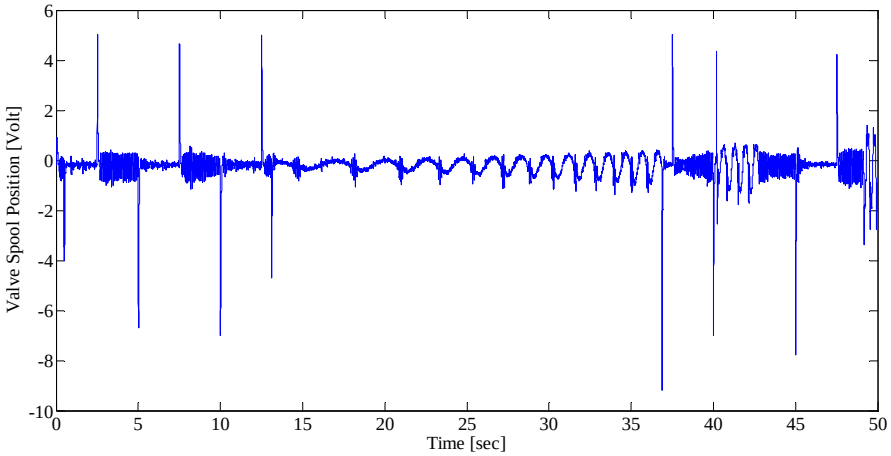

b) Valve spool position.

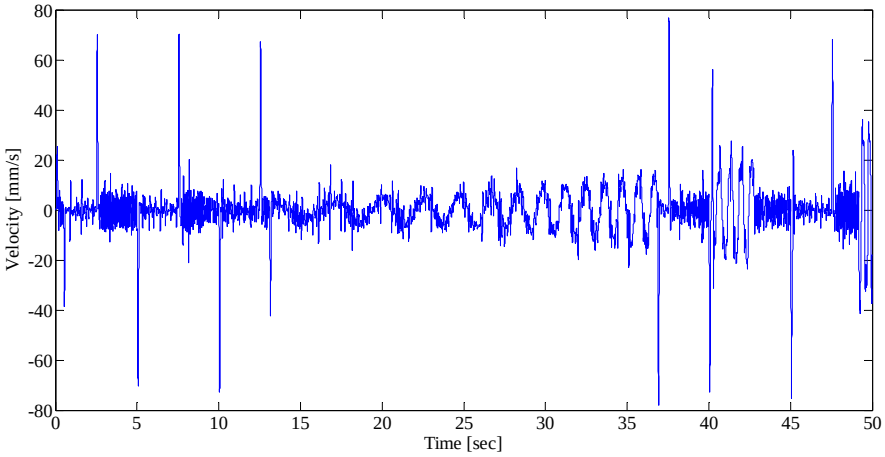

c) Calculated actuator velocity from filtered actuator position signal

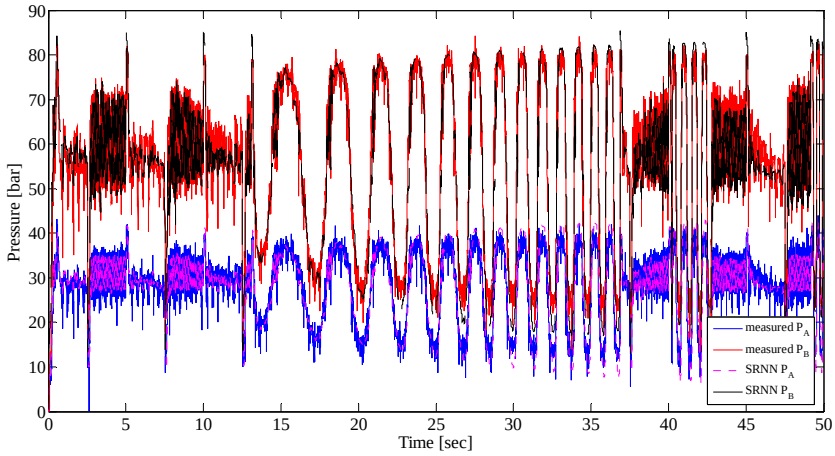

d) Cylinder chamber pressures predicted by SRNN.

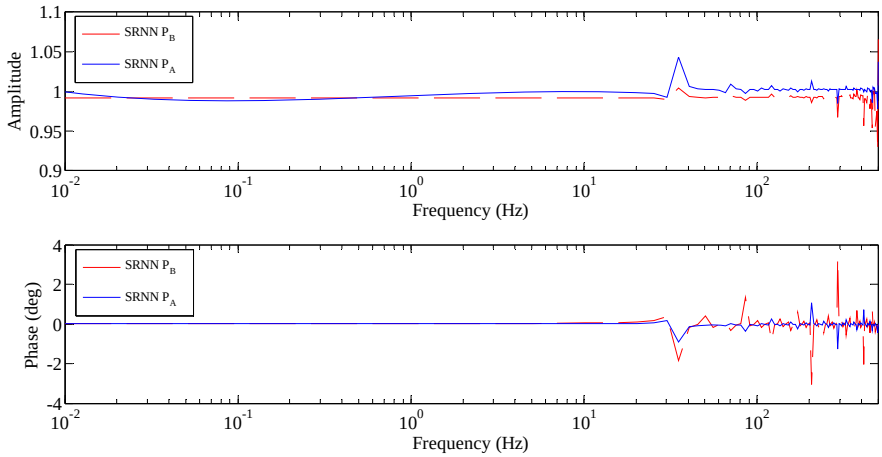

e) Accuracy frequency response functions.

Fig. 5.21 Validation study (v6) results.

5.5 Closure

This study presented a NN-based modeling/identification procedure to predict the long-term pressure dynamics of a valve controlled EHSS. Apart from well-known black-box approaches (NARX and NOE), the study includes a gray-box approach in which a SRNN is employed. The developed black-box models consists of a NN with one hidden layer of sigmoidal neurons and a linear output neuron for the purpose of mapping the regression vector to the predicted chamber pressures. Even though the black-box models yielded acceptable training performance, they have

failed to predict the chamber pressures in the validation scenarios. Therefore, black-box model development paradigms to capture the essence of the pressure dynamics have significant drawbacks.

As an alternative, a gray-box model, which makes good use of a priori information on the process, is developed. In this approach, a specialized network is devised with the sketchy guidance of the mathematical models available. Hence, the pressure dynamics of the EHSS was divided into its sub-systems based on the available mathematical model. Later, a number of smaller neural networks (i.e. *flow-rate models* and *pressure models*) were designed in order to capture the assigned task on them. Then, all these networks were combined to yield a tailored SNN (namely SRNN) for the solution of challenging long-term pressure prediction task problem. The prediction performances of the SRNN were evaluated through a number of (simulation & experimental) case studies. These investigations demonstrated that the SRNN, which has been developed via strong assumptions on the system, exhibited much better (long-term) prediction performance if compared to its counterparts employing weak assumptions. The key points (and contributions) of the study can be summarized as follows:

- Using advanced modeling/filtering/system identification techniques, the long-term prediction of the chamber pressures of an EHSS is not fully explored in the current technical literature. Therefore, the devised SRNN is the first observer system that can be tailored to capture the long-term pressure dynamics of such nonlinear systems accurately.

- All the advanced controllers in the current state of the art exclusively require the measurement of hydraulic (actuator chamber) pressures which in turn increases the overall cost due to pressure sensors and interface circuitry incorporated to the system. Therefore, this study, which concentrates on the accurate estimation of these chamber pressures using ANN models (for the possibility of eliminating costly sensors), complements these research efforts in the literature.

- Study illustrates the adaptation of the SRNN whose free parameters (i.e. synaptic weights) are adjusted via a detailed simulation study on a generic valve-controlled EHSS. The same network (with initial weights intact) was directly applied to model the pressure dynamics of an actual EHSS. After a brief training session, this network was able to predict the chamber pressures of this new experimental system quite accurately (error values of the SRNN are about ±5 bars) in the long run (50000 steps). Training of the presented network is efficient since the SRNN quickly converges to the global optimum point (yielding accurate prediction results) as it does not need to start the training session in any arbitrary point in the huge weight space. Additionally, the study also investigated the changes in the free parameters as the adaptation to the new system (elaborated as experimental test setup) completed. The study shows that no noticeable changes in the hidden layer weights are observed. Similarly, the output weights change slightly but have a considerable influence on the prediction performance of the network.

- The experimental studies revealed that the SRNN could predict the chamber pressures quite accurately (± 5 bars) in relatively long intervals. Apart from advanced control applications, designed structured neural networks could be of special importance in some special applications (like military-, and aerospace systems) where sensor failures could have detrimental effects. Therefore, the presented network could reliably serve as a sensor backup system for degraded mode of operation where some of the pressure sensors in the hydraulic system malfunction.

CHAPTER 6

PRESSURE PREDICTION OF A VARIABLE-SPEED PUMP CONTROLLED HYDRAULIC SYSTEM

6.1 Introduction

In electro-hydraulic servo-systems, the hydraulic power is either controlled by throttling principle (using servo-valves) or by volumetric control principle (via adjusting the rotational speed of a constant-displacement pump by a servo motor or via adjusting the pump displacement by a swash plate).

The former principle offers good dynamic behavior at the expense of substantial energy losses at the flow control device. On the other hand, the latter principle yields increased efficiency with a poor dynamic response. When the emphasis is placed on the high power transmission with low energy losses (i.e. cost-effectiveness), variable-speed pump-controlled hydraulic systems are generally preferred in the drive systems of the contemporary machine systems (Helbig, 2002; Helduser, 2003; Lovrec and Ulaga, 2007; Lovrec et al., 2008).

As similar to the Chapter 5, the objective of this work is to predict the long-term pressure dynamics of a variable speed pump controlled hydraulic system as the pressures in cylinder chambers of a hydraulic actuator are needed in various control tasks. Again, a structured recurrent neural network is proposed as the solution of long-term pressure prediction problem after seeing that black-box models could not deal with such a challenging task at hand.

The rest of the chapter is organized as follows: After this brief introduction part in Section 6.1, a variable speed pump controlled hydraulic system and its model is given in Section 6.2. Following that, some RNN models are trained in order to predict the cylinder chamber pressures using black-box- and gray-box modeling approaches in Section 6.3. Next, Section 6.4 illustrates the practical usage of the structured RNN (as devised in Section 6.3) on the hydraulic experimental test set up. Finally, concluding remarks are presented in Section 6.5.

6.2 Pump Controlled Hydraulic System

The hydraulic experimental test setup was explained in Section 5.4.1 in a detailed manner. In addition, hydraulic circuit of the variable-speed pump controlled mode of the experimental setup and its position controller topology is now illustrated in Fig. 6.1.

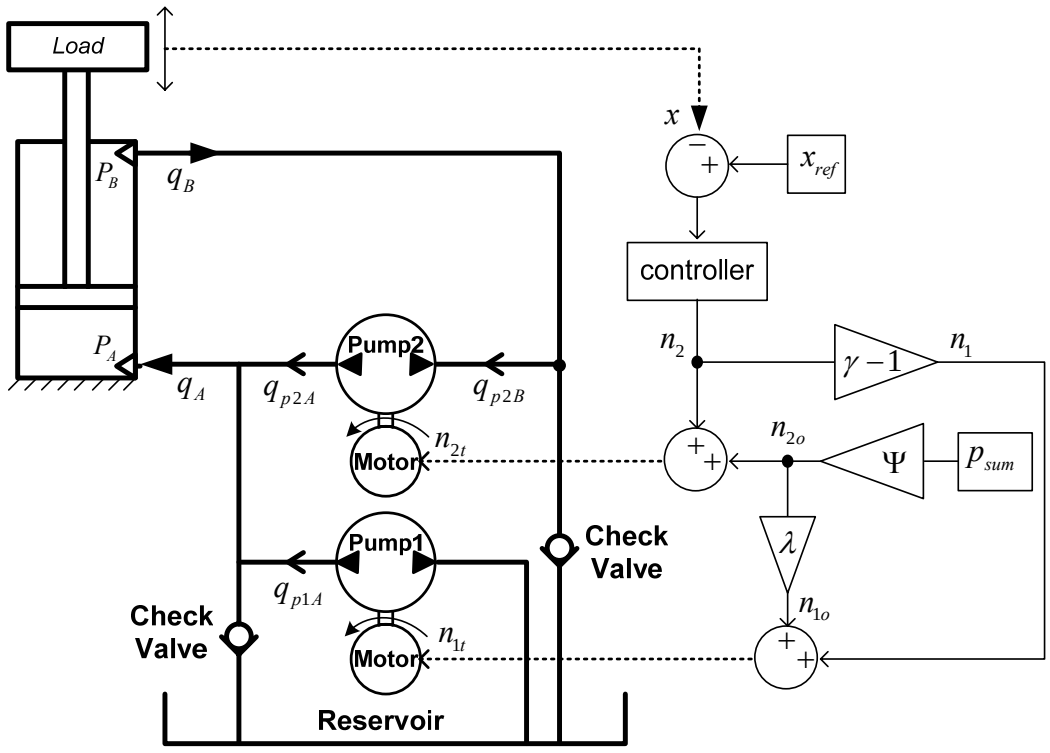

Fig. 6.1 Schematic diagram of the experimental test setup (Caliskan, 2009).

6.2.1 Mathematical Model

First of all, the model describing the pump controlled mode of the system must be devised in order to apply the structured neural network (SNN) methodology (Dolen, 2000). All the relevant equations, which are related to the pressure dynamics of the hydraulic setup, are elaborated here to reveal the interactions among the sub-systems.

The flow rates of the pumps are adjusted via manipulating the drive speeds of the servo-motors in order to control the position of the hydraulic actuator. Pumps rotate in either direction according to the flow needed by the system. As could be seen from the controller topology, there are two control loops which regulate the piston pressure and the position, separately. Therefore, the reference inputs of the independent controllers are the reference position (x_{ref}) and the desired value for the sum of chamber pressures at steady state (p_{sum}) as presented below.

$$p_{sum} = P_{A\_steady\,state} + P_{B\_steady\,state} \tag{6.1}$$

The pressure control-loop is used both to pressurize the cylinder chambers to a predetermined value and to compensate the pump leakages so as to maintain the stability of the hydraulic cylinder. Similarly, the *offset speeds of pump 1 (n_{1o})* and *pump 2* (n_{2o}) are related to each other as

$$n_{1o} = \lambda n_{2o} \tag{6.2}$$

where λ has a negative value. Furthermore, Ψ is another constant used in the pressure controller in order to determine the ratio between p_{sum} and n_{2o}. The steady state dynamics of the hydraulic system is utilized to find the value of these constants.

Furthermore, the task of the position control loop is to create a manipulated input signal n_2. The cylinder used in the system is a single rod differential cylinder with an area ratio defined as

$$\gamma = \frac{A_A}{A_B} \tag{6.3}$$

where A_A and A_B are the piston annulus areas in the actuator chambers A and B, respectively. In this controller topology, the hydraulic cylinder is actually moved by *pump 2*. On the other hand, *pump 1*is only used for the compensation of the asymmetric flow rate due to this differential cylinder. In order to perform this task, the ratio between the dynamic pump speeds is defined as

$$n_1 = (\gamma - 1) n_2 \tag{6.4}$$

As shown in Fig. 6.1, when the pumps rotate in the counter clockwise direction, the flow continuity equations of this hydraulic system could be written from Fig. 6.1 as follow

$$q_{p2A} = D_P n_{2t} - C_i (P_A - P_B) - C_{ea} P_A \tag{6.5}$$

$$q_{p2B} = D_P n_{2t} - C_i (P_A - P_B) + C_{eb} P_B \tag{6.6}$$

$$q_{p1A} = D_P n_{1t} - C_i P_A - C_{ea} P_A \tag{6.7}$$

$$q_A = q_{p2A} + q_{p1A} \tag{6.8}$$

$$q_B = q_{p2B} \tag{6.9}$$

where the terms P_A and P_B represent the hydraulic cylinder cap end side and rod end side chamber pressures, D_P is the pump displacement, C_i is the internal leakage, C_{ea}

and C_{eb} are the external leakage coefficients of the *pump 1* and *pump 2*, respectively. Moreover, n_{1t} and n_{2t} represent the rotational speed of *pump 1* and *pump 2* in terms of revolution per second (rps).

Similar to the servo-valve controlled mode of the hydraulic system, the flow continuity equations for the cylinder chambers are as below

$$q_A = A_A \dot{x} + \frac{V_A(x)}{\beta} \frac{dP_A}{dt} \tag{6.10}$$

$$q_B = A_B \dot{x} - \frac{V_B(x)}{\beta} \frac{dP_B}{dt} \tag{6.11}$$

where β is the bulk modulus of the oil. In (6.10) and (6.11), the hydraulic cylinder chamber volumes are not constant but do change with the hydraulic cylinder position as $V_A(x) = A_A x + V_{A0}$ and $V_B(x) = -A_B x + V_{B0}$ where V_{A0} and V_{B0} are initial chamber volumes when the piston is at the midpoint of the hydraulic cylinder.

Defining the load pressure as shown below

$$P_L = \gamma P_A - P_B \tag{6.12}$$

The force transmitted to the load becomes

$$f_L = P_L A_B \tag{6.13}$$

Next, the Newton's 2nd law could be applied to the load as

$$f_L = m\ddot{x} + b\dot{x} + mg + f_{fric} \tag{6.14}$$

In Eq. (6.14), friction force is defined by again a LuGre model as it is given in (5.7) and (5.8). The numerical values of the physical parameters used in the simulation study are presented in Table 6.1.

Table 6.1 Model parameters used in the simulation study.

Parameter	Value	Parameter	Value
m	12.3 *kg*	σ_0	$12\text{x}10^2$ *N/mm*
A_A	1.9635 mm^2	σ_1	2.6 *Ns/mm*
A_B	1.0014 mm^2	σ_2	2.6 *Ns/mm*
V_{Ao}	$1.4258\ \text{x}10^5$ mm^3	F_c	330 *N*
V_{Bo}	$7.6821\ \text{x}10^4$ mm^3	F_s	360 *N*
D_p	$15.6\ \text{x}10^3$ mm^3/rev	v_s	100 *mm/s*
C_i	1027 $mm^3/(s \cdot MPa)$	λ	-1.2294
C_{ea}	120 $mm^3/(s \cdot MPa)$	Ψ	-0.0265
C_{eb}	120 $mm^3/(s \cdot MPa)$	β	1300 *MPa*

6.3 Prediction Models and Parameter Estimation

In this section, the problem of creating accurate ANN models for the long-term pressure prediction in the cylinder chambers for a (variable-speed) pump-controlled hydraulic system is to be handled by black-box- and gray-box (i.e SNN) modeling approaches. These predictive models are initially developed via simulation data rather than experimental data due to two main reasons:

First of all, black-box- and gray-box models devised in Sections 6.3.1 and 6.3.2 via a simulated hydraulic system, whose physical system parameters are close to those of the actual system, will yield reliable initial conditions (i.e. start-off weights) for further training of the network via experimental data. Note that, despite the devised SNN is shown to have optimal architecture (i.e. reduced-order nonlinear state observer), the resultant network totally fails to yield expectable performance in the training session if its weights are initialized randomly. That is, the training

operation with arbitrary initial weights will increase the possibility of catching by a local minimum in the huge weight (search) space.

Secondly, the design (and also the training) of the gray-box (namely, SNN) modeling approach will need (normally) the unmeasured states such as the flow rates (q_A and q_B) when the long-term pressure prediction problem is divided into its fundamental components as will be shown in Section 6.3.2. It is seen that capturing the exact pressure dynamics of the simulated hydraulic system without the measurements of the control flow rates is extremely difficult. Since there are no flow meters on the experimental set-up, the gray-box model is developed first for a simulation based study and then applied (e.g. trained / fine-tuned and tested) on the experimental setup.

6.3.1 Black-box Approach

First, some neural networks, using the black-box modeling approach, are to be devised for the long-term pressure prediction of the cylinder chambers in the simulated system. It is important to note that only the position of the hydraulic actuator ($x(k)$) and the rotational speed of the pumps (n_{1t} and n_{2t}) are used as inputs to the devised models.

A PRMS type signal, given in Fig. 6.2.a, is applied to system and then, the n_{1t} and n_{2t} signals are formed based on this n_2 signal as shown in Fig. 6.1. Note that p_{sum} is set to 12 MPa in the simulated study. Furthermore, Fig. 6.2.b represents the position and velocity profile of the hydraulic actuator and Fig. 6.2.c shows chamber pressures for this training scenario.

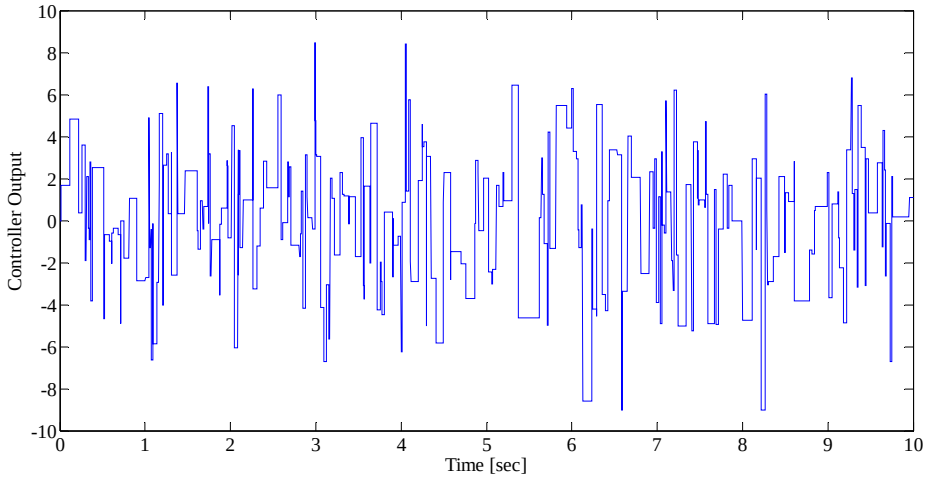

a) Controller signal.

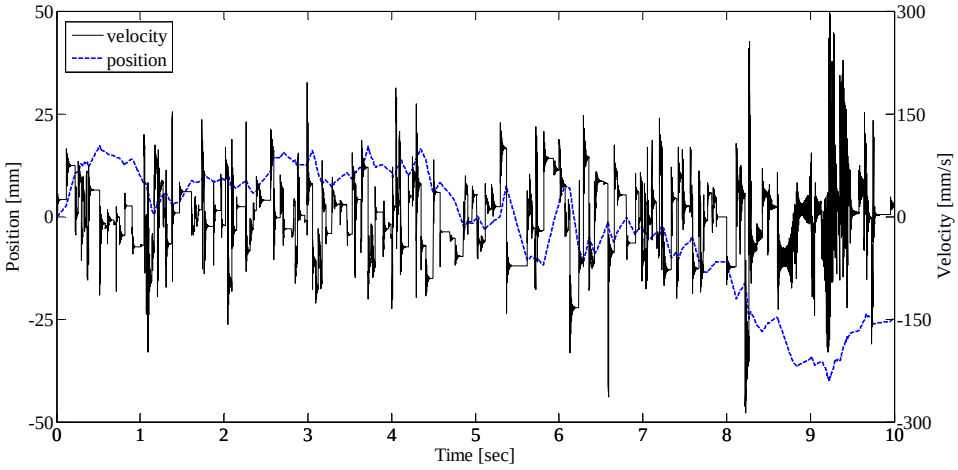

b) Cylinder position and velocity.

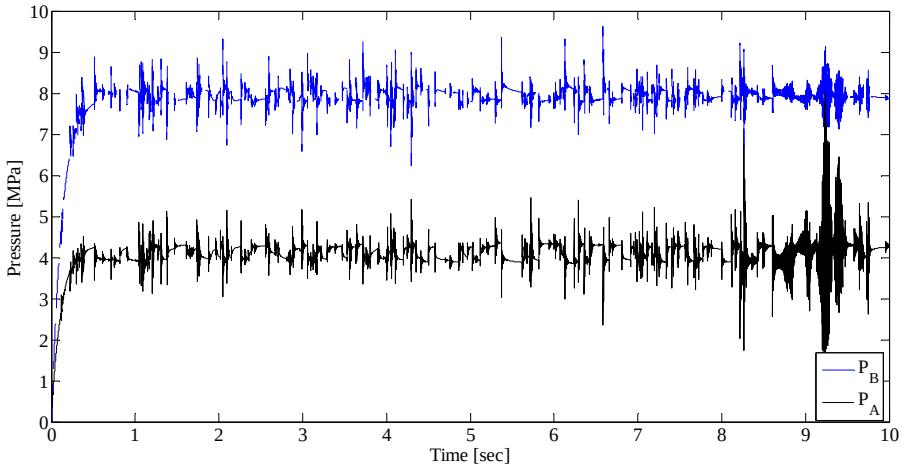

c) Pressures in the cylinder chambers.

Fig. 6.2 Training scenario for the variable speed pump controlled hydraulic system.

Next, the elements of the input vector of the black-box models should be determined as in the form given below.

$$\varphi(k) = [n_{1t}(k),\ldots, n_{1t}(k-l), n_{2t}(k),\ldots, n_{2t}(k-l), x(k),\ldots, x(k-m), \\ v(k),\ldots, v(k-n), P_A(k-1),\ldots, P_A(k-p), \quad P_B(k-1),\ldots, P_B(k-p)]^T \tag{6.15}$$

For that purpose, various NARX models, which utilize different order of TDL input signals, are trained in a feed-forward fashion. That is, the old pressure values coming from the "simulated" pressure sensors are directly fed to the network as could be seen from (6.15).

The training performance of these black-box models are summarized in Table 6.2. Architecture #8 is chosen as the topology for the black-box model since it has the minimum RMS error value. Note that the training performances all of the NARX models are very satisfactory since they are utilizing measured pressure states directly in the regression vector. However, the models must be arranged in recurrent (feedback) form meaning that the previous pressure values must come from the network's output itself in the validation case of which is expected to differ significantly from the training scenario.

Following that, the outputs of the architecture #8 are delayed as necessary and connected to its 1st layer. As the architecture of the network is now changed due this feedback, the resulting network will be named as NOE from that point on. The NOE could train itself without any problem in a recurrent form provided that the initial weight values are taken from the NARX model. After a training process (10 epoch) in which the training duration is 70 minute, it is found that the training error of the NOE was about 0.2 MPa. Hence, the final NOE network is able to predict the pressure states without utilizing any pressure sensors. The model validation performance of the resulting network will be evaluated in Section 6.3.3.

Table 6.2 Trained NARX models in black-box approach [*].

Architecture	**#1**	**#2**	**#3**	**#4**	**#5**	**#6**	**#7**	**#8**	**#9**
Inputs	$n_{1t}(k)$ $n_{2t}(k)$ $x(k)$ $v(k)$ $P_A(k-1)$ $P_B(k-1)$			$n_{1t}(k)$, $n_{1t}(k-1)$ $n_{2t}(k)$, $n_{2t}(k-1)$ $x(k)$, $x(k-1)$ $v(k)$, $v(k-1)$ $P_A(k-1)$, $P_A(k-2)$ $P_B(k-1)$, $P_B(k-2)$			$n_{1t}(k)$, $n_{1t}(k-1)$, $n_{1t}(k-2)$ $n_{2t}(k)$, $n_{2t}(k-1)$, $n_{2t}(k-2)$ $x(k)$, $x(k-1)$, $x(k-2)$ $v(k)$, $v(k-1)$, $v(k-2)$ $P_A(k-1)$, $P_A(k-2)$, $P_A(k-3)$ $P_B(k-1)$, $P_B(k-2)$, $P_B(k-3)$		
Outputs	$P_A(k)$ and $P_B(k)$								
Training error in (*MPa*)	0.09	0.07	0.07	0.02	0.01	$8\text{x}10^{-3}$	0.01	$5\text{x}10^{-3}$	$6\text{x}10^{-3}$
Training data	10001 Sample for each variable								
Epochs	1000						2000		
Training time (min)	1.5	3	5	2	5	9	6	15	25
1st layer neurons	5	10	15	5	10	15	5	10	15
Act. function	Tangent sigmoid								
Training method	Levenberg-Marquardt								

[*] Linear activation function is utilized at the output layers.

6.3.2 Gray-box (SNN) Approach

If the mathematical model of this hydraulic system is examined from Section 6.2.1, it is seen that the model could be easily separated into two parts: *flow-rate model* and *pressure model*. Fig. 6.3 illustrates the topology of the devised structured recurrent neural network where $G = (\beta\, q_{\max} T) / (V_{x0}\, P_{\max})$ is a connection gain due to the normalization operation and the subscript x denotes a placeholder for letters *A* and *B*. Moreover, *T* denotes the sampling period, again. The modules of the devised SRNN are explained in the following sections.

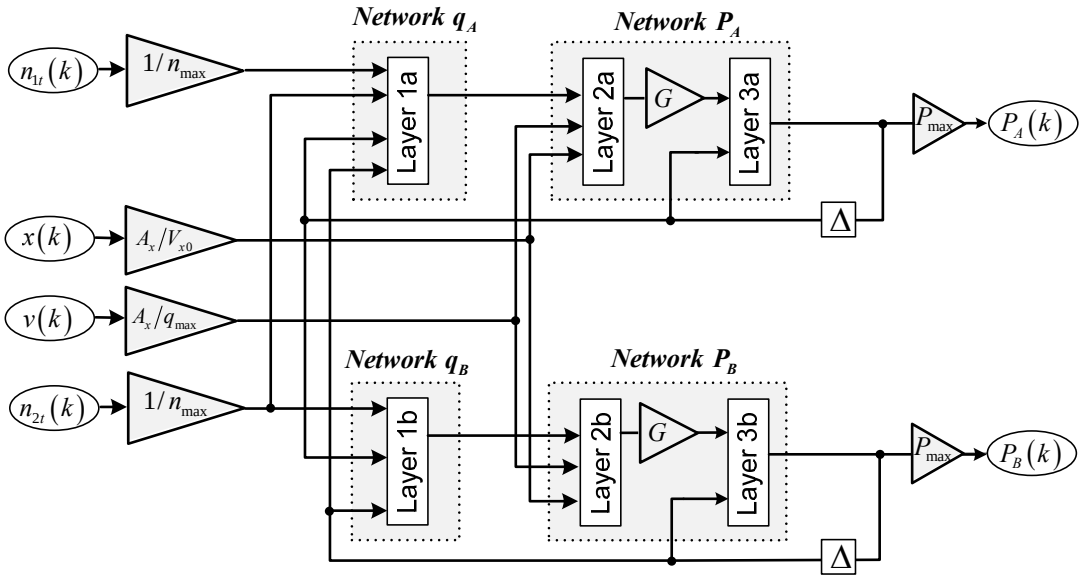

Fig. 6.3 Schematic of the structured recurrent neural network.

6.3.2.1 Flow-rate Model

Normalized flow-rates could be estimated by a simple linear model using *a priori* information about the process using (6.5) to (6.9) as below

$$\overline{q}_x(k) = \theta_x^T \overline{\varphi}_x(k) \tag{6.16}$$

$$\overline{\varphi}_A(k) = [\overline{n}_{1t}(k), \overline{n}_{2t}(k), \overline{P}_A(k), \overline{P}_B(k)]^T \tag{6.17a}$$

$$\overline{\varphi}_B(k) = [\overline{n}_{2t}(k), \overline{P}_A(k), \overline{P}_B(k)]^T \tag{6.17b}$$

Hence, (6.5-6.9) are linear equations; they are modeled using a network with only a one neuron having a linear activation function so that this network model simply boils down to an ARX model. Again, the training input signal in Fig. 6.2.a is applied and then the normalized forms of the related input and output signals, which will be required in the training operation of the *flow-rate models*, are captured from the simulated system. Table 6.3 shows the training performances of the linear

models (labeled as *Network* q_A and *Network* q_B) that are used to predict the flow rates in each chamber. It is critical to notice that this flow-rate model requires the pressure estimates at time instant *kT*. But, such an estimate will not be available at the desired time while the SRNN is running for a prediction task. Therefore, pressure estimates at $t = (k-1)T$ will be utilized as the inputs of the flow rate models assuming that the pressure values are almost same within one sampling interval.

Table 6.3 Trained *flow rate models* in gray-box approach.

Architecture	***Network*** q_A	***Network*** q_B
Inputs	$\bar{n}_{1t}(k), \bar{n}_{2t}(k), \bar{P}_A(k), \bar{P}_B(k)$	$\bar{n}_{2t}(k), \bar{P}_A(k), \bar{P}_B(k)$
Output	$\bar{q}_A(k)$	$\bar{q}_B(k)$
Training data	10001 Sample	
Training error in (mm^3/s)	2.151×10^{-6}	1.4034×10^{-6}
Epochs	1	
1st layer neurons	1	
Activation function	Linear	
Training method	Least mean square	

6.3.2.2 Pressure Model

It is obvious that the chamber pressures could be computed via (6.10) and (6.11) in a similar way as done in Section 5.3.2.2. Therefore, the same pressure models, named as *Network* P_A and *Network* P_B, are utilized to solve the pressure dynamics in the cylinder chambers. It is critical to note that the pressure states are directly taken from the simulated system and utilized in the regression vector of these models during the training session in order to increase their training performance. But, all the related models are then reconfigured in a recurrent arrangement as presented in Fig. 6.3.

Next, all the modules are connected to each other to form the unified network, called SRNN. Furthermore, this SRNN model could be trained in the unified form

for fine tuning of its weight parameters based on the training scenario. It is seen that the training RMS error of the SRNN decreases from 0.4 MPa level to 0.2 MPa level within 5 epochs while training session lasts about 35 minutes. The model validation performance of the SRNN network is evaluated in the next section.

6.3.3 Prediction Results

A validation study is conducted on the simulated system via the rotational speed of the pumps, realistic input signals which are collected from the experimental setup as shown in Fig. 6.4.a, are used in the simulated system to create a 50000 step-ahead prediction task. The hydraulic system presented in Fig. 6.1 is simulated with these chirp signals (0.1 Hz to 10 Hz in 50 seconds) with increasing amplitude. Fig. 6.4.b represents the validation performance of the NOE network and it is seen that the validation performance of this network model is unacceptable for all practical purposes. On the other hand, Fig. 6.4.c represents the pressure values in the cylinder chambers calculated from the simulated system model and the SRNN model. It is found that the RMS errors of the SRNN model are 0.0547 MPa and 0.0911 MPa for the prediction of P_A and P_B respectively. Therefore, it could be inferred that the pressure dynamics of the simulated system is accurately captured by the SRNN model.

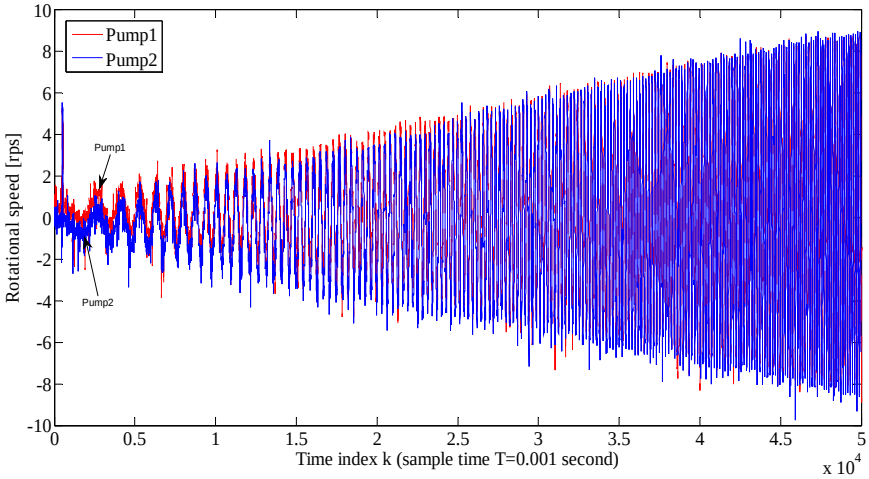

a) Rotational speed of pumps.

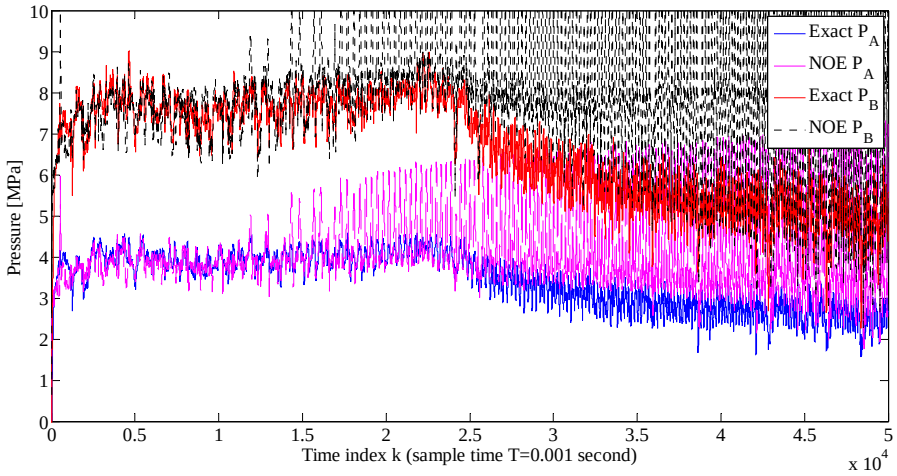

b) Prediction via NOE.

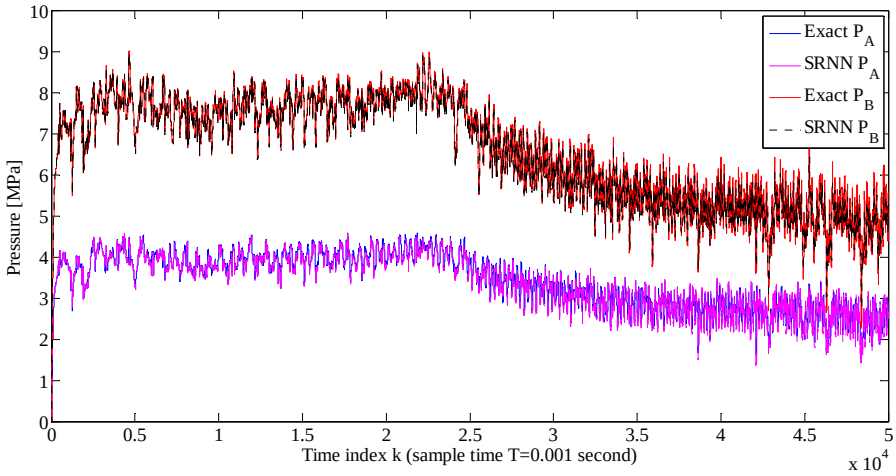

c) Prediction via SRNN.

Fig. 6.4 Model validation test results.

6.4 Experimental Pressure Prediction Results and Discussion

In this section, the versatility of the SRNN (as elaborated in Section 6.3.2) is to be tested on the experimental setup. Therefore, the network, which was developed in a simulation environment, is to be trained via the data collected on the experimental setup. Unfortunately, training the SRNN as a whole is a very difficult feat for a test duration of 50 seconds (meaning that 50,000 step ahead prediction is required) where the workstation (with Intel Core i5 processor and a SDRAM of 4GB) used in

the study will be stretched to its limits. For that reason, the SRNN shown in Fig. 6.3 is divided into two (titled as *RNN* P_A and *RNN* P_B) parts and are trained (separately) to predict the pressure change in each chamber assuming that the opposite chamber pressure is known in the training session. Figs. 6.5 and 6.6 illustrate the networks in such a configuration.

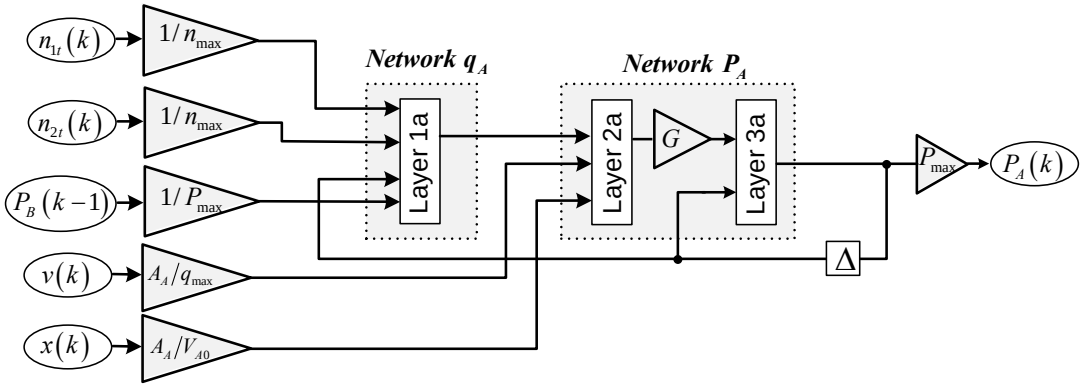

Fig. 6.5 *RNN* P_A for the pressure prediction in chamber *A*.

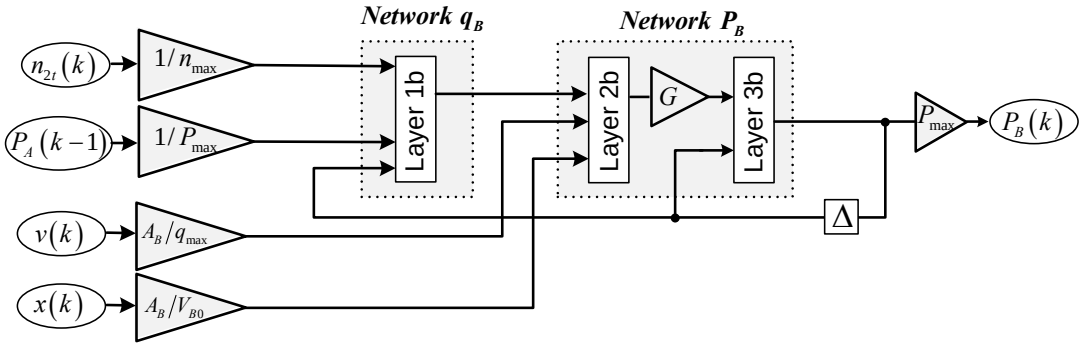

Fig. 6.6 *RNN* P_B for the pressure prediction in chamber *B*.

Next, the formed RNNs are trained using the measured signals that are presented in Fig. 6.7. That is, the rotational speeds of the pumps are given in Fig. 6.7.a. On the other hand, Fig. 6.7.b shows the measured position of the cylinder in this training

scenario. As could be seen, the noise on the position transducer will aggravate the noise on the calculated velocity significantly unless any filtering operation is applied on position signal. Therefore, the position signal is filtered before the velocity calculation. For that purpose, a discrete-time low-pass filter with a cut off frequency of 30 Hz is used. Fig. 6.7.c presents the calculated cylinder velocity (as required in the regression vector) from the filtered actuator position signal using the first-order difference method. Similarly, the target pressure values and the RNN outputs after the training operation is given in Fig. 6.7.d while Table 6.4 represents the training performances of the RNNs. To assess the generalization performance, a validation scenario, which is illustrated in Fig. 6.8, is considered. As can be seen, the performances of the RNNs are very satisfactory (since RMS prediction error in P_A is 0.112 MPa and in P_B is 0.195 MPa) when the assumption on opposite chamber pressure is satisfied.

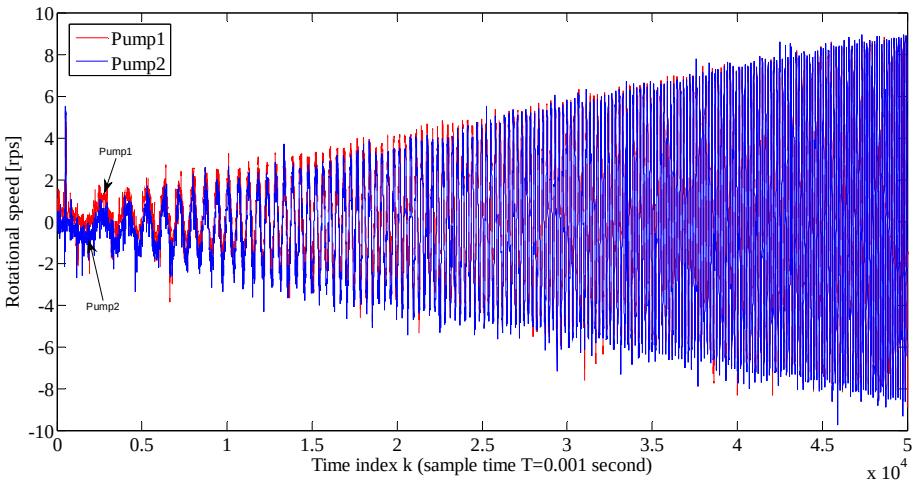

a) Rotational speed of the pumps.

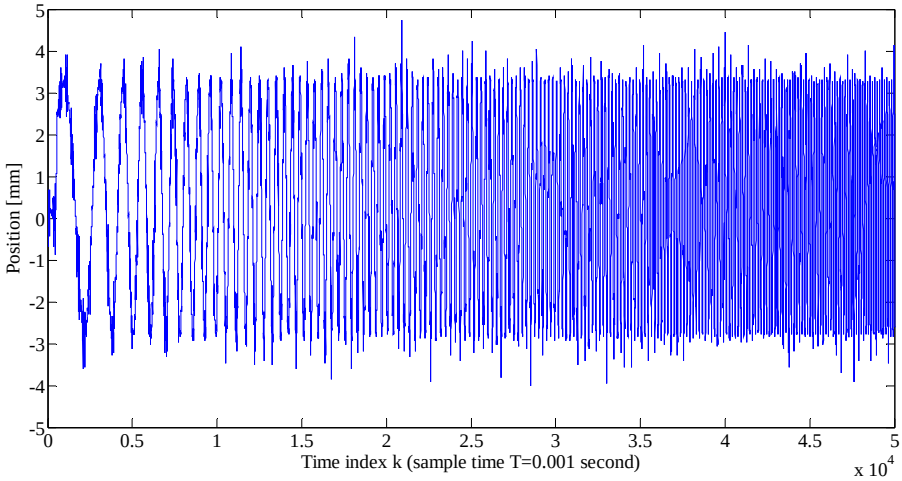

b) Measured cylinder position.

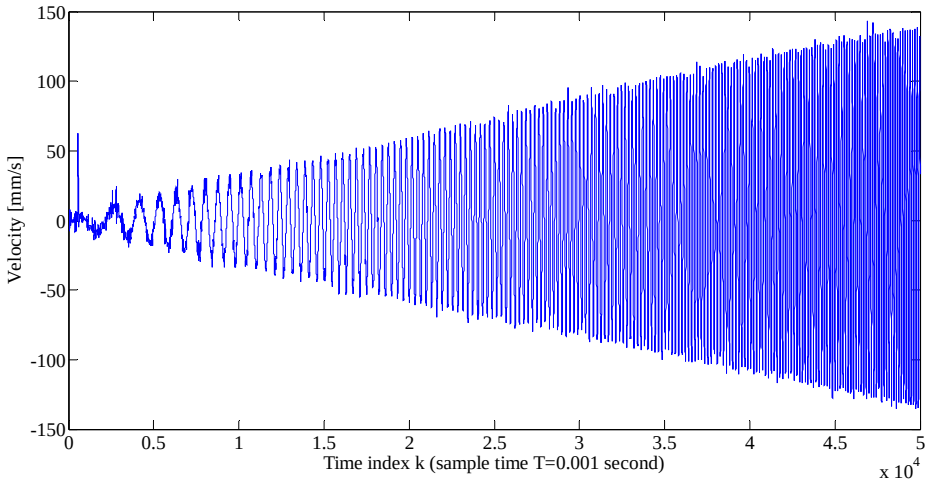

c) Calculated cylinder velocity from the filtered position signal.

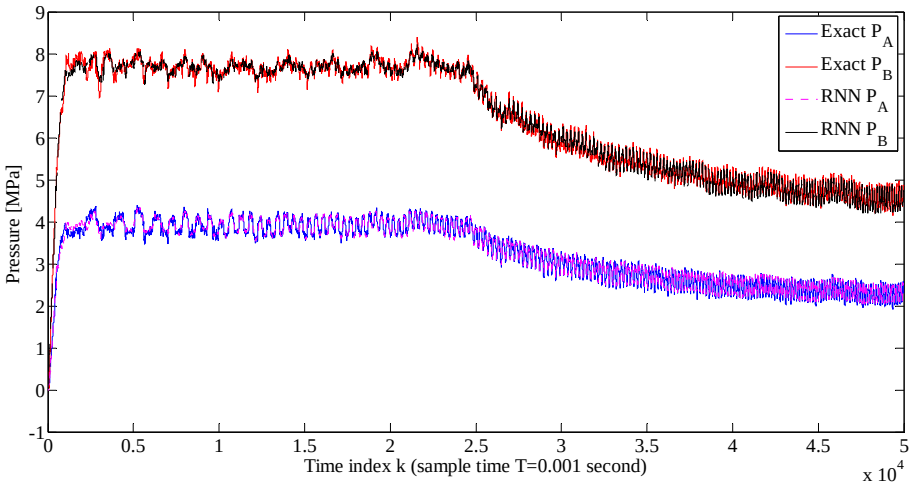

d) Target pressures and model outputs after the training session.

Fig. 6.7 Training signals for the experimental study.

Table 6.4 Training properties of the RNNs.

Architecture	***RNN P_A***	***RNN P_B***
Inputs	$n_{1t}(k), n_{2t}(k), P_B(k-1), v(k), x(k)$	$n_{2t}(k), P_A(k-1), v(k), x(k)$
Output	$P_A(k)$	$P_B(k)$
Training data	50001 Sample	
Training error	0.092 *MPa*	0.116 *MPa*
Epochs	10	
Training time	365 minute	
1st layer neurons	1Linear	
2nd layer neurons	20 Tangent Sigmoid	
3rd layer neurons	1Linear	

Finally, the *RNN* P_A and *RNN* P_B are coupled to each other to form the SRNN. Therefore, the inputs to the designed model without any feedback (at any rate) from the pressure sensors will only be the rotational speed of *pump 1* and *pump 2*, the position and the velocity of the hydraulic cylinder. However, the SRNN outputs deviate significantly from the chamber pressures measured on the experimental setup at long intervals as could be seen from the validation performance of this network given in Fig. 6.9. Since the two outputs of the SRNN are highly cross coupled to each other, the presented model could not satisfactorily predict the pressure states in the cylinder chambers. At least, one of the chamber pressure should be known beforehand to predict the opposite chamber pressure accurately. In any way, the presented model could be used to predict the pressure in one chamber quite accurately with an RMS error of 0.2 MPa (where the pressure varies in between *0* and *10* MPa) when the pressure value of the opposite chamber is available. Therefore, one of the advantages of the developed SRNN for the hydraulic system at hand is to reduce the total number of pressure sensors in such hydraulic systems from two to one or the model could be used as a (software) sensor backup system when a fault is occurred in one of the pressure sensors.

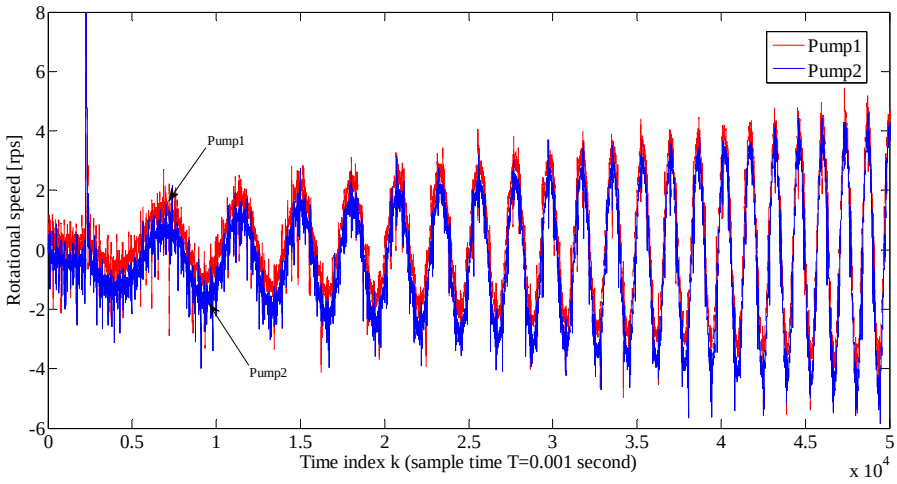

a) Rotational speed of pumps.

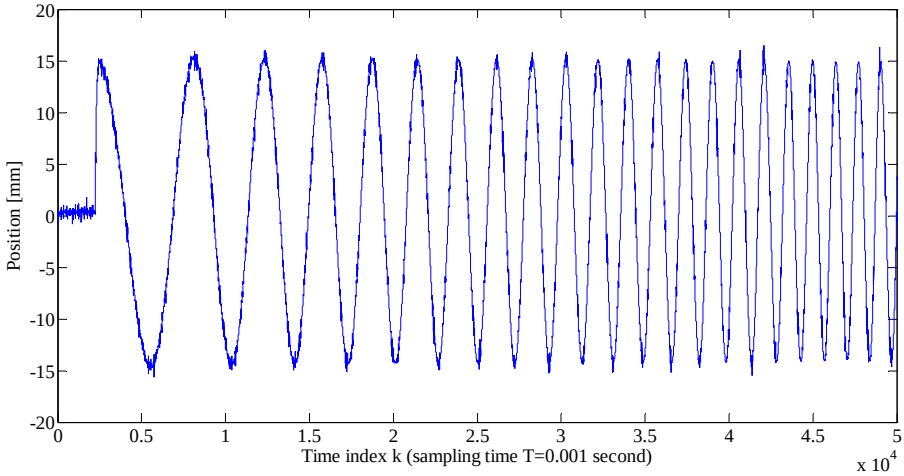

b) Cylinder position.

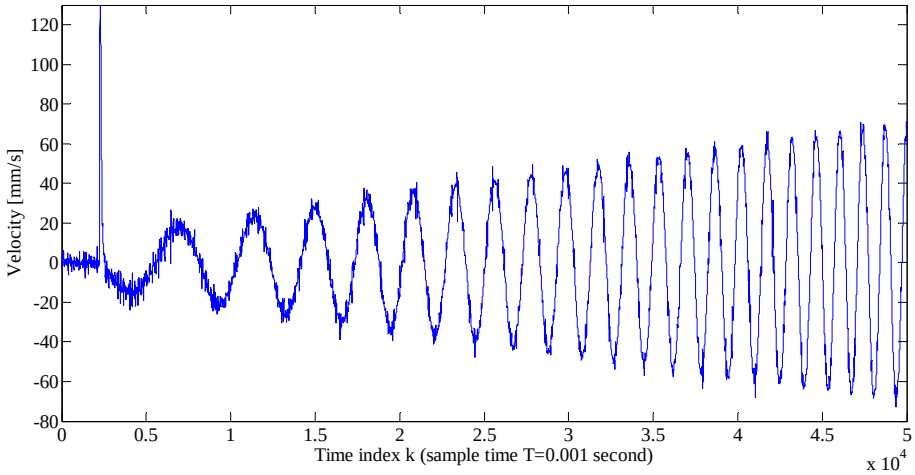

c) Cylinder velocity.

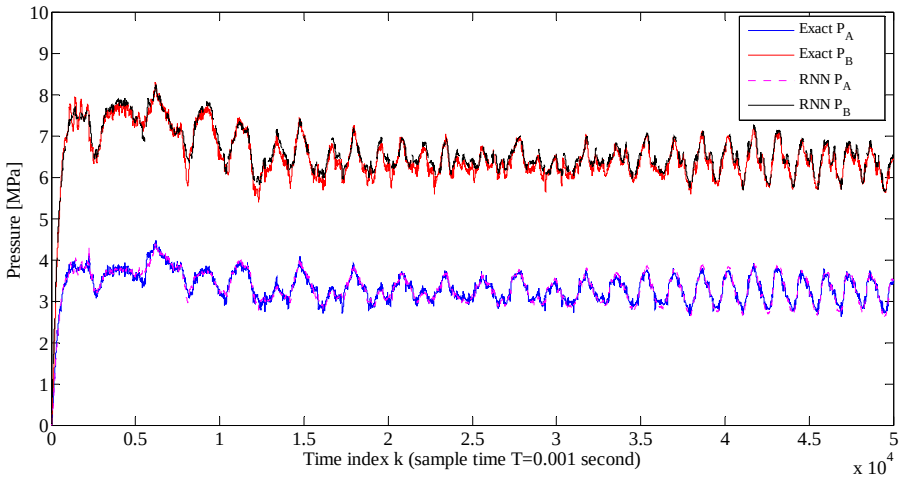

d) Measured pressures and RNNs outputs.

Fig. 6.8 Validation test of the *RNNs.*

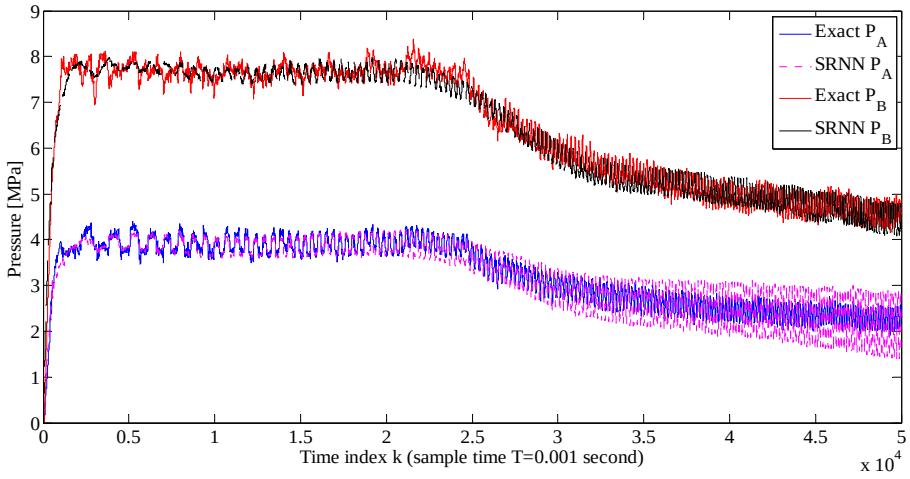

Fig. 6.9 Validation test of the *SRNN.*

Another interesting point worth mentioning is that when this SRNN architecture is to be trained by starting off with an arbitrary set of initial weights, the network could not capture the dynamic behavior of the system. Therefore, determining the optimal architecture (size, correct regression vector, etc.) does not guarantee the solution of the estimation problem at hand. In fact, the SRNN network, which was trained initially via the data on simulated plant, can be easily adapted to any

experimental case since the resulting network will not start training in any arbitrary location in the huge weight domain but nearly about the global optimum point.

6.5 Closure

This study presented an SRNN based modeling/identification procedure for the pressure dynamics of a variable-speed pump controlled electro-hydraulic system. The signals, used for the long-term pressure prediction task, were the rotational speed of the pumps, the position and the average velocity of the hydraulic actuator. A gray-box approach (SRNN) beside the well known black-box approaches (NARX and NOE) were utilized in the identification process. The study elaborated the performance of these models through a detailed simulation and experimental cases where black-box modeling approaches failed to yield acceptable performance even in the simulation studies. On the other hand, it was seen that the SRNN has showed excellent performance in the simulation study and has been able predicted the pressures in both chambers of the cylinder quite accurately in relatively long intervals (i.e. 50s). Unfortunately, the experimental studies revealed that the outputs of the SRNN diverged in the extended time periods due to the fact the outputs of the predictor model were highly coupled to each other and the errors introduced by a number of sources (e.g. noise in the position sensor, the time delay in the velocity computation, etc.). However, if a pressure sensor were utilized to provide a feedback to the network, it was able to estimate the other pressure component quite accurately without any divergence. Hence, the presented network model could reliably serve as a sensor backup in certain applications where sensor failures could have catastrophic consequences.

CHAPTER 7

POSITION ERROR PREDICTION FOR CABLE-DRUM SYSTEMS

7.1 Introduction

Cable-drum mechanisms, which are considered to be a subclass of friction/traction/capstan drive systems, are commonly used to convert the rotary motion of a drum into a translational one with the utilization of the friction force induced at the interface of contacting material pair. Apart from their use in conventional machines such as printing presses, textile machinery, cranes etc; cable-drum systems are also employed as motion transmission elements in many precision engineering devices including photocopiers, printers, plotters, rapid prototyping machines, haptic devices and more. Despite their primary role as power transmission elements; the cable-drum systems could serve as integral components of linear position sensors as well. In fact, the mechanisms accommodating an angular position sensor on the drum shaft do find their commercial uses as inexpensive sensors for certain industrial applications that do not require high positioning accuracy such as presses, punching / injection machines, wood- and sheet-metal working machinery etc. In commercial sensors such as “wire draw encoders” and “cable encoders”, the cable is often times attached onto a spring-loaded capstan to create a kinematically-coupled motion. However, the resulting mechanical system becomes quite complicated (Kautz, 1993; Steinich, 2007) to be suitable for precision products. Judging by the earlier applications; a cable directly wound on the capstan does have certain advantages over the “wire drawn” devices

including its simplicity, ease-of-manufacture, (almost) unlimited travel spans (range), linearity, wider bandwidth (better frequency response), etc.

Emphasizing power transmission efficiency, dynamic stiffness, and vibrations; numerous investigations in the literature have directly focused on the capstan drives that possess some of the characteristics of the cable-drum mechanisms. In fact, many studies concentrate on the attributes of traction drives as power transmission elements rather than their measurement characteristics. The earliest known work is attributed to Euler (1762) who investigated the balance of a string wrapped around a fixed drum while Grashoff (1883) revised the friction on belt-pulley mechanisms at steady-state and laid the ground work on the creep theory. In this classical (and widely adopted) approach, the pulley/drum is divided into two regions. In the first region (called slip zone), the cable/belt is to creep against the drum which in turn enables the power transmission via the friction forces produced at the interface in accordance with the Coulomb friction law. In the second region (commonly referred to as adhesion zone), the cable/belt is assumed to adhere to the drum and thus no friction force is developed to transmit the mechanical power between two media. Fawcett (1981), Johnson (1985) and Gerbert (1999) review and elaborate the classical creep theory. In fact, the evolution of the theory has continued in time. For instance, Bechtel et al. (2000) considered the unaccounted inertial effects in the slip zone. Moreover, Leamy and Wasfy (2002) conducted a detailed analysis on the belt-drives using a modified Coulomb friction law. On the other hand, shear model is the second theory, which was first proposed by Firbank (1970). Next, Gerbert (1996) studied the shear model by considering the extension of the belt. Later, Kong and Parker (2005) were the first who compared the two theories applied on a two-pulley system and they proposed an iterative method for calculating the steady state behavior of the mechanism. Furthermore, Kong and Parker (2006) have incorporated the compliances of various (like pulley grooves) on belt-drive dynamics. Lastly, Tu and Fort (2004) considered the effects of lubricants on the friction between fiber and capstan while Smith (1998) investigated micro-tribological interactions among various interfaces in a belt-driven data-tape.

Comprehensive review of the relevant literature reveals that the evaluation of the cable-drum mechanism within the context of precision motion/sensing are not fully stuied. Only, Werkmeister and Slocum (2007) looked into the (dynamic) stiffness of a wire capstan drive through a rigorous analytical and experimental study. Based on this study, Baser and Konukseven (2010) developed an analytical method in order to calculate the slippage between the cable and drum. It was seen that the analytical method, whose parameters were determined in an accurate way, could only predict the slippage within 10% difference from the experimental results. As a result, the resulting analytical method could not be used for position error estimation for cable-drum systems since some parameters (such as eccentricity of the drum and friction coefficient between the cable and drum) and variables (such as external load and preload on the cable) must be measured in order to manipulate the calculations. Furthermore, external load on the cable and also the reference velocity profile of the output drum were constant in the above-mentioned study; therefore, it eliminates all the inertia effects and velocity dependent slip dynamics of the device. However, Kilic et al. (2011) show that the slippage between the cable and drum is highly dependent on the velocity of the output drum and the external load on the cable which are continuously changing during the operating conditions of the mechanism. Therefore, it is seen that the applicability of the analytical method to predict the transmission error due to slippage is not feasible. Eventually, the main objective of this study is to devise a practical position error prediction scheme for cable-drum mechanisms that accept only a position signal from a rotary encoder coupled to the drum itself.

After this detailed introduction, Section 7.2 introduces a cable drum mechanism as a linear motion sensor. Following that, the Section 7.3 introduces a test set-up and investigates the actual dynamic behavior of the device through an experimental study. In Section 7.4, ANNs are designed to predict the slippage between the cable and drum. It is shown that black-box modeling approaches are not sufficient for the estimation of the slip error of the device and hence a structured recurrent neural network model is devised and (proposed also) to predict the slippage. Finally, the

merit of the proposed network is assessed based on a random input test scenario and thus the crucial points of the study are discussed in Section 7.5.

7.2 Cable-drum Mechanism as Motion Sensor

A generic mechanism serving as a part of a linear motion sensor is illustrated in Fig. 7.1. In this arrangement, a digital rotary position sensor is directly coupled to the drum (pulley / capstan). The engagement angle of this drum, which plays a critical role in the induction of traction force between the cable and the drum, is controlled by the adjustment wheels shown in the figure. Similarly, the preload adjustment mechanism, which is usually composed of a helical spring and a screw, can be utilized to set the cable tension to the desired level. Note that the cable is subjected to an alternating load as the direction of the mechanism changes. Considering that the cable does not carry any compressive loads, the preload on the cable must be selected higher than the magnitude of the alternating load itself.

It is critical to note that the mechanism in Fig. 7.1 can be regarded as a simple belt-drive where the "creep" of the cable against the drum intrinsically induces the traction (torque) that creates the rotation of the drum. However, unlike conventional belt drives, the system under investigation has major differences:

- The center of the drum moves along an axis while the cable velocities at entry and exit points on the drum are essentially zero.
- Effective friction torque acting on the drum's shaft due to the sensor + bearings is quite low.
- Cable's mass along with the inertia of the drum are insignificant.
- Typical cable engagement (winding) angle is relatively large ($>\pi$).
- If compared to the circumferential speeds of belt drives, the average velocity of mechanism (i.e. carriage) is low.

Consequently, this system is expected to work reasonably well (without significant slip) under ideal circumstances. The next section investigates the actual dynamic behavior of a generic cable/drum system through an experimental study.

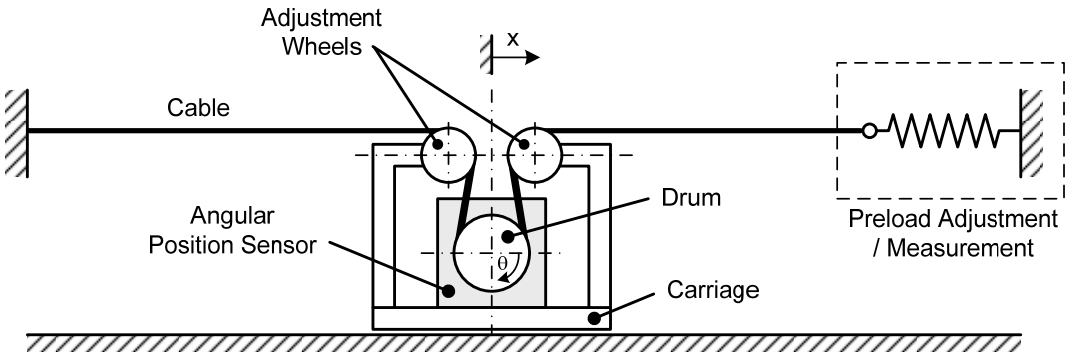

Fig. 7.1 A generic cable-drum mechanism used as linear motion sensor.

7.3 Test Setup and Experimental Results

As for experimental setup, a carriage system housing a drum assembly has been designed as illustrated in Fig. 7.2. In this setup, a DC motor under the guidance of a custom-built motion controller card drives this carriage system via a preloaded ball-screw mechanism. Hence, the resulting system is capable of generating accurately the desired acceleration / deceleration profiles for the cable-drum mechanism.

A schematic of this setup is given in Fig. 7.2.a. As can be seen in Fig. 7.2, a high-resolution optical position encoder, which has been directly coupled to the main drum, provides secondary information on the position of the carriage while a linear scale (LS) is directly coupled to the carriage for verification purposes. In this arrangement, the cable winding (engagement) angle could be easily adjusted by changing the locations of the wheels on the carriage assembly (Fig. 7.2.b). Likewise, the tension on the cable can be set by either calibrated weights on the side (Fig. 7.2.c) or helical coil connected to screw (Fig. 7.2.b). In fact, the test setup enables the investigation of various conditions that affect the measurement accuracy as well as precision of the device:

- Drum material and its diameter
- Cable material and its diameter

- Cable tension and cable engagement angle
- Steady-state velocity of the carriage

All these factors to the slip dynamics are well studied and presented in (Kilic et al., 2011).

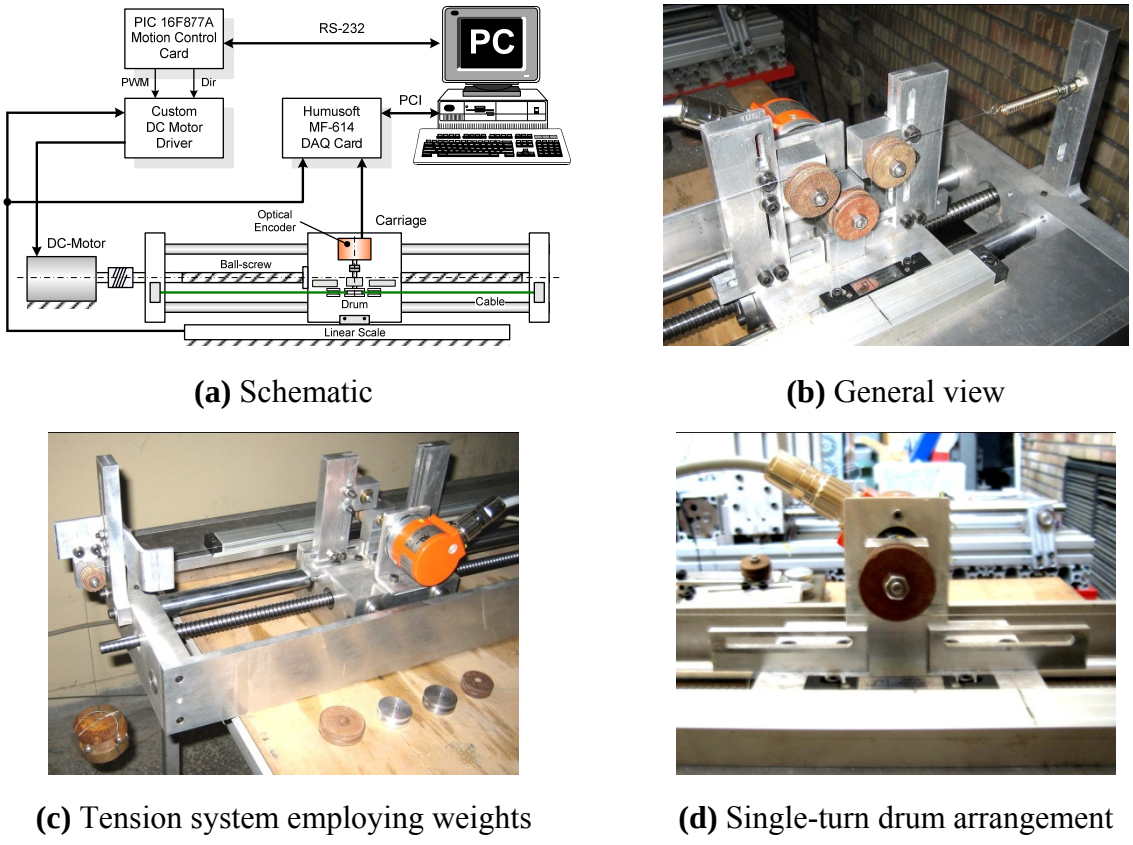

(a) Schematic

(b) General view

(c) Tension system employing weights

(d) Single-turn drum arrangement

Fig. 7.2 Test setup.

As an experiment, a (thin) plastic-coated steel cable with a diameter of 0.4 mm, which is specifically devised for precision instruments, is wrapped around the drum once as can be seen from Fig. 7.2.d (i.e. the cable engagement angle is 360^0) while one of its ends is fixed to the post. Likewise, the other end has been directly connected to a screw mechanism so as to improve the overall stiffness of the preloading system. Since the rigidity values (*AE*) of the cable materials are known

beforehand, the cable tensions can be adjusted to the desired levels by turning the screw accurately.

After setting the tension to approximately 40 *N*, the carriage housing the drum plus the sensor is programmed to travel back and forth sixteen times to a distance of 0.6 *m* at uniform speeds of 50, 100, and 140 *mm/s* respectively The slip errors versus total travel distance for these tests are presented in Fig. 7.3.a. Moreover, Fig. 7.3.b shows the average of errors in both directions. The sinusoidal waveforms on the position error signal take place due to the eccentricity of the drum. It turns out that the position error induced by micro-slip is highly dependent upon the direction of motion as well as the speed of the carriage assembly and eccentricity of the drum. Note that "error" (or slippage) in these figures are defined as

$$e = x_{LS} - R.\theta_{PE} \tag{7.1}$$

where ;

x_{LS}: Linear scale measurement,

θ_{PE}: Measurement of optical position encoder on the drum shaft,

R: Radius of the drum

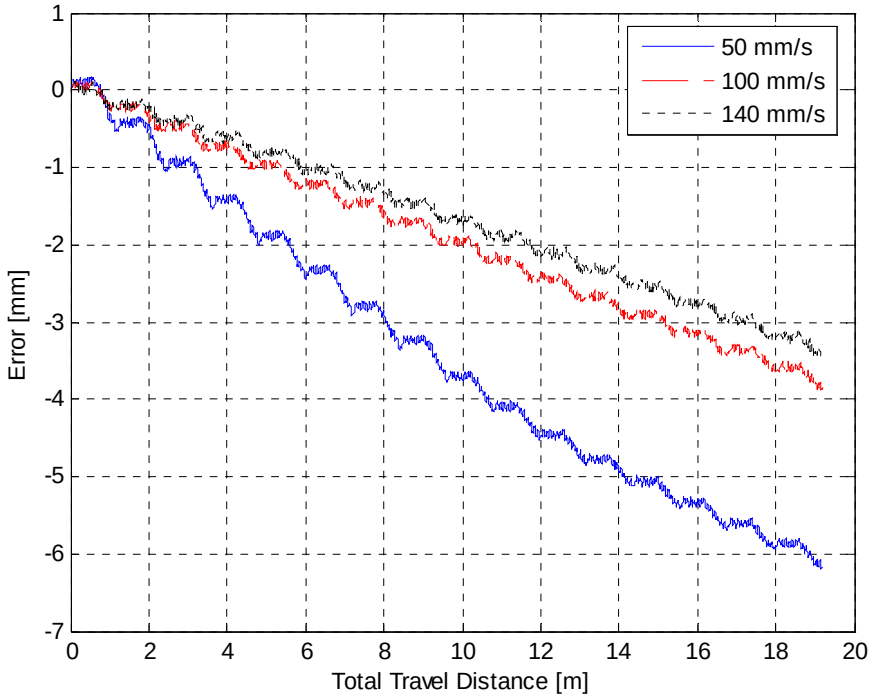

a) Overall drift (16 repetitions).

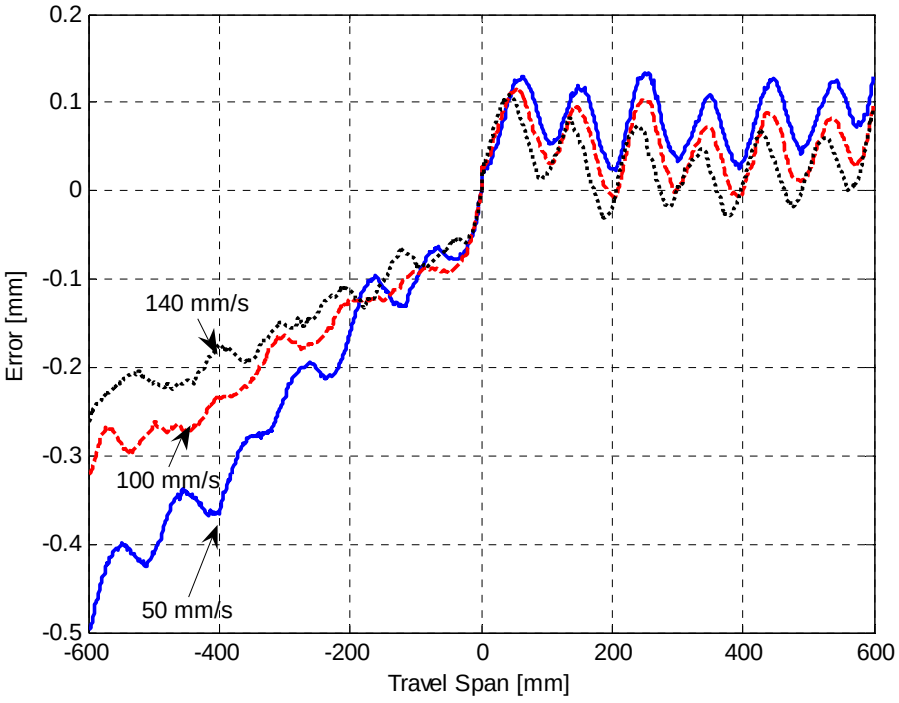

b) Average of slip errors vs. direction.

Fig. 7.3 Experimental results.

7.4 Position Error Prediction Using Artificial Neural Networks

Despite the apparent drift being observed when using the cable-drum system as a linear motion sensor in the preceding section; the standard deviations calculated using the data for 16 round-trips indicate that the dynamics of the slip error is repetable or systematic. The detailed experimental studies show that the slip error is a function of many parameters such as the position, velocity and eccentricity of the drum, and the preload and external load on the cable. Provided that the test conditions are about the same (preload on the cable / diameter, material and eccentricity of the drum / material and diameter of the cable are all fixed); it is now tried to predict the slip error of the device by using artificial neural networks.

7.4.1 Black-box Approach

First, a training scenario is highly needed in order to capture the dynamics of the slippage by ANN models. Only the rotary encoder output signal is to be used in the elements of the input vector (or regression vector). Therefore, regression vector could be formed from the position and velocity of the drum as represented in Fig. 7.4.a. All the position error data corresponding to this training scenario is presented in Fig. 7.4.b. Before training any type of black-box models, the regression vector size along with the model orders must be determined. That is, the regression vector could be given as:

$$\varphi(k) = [x_{PE}(k),\ldots, x_{PE}(k-n), v_{PE}(k),\ldots, v_{PE}(k-m)]^T \tag{7.2}$$

where k refers to the discrete-time index and v_{PE} is the calculated velocity of the drum from the position of the drum, x_{PE}, in linear coordinates using the first-order difference (*Euler*) method. The orders (n and m) of tapped-delayed signals are to be determined via trial and error since slippage also depends on the external load on the cable. Unfortunately, this force could not measured during the experiments. But, it is expected that inertial forces could be captured by the network models using the tapped-delayed position and velocity signals.

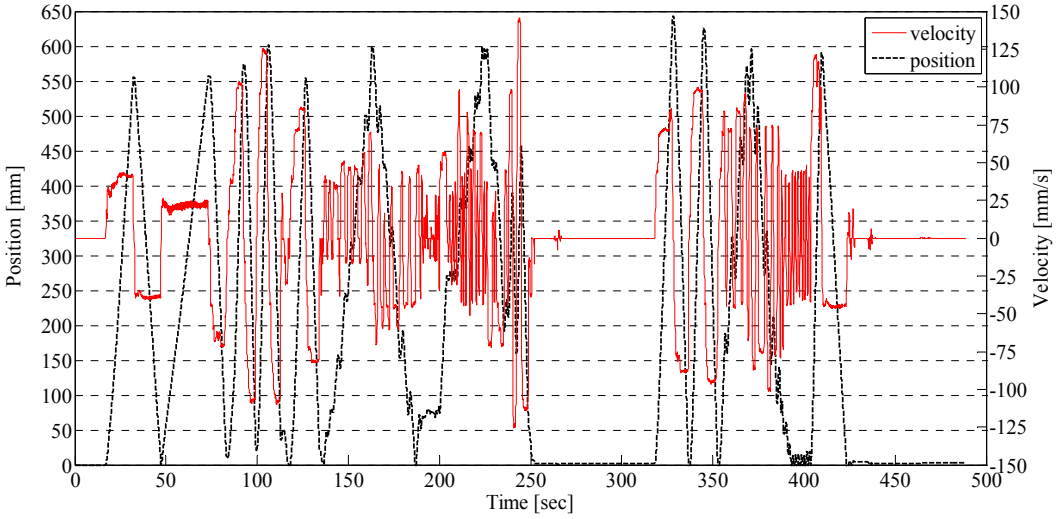

a) Position and velocity profile of the drum.

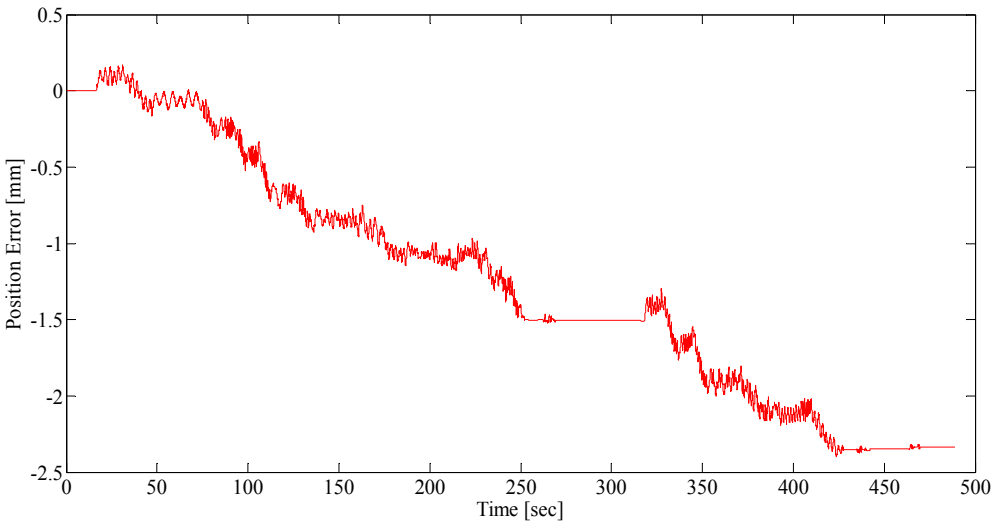

b) Position error of the cable-drum system.

Fig. 7.4 Training scenario.

First of all, FNNs are used to capture the slip dynamics from the position and velocity signal of the drum since a FNN with tapped delay position and velocity of the drum is theoretically capable of capturing the desired relationship as shown in Fig. 7.5. For this purpose, FNNs with different architectures are tried as presented

in Table 7.1. But, it is observed that all these networks fail to learn the presented pattern successfully.

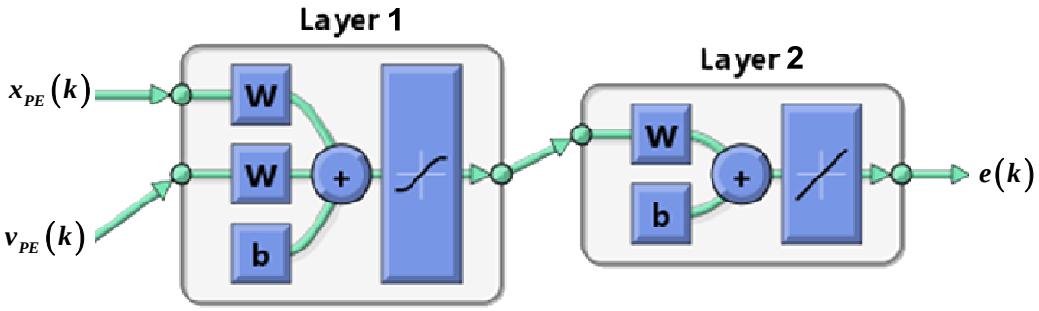

Fig. 7.5. Architecture of the FNN.

Table 7.1 Trained FNN models*.

Architecture	**#1**	**#2**	**#3**	**#4**	**#5**	**#6**	**#7**	**#8**	**#9**
Inputs	x_{PE} (k), v_{PE} (k)			x_{PE} (k), x_{PE} (k-1), v_{PE} (k), v_{PE} (k-1)			x_{PE} (k), x_{PE} (k-1), x_{PE} (k-2), v_{PE} (k), v_{PE} (k-1), v_{PE} (k-2)		
Output	*e(k)*								
Training error [mm]	0.6	0.572	0.654	0.576	0.520	0.506	0.592	0.569	0.495
Training data	9776 Sample								
Epochs	100								
Training time (sec)	7	13	20	8	15	25	10	19	31
1st layer neurons	10	20	30	10	20	30	10	20	30
Activation function	Tangent sigmoid								
Training method	Levenberg-Marquardt								

* Linear activation function is utilized at the output layers.

Following that, a NARX architecture as presented in Fig. 7.6 is to be designed to predict the slip dynamics. Again, using different number of neurons in the first layer of the NARX and changing the order of tapped delay input signals, the best

combination is to be determined via experimentation (trial). Training results of the various NARX models are given in Table 7.2.

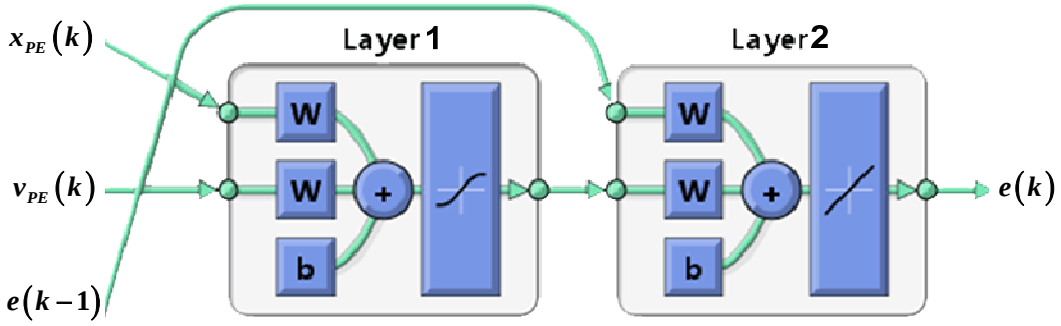

Fig. 7.6 Architecture of the NARX.

Table 7.2 Trained NARX models*.

Architecture	**#1**	**#2**	**#3**	**#4**	**#5**	**#6**	**#7**	**#8**	**#9**
Inputs	x_{PE} (k), v_{PE} (k), e(k-1)			x_{PE} (k), x_{PE} (k-1), v_{PE} (k), v_{PE} (k-1), e(k-1)			x_{PE} (k), x_{PE} (k-1), x_{PE} (k-2) v_{PE} (k), v_{PE} (k-1), v_{PE} (k-2) e(k-1)		
Outputs	e(k)								
Training error [μm]	10.5	10.5	10.6	10.7	10.7	10.6	10.6	10.5	9.5
Training data	9776 Sample								
Epochs	100								
Training time (sec)	7	13	20	8	15	24	10	20	29
1st layer neurons	10	20	30	10	20	30	10	20	30
Activation function	Tangent sigmoid								
Training method	Levenberg-Marquardt								

* Linear activation function is utilized at the output layers.

Hence, all of the NARX networks are trained in a feed-forward manner; their training performances are quite acceptable (near 10 μm). However, those models must be used in a recurrent form (meaning that the previous error value at time

index *k-1*must come from the network model itself). Therefore, the next step is to feed back the output of the NARX network, which is delayed one sampling period, to its first layer as could be seen from Fig. 7.7.

Following that, these recurrent networks, which are referred to as NOE models, are additionally trained via RTRL algorithm. As could be seen from Table 7.3, the networks could be trained without any problem in a recurrent form provided that the initial weight values are taken from the NARX model. It is seen that NOE #9 has the smallest training error (31.1 μm). Note that this particular network could not track the sinusoidal waveform superimposed onto the error signal due to the eccentricity of the drum as this situation can be easily seen from Fig. 7.8. For that reason, the regression vector should be updated as shown below in order to capture the drum eccentricity effects on the position error:

$$\varphi(k) = [x_{PE}(k), x_{PE}(k-1),, x_{PE}(k-2), v_{PE}(k), v_{PE}(k-1), v_{PE}(k-2), \cos(\theta_{PE}(k)), sin(\theta_{PE}(k))]^T \quad (7.3)$$

Table 7.3 Trained NOE models*.

Architecture	**#1**	**#2**	**#3**	**#4**	**#5**	**#6**	**#7**	**#8**	**#9**
Inputs	x_{PE} (k), v_{PE} (k)			x_{PE} (k), x_{PE} (k-1), v_{PE} (k), v_{PE} (k-1)			x_{PE} (k), x_{PE} (k-1), x_{PE} (k-2), v_{PE} (k), v_{PE} (k-1), v_{PE} (k-2)		
Outputs	e(k)								
Training error in (μm)	47	42.2	38.2	50.6	39.4	39.2	53.1	38.6	31.1
Training data	9776 Sample								
Epochs	10								
Training time (sec)	390	403	410	392	411	413	399	414	428
1st layer neurons	10	20	30	10	20	30	10	20	30
Activation function	Tangent sigmoid								
Training method	RTRL								

* Linear activation function is utilized at the output layers.

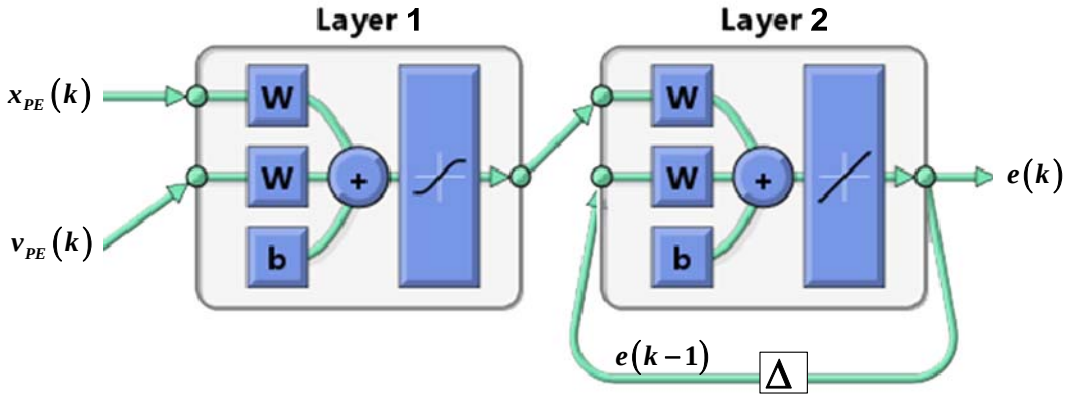

Fig. 7.7 Architecture of the NOE.

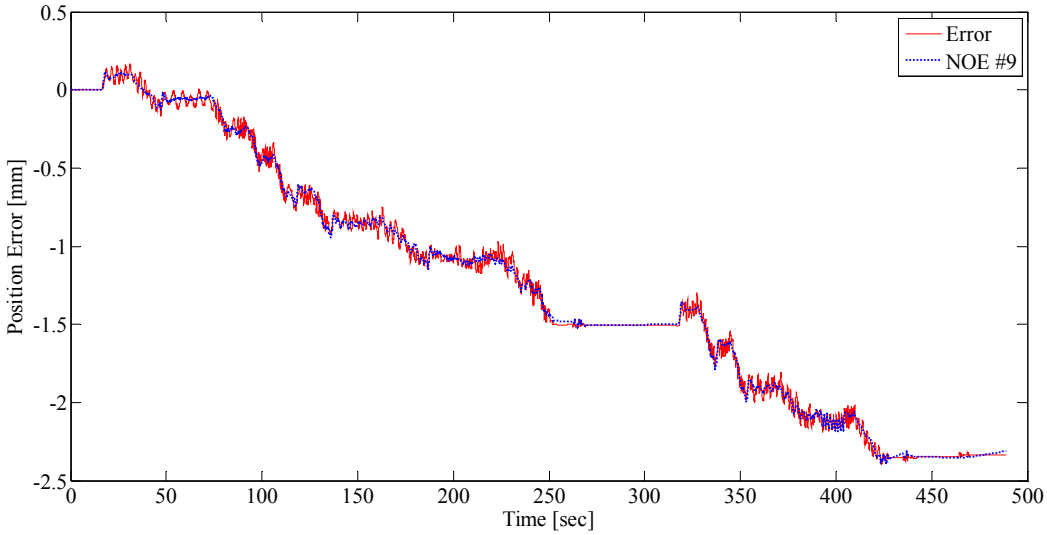

Fig. 7.8 Training performance of the NOE #9.

Maintaining the train operation of the network NOE#9 with using this new regression vector, a new network, called NOE #10, is obtained as shown in Fig.7.9. The training error now decreases to *16.6* μm where the training performance of this new network in time domain is given in Fig. 7.10. As can be seen from the first inset in Fig. 7.10, NOE #10 is now able to capture the slippage dynamics due to eccentricity of the drum. However, there is an important drift problem if one looks into the second inset in Fig. 7.10. Although the drum velocity is exactly zero

(meaning that the position error must be constant at these time intervals), the outputs of the NOE models are not constant but do drift in time. Therefore, the black-box modeling approaches are not sufficient to predict the position error of the cable-drum mechanism accurately. In any way, one needs to apply structured neural network topology for this specific prediction task problem.

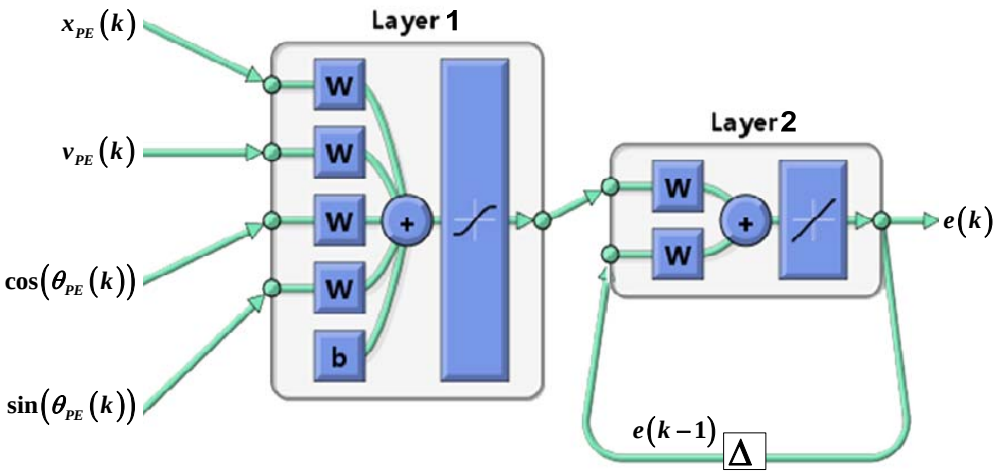

Fig. 7.9 Architecture of the NOE#10.

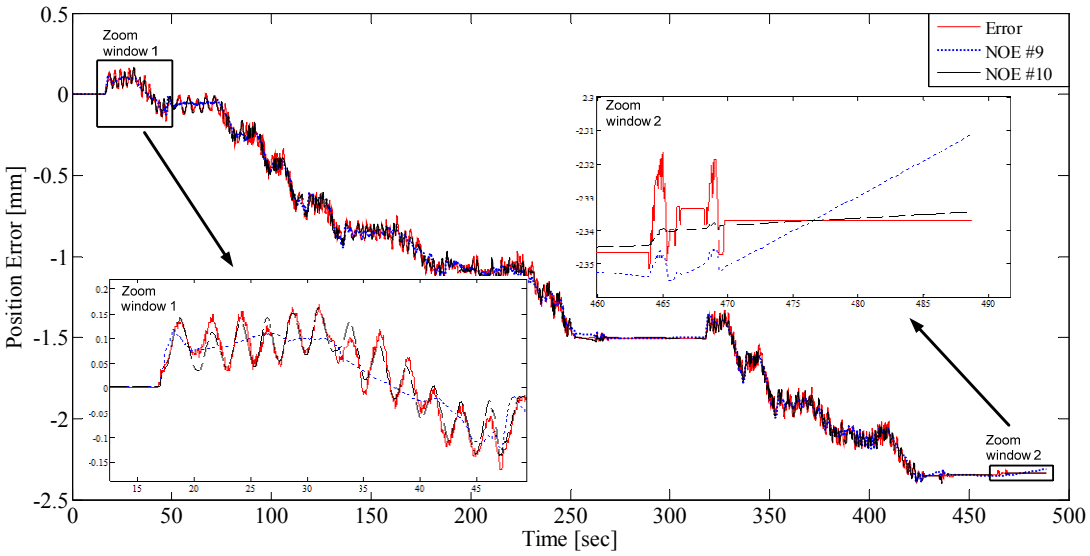

Fig. 7.10 Training performance of the NOE #9 *and* NOE #10.

7.4.2 Structured Neural Network Design

Since the prediction problem of NOE#10 is an output drift problem at zero-velocity, one needs some auxiliary networks beside that network to make its output constant when the drum velocity is exactly zero. For that purpose, first a specific network, called zero region detector (ZRD), is designed to capture the velocity of the drum near zero velocity region. The architecture of this network is given in Fig.7.11 and the implemented mathematical functional could be given below:

$$y = \begin{cases} +1, & -0.001 \le x \le +0.001 \\ -1, & otherwise \end{cases} \tag{7.4}$$

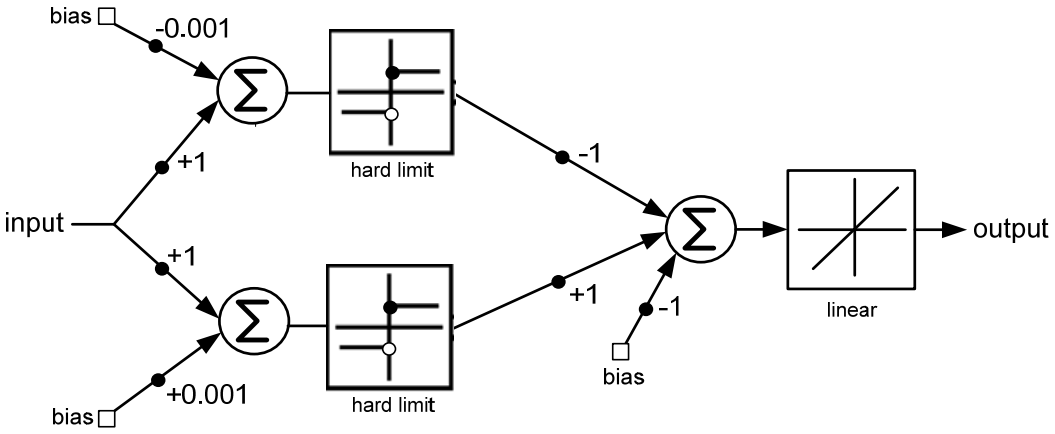

Fig. 7.11 Architecture of the ZRD network.

As could be seen from Fig. 7.11, ZRD is a two layered feed-forward network with two hard-limit (type) neurons in the first layer and one linear neuron at the output layer. The zero velocity range is adjusted by the bias weight values of the first layer. Consequently, a *switching* network is also utilized while constructing the SNN model. Eventually, the velocity signal is to be connected to the input of the ZRD network to detect the low velocities. Finally, the output of the ZRD network is

connected to the "*switch*" port of the *switching network* in order to direct the output of this network. The overall SNN is presented in Fig. 7.12. Note that in this topology, it is guaranteed that when the speed of the drum is below 0.001 *mm/s*, the predicted position error does not drift in time as zero input is fed to the integrator (present at the output layer of the SNN) for this particular case.

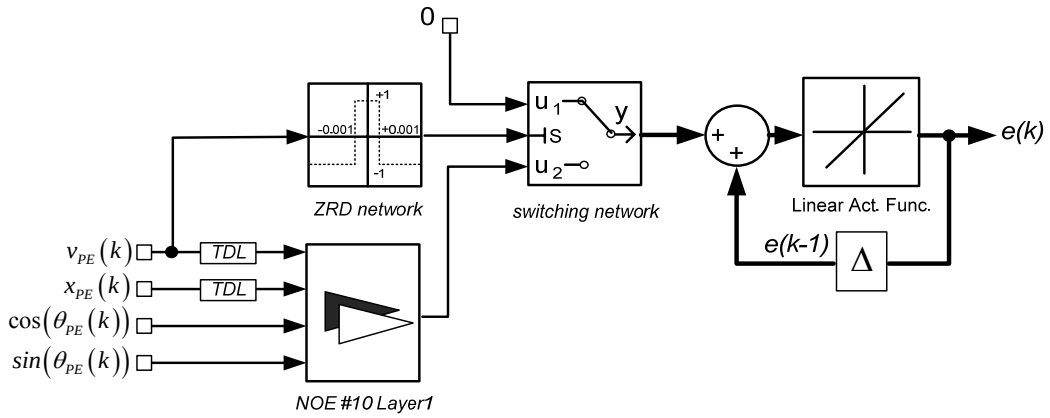

Fig. 7.12 Structured neural network.

7.5 Results and Discussions

Up to now, the trained networks are not validated through a scenario different than the training case. For that purpose, a validation test is performed based on a scenario presented in Fig. 7.13. The position and velocity profile of the drum are shown in Fig. 7.13.a for this validation scenario. On the other hand, Fig. 7.13.b presents the measured position error for this experiment and the position error predicted by the devised SNN. The unpredicted part of the position error, which gradually increases in time, is shown in Fig. 7.13.c. It is found that the root-mean-square (RMS) of the unpredicted position error (residual) is about 77 μm for this random motion profile which lasts about 250 seconds.

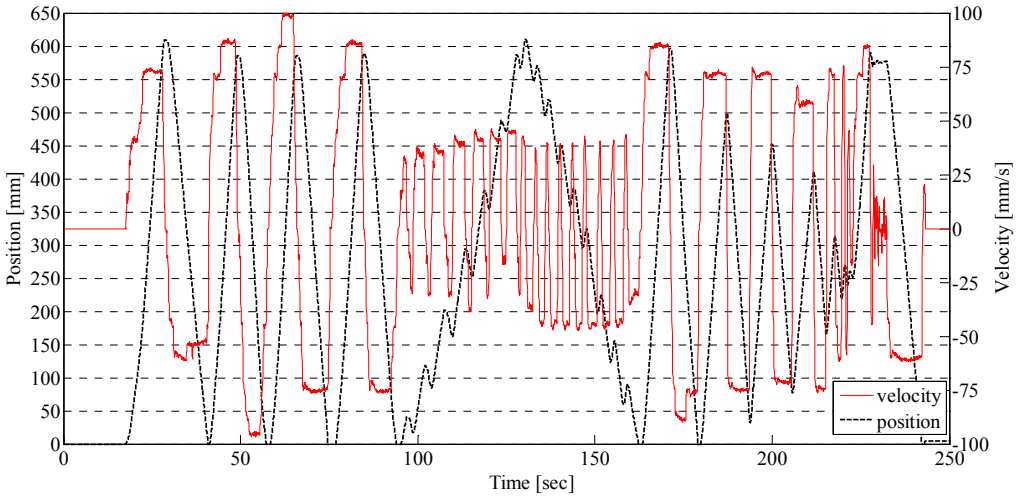

a) Position and velocity profile of the drum.

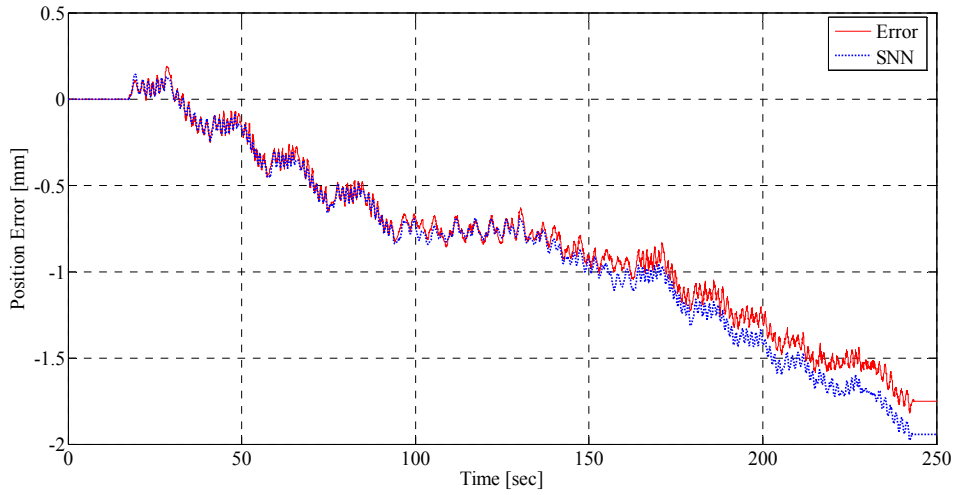

b) Position error of the cable-drum system.

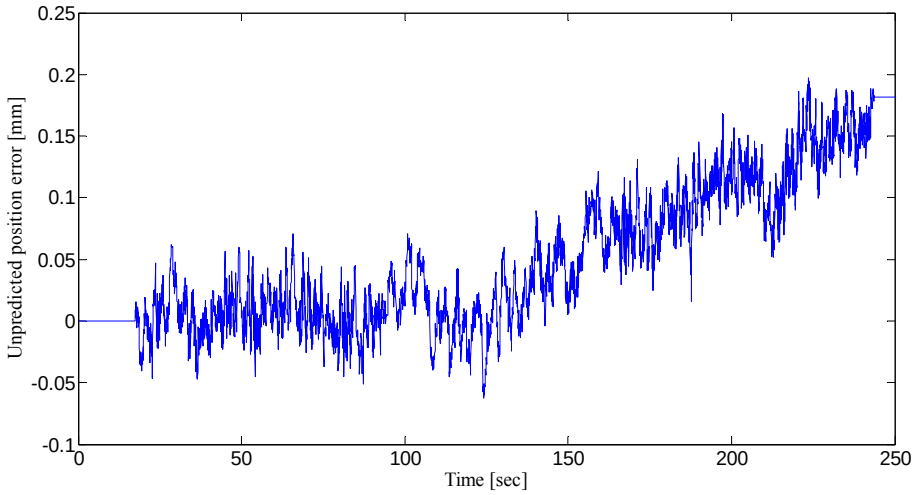

c) Unpredicted position error.

Fig. 7.13 Validation test.

It is evident that to predict the slip dynamics without any error is not an easy task as this friction based phenomenon depends on a large number of parameters. For that reason, the developed SNN model could not capture the dynamics of the slip with only using the position information of the drum. Furthermore, other physical parameters (like external load on the cable) could be utilized as an input to the network models to enhance the accuracy of the predictions. However, such requirements would clearly hinder the practical value of the estimator and would limit its applicability. As a practical and inexpensive solution, a beacon (or a limit switch) could be placed at home position (HP) of the carriage to reset the overall position error when carriage returns to this HP. With this new arrangement, Fig. 7.14.a shows the performance of the SNN using HP solution to the same validation scenario, given in Fig. 7.14.a. Again, the unpredicted part of the position error is presented, given in Fig. 7.14.b. The RMS of the unpredicted error is now calculated as 29 μm. Moreover, it isobserved that the minimum- and the maximum error of the SNN model are in the 100 μm bandwidth, which is a critical level for precision systems, for this arbitrary validation scenario.

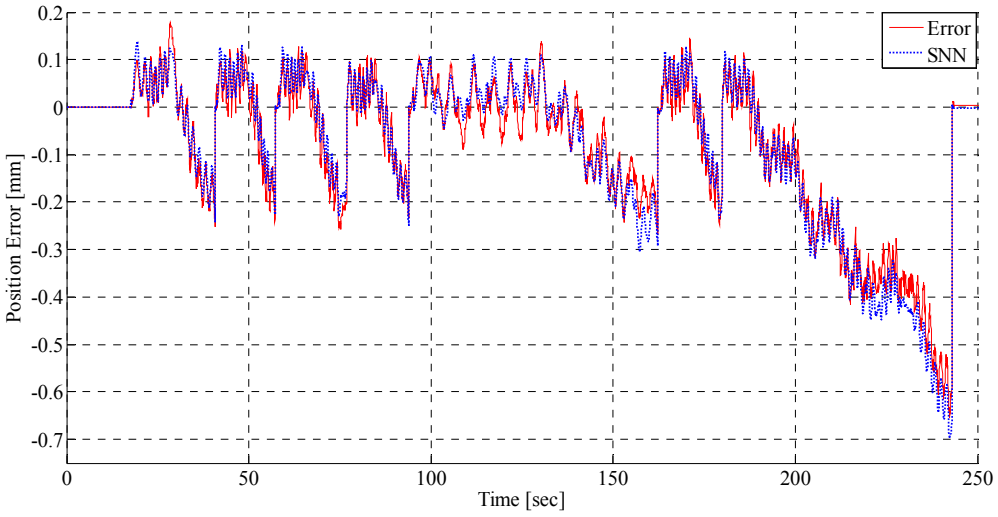

a) Position error of the cable-drum system.

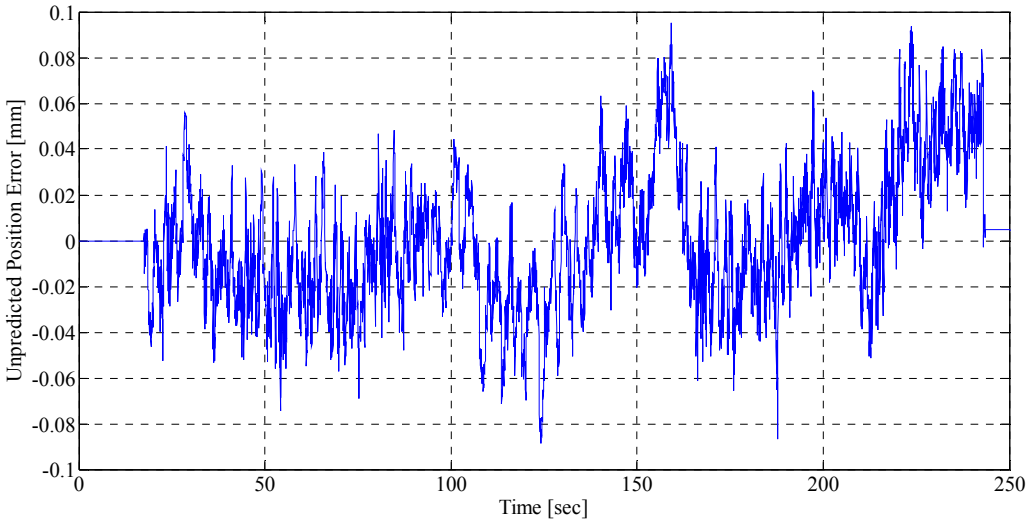

b) Unpredicted position error.

Fig. 7.14 Validation scenario using HP approach.

7.6 Closure

This chapter has evaluated the cable-drum mechanisms as linear motion sensor for certain machine systems. Literature survey of such systems showed that the slippage between the cable and drum depended on many physical factors such as eccentricity of the drum, kinematic friction coefficient between the cable and drum, external and preload force on the cable. Furthermore, the complementary experimental study indicated that the small fluctuations in mechanism's speed yielded a considerable (micro) slip at the interface. Therefore, it has been seen that the calculation of this slippage by an analytical method was obviously unpractical. Therefore, it is aimed to calculate this slippage via a SNN model. The work illustrated that if the accumulated position error (drift) of the drum was reset periodically via an absolute reference (beacon), the devised model could estimate the position of a carriage, housing a cable-drum mechanism, with in an acceptable error band (<100 μm).

CHAPTER 8

CONCLUSIONS AND RECOMMENDATIONS

8.1 Significance of this Research

This work seeks the solution of rather difficult problem: system modeling and identification of some nonlinear systems from mechanical engineering domain using ANNs. It has been seen that using conventional neural network structures (black-box models) was not sufficient to handle the complex dynamic behavior of these mechanical systems. Chapter 2 has highlighted the accurate modeling and identification capability of structured neural networks in the current state of the art. But, it was seen that the design strategies for SNNs were either incomplete when viewed from a general perspective. For that purpose, a general methodology (proposed in Chapter 3) deals with how to design SNNs using the *a priori* information available from the engineering knowledge. In this approach, the task is first decomposed into subtasks and then some networks are trained (or directly taken from the standard library) considering these subtasks. Therefore, SNNs consist of some independent neural networks cooperating with each other in order to model the behavior of system within the framework of prediction/estimation. It is important to note that each independent network operates as a single module and works in its own domain to full its assigned task. In the corresponding chapters, a unique SNN was designed for each of the nonlinear mechanical systems under study (i.e. timing-belt drive, cable-drum mechanism and hydraulic systems). The experimental results provided the accurate verification of the devised SNNs under challenging conditions. It was observed that that the modular design of neural network has enhanced the training and generalization performances of these ANNs,

resulting in a more robust and reliable network models. Consequently, this dissertation has demonstrated the great potential of using SNNs to estimate or predict successfully the (unavailable) states of the mechanical systems with their complex nonlinearities such as dead-zone, backlash, hysteresis and friction elements. Therefore, the contributions of this thesis work could be summarized as follows:

1. A design methodology of SNNs for modeling and identification of nonlinear systems is almost completed. The proposed modeling technique will be of primary importance since the SNNs, which are developed especially using a sketchy guidance of *a priori* knowledge on the investigated process, will have a great capability of capturing the unaccounted system dynamics which is not taken into consideration during the mathematical modeling of the process. Furthermore, these *a priori* information-based neural networks have another significant characteristic of modularization in which some parts of the models could be added, deleted or changed in order to identify similar systems accurately.

2. A new entropy based pruning algorithm is proposed to delete the redundant neurons in a network and explained in Chapter 3 in a detailed manner. Through some benchmark systems (taken from the literature), it has been demonstrated that the technique effectively prunes the redundant units (neurons) of a complex network.

3. Chapter 4 concentrates on devising a feasible SNN model for the position estimation of a carriage system which is driven by a timing-belt mechanism. Only the indirect measurements of the carriage system, recorded via low-cost rotary encoder, is utilized in the designed estimator. Model validation tests show that the devised SNN could estimate all the transmission errors of the drive system, which are the backlash in the gear-box of the motor, friction and hysteresis phenomenon between the teeth of the motor pinion and belt pinion, in an acceptable error band (about 30 μm). Therefore, this model could be

effectively used as an open-loop controller for compensating the position error of timing-belt driven mechanical systems.

4. In Chapter 5, an SRNN is proposed to predict the pressure dynamics for servo-valve controlled hydraulic systems quite acceptable (±5 bars) in relatively long-term periods (50000 steps). The major contribution of this study is the design/development of a SNN topology which is tailored to capture the long-term pressure dynamics of electro-hydraulic servo-systems which is inherently nonlinear in nature. Searching the current literature comprehensively, there is not any ANN models (whether generic or structured) that can predict the long-term chamber pressures of such systems. It is shown that utilizing an experimental data, one can easily adjust the weights of this particular SRNN to characterize pressure dynamics of a servo-controlled hydraulic system.

5. Chapter 6 illustrates the design of another SRNN to predict the chamber pressures of a speed variable pump controlled hydraulic system in extended time periods. It is observed that the devised model could be used in a successful manner to predict the pressure in one chamber with a RMS error about *1-2 (bars)* when the pressure value of the opposite chamber is available. Therefore, the main contribution of this study is to reduce the number of pressure sensors in such hydraulic systems since the use of pressure sensors adds to the cost, size, weight and complexity of the overall system. Especially, if the studies of Guo et al. (2008) and Pi and Wang (2011), in which they are using 12 pressure sensors for controlling a 6-DOF parallel mechanism based robotic manipulators, are taken into consideration, the contribution of the study will be seen more clearly.

6. A particular SNN is devised as a feasible position estimation scheme for cable-drum mechanisms in Chapter 7. The experimental results of the work indicate that the proposed model (SNN) could compensate the position error of the mechanism within the 100 μm error band. Therefore, such a simple mechanism

with the devised SNN model could be used as a linear motion sensor for low-end (and cost sensitive) machine systems.

8.2 Recommendations

Although this research has proposed a general methodology for devising SNNs in a systematic fashion, all stages were not completely applied while designing neural network models for the investigated mechanical systems. That is, the devised SNNs were left in a modular form and no further attempt was made to optimize the SNNs (which happens to be the most essential step for hardware implementation of such networks). The SNNs were not converted into a generic (standard) type network models since it is desired to preserve the physical structure of the network. Otherwise, the modularity feature of the SNNs will disappear. Hence, it will also reduce the utilization of these models for the modeling of other similar systems. For instance, despite the fact that the presented study in Chapter 5 concentrates on an EHSS with zero-lapped servo-valve, other hydraulic system topologies employing different types of servo-valves (e.g. under lapped or over lapped) can also be easily accommodated by the presented SRNN due to its modular structure. Provided that specialized flow-rate NN models are designed to mimic the dynamics of the above mentioned servo-valves (via the presented approach in this work), one can devise a specialized SRNN conveniently by simply replacing the existing flow-rate networks with the new ones in a modular fashion without altering the other parts of the network. In any way, there exists an opportunity to blend and prune the network modules to create a generic recurrent network topology. Research efforts on this issue will be go on. The other recommendations and future work of the thesis work could be stated as follows:

1. All the stages of the proposed SNN methodology are now applied manually. However, an automation of the whole design process by some expert systems will have a great impression in the research field of nonlinear system identification and modeling.

2. The proposed (entropy based) pruning algorithm deletes only the redundant neurons in a network. Although pruning a neuron rather than its weight is more effective from the reduction of computation burden point on the hardware platform, remaining excessive weight values should also be removed. Therefore, other well-known pruning methods such as saliency- (OBD, OBS, unit-OBS, mw-OBS), perturbation- or evolutionary based algorithms could be further utilized as a part of the proposed method.

3. It is known that model predictive controllers require the future values of the predicted plant outputs while reducing the difference (error) between the command tracking signal and the predicted values of the process. Hence, the networks, which are especially devised for the long-term prediction tasks in this thesis work, could be used to realize more effective predictive controllers as a future work.

4. In Chapter 5, the leakage effects in the hydraulic actuator was neglected to avoid the design of a cross-coupled model (i.e. the outputs of the model must feed each other) when applying the SNN methodology. No doubt, this cross-coupled model will yield a more complex SRNN model. Considering the other factors beside the leakage such as temperature and viscosity, much more complex SRNN models could be devised in the future.

5. This thesis has not dealt with the hardware implementation of the devised SNNs. As a future study, the well-performed networks could be implemented on cost effective platforms such as FPGAs, FPAAs and GPUs in order to produce customized network models for application specific systems (a network system on a chip).

REFERENCES

1. Aadaleesan, P., Miglan, N., Sharma, R. and Saha, P. 2008. Nonlinear system identification using Wiener type Laguerre-Wavelet network model. Chemical Engineering Science, 63, 3932-3941.

2. Abrate, S. 1992. Vibrations of belts and belt drives. Mechanism and Machine Theory, 27(6), 645–659.

3. Agarwal, M. 1997. Combining neural and conventional paradigms for modeling, prediction and control. International Journal of Systems Science, 28(1), 65-81.

4. Aguirre, L.A., Coelho, M.C.S. and Correa, M.V. 2005. On the interpretation and practice of dynamical differences between Hammerstein and Wiener models. Control Theory and Applications, 152 (4), 349-356.

5. Akiyema, Y., Yamashita A., Kajiura M., Anzai Y. and Aiso H. 1991. The Gaussian Machine: A Stochastic Neural Network for Solving Assignment Problems. Journal of Neural Network Computing, 3, 43-51.

6. Al-Ghoneim, K. and Kumar, V. 1995. Learning ranks with neural networks. In Applications and Science of Artificial Neural Networks, 2492, 446-464.

7. Ankenbrand, T. and Tomassini, M. 1996. Forecasting financial multivariate time series with neural networks. International Symposium on Neuro-Fuzzy Systems, 95-101.

8. Ardalani-Farsa, M. and Zolfaghari, S. 2010. Chaotic time series prediction with residual analysis method using hybrid Elman-NARX neural networks. Neurocomputing, 73, 2540-2553.

9. Artmeyer, M., Lorenz, R.D. and DeVries, M.F. 1995. Process identification and modeling using structured topologies of artificial neural networks. In Proceedings of CIRP/VDI Conference, pp. 127-140.

10. Astrom, K.J. and Canudas-De-Wit, C. 2008. Revisiting the LuGre model. IEEE Control Systems Magazine, 28(6), 101-114.

11. Atuonwu, J.C., Cao, Y., Rangaiah, G.P. and Tade, M.O. 2010. Identification and predictive control of a multistage evaporator. Control Engineering Practice, 18, 1418-1428.

12. Auda, G. and Kamel, M. 1998. Modular neural network classifiers: a comparative study. Journal of Intelligent and Robotic Systems, 21, 117-129.

13. Ayalew, B. and Kulakowski, B. 2005. Modeling supply and return dynamics for an electrohydraulic actuation system. IISA Transactions, 44, pp. 329-343.

14. Azaam, F. 2000. Biologically Inspired Modular Neural Networks. Ph.D. thesis, Virginia Polytechic Institute.

15. Bade, S.L. and Hutchings, B.L. 1994. FPGA-Based Stochastic Neural Networks – Implementation. IEEE Workshop on FPGAs for Custom Computing Machines Workshop, Napa, pp. 189-198.

16. Baltersee, J. and Chambers, J.A. 1998. Nonlinear adaptive prediction of speech with a pipelined recurrent network. IEEE Trans. Signal Process., 46(8), 2207-2216.

17. Banakar, A. and Azeem, M.F. 2012. Local recurrent sigmoidal-wavelet neurons in feed-forward neural network for forecasting of dynamic systems: Theory. Applied Soft Computing, 12, 1187-1200.

18. Barbosa, B.H.G., Aguirre, L.A., Martinez, C.B. and Braga, A.P. 2011. Black and gray-box identification of a hydraulic pumping system. IEEE Transactions on Control Systems Technology, 19(2), 398-406.

19. Barbounis, T.G. and Theocharis, J.B. 2007. Locally recurrent neural networks for wind speed prediction using spatial correlation. Information Sciences, 177, 5775-5797.

20. Bartfai, G. 1994. Hierarchical clustering with ART neural networks. World Congress on Computational Intelligence, 2, 940-944.

21. Baruch, I.S., Beltran, R., Garrido, R. and Nenkova, B. 2005. A recurrent neural multi-model for mechanical systems dynamics compensation. Cybernetics and Information Technologies, 5(2), 21-31.

22. Baruch, I.S., Flores, J.M., Nava R.F., Ramirez P, I.R. and Nenkova, B. 2002. An advanced neural network topology and learning, applied for identification and control of a DC motor. In Proceedings of IEEE Symposium on Intelligent Systems,1, pp. 289-295.

23. Baser, O. and Konukseven, E.I. 2010. Theoretical and Experimental Determination of Capstan Drive Slip Error. Mechanism and Machine Theory, 45, 815-827.

24. Battiti, R. and Colla, A. 1994. Democracy in neural nets: Voting schemes for classification. Neural Networks, 7(4), 691-707.

25. Baum, E.B. 1991. Neural net algorithms that learn in polynomial time from examples and queries. IEEE Trans. on Neural Networks, 2 (1), 5-19.

26. Baum, E.B. and Haussler, D. 1989. What size gives valide generalization. Neural Computing, 1, 151-160.

27. Bechtel, S.E, Vohra, S., Jacob, K.I. and Carlson, C.D. 2000. The Stretching and Slipping of Belts and Fibers on Pulleys. ASME J. of Applied Mechanics, 67, 197-206.

28. Bengio, Y., Simard, P. and Frasconi, P. 1994. Learning long-term dependencies with gradient descent is difficult. IEEE Transactions on Neural Networks 5, 157-166.

29. Billings, S.A. and Zhu, Q.M. 1994. Nonlinear model validation using correlation tests. International Journal of Control, 60, 1107-1120.

30. Blum, A.L. and Riyest, R.L. 1992. Training a 3-node neural network is NP-complete. Neural Networks, 5 (1), 117-127.

31. Bohte, S.M., Poutr´e, H.L. and Kok, J.N. 2002. Error-backpropagation in temporally encoded networks of spiking neurons. Neurocomputing, 48, 17–37.

32. Caliskan, H. 2009. Modeling and Experimental Evaluation of Variable Speed Pump and Valve Controlled Hydraulic Servo Drives. Ms. thesis at Middle East Technical University, Ankara, Turkey.

33. Cernansky, M. 2009. Training Recurrant Neural Network Using Multistream Extended Kalman Filter on Multicore Processor and Cuda Enabled Graphic Processor Unit. International Conference on Artificial Neural Networks, 1, pp. 381-390.

34. Chan L. and Li, Y. 2000. Dynamic Modelling and Time Series Prediction by Incremental Growth of Lateral Delay Neural Networks. IEEE Symposium on Combinations of Evolutionary Computation and Neural Networks, 216-223.

35. Che, S., Boyer, M., Meng, J., Tarjan, D., Sheaffer, J.W. and Skadron, K. 2008. A performance study of general-purpose applications on graphics procesors using CUDA. J. Parallel Distrib. Comput., 68, 1370-1380.

36. Chen, S., Wang, X.X. and Harris, C.J. 2008. NARX Based Nonlinear System Identification Using Orthogonal Least Squares Basis Hunting. IEEE Transactions on Control Systems Technology, 16 (1), 78-84.

37. Chi, C.W., Hsia, S.T.C., Tseng, H.C. 1997. Adaptive aggregation of modular fuzzy control. IEEE International Conference on Systems, Man, and Cybernetics, Orlando, Florida.

38. Coelho, L.S., Pessoa, M.W. 2009. Nonlinear identification using a B-spline neural network and chaotic immune approaches. Mechanical Systems and Signal Processing, 23, 2418-2434.

39. Corwin, E., Greni, S., Logar, A. and Whitehead, K. 1994. A multi-stage neural network classifier. World Congress on Computational Intelligence, 3, 198-203.

40. Cun, Y.L., Denker, J.S. and Solla, S.A. 1990. Optimal brain damage. In Proceedings of the Neural Information Processing Systems, 2, pp. 598–605.

41. Dang, X. and Tan, Y. 2007. RBF neural networks hysteresis modeling for piezoceramic actuator using hybrid model. Mechanical Systems and Signaş Processing, 21, 430-440.

42. Dempster, A.P., Laird, N.M. and Rubin, D.B. 1977. Maximum likelihood from incomplete data via the EM algorithm. Journal of the Royal Statistical Society, 39 (1), 1-38.

43. Deng, L., and Tan, Y. 2008. Diagonal recurrent neural network with modified backlash operators for modeling of rate-dependent hysteresis in piezoelectric actuators. Sensors and Actuators A: Physical, 148, 259-270.

44. Dolen, M. 2000. Modeling and Estimation by Structured Neural Networks for CNC Machine Tools. Ph.D. thesis, University of Wisconsin, USA.

45. Dolen, M. and Lorenz, R.D. 2002. General Methodologies for Neural Network Programming. Smart Engineering System Design, 4, 63-73.

46. Dong, P., Bilbro, G.L. and Chow, M. 2006. Implementation of artificial neural network for real time applications using field programmable analog arrays. International Joint Conf. on Neural Networks, Vancouver, Canada, pp. 1518-1524.

47. Endisch, C., Brache, M., Endish, P., Schroder, D. and Kennel, R. 2009. Identification of Mechatronic Systems with Dynamic Neural Networks using Prior Knowledge. In Proceedings of the World Congress on Engineering and Computer Science, pp. 859-865.

48. Engelbrecht, A.P. 2001. A new pruning heuristic based on variance analysis of sensitivity information. IEEE Trans. Neural Networks, 12, 1386–1399.

49. Euler, M.L. 1762. Remarques sur l'effect du Frottement dans l'equilibre (Remarks on the effect of friction in balance). *Mém. Acad. Sci.*, 265-278.

50. Fahlman, S.E. and Lebiere, C. 1990. The cascade-correlation learning architecture, in: D.S. Touretzky (Ed.). Advances in Neural Information Processing, 2, 524–532.

51. Fawcett, J.N. 1981. Chain and Belt Drives – A Review. *Shock and Vibration Digest*, 13(5), 5-12.

52. Finnoff, W., Hergert, F., and Zimmermann, H.G. 1993. Improving model selection by nonconvergent methods. Neural Networks, 6, 771-783.

53. Firbank, T.C. 1970. Mechanics of the Belt Drive. Int. J. of Mech. Sci., 12, 1053-1063.

54. Garcia, P., Briz, F., Raca, D. and Lorenz, R.D. 2007. Saliency-tracking – based sensorless control of AC machines using structured neural networks. IEEE Transactions on Industry Applications, 43(1), 77-86.

55. Ge, H., Qian, F., Liang, Y., Du, W. and Wang, L. 2008. Identification and control of nonlinear systems by a dissimilation particle swarm optimization-based Elman neural network. Nonlinear Analysis: Real World Applications, 9, 1345-1360.

56. Gerbert, G.G. 1996. Belt Slip – A Unified Approach. *ASME J. of Mech. Design*, 118, 432-438.

57. Gerbert, G.G. 1999. *Traction Belt Mechanics,* Chapters 7-10, Chalmers Univ. of Tech. Press, Sweden.

58. German, S., Bienenstock, E. and Doursat, R. 1992. Neural networks and the bias/variance dilemma. Neural Computation 4(1), 1-58.

59. Girolami, M. and Gyfe, C. 1997. Extraction of independent signal sources using a deflationary exploratory projection pursuit network with lateral inhibition. IEE Proceedings on Vision, Image and Signal, 144 (5), 299-306.

60. Girosi, F., Jones, M. and Poggio, T. 1995. Regularization theory and neural network architectures. Neural Computing, 7, 219–269.

61. Goh, S.L. and Mandic, D.P. 2005. Nonlinear adaptive prediction of complex-valued signals by complex-valued PRNN. IEEE Transactions on Signal Processing, 53(5), 1827-1836.

62. Goldberg, D.E. 1989. Genetic Algorithms in Search, Optimization and Machine Learning. Addison Wesley.

63. Gonzales-Olvera, M.A. and Tang, Y. 2007. A new recurrent neurofuzzy network for identification of dynamic systems. Fuzzy Sets and Systems, 158, 1023-1035.

64. Grashof, B.G. 1883. *Theoretische Machinenlehre*, Band 2, Leopold Voss, Hamburg.

65. Guan, C. and Pan, S. 2008. Adaptive sliding mode control of electro-hydraulic system with nonlinear unknown parameters. Control Engineering Practice, 16, 1275-1284.

66. Guan, G.Q. and Chen, J.Q. 2005. Building optimal back-propogation trained neural networks for firm bankruption predictions. In Proceedings of the Information Resources Management Association International Conference, pp. 449- 452.

67. Guo, H., Liu, Y., Liu, G. and Li, H. 2008. Cascade control of hydraulically driven 6-DOF parallel robot manipulator based on a sliding mode. Control Engineering Practice, 16, 1055-1068.

68. Hace, A., Jezernik, K. and Sabanovic, A. 2005. Improved design of VSS Controller for a linear belt-driven servomechanism. IEEE/ASME Transactions on Mechatronics, 10(4), 385–390.

69. Hametner, C. and Jakubek, S. 2011. Nonlinear identification with local model networks using GTLS techniques and equality constraints. IEEE Transactions on Neural Networks, 22(9), 1406-1418.

70. Hamming, R.W. 1986. Coding and Information Theory, Second edition. New Jersey: Prentice Hall.

71. Hamrouni, L., Kherallah, M. and Alimi, A.M. 2011. Textile plant modeling using recurrent neural networks. In Proceedings of the IEEE International Conference on Systems, Man, and Cybernetics, pp. 1580-1584.

72. Han, X., Xie, W.F., Fu,Z. and Luo, W. 2011. Nonlinear systems identification using dynamic multi-time scale neural networks. Neurocomputing, 74, 3428-3439.

73. Han, Z., Yingrong, L. and Qian, L. 2006. MW-OBS: an improved pruning method for topology design of neural networks. Tsinghua Science and Technology, 11, 307-312.

74. Hassibi, B. and Stork, D.G. 1992. Second-order derivatives for network pruning: optimal brain surgeon. In Proceedings of the Neural Information Processing Systems, 5, pp. 164–171.

75. Hassibi, B., Stork, D.G. and Wolff, G. 1993. Optimal brain surgeon and general network pruning. In Proceedings of IEEE International Conference on Neural Networks, pp. 293–299.

76. Haykin, S. and Li, X.B. 1995. Detection of signals in chaos. In Proceedings of the IEEE 83(1), 95-122.

77. He, S. and Sepehri, N. 1999. Modeling and prediction of hydraulic servo actuators with neural networks. In Proceedings of the American Control Conference, San Diego, California, pp. 3708-3712.

78. He, X. and Asada, H. 1993. A new method for identifying orders of input-output models for nonlinear dynamical systems. In Proceedings of American Control Conference, San Francisco, USA, pp. 2520-2523.

79. Heaton, J. 2008. Introduction to Neural Networks with Java, 2nd edition. Heaton Research Inc.

80. Hebb, D.O. 1949. The organization of behavior. New York: Wiley & Sons.

81. Hecht-Nielsen, R. 1987. Counterpropagation networks. Applied Optimization, 26(23), 4979-4984.

82. Helbig, A., 2002. Injection molding machine with electric-hydrostatic drives. 3rd International Fluid Power colloquium, 1, 67-81.

83. Helduser, S., 2003. Improved energy efficiency in plastic injection molding machines. 8th Scandinavian International Conference on Fluid Power, Tampere, Finland.

84. Hikawa, H. 1999. Frequency Based Multilayer Neural Network with on chip learning and Enhanced Neuron characteristics. IEEE Transactions on Neural Networks, 10(3), 545-553.

85. Hikawa, H. 2003. A New Digital Pulse-Mode Neuron with Adjustable Activation Function. IEEE Transactions on Neural Networks, 14(1), 236-242.

86. Hinton, G.E., Sejnowski, T.J. and Ackley, D.H. 1984. Boltzmann machines: constraint satisfaction network that learn. Carnegie Mellon University technical report, CMU-CS-84-119.

87. Hintz, C., Rau, M. and Schroder, D. 2000. Identification of a nonlinear multi stand rolling system by a structured recurrent neural network. In Proceedings of IEEE Industry Applications Conference, pp. 1121–1128.

88. Hong, X. and Chen, S. 2011. Modeling of complex-valued Wiener systems using B-spline neural network. IEEE Transactions on Neural Networks, 22(5), 818-825.

89. Hunt, K.J., Sbarbaro, D., Zbikowski, R. and Gawthrop, P.J. 1992. Neural networks for control systems- a survey. Automatica, 28, 1083-1112.

90. Ishikawa, M. 1996. Structural learning with forgetting. Neural Networks, 9, 509–521.

91. Iwata, A., Nagasaka, Y. and Suzumura, N. 1990. Data compression of the ECG using neural network for digital Holter monitor. IEEE Engineering in Medicine and Biology Magazine, 9 (3), 53-57.

92. Jacobs, R.A. 1995. Methods of combining expert's probability assessments. Neural Computation, 7, 867-888.

93. Jang, H. Park, A. and Jung, K. 2008. Neural Network Implementation using CUDA and OpenMP. IEEE Digital Image Computing: Techniques and Applications, DOI: 10.1109/DICTA.2008.82, 155- 161.

94. Januszewski, M. and Kostur, M. 2010. Accelerating numerical solution of stochastic differential equations with CUDA. Computer Physics Communications, 181, 183-188.

95. Jelali, M. and Kroll, A. 2003. Hydraulic Servo-systems Modelling, Identification and Control. London: Springer.

96. Johansen, T.A. and Foss, B.A. 1995. Identification of non-linear system structure and parameters using regime decomposition. Automatica, 31, 321-326.

97. Johansen, T.A. and Foss, B.A. 1997. Operating regime based process modeling and identification. Computers and Chemical Engineering, 21, 159-176.

98. Johnson, K.L. 1985. *Contact Mechanics,* Cambridge Univ. Press, London.

99. Jordan, M.I. and Jacobs, R.A. 1994. Hierarchical mixture of experts and EM algorithm. Neural Computation, 6, 181-214.

100. Juang, C.F. and Hsieh, C.D. 2010. Alocally recurrent fuzzy neural network with support vector regression for dynamic-system modeling. IEEE Transactions on Fuzzy Systems, 18(2), 261- 273.

101. Kaddissi, C., Kenne, J.P. and Saad, M. 2007. Identification and real-time control of an electrohydraulic servo system based on nonlinear backstepping. IEEE/ASME Transactions on Mechatronics 12(1), 12-22.

102. Kaddissi, C., Kenne, J.P. and Saad, M. 2011. Indirect adaptive control of an electrohydraulic servo system based on nonlinear backstepping. IEEE/ASME Transactions on Mechatronics, 16(6), 1171-1177.

103. Kagotani, M., Ueda, H. and Koyama, T. 2001. Transmission error in helical timing belt drives. Transactions of the ASME, 123, 104-110.

104. Kang, R., Jiao, Z., Wu, S., Shang, Y., and Mare, J.C. 2008. The nonlinear accuracy model of electro-hydrostatic actuator. IEEE Conference on Robotics, Automation and Mechatronics, Chengdu, China, pp. 107-111.

105. Karnin, E.D. 1990. A simple procedure for pruning back-propagation trained neural networks. IEEE Trans. Neural Networks, 1, 239–242.

106. Karpenko, M. and Sepehri, N. 2010. On quantitative feedback design for robust position control of hydraulic actuators. Control Engineering Practice 18, 289-299.

107. Kautz, T.O. 1993. Cable extension linear position transducer. U.S. Patent 5 236 144.

108. Kilic, E. 2007. Novel Position Measurement and Estimation Methods for CNC Machine Systems. M.Sc. Thesis, Middle East Technical University – Ankara, Turkey.

109. Kilic, E., Dolen, M. and Koku, A.B. 2011. Experimental Evaluation of Cable-Drum Systems as Linear Motion Sensors. In Proceedings of IEEE International Conference on Mechatronics, Turkey, 666-671.

110. Kilic, E., Dolen, M., Koku, A.B. and Dogruer, C.U. 2007. Novel position estimators for timing belt drives. Journal of Automation, Mobile Robotics and Intelligent Systems, 1(2), 55-61.

111. Kim, K. and Park, J. 1993. Application of hierarchical neural networks to fault diagnosis of power systems. International Journal on Electrical Power and Energy System, 15(2), 65-70.

112. King, S.-Y. and Hwang, J.-N. 1989. Neural network architectures for robotic applications. IEEE Transactions on Robotics and Automation, 5 (5), 641-657).

113. Kiong, L.C, Rajeswari, M. and Rao, M.V.C. 2003. Nonlinear dynamic system identification and control via constructivism inspired neural network. Applied Soft Computing, 3, 237-257.

114. Kirkpatrick, S., Gelatt, C.D. and Vecchi, M.P. 1983. Optimization by simulated annealing. Science, 220, 671-680.

115. Kolen, J.F. and Kremer, S.C. 2001. A Field Guide to Dynamical Recurrent Networks. New York: IEEE Press.

116. Kong, L. and Parker, R.G. 2005. Microslip friction in flat belt drives. Proc. *IMechE Mechanical Engineering Science.*, 219, 1097-1106.

117. Kong, L. and Parker, R.G. 2006. Mechanics and Sliding Friction in Belt Drives with Pulley Grooves. *ASME J. of Mech. Design*, 128, 494-502.

118. Krips, M., Lammert, T. and Kummert, A. 2002. FPGA Implementation of a Neural Network for a Real-Time Hand Tracking System. In proceedings of the First IEEE International Workshop on Electronic Design, Test and Applications.

119. Kulkarni, A.S. and El-Sharkawi, M.A. 2001. Intelligent precision position control of elastic drive systems. IEEE Trans. on Energy Conv., 16 (1), 26-31.

120. Kurkova, V. 1991. Kolmogorov's theorem is relevant. Neural Computations, 3(4), 617-622.

121. Kwan, H.K. 1992. Simple sigmoid like activation function suitable for digital hardware implementation. Electronic Letters , 28, 1379 – 1380.

122. Kwok, T. and Yeung, D. 1997. Constructive algorithms for structure learning in feedforward neural networks for regression problems. IEEE Trans. Neural Networks, 3, 630–645.

123. Lawrynczuk, M. 2010. Training of neural models for predictive control. Neurocomputing, 73, 1332-1343.

124. Lazar, M. and Pastravanu, O. 2002. A neural predictive controller for non-linear systems. Mathematics and Computers in Simulation, 60, 315-324.

125. Leamy, M.J. and Wasfy, T.M. 2002. Analysis of Belt-Drive Mechanics using a Creep-Rate Dependent Friction Law. *ASME J. of App. Mechanics*, 69, 763-771.

126. LeCun, Y., Boser, B., Denker, J., Henderson, D., Howard, R., Hubbard, W. and Jackel, L. 1989. Backpropagation applied to handwritten zip code recognition. Neural Computation, 1, 541-551.

127. Lemma, D.T., Ramasamy, M. and Shuhaimi, M 2010. System identification using orthonormal basis filters. Journal of Applied Sciences 10(21), 2516-2522.

128. Li, C.J. 1995. Mechanical system modeling using recurrent neural networks via quasi-Newton learning methods. Applied Mathematical Modelling, 19(7), 421-428.

129. Li, W. and Rehani, M. 1996. Modeling and control of a belt-drive positioning table. In Proceedings of the 22nd IEEE International Conference of Industrial Electronics, Taipei, 1996, pp. 1984–1989.

130. Liberati, M., Beghi, A., Mezzalira, S. and Peron, S. 2004. Grey-box Modelling of a Motorcycle Shock Absorver. Conference on Decision and Control, 755- 760.

131. Lien, J.P., York, A., Fang, T. and Buckner, G.D. 2010. Modeling piezoelectric actuators with hysteretic recurrent neural networks. Sensors and Actuators A, 163, 516-525.

132. Lightbody, G., O'Reilly, P., Irwin, G.W., Kelly, K. and McCormick, J. 1997. Neural modelling of chemical plant using MLP and B-spline networks. Control Engineering Practice, 5(11), 1501-1515.

133. Lima C.A.M, Coelho, A.L.V. and Von Zuben, F.J. 2007. Hybridizing mixture of experts with support vector machines: Investigation into nonlinear dynamic systems identification. Information Sciences, 177, 2049-2074.

134. Lin, T., Horne, B.G and Giles, C.L. 1998. How embedded memeory in recurrent neural network architectures helps learning long-term temporal dependencies. Neural Networks, 5, 861-868.

135. Lippmann, R. 1989. Review of neural networks for speech recognition. Neural Computation, 1, 1-38.

136. Liu, G.P., Kadirkamanathan, V. and Billings, S.A. 1998. On-line identification of nonlinear systems using Volterra polynomial basis function neural networks. Neural Networks 11, 1645-1657.

137. Liu, J.N.K. and Lee, R.S.T. 1999. Rainfall forecasting from multiple point sources using neural networks. IEEE International Conference on Systems, Man, and Cybernetics, 3, 429-434.

138. Ljung, L. 1999. System Identification: Theory for the User. London: Prentice Hall.

139. Lovrec, D., Kastrevc, M., Ulaga, S., 2008. Electro-hydraulic load sensing with speed-controlled hydraulic supply system on forming machines. International Journal Advanced Manufacturing Technology 1, 1066-1075.

140. Lovrec, D., Ulaga, S., 2007. Pressure control in hydraulic systems with variable or constant pumps. Experimental Techniques 31 (2), 33-41.

141. Lu, B.L. and Ito, M. 1999. Task decomposition and module combination based on class relations: a modular neural network for pattern classification. IEEE Transactions on Neural Networks, 10(5), 1244-1256.

142. Macleod, C., Maxwell, G. and Muthuraman, S. 2009. Incremental growth in modular neural networks. Engineering Applications of Artificial Intelligence, 22, 660-666.

143. MacQueen, J.B. 1967. Some methods for classification and analysis of multivariate observations. Proceedings of the 5th Berkeley Symposium on Mathematical Statistics and Probability, 281-297.

144. Maeda, Y. and Tada, T. 2003. FPGA implementation of a pulse density neural network with learning ability using simultaneous perturbation. IEEE Transactions on Neural Networks, 14(3), 688-695.

145. Maeda, Y., Hiramatsu, T., Miyoshi, S. and Hikawa, H. 2009. Pulse Coupled Oscillator with Learning Capability Using Simultaneous Perturbation and Its FPAA Implementation. ICROS-SICE International Joint Conference, Fukuoka, Japan, pp. 3142-3145.

146. Maher, J., Ginley, B., Rocke, P. and Morgan, F. 2006. Intrinsic Hardware Evolution of Neural Networks in Reconfigurable Analogue and Digital Devices. IEEE Symposium on Field-Programmable Custom Computing Machines.

147. Maria, J., Menezes, P. and Baretto, G. 2008. Long-term time series prediction with the NARX network: An empirical evaluation. Neurocomputing, 71, 3335-3343.

148. Mayergoyz, I.D. 1991. Mathematical Models of Hysteresis. NewYork: Springer.

149. Melin, P., Mancilla, A., Lopez, M. and Mendoza, O. 2007. A hybrid modular neural network architecture with fuzzy Sugeno integration for time series forecasting. Applied Soft Computing, 7, 1217-1226.

150. Merritt, H.E. 1967. Hydraulic Control Systems. New York: John Wiley & Sons.

151. Michalkiewicz, J. 2012. Modified Kolmogorov's neural network in the identification of Hammerstein and Weiner systems. IEEE Transactions on Neural Networks and leraning Systems, 23(4), 657- 662.

152. Mihajlov, M., Nikolic, V. and Antic, D. 2002. Position control of an electro-hydraulic servo system using sliding mode control enhanced by fuzzy PI controller. Mechanical Engineering, 1(9), 1217-1230.

153. Mirzaee, H. 2009. Long-term prediction of chaotic time series with multi-step predictipn horizons by a neural network with Levenberg-Marquardt learning algorithm. Chaos, Solitons and Fractals 41, 1975-1979.

154. Moallemi, C. 1991. Classifying cells for cancer diagnosis using neural networks. IEEE Expert, 6 (6), 8-12.

155. Mohanty, A., and Yao, B. 2011. Indirect adaptive robust control of hydraulic manipulators with accurate parameter estimates. IEEE Transactions on Control Systems Technology, 19(3), 567-575.

156. Mozer, M.C. and Smolensky, P. 1989. Skeletonization: A technique for trimming the fat from a network via relevance assessment. In Proceedings of the Neural Information Processing Systems, 1, pp. 107–115.

157. Mustafaraj, G., Lowry, G. and Chen, J. 2011. Prediction of room temperature and relative humidity by autoregressive linear and nonlinear neural network models for open office. Energy and Buildings, 43, 1452-1460.

158. Nageswaran, J.M., Dutt, N., Krichmar, J.L., Nicolau, A. and Veidenbaum, A.V. 2009. A configurable simulation environment for the efficient simulation of large spiking neural networks on graphics processors. Neural Networks, 22, 791-800.

159. Narendra, K.S. and Parthasarathy, K. (1989). Neural Network and Dynamical Syetms Part II: Identification. Report No. 8002, Yale University.

160. Narendra, K.S. and Parthasarathy, K. 1990. Identification and control of dynamical systems using neural networks. IEEE Trans. Neural Networks, 1, 4-27.

161. Nelles, O. 2001. Nonlinear System Identification. New York: Springerlink.

162. Ni, J. and Song, Q. 2006. Dynamic pruning algorithm for multilayer perceptron based neural control systems. Neurocomputing, 69, 2097-2111.

163. Nørgaard, M. 2000. Neural network based system identification toolbox, Technical Report 00-E-891, Department of Automation, Technical University of Denmark.

164. Nuno-Maganda, M.A., Arias-Estrada, M., Torres-Huitzil, C. and Girau, B. 2009. Hardware Implementation of Spiking Neural Network Classifiers based on Backpropagation-based Learning Algorithms. In Proceedings of International Conference on Neural Networks, Atlanta, USA.

165. Omondi, A.R. and Rajapakse, J.C. 2006. FPGA implementations of Neural Networks. New York: Springer.

166. Orlando, J.R., Mann, R. and Haykin S. 1990. Classification of sea-ice images using a dual-polarized radar. IEEE Journal of Oceanic Engineering, 15 (3), 228-237.

167. Oyama, E., Agah, A., MacDorman, K.F., Maeda, T. and Tachi S. 2001. A modular neural network architecture for inverse kinematics model learninig. Neurocomputing, 38, 797-805.

168. Pan, Y. and Sensen, C. 2005. Modular neural networks and their applications in exon prediction. In Advances in bioinformatics and its applications series in mathematical biology and medicine, 8, 47-61.

169. Parlos, A.G., Rais, O.T. and Atiya, A.F. 2000. Multi-step-ahead prediction using dynamic recurrent neural networks. Neural Networks 13, 765-786.

170. Patel, A. and Dunne, J.F. 2010. NARX Neural Network Modelling of Hydraulic Suspension Dampers for Steady-state and Variable Temperature Operation. Vehicle System Dynamics, 40 (5), 285-328.

171. Pi, Y. and Wang, X. 2011. Trajectory tracking control of a 6-DOF parallel robot manipulator with uncertain load disturbances. Control Engineering Practice, 19, 185-193.

172. Piroddi, L. and Spinelli, W. 2003. An identification algorithm for polynomial NARX models based on simulation error minimization. International Journal of Control, 76, 1767-1781.

173. Pukrittayakameei, A., Hagan, M., Raff, L., Bukkapatnam, S. and Komanduri, R. 2009. A network pruning algorithm for combined function and derivative approximation. In Proceedings of International Joint Conference on Neural Networks, Atlanta, USA.

174. Qiao, J., Zhang, Y. and Han, H. 2008. Fast unit pruning algorithm for feedforward neural network design. Applied Mathematics and Computation, 205, 622-627.

175. Ramirez-Agundis, A., Gadea-Girones, R. and Colom-Palero, R. 2008. A hardware design of a massive-parallel, modular NN-based vector quantizer for real-time video coding. Microprocessors and Microsystems, 32, 33-44.

176. Reed, R. 1993. Pruning algorithm - a survey. IEEE Trans. Neural Networks, 5, 740-747.

177. Ren, X. and Lv, X. 2011. Identification of extended Hammerstein systems using dynamic self-optimizing neural networks. IEEE Transactions on Neural Networks, 22(8), 1169-1179.

178. Reuter, H.B. 1995. Zur Identifikation nichtlinearer Systemmodelle mit wenig A-priori-Informationen. Dissertation in University of Duisburg, Düsseldorf, Germany.

179. Rogova, G. 1994. Combining results of several neural network classifiers. Neural Networks, 7, 771-781.

180. Sato, M. and Sato, Y. 1995. Neural clustering-implementation of clustering model using neural networks. IEEE International Conference on Systems, Man and Cybernetics, 4, 3609-3614.

181. Schenker, B. and Agarwal, M. 1998. Output prediction in systems with backlash. IMechE, 212, 17-26.

182. Schittenkopf, C., Deco, G. and Brauer, W. 1997. Two strategies to avoid overfitting in feedforward neural networks. Neural Networks, 10, 505–516.

183. Schrauwen, B., D'Haene, M., Verstraeten, D. and Van Campenhout, J. 2008. Compact hardware liquid state machines on FPGA for real-time speech recognition. Neural Networks, 21, 511-523.

184. Seidl, D.R. 1996. Motion and Motor Control Using Structured Neural Networks. Ph.D. thesis, University of Wisconsin, USA.

185. Seidl, D.R. and Lorenz, R.D. 1991. A structure by which a recurrent neural network can approximate a nonlinear dynamic system. In Proceedings of International Joint Conference on Neural Networks, pp. 709-714.

186. Seidl, D.R. and Lorenz, R.D. 1993. One-step optimal space vector PWM current regulation using a neural network. In Proceedings of the IEEE IAS Conference, pp. 2027-2034.

187. Seidl, D.R., Lam, S.L., Putman, J.A. and Lorenz, R.D. 1993. Neural network identification and compensation of gear backlash hysteresis in position controlled mechanisms. In Proceedings of the IEEE IAS Conference, pp. 2027-2034.

188. Seidl, D.R., Reineking, T.L. and Lorenz, R.D. 1992. Use of neural networks to identify and compensate for friction in precision position controlled mechanism. In Proceedings of the IEEE IAS Conference, pp. 1937-1944.

189. Sharma, S.K., Irwin, G.W., Tokhi, M.O and McLoone, S.F. 2003. Learning soft computing strategies in a modular neural network architecture. Engineering Applications of Artificial Intelligence. 16, 395-405.

190. Sibte, S. and Abidi, R. 1996. Neural networks and child language development: A simulation using a modular neural network architecture. In Proceedings of IEEE International Conference on Neural Networks, pp. 840-845.

191. Siebel, N., Bötel, J. and Sommer, G. 2009. Efficient neural network pruning during neuro-evolution. In Proceedings of International Joint Conference on Neural Networks, Atlanta, USA.

192. Sietsma, J. and Dow, R.F.J. 1991. Creating artificial neural networks that generalize. Neural Networks, 4(1), 67-69.

193. Smith, D.P. 1998. Tribology of the Belt Driven Data Tape Cartridge. *Tribology International,* 31(8), 465–477.

194. Sola, J. and Sevilla, J. 1997. Importance of input data normalization for the application of neural networks to complex industrial problems. IEEE Transactions on Nuclear Science, 44(3), 1464-1468.

195. Sorjamaa, A., Reyhani, J.H.N., Ji, Y. and Lendasse, A. 2007. Methodology for long-term prediction of time series. Neurocomputing 70, 2861-2869.

196. Soukoulis, C.M., Levin, K. and Grest, G.S. 1983. Irreversibility and Metastability in Spin-Glasses. I. Ising Model. Physical Review, 28, 1495-1509.

197. Söderström, T. and Stoica, P. 1989. System Identification. Prentice Hall.

198. Sprecher, D.A. 1996. A numerical implementation of Kolmogorov's superpositions. Neural Networks, 9(5), 765-772.

199. Stahlberger, A. and Riedmiller, M. 1996. Fast network pruning and feature extraction using the unit-OBS algorithm. Advances in Neural Information Processing Systems, Denver, pp. 2-5.

200. Stavrakoudis, D.G. and Theocharis, J.B. 2007. Pipelined recurrent fuzzy neural networks for nonlinear adaptive speech prediction. IEEE Trans. Syst. Man Cybern., 37(5), 1305-1320.

201. Steinich, K.M. 2007. Cable actuated position sensor with spring located inside the cable drum. U.S. Patent 7 263 782.

202. Stepniewski, S.E. and Keane, A.J. 1997. Pruning backpropagation neural networks using modern stochastic optimization techniques. Neural Computing & Applications, 5, 76-98.

203. Tagliarini, G.A., Christ, J.F. and Page, E.W. 1991. Optimization using neural networks. IEEE Transactions on Computers, 40 (12), 1347-1358.

204. Tan, C.L., Quah, T.S. and Teh, H.H. 1996. An artificial neural network that models human decision making. Computers, 29 (3), 64-70.

205. Te Braake, H.A.B., Babuska, R. and Van Can, H.J.L. 1994. Fuzzy and neural models in predictive control. Journal A, 35, 44-51.

206. Tellez, F.O., Loukianov, A.G., Sanchez, E.N. and Corrochano, E.J.B. 2010. Decentralized neural identification and control for uncertain nonlinear systems: Application to planar robot. Journal of the Franklin Institute, 347, 1015-1034.

207. Tenorio, M.F. and Lee, W.T. 1990. Self-organizing network for optimum supervised learning. IEEE Trans. Neural Networks, 1, 100–110.

208. Thayer, W.J. 1965. Transfer function for Moog servovalves. Technical Bulletin I03 MOOG 103, East Aura, NY, USA.

209. Tokunaga, K. and Furukawa, T. 2009. Modular network SOM. Neural Networks, 22, 82-90.

210. Treesatayapun, C. 2010. Nonlinear discrete-time controller with unknown systems identification based on fuzzy rules emulated network. Applied Soft Computing, 10, 390-397.

211. Tseng, H.C. and Almogahed, B. 2009. Modular neural networks with applications to pattern profiling problems. Neurocomputing, 72, 2093-2100.

212. Tseng, H.C. and Chi, C.W. 1995. Modular intelligent control. Advances in Fuzzy Theory and Technology III.

213. Tu, C.F. and Fort, T. 2004. A Study of Fiber–Capstan Friction. 1: Stribeck Curves. *Tribology International,* 37, 701–710.

214. Tufa, L.D., Ramasamy, M., Patwardhan, S.C. and Shuhaimi, M. 2010. Development of Box-Jenkins time series models by combining conventional and orthonormal basis filter approaches. Journal of Process Control, 20, 108-120.

215. Tumer, K. and Ghosh, J. 1996. Error correlation and error reduction in ensemble classifiers. Connection Science, 8, 385-404.

216. Van den Hof, P., Paul, M.J., Heuberger, P. and Wahlberg, B. 2005. Modeling and Identification with Rational Orthogonal Basis Functions. London: Springer.

217. Van Hulle, M. M. and Tollenacre, T. 1993. A modular artificial neural network for texture processing. Neural Networks, 6(1), 7-32.

218. Waibel, A. 1989. Modular construction of time-delay neural networks for speech recognition. Neural Computation, 1(1), 39-46.

219. Wang, L., Der, S. and Nasrabadi, N. 1998. Automatic target recognition using a feature-decomposition and data-decomposition modular neural network. IEEE Transactions on Image Processing, 8, 11113-1121.

220. Wang, P., Xu, L., Zhou, S.M., Fan, Z., Li, Y. and Feng, S. 2010. A novel Bayesian learning method for information aggregation in modular neural networks. Expert Sytems with Applications, 37, 1071-1074.

221. Watanabe, E. and Mori, K. 2001. Lossy image compression using a modular structured neural network. In Proceedings of the IEEE Signal Processing Society Workshop, pp. 403-412.

222. Watanabe, S. and Yoneyama, M. 1992. An ultrasonic visual sensor for three-dimensional object recognition using neural networks. IEEE Transactions on Robotics and Automation, 8 (2), 240-249.

223. Watton, J. and Xue, Y. 1997. Simulation of fluid power circuits using artificial network models Part1: selection of components models. Proc. Instn. Mech. Engrs, 211, 417-428.

224. Weber, M., Crilly, P.B. and Blass, W.E. 1991. Adaptive noise filtering using an error-backpropagation neural network. IEEE Transactions on Instrumentation and Measurement, 40 (5), 820-825.

225. Wei, H.L., Zhu, D.Q., Billings, S.A. and Balikhin, M.A. 2007. Forecasting the geomagnetic activity of the *Dst* index using multiscale radial basis function networks. Advances in Space Research, 40, 1863-1870.

226. Werbos, P.J. 1974. Beyond Regression: New Tools for Prediction and Analysis in the Behavioral Sciences. Ph.D. thesis, Harvard University.

227. Werkmeister, J. and Slocum, A. 2007. Theoretical and Experimental Determination of Capstan Drive Stiffness. *Precision Engineering*, 31, 55-67.

228. Widrow, B. and Walach, E. 1996. Adaptive Inverse Control. New Jersey: Prentice Hall.

229. Williams, R.J. and Zipser, D. 1989. A learning algorithm for continually running fully recurrent neural networks. Neural Computation, 1, 270-280.

230. Witters, M. and Swevers, J. 2010. Black-box model identification for a continuously variable, electro-hydraulic semi-active damper. Mechanical Systems and Signal Processing, 24, 4-18.

231. Wong, C.X. and Worden, K. 2007. Generalised NARX shunting neural network modeling of friction. Mechanical Systems and Signal Processing 21, 553-572.

232. Wongputorn, P., Hullender, D., Woods, R. and King, J. 2005. Application of MATLAB functions for time domain simulation of systems with lines with fluid transients. Journal of Fluids Engineering, 127, 177-182.

233. Xu, J. and Ho, D.W.C. 2006. A new training and pruning algorithm based on node dependence and Jacobian rank deficiency. Neurocomputing, 70, 544-558.

234. Xu, P.X. 1997. Experimental Modeling of a Hydraulic Load Sensing Pump using Neural Networks. Ph.D. thesis, University of Saskatchewan, Canada.

235. Xue-miao, P., Yuan, Z., Zong-yi, X., Yong, Q. and Li-min, J. 2010. Research on neural networks based modeling and control of electrohydraulic system. In Proceedings of the 2nd International Conference on Advanced Computer Control, Shenyang, China, pp. 34-38.

236. Yang, W.C. and Tobler, W.E. 1991. Dissipative modal approximation of fluid transmission lines using linear friction model. Journal of Dynamic Systems, Measurement and Control, 113, 152-162.

237. Yao, B., Bu, F., Reedy, J. and Chiu, G.T.C. 2000. Adaptive robust motion control of single-rod hydraulic actuators: theory and experiments. IEEE/ASME Transactions on Mechatronics, 5(1), 79-91.

238. Yilmaz, S. and Oysal, Y. 2010. Fuzzy wavelet neural network models for prediction and identification of dynamical systems. IEEE Transactions on Neural Networks, 21(10), 1599-1609.

239. Yousefi, H., Handroos, H. and Soleymani, A. 2008. Application of differential evolution in system identification of a servo-hydraulic system with a flexible load. Mechatronics, 18, 513-528.

240. Zaki, A., Sollmann, K., Jouaneh, M. and Anderson, E. 2008. Nonlinear control of a belt-driven two-axis positioning system. In Proceedings of ASME International Mechanical Engineering Congress and Exposition, pp. 807-814.

241. Zamarreno, J.M. and Vega, P. 1998. State space neural network. Properties and application. Neural Networks, 11, 1099-1112.

242. Zemouri, R., Gouriveau, R. and Zerhouni, N. 2010. Defining and applying prediction performance metrics on a recurrent NARX time series model. Neurocomputing, 73, 2506-2521.

243. Zeng, X. and Yeung, D.S. 2006. Hidden neuron pruning of multilayer perceptrons using a quantified sensitivity measure. Neurocomputing, 69, 825-837.

244. Zhang, H. 1997. Neural Adaptive Control of Nonlinear MIMO Electrohydraulic Servosystem. PhD thesis at University of Saskatchewan, Department of Mechanical Engineering, Canada.

245. Zhang, M. and Fulcher, J. 1996. Face recognition using artificial neural network group-based adaptive tolerance (GAT) trees. IEEE Transactions on Neural Networks. 7 (3), 555-567.

246. Zhang, Q. and Benveniste, A. 1992. Wavelet networks. IEEE Transactions on Neural Networks, 3(6), 889-898.

247. Zhang, X. and Tan, Y. 2010. A hybrid model for rate-dependent hysteresis in piezoelectric actuators. Sensors and Actuators, 157, 54-60.

248. Zhao, H. and Zhang, J. 2009. Nonlinear dynamic system identification using pipelined functional link artificial recurrent neural network. Neurocomputing, 72, 3046-3054.

249. Zhao, X. and Tan, Y. 2008. Modeling hysteresis and its inverse model using neural networks based on expanded input space method. IEEE Transactions On Control Systems Technology, 16(3), 484-490.

250. Zhao, Z. and Cai, L. 1996. On the improvement of tracking performance of positioning tables. In Proceedings of the 22nd IEEE International Conference of Industrial Electronics, Taipei, Taiwan, pp. 1990–1995.

251. Zhuang, H., Low, K.S., and Yau, W.Y. 2007. A pulse neural network with on-chip learning and its practical applications. IEEE Transactions on Industrial Electronics, 54(1) 34-42.

APPENDIX A

DETAILED MODELING OF THE HYDRAULIC SERVO SYSTEM

The mathematical model of the simulated servo-valve controlled hydraulic system, utilized in Chapter 5, is now explained in a detailed manner. As remembered, the model of the hydraulic servo-system was used to generate input-output data sets for designing ANNs. Therefore, the simulated hydraulic model should accurately represent the nonlinear dynamic behavior of a real hydraulic system. In other words, it should be possible to identify ANN models from an input-output data taken from the constructed theoretical model as if it was experimental results of a real system. In fact, it is required that the model should be of the same order as the relevant dynamics of a real system. For that purpose, the model must house pump, pressure relief valve and accumulator dynamics and also the pipe line.

As could be seen from Fig. 5.1, a fixed displacement pump feeds the system with hydraulic fluid from a reservoir (tank). This pump is essentially a constant flow device. The pump simply moves an amount of fluid, and it does not determine the output or supply pressure. The pressure is determined primarily by the load to which the pump is connected. Pump output pressure increase rapidly as the integral of flow. To avoid rupture due to the very high pressure at the pump casing or pipe lines, a pressure relief valve is used as a safety device. This relief valve is installed on the discharge side of the pump to limit the maximum operating pressure. Moreover, an accumulator is located on the pump exit side satisfying an energy source in case of additional power need on the hydraulic power supply. Therefore, it is wanted a constant supply pressure at the pump discharge by means of the

accumulator and the relief valve. Moreover, servo-valve directs the oil flow through the appropriate position of its spool to determine the direction of motion and speed of the hydraulic actuator. Eventually, the aim of this section is to derive the mathematical models of the all used hydraulic elements and to give the value of the parameters which are used in the detailed simulation study. A problem with modeling of these subsystems is to choose the value of the large number of physical parameters in order to give out a valid simulation results. Although the theoretical model does not give the same response as the real system output, it will be useful for analyzing the dynamic behavior of the hydraulic servo system. Therefore, simulation results will provide the necessary insight to decide which nonlinearities of the hydraulic system should be taken into consideration while designing ANNs.

A.1 Servo Valve

Electro hydraulic servo-valve is a complicated device composed from mainly a spool valve, flapper-nozzle and torque motor as can be seen in Fig. A.1. Therefore, it has many dynamic and non-linear effects such as backlash, saturation, hysteresis, square-root function for the flows, friction forces, lateral and axial flow forces (or known as Bernoulli force, also).

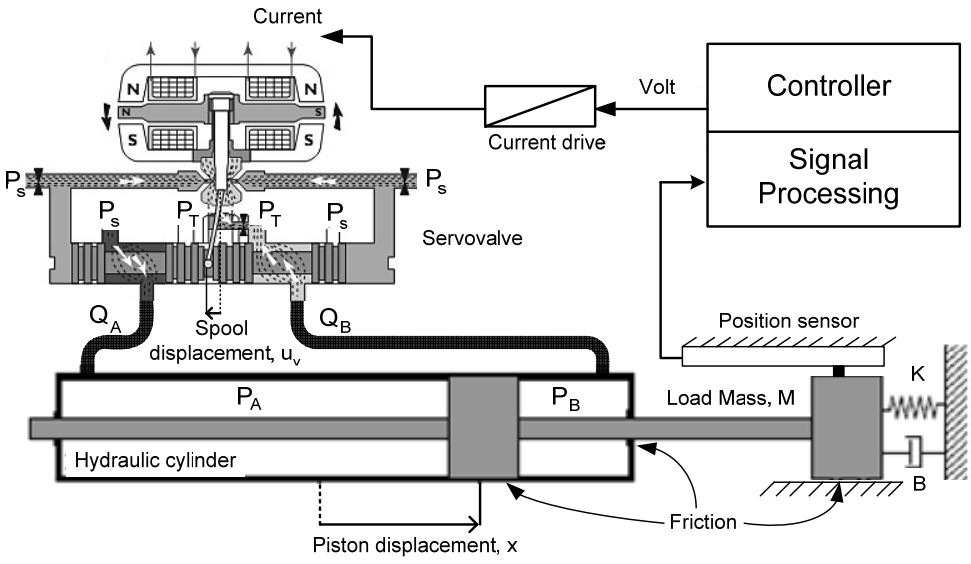

Fig. A.1 A servo-valve controlling a hydraulic actuator (Courtesy of Moog Corporation).

Although there are a lot of nonlinearities in servo valves, it is often convenient in servo analysis to represent an electro-hydraulic servo-valve by simplified functions. All the assumptions (and approximations) made in the simulation study are frequently utilized in the relevant technical literature and can be presumed reasonable for all practical purposes. For instance, Thayer (1965) shows that a servo-valve can be represented as a linear time-invariant system at frequencies up to 100 Hz provided that the servo-valve's response is much faster than the rest of the hydraulic system itself. Appropriate transfer functions are generally derived by the valve firms especially for the relationship between the control input and the main spool valve displacement such as given in (5.9) and (5.10) in this thesis work.

After, knowing the spool position with respect to the control input, relationship between the flow rates to the actuator cylinder chambers and main spool position must be derived. It is well known from the fluid mechanics that the flow through an orifice mainly depends on the port distance, pressure drop across the orifice and the direction of the pressure drop, also. Before writing the flow equations through the valve, the center type of the valve must be determined. If the overall length of the valve port is greater than the length of the spool (when the spool is at the neutral position), valve is known as open centre (or under lapped). On the contrary, if the length of the spool is greater than the length the valve port, valve is called as closed centre (or over lapped). Critical centre (or zero lapped) valves have a port length which is equal to its spool length. Therefore, the backlash characteristics of the valve is minimized. But, they are much more expensive than the other type of valves due to the high accuracy machining tolerances.

Considering a generic 4 way servo-valve as shown in Fig. A.2, the flow equations for a zero lapped valve could be written as below.

$$\begin{aligned} Q_A &= Q_1 - Q_2 \\ &= K_v f(u_v)\, sign(P_S - P_A)\sqrt{|P_S - P_A|} - K_v f(-u_v)\, sign(P_A - P_T)\sqrt{|P_A - P_T|} \end{aligned} \quad \text{(A.1)}$$

$$\begin{aligned} Q_B &= Q_3 - Q_4 \\ &= K_v f(-u_v)\, sign(P_S - P_B)\sqrt{|P_S - P_B|} - K_v f(u_v)\, sign(P_B - P_T)\sqrt{|P_B - P_T|} \end{aligned} \quad \text{(A.2)}$$

where K_v is the servo-valve flow gain and u_v refers to the displacement of the valve spool. Moreover, the function *f(x)* is defined by;

$$f(x)=\begin{cases} x, & x \geq 0 \\ 0, & x < 0 \end{cases} \tag{A.3}$$

The corresponding flow equations for *under lapped valves* could be modified and written as;

$$\begin{aligned} Q_A = {} & K_v f(u_{u1}+u_v)\, sign(P_S - P_A)\sqrt{|P_S - P_A|} \\ & - K_v f(u_{u2}-u_v)\, sign(P_A - P_T)\sqrt{|P_A - P_T|} \end{aligned} \tag{A.4}$$

$$\begin{aligned} Q_B = {} & K_v f(u_{u3}-u_v)\, sign(P_S - P_B)\sqrt{|P_S - P_B|} \\ & - K_v f(u_{u4}+u_v)\, sign(P_B - P_T)\sqrt{|P_B - P_T|} \end{aligned} \tag{A.5}$$

where $u_{ui} > 0,\ i=1,..4$ are the underlaps of the valve orifices. Moreover, flow equations for the *over lapped valves* could be written as;

$$\begin{aligned} Q_A = {} & K_v f(-u_{o1}+u_v)\, sign(P_S - P_A)\sqrt{|P_S - P_A|} \\ & - K_v f(-u_{o2}-u_v)\, sign(P_A - P_T)\sqrt{|P_A - P_T|} \end{aligned} \tag{A.6}$$

$$\begin{aligned} Q_B = {} & K_v f(-u_{o3}-u_v)\, sign(P_S - P_B)\sqrt{|P_S - P_B|} \\ & - K_v f(-u_{o4}+u_v)\, sign(P_B - P_T)\sqrt{|P_B - P_T|} \end{aligned} \tag{A.7}$$

where the overlaps are $u_{oi} > 0,\ i=1,..4$

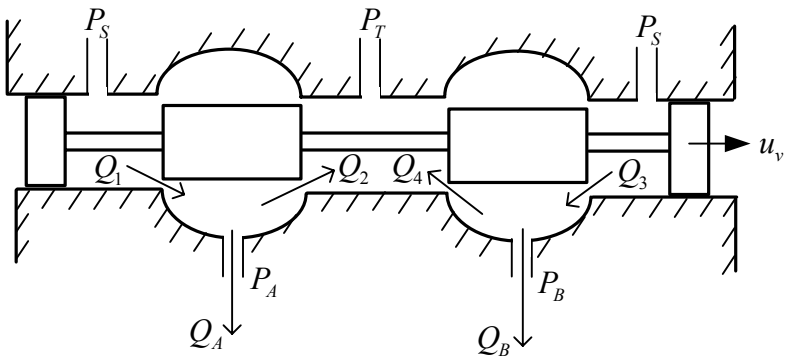

Fig. A.2 A schematic of a generic four way valve.

It is important to note that a zero lapped valve is used in the simulation study, whose mathematical model and used parameters are given in Section 5.2 in a detailed manner.

A.2 Pressure Relief Valve

Pressure relief valve is an auxiliary hydraulic device which is normally closed to create a high pressure value at its inlet port. But, it is opened whenever the pressure value in its control chamber exceeds the predetermined threshold pressure value (which is adjusted by the help of a spring) and bypasses the flow from pump to the tank (reservoir) in order to decrease the supply pressure value to the servo-valve inlet as shown in Fig. A.3. Mathematical model of this valve is given below and Table A.1 gives the parameter values used in the simulation study.

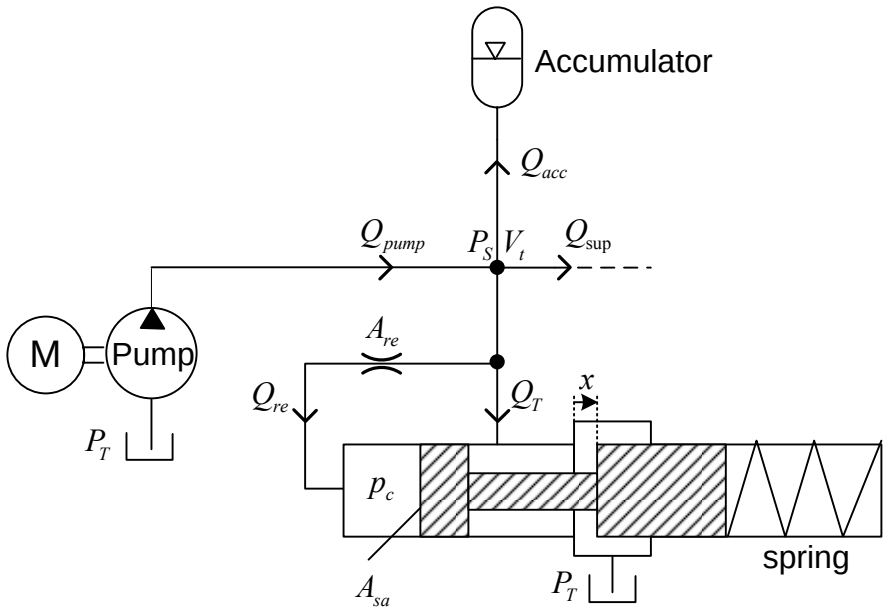

Fig. A.3 Pressure Relief Valve.

Spool motion of the relief valve could be written as;

$$m_e \ddot{x} + b_e \dot{x} + k_e x + F_{ax}(x, P_S) = A_{sa}\, p_c - F_0 \tag{A.8}$$

$$F_{ax}(x, P_S) = 0.43\, w\, x (P_S - P_T) \tag{A.9}$$

where m_e is the spool mass, b_e is the viscous force coefficient, x is the relief valve spool displacement, k_e is the spring stiffness, F_{ax} is the axial flow force, w is the width of the spool, P_S is the supply pressure, P_T is the tank pressure, A_{sa} is the spool area, p_c is the control pressure and F_0 is the spring pre-load force.

Moreover, the control pressure dynamics could be written as below by applying the flow continuity equations to the control chamber;

$$\dot{p}_c = \frac{\beta}{V_c(x)}\left(Q_{re} - A_{sa}\dot{x}\right) = \frac{\beta}{V_{co} + A_{sa}x}\left[\alpha_d A_{re} sign\left(p_c - P_S\right)\sqrt{\frac{2}{\rho}\left|p_c - P_S\right|} - A_{sa}\dot{x}\right] \quad \text{(A.10)}$$

where V_c is the volume of the control chamber, V_{co} is the initial control chamber volume when the relief valve spool is completely closed, α_d is the discharge coefficient, Q_{re} is the flow through the restrictor and A_{re} is the area of the fixed restrictor.

Applying the continuity equation to the chamber of the supply pressure leads to

$$\dot{P}_S = \frac{\beta}{V_t}\left(Q_{pump} - Q_{re} - Q_{\sup} - Q_T - Q_{acc}\right) \quad \text{(A.11)}$$

$$Q_T = \alpha_d\, w x\, sign\left(P_S - P_T\right)\sqrt{\frac{2}{\rho}\left|P_S - P_T\right|} \quad \text{(A.12)}$$

where V_t is the total volume of the chamber where pressure is controlled, Q_{pump} is the pump flow, Q_{sup} is the supply flow to the servo-valve inlet port, Q_T is the flow through the main orifice of the relief valve and Q_{acc} is be the flow to the accumulator. The parameter values used in the simulation model are given in Table A.1.

Table A.1 Parameters used in the relief valve model.

Parameter	**Value**	**Parameter**	**Value**
m_e	0.1 kg	b_e	300 Ns/m
k_e	10000 N/m	A_{sa}	1×10^{-4} m^2
F_0	2000 N	w	0.022 m
V_{co}	1×10^{-5} m^3	α_d	0.7
B	1.4×10^{9} Pa	V_t	2×10^{-3} m^3
A_{re}	5×10^{-8} m^2	x_{max}	0.01 m

A.3 Accumulator

Accumulators are primarily used to filter pressure pulsations from the pump and to provide additional fluid flow in the necessary direction as shown in Fig. A.4.

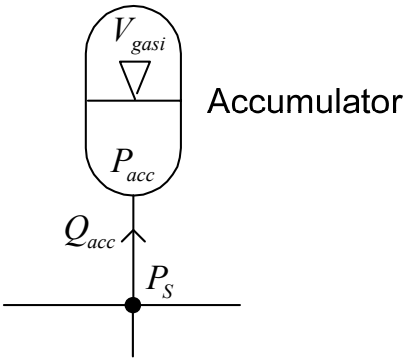

Fig. A.4 Accumulator dynamics.

The relationship between Q_{acc} and P_{acc} could be written as follow (Kang et al., 2008);

$$P_{acc} = P_{acci} V_{gasi}^{k} \Big/ \left(V_{gasi} - \int Q_{acc} dt \right)^{k} \tag{A.13}$$

$$Q_{acc} = K_{acc-leak} \left(P_s - P_{acc} \right) \tag{A.14}$$

where P_{acci} is the initial pressure, V_{gasi} is the initial volume of gas, k is the polytropic exponent of gas and $K_{acc\text{-}leak}$ is the leakage coefficient of the accumulator. The parameter values used in the simulation study are given in Table A.2.

Table A.2 Parameters used in the accumulator model.

Parameter	Value	Parameter	Value
P_{acci}	$2\times10^{7}\ Pa$	V_{gasi}	$150\ ml$
k	1.4	$K_{acc\text{-}leak}$	$2\times10^{-10}\ m^3/(Pa\cdot s)$

A.4 Pump and Motor

In this section, mathematical models of the pump and motor are derived. First, a gear-box headed DC motor is utilized as the motor of the pump device and then, a fixed displacement pump is used for flow supply to the hydraulic circuit from the

pump exit. It is assumed that a motor having a maximum speed of 12000 *rev/min* is used in the simulation study. Moreover, the nominal voltage and power of the motor are assumed 240 *V* and 10 *kW*, respectively. The mathematical equations of the DC motor and the pump flow (Q_{pump}) are given as below;

$$U = E + L\frac{di}{dt} + Ri \tag{A.15}$$

$$E = K_c K_g \omega \tag{A.16}$$

$$T_e = K_t K_g i \tag{A.17}$$

$$T_e = J\dot{\omega} + k_{fric}\omega + T_L \tag{A.18}$$

$$T_L = D\,p/\eta_{mech} \tag{A.19}$$

$$Q_{pump} = D\,\omega - K_{ilp}\,P_S \tag{A.20}$$

where U is the nominal voltage, L is the inductance, R is the resistance, E is the back electromotive force voltage, K_c is the back *emf* constant, K_g is the gearbox ratio, T_e is the electromagnetism torque, K_t is the torque constant, J is the total inertia (motor plus pump system), k_{fric} is the viscous coefficient, ω is the rotational speed of gear-box output, T_L is the load torque, D is the pump displacement, p is the pressure differential across the pump (if one assumes that tank pressure P_T is exactly zero then p equals to P_S) and η_{mech} is the pump mechanical efficiency. The parameter values used in the simulation study are given in Table A.3.

Table A.3 Parameters used in the motor and pump model.

Parameter	Value	Par.	Value
U	240 *V*	L	2.5×10^{-3} *H*
R	1 *ohm*	K_c	0.2 *V/(rad/s)*
K_t	0.2 *Nm/A*	K_g	7:1
J	1.2×10^{-3} *kg·m²*	k_{fric}	4×10^{-4} *N·m/(rad/s)*
D	16 *cm³/rev*	η_{mech}	0.80
K_{ilp}	1×10^{-13} *m³/(s·Pa)*		

A.5 Pipelines

Pipelines are used to connect the hydraulic elements to each other. Pipeline dynamics can be neglected assuming the pipe lengths are small. In that case, their

volume should be added to the corresponding chamber volumes while solving the related pressure dynamics there. In the simulation study, only the pipeline dynamics between the pump and the supply port of the servo-valve is taken into consideration while assuming the other pipeline lengths are small.

Taking the supply line (going from the pump to the servo-valve inlet) as an example, p_1 and q_1 will indicate the pump side pressure and the flow rate at the head of the pipeline and p_2 and q_2 will indicate the supply pressure value and supply flow rate at the inlet of the servo-valve as could be seen from Fig. A.5. The pipeline effects could be modeled by a four-pole equation (Ayalew and Kulakowski, 2005).

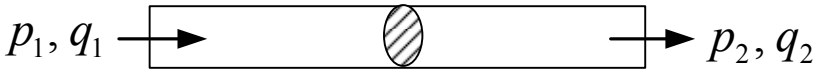

Fig. A.5 A fluid transmission line.

The four-pole equations in the Laplace domain could be arranged to give the $p_2(s)$ and $q_1(s)$ as outputs while the inputs are $p_1(s)$ and $q_2(s)$ as shown below:

$$\begin{bmatrix} p_2(s) \\ q_1(s) \end{bmatrix} = \begin{bmatrix} \dfrac{1}{\cosh\Gamma(s)} & -\dfrac{Z_c(s)\,sinh\Gamma(s)}{\cosh\Gamma(s)} \\ \dfrac{sinh\Gamma(s)}{Z_c(s)\cosh\Gamma(s)} & \dfrac{1}{\cosh\Gamma(s)} \end{bmatrix} \begin{bmatrix} p_1(s) \\ q_2(s) \end{bmatrix} \tag{A.21}$$

The propagation operator Γ(s) and the line characteristic impedance $Z_c(s)$ are defined by

$$\Gamma(s) = D_n \frac{sd^2}{4v} \sqrt{\alpha^2 + \frac{32\alpha\chi\upsilon}{sd^2}} \tag{A.22}$$

$$Z_c(s) = Z_0 \sqrt{\alpha^2 + \frac{32\alpha\chi\upsilon}{sd^2}} \tag{A.23}$$

where α is the natural frequency modification factor and χ is the damping modification factor, which could be determined from Yang and Tobler (1991).

Moreover, υ is the kinematic viscosity. D_n is the dissipation number and Z_0 is the line impedance as given below

$$D_n = \frac{4l\upsilon}{cd^2} \tag{A.24}$$

$$Z_0 = \frac{4\rho c}{\pi d^2} \tag{A.25}$$

$$c = \sqrt{\frac{\beta}{\rho}} \tag{A.26}$$

where l and d is the length and diameter of the pipeline, respectively. Moreover, c is the speed of sound which is expressed in terms of bulk modulus and density of the hydraulic oil.

Table A.4 shows the value of the parameters used in the pipeline model and a least-squares curve fit algorithm (Wongputorn et al., 2005) named '`invfreqs`' in the MATLAB Signal Processing Toolbox is used to approximate the three casual functions as below

$$\frac{1}{\cosh\Gamma(s)} = \frac{\begin{array}{r}0.358s^5 + 1.073\times10^6 s^4 + 4.557\times10^7 s^3 - 1.532\times10^{14} s^2 \\ - 4.11\times10^{15} s + 9.078\times10^{21}\end{array}}{\begin{array}{r}s^6 + 102.3s^5 + 1.052\times10^8 s^4 + 6.964\times10^9 s^3 + 2.732\times10^{15} s^2 \\ + 8.823\times10^{16} s + 9.078\times10^{21}\end{array}} \tag{A.27}$$

$$\frac{Z_c(s)sinh\Gamma(s)}{\cosh\Gamma(s)} = \frac{\begin{array}{r}2.091\times10^{14} s^7 + 5.144\times10^7 s^6 + 3.764\times10^{21} s^5 + 7.134\times10^{24} s^4 \\ +4.673\times10^{27} s^3 + 1.17\times10^{30} s^2 + 9.951\times10^{31} s + 1.732\times10^{33}\end{array}}{\begin{array}{r}s^8 + 3675s^7 + 8.32\times10^7 s^6 + 1.75\times10^{11} s^5 + 4.012\times10^{14} s^4 \\ +5.856\times10^{17} s^3 + 3.44\times10^{20} s^2 + 7.548\times10^{22} s + 4.775\times10^{24}\end{array}} \tag{A.28}$$

$$\frac{sinh\Gamma(s)}{Z_c(s)\cosh\Gamma(s)} = \frac{\begin{array}{r}8.758\times10^7 s^7 + 0.0024s^6 + 16.08s^5 + 3.621\times10^4 s^4 \\ +2.573\times10^7 s^3 + 6.225\times10^9 s^2 + 4.121\times10^{11} s - 9.943\times10^5\end{array}}{\begin{array}{r}s^8 + 2954s^7 + 7.387\times10^7 s^6 + 1.925\times10^{11} s^5 + 4.012\times10^{14} s^4 \\ +6.773\times10^{17} s^3 + 4.615\times10^{20} s^2 + 1.11\times10^{23} s + 7.345\times10^{24}\end{array}} \tag{A.29}$$

Table A.4 Parameters used in the pipeline model.

Parameter	Value	Parameter	Value
d	0.005 m	l	1 m
v	100 mm^2/s	ρ	890 kg/m^3
β	1.4×10^9 Pa	α	1
χ	1		

A.6 Hydraulic Cylinder Dynamic and Friction Model

Here, the model of the hydraulic cylinder is developed by taking the effects of position dependent actuator chamber volumes and friction forces. The internal and external leakages are also taken into consideration as shown in Fig. A.6.

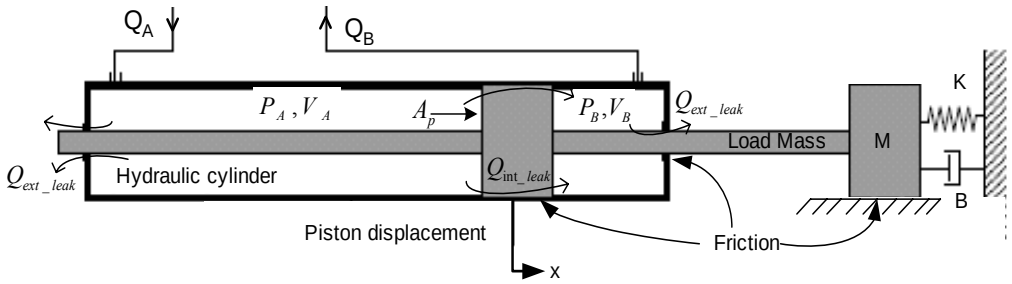

Fig. A.6 Hydraulic cylinder.

Applying the continuity equations to each cylinder chamber will give the chamber pressure dynamics as below.

$$Q_A - Q_{\text{int}\_leak} - Q_{ext\_leak} - A_p\,\dot{x} = \left(\frac{V_{A0} + A_p x}{\beta}\right)\frac{dP_A}{dt} \tag{A.30}$$

$$-Q_B + Q_{\text{int}\_leak} - Q_{ext\_leak} + A_p\,\dot{x} = \left(\frac{V_B - A_p x}{\beta}\right)\frac{dP_B}{dt} \tag{A.31}$$

Moreover, the nonlinear equation describing the relationship among the chamber pressures and the actuator position (x) can be written as

$$\left(P_A - P_B\right) A_p = M\,\ddot{x} + B\,\dot{x} + Kx + F_{fric} \tag{A.32}$$

where M is the mass of the piston/load; B is the the effective viscous damping; K is the stiffness of the equivalent spring, A_p is the piston annulus area and β refers to the bulk modulus of the hydraulic fluid. P_A and P_B denote the hydraulic pressures in

each of the actuator chambers. Note that the volumes of hydraulic oil on each side of the piston are given by variables $V_A=A_p x+V_{A0}$ and $V_B=-A_p x+V_{B0}$ where V_{A0} and V_{B0} are the initial chamber volumes. The internal and external leakages (Q_{int_leak} and Q_{ext_leak}) can be calculated as $C_{int}(P_A-P_B)$ and $C_{ext}P_A$ (or $C_{ext}P_B$), respectively, where C_{int} and C_{ext} will be the leakage coefficients. On the other hand, friction process in (A.33) can be characterized by the LuGre model as its mathematical model is given in (5.7) and (5.8). The parameter values used in the simulation study are also given in Table 5.1.

APPENDIX B

MATLAB FILES

The below M-Files are used to create and to train network objects which are presented in Chapter 5. In Appendix B.1, *Network_Qa* (in Fig. 5.4) is devised. In a similar way, *Network_Qb* could also be created. Next, Appendix B.2 represents the M-File for the creation of the *divider network* as illustrated in Fig. 5.5. Furthermore, the construction of the SRNN from its modules (*Network_Qa, Network_Qb and divider network)* is realized by the M-File given in Appendix B.3.

B.1 M-File for the *Network_Qa*

```
u = linspace(-1,1,99)';
p = linspace(0,1,99)';
q = zeros(99,99);
output=zeros(1,9801);
input=zeros(2,9801);

k=1;
for i = 1:99
  for j = 1:99
    if(u(j)>0)
      q(i,j) = u(j)*sqrt(1-p(i));
    else
      q(i,j) = u(j)*sqrt(p(i));
    end
  output(k)=q(i,j);
  input(1,k) = u(j);
  input(2,k) = p(i);
  k=k+1;
  end
end

net = network;
net.numInputs = 2;
net.numLayers = 3;
net.biasConnect = [1; 1; 1];
net.inputConnect(1,1) = 1;
net.inputConnect(1,2) = 1;
net.layerConnect = [0 0 0;1 0 0;0 1 0];
net.outputConnect = [0 0 1];
net.inputs{1}.size = 1;
```

```
net.inputs{1}.range = [-1 1];
net.inputs{2}.size = 1;
net.inputs{2}.range = [0 1];
net.layers{1}.size = 10;
net.layers{1}.transferFcn = 'tansig';
net.layers{1}.initFcn = 'initnw';
net.layers{2}.size = 10;
net.layers{2}.transferFcn = 'tansig';
net.layers{2}.initFcn = 'initnw';
net.layers{3}.initFcn = 'initnw';
net.initFcn = 'initlay';
net.performFcn = 'mse';
net.trainFcn = 'trainlm';
net = init(net);
net.trainParam.goal = 1e-10;
net.trainParam.epochs=2500;
net = train(net,input,output);
Network_Qa=net;
```

B.2 M-File for the *divider network*

```
u = linspace(-1,1,100)';
p = linspace(-0.9,0.9,100)';
q = zeros(100,100);
output=zeros(1,10000);
input=zeros(2,10000);

k=1;
for i = 1:100
  for j = 1:100
      q(i,j) = u(j)/(p(i)+1);
  output(k)=q(i,j);
  input(1,k) = u(j);
  input(2,k) = p(i);
  k=k+1;
  end
end

net = network;
net.numInputs = 2;
net.numLayers = 2;
net.biasConnect = [1; 1];
net.inputConnect(1,1) = 1;
net.inputConnect(1,2) = 1;
net.layerConnect = [0 0;1 0];
net.outputConnect = [0 1];
net.inputs{1}.size = 1;
net.inputs{1}.range = [-1 1];
net.inputs{2}.size = 1;
net.inputs{2}.range = [-0.9 0.9];
net.layers{1}.size = 20;
net.layers{1}.transferFcn = 'tansig';
net.layers{1}.initFcn = 'initnw'
net.layers{2}.initFcn = 'initnw';
net.initFcn = 'initlay';
net.performFcn = 'mse';
```

```
net.trainFcn = 'trainlm';
net = init(net);
net.trainParam.goal = 1e-20;
net.trainParam.epochs=1000;
net = train(net,input,output);
divider=net;
```

B.3 M-File for the SRNN

```
net = network;
net.numInputs = 4;
net.numLayers = 10;
net.biasConnect = [1; 1; 1; 1; 1; 1; 1; 0; 1; 0];
net.inputConnect(1,1) = 1;
net.inputConnect(4,1) = 1;
net.inputConnect(7,2) = 1;
net.inputConnect(9,4) = 1;
net.inputConnect(7,3) = 1;
net.inputConnect(9,3) = 1;
net.layerConnect = [0 0 0 0 0 0 0 1 0 0;
                    1 0 0 0 0 0 0 0 0 0;
                    0 1 0 0 0 0 0 0 0 0;
                    0 0 0 0 0 0 0 0 0 1;
                    0 0 0 1 0 0 0 0 0 0;
                    0 0 0 0 1 0 0 0 0 0;
                    0 0 1 0 0 0 0 0 0 0;
                    0 0 0 0 0 0 1 1 0 0;
                    0 0 0 0 0 1 0 0 0 0;
                    0 0 0 0 0 0 0 0 1 1];
net.outputConnect = [0 0 0 0 0 0 0 1 0 1];
net.layerWeights{1,8}.delays = [1];
net.layerWeights{4,10}.delays = [1];
net.layerWeights{8,8}.delays = [1];
net.layerWeights{10,10}.delays = [1];
net.layers{1}.size = 10;
net.layers{1}.transferFcn = 'tansig';
net.layers{1}.initFcn = 'initnw';
net.layers{2}.size = 10;
net.layers{2}.transferFcn = 'tansig';
net.layers{2}.initFcn = 'initnw';
net.layers{3}.initFcn = 'initnw';
net.layers{7}.size = 20;
net.layers{7}.transferFcn = 'tansig';
net.layers{7}.initFcn = 'initnw';
net.layers{8}.initFcn = 'initnw';
net.layers{4}.size = 10;
net.layers{4}.transferFcn = 'tansig';
net.layers{4}.initFcn = 'initnw';
net.layers{5}.size = 10;
net.layers{5}.transferFcn = 'tansig';
net.layers{5}.initFcn = 'initnw';
net.layers{6}.initFcn = 'initnw';
net.layers{9}.size = 20;
net.layers{9}.transferFcn = 'tansig';
net.layers{9}.initFcn = 'initnw';
net.layers{10}.initFcn = 'initnw';
net.performFcn = 'mse';
net.trainFcn = 'trainlm';
```

```
net.initFcn = 'initlay';
net = init(net);

net.IW{1,1}=Network_Qa.IW{1,1};
net.IW{4,1}=Network_Qb.IW{1,1};
net.LW{1,8}=Network_Qa.IW{1,2};
net.LW{4,10}=Network_Qb.IW{1,2};
net.LW{2,1}=Network_Qa.LW{2,1};
net.LW{5,4}=Network_Qb.LW{2,1};
net.LW{3,2}=Network_Qa.LW{3,2}*Kv*sqrt(Ps)*Uv_max/q_max;
net.LW{6,5}=Network_Qb.LW{3,2}*Kv*sqrt(Ps)*Uv_max/q_max;
net.IW{7,2}=divider.IW{1,2};
net.IW{9,4}=divider.IW{1,2};
net.IW{7,3}=-divider.IW{1,1};
net.IW{9,3}=divider.IW{1,1};
net.LW{7,3}=divider.IW{1,1};
net.LW{9,6}=-divider.IW{1,1};
net.LW{8,7}=divider.LW{2,1}*q_max*Bulk/v_A*Ts/Ps;
net.LW{10,9}=divider.LW{2,1}*q_max*Bulk/v_B*Ts/Ps;
net.LW{8,8}=1;
net.LW{10,10}=1;
net.b{1,1}=Network_Qa.b{1,1};
net.b{2,1}=Network_Qa.b{2,1};
net.b{3,1}=Network_Qa.b{3,1}*Kv*sqrt(Ps)*Uv_max/q_max;
net.b{4,1}=Network_Qb.b{1,1};
net.b{5,1}=Network_Qb.b{2,1};
net.b{6,1}=Network_Qb.b{3,1}*Kv*sqrt(Ps)*Uv_max/q_max;
net.b{7,1}=divider.b{1,1};
net.b{9,1}=divider.b{1,1};
SRNN=net;
View(SRNN)
```

CIRRICULUM VITAE

PERSONEL INFORMATION:

Name : Ergin Kılıç

Place of Birth : Tokat

Adress : Middle East Technical University,
Mechanical Engineering Department,
A-102, 06800, Ankara.

GSM : [+90] (505) 418 07 15

e-mail : kergin@metu.edu.tr
ergink81@gmail.com

Nationality : Turkish

EDUCATION:

2007 – : Ph.D. Programme at METU
CPGA: 3.75/4 (Graduate Courses Performance Award)

2004 – 2007 : M.Sc. Programme at METU
CPGA: 3.6/4

1999 – 2003 : B.Sc. Programme at Gazi University
CPGA: 3.38/4 (Honor Student)

1992 – 1999 : High School Degree from Çankaya Atatürk Anadolu Lisesi, Ankara

LANGUAGES:

English : Intermediate (KPDS=72)

WORK EXPERIENCE:

2005 – : Teaching Assistant at ME Department, METU, Ankara.

2008 - 2010 : Researcher in a TUBITAK project named as “Development of Personal Computer based Universal Motion Control Systems” (project no: 108E048).

2003 – 2004 : Sales Engineer at Altar Teknoloji, Kavaklıdere, Ankara .

COMPUTER SKILLS:

Autodesk\ AutoCAD : Medium

Autodesk\ Inventor : Professional

SolidWorks : Medium

KeyCreator : Medium

EdgeCAM : Medium

MATLAB : Professional

JAVA : Beginner

C# : Beginner

Verilog : Medium

VHDL : Beginner

INTERESTS AND HOBBIES:

Fitness, Traveling, Electronics

PUBLICATIONS:

Kilic, E., Dolen, M., Koku, A.B., Caliskan, H. and Balkan, T. Accurate pressure prediction of a servo-valve controlled hydraulic system. Mechatronics, doi: 10.1016/j.mechatronics.2012.08.001

Kilic, E., Dogruer, C.U., Dolen, M. and Koku, A.B. 2012. Position estimation for timing belt drives of precision machinery using structured neural networks. Mechanical Systems and Signal Processing, 29, 343-361.

Kilic, E., Dolen, M. and Koku, A.B. 2010. Analysis and estimation of motion transmission errors of a timing belt drive. Turkish Journal of Electrical Engineering and Computer Sciences, 18(5), 883-897.

Dogruer, C.U., Kilic, E., Dolen, M., and Koku, A.B. 2007. Nonlinear position estimators based on artificial neural networks for low costs manufacturing systems. Journal of Automation, Mobile Robotics and Intelligent Systems, 1(2), 40-44.

Kilic, E., Dolen, M., Koku, A.B. and Dogruer, C.U. 2007. Novel position estimators for timing belt drives. Journal of Automation, Mobile Robotics and Intelligent Systems, 1(2), 55-61.

Kanburoglu, F.A., Kilic, E., Dolen, M. and Koku, A.B. 2007. A test setup for evaluating long-term measurement characteristics of optical mouse sensors. Journal of Automation, Mobile Robotics and Intelligent Systems, 1(2), 71-75.

INTERNATIONAL CONFERENCES:

Kilic, E., Dolen, M. and Koku, A.B. 2011. Experimental Evaluation of Cable-Drum Systems as Linear Motion Sensors. In Proceedings of IEEE International Conference on Mechatronics, Turkey, pp. 666-671.

Kilic, E., Dolen, M. and Koku, A.B. 2011. Long-term prediction of hydraulic system dynamics via structured recurrent neural networks. In Proceedings of IEEE International Conference on Mechatronics, Turkey, pp. 330-335.

Kilic, E., Baser, O., Dolen, M. and Konukseven, E.I. 2010. An enhanced adaptive windowing technique for velocity and acceleration estimation using incremental position encoders. In Proceedings of the International Conference on Signals and Electronic Systems, Gliwice, Poland, pp. 61-64.

Baser, O., Kilic, E., Konukseven, E.I. and Dolen, M. 2010. A hybrid method to estimate velocity and acceleration using low-resolution optical incremental encoders. In Proceedings of the International Conference on Signals and Electronic Systems, Gliwice, Poland, pp. 57-60.

NATIONAL CONFERENCES:

Ergin Kılıç, Hakan Çalışkan, Melik Dölen, A. Buğra Koku, and Tuna Balkan. 2011. Yapay sinir ağ modellerinin valf denetimli hidrolik bir sistemin uzun süreli basınç tahmininde kullanılması. 6th National Hydarulic Pneumatic Congress and Exhibition (HPKON 2011), 12-15 October, Izmir, pp. 211- 225.

Furkan A. Kanburoğlu, Ergin Kılıç, Melik Dölen and A. Buğra Koku. 2009. Bilgisayar denetimli takım tezgahları için dağıtık bir hareket denetim sistemi. National Conference on Automatic Control (TOK'09), 13-16 October, Istanbul, pp. 483-489.

Ergin Kılıç, Melik Dölen ve A. Buğra Koku. 2008. Dişli kayış mekanizmalarında iletim hatalarının incelenmesi. National Conference on Automatic Control (TOK'08), 13-15 November, Istanbul, pp. 200-205.